The Dissertation Committee for Fei Cao Certifies that this is the approved version of the following dissertation:

DEVELOPMENT OF A TWO-PHASE FLOW COUPLED CAPACITANCE RESISTANCE MODEL

Committee:

Larry W. Lake, Supervisor

Thomas F. Edgar

Leon S. Lasdon

Kishore K. Mohanty

Tad W. Patzek

DEVELOPMENT OF A TWO-PHASE FLOW COUPLED CAPACITANCE RESISTANCE MODEL

by

Fei Cao, B.E.; M.S.E

Dissertation

Presented to the Faculty of the Graduate School of

The University of Texas at Austin

in Partial Fulfillment

of the Requirements

for the Degree of

Doctor of Philosophy

The University of Texas at Austin

December 2014

Dedication

To my parents

To Haishan Luo and Chloe Luo

To the memory of my grandparents

Acknowledgements

First and foremost, I would like to thank my supervisor Dr. Larry W. Lake for giving me this precious opportunity to work with him. I deeply appreciate his professional knowledge, patience, guidance and encouragement. My study at UT-Austin under his supervision is the most valuable and unique experience that has broadened my horizon. Special thanks are due to Dr. Leon Lasdon and Mr. Emilio Nunez for their suggestions and support. Thanks are also due to Dr. Kishore Mohanty, Dr. Tad Patzek, and Dr. Thomas Edgar for serving on my dissertation committee. I would also like to thank Dr. Jean-Philippe Nicot and Dr. Susan Hovorka for their guidance and support for this research.

Many thanks to Eric Ziegel and Shawn Shirzadi in BP America for the opportunity to work in their team during summer 2013. Their professionalism, enthusiasm, and hard-working attitude greatly inspired me. I am also thankful for other members of the Field of the Future team in BP. Their help is greatly appreciated.

Special thanks are due to Scott Birkhead and other petrophysicists in Anadarko Petroleum Corporation. I am thankful for their openness and willingness to help me during my internship with Anadarko in summer 2012.

I am grateful to the faculty and staff of the Petroleum and Geosystems Engineering Department at the University of Texas at Austin for being supportive during my time here. Special thanks are due to Heather Felauer and Frankie Hart for their help and patience. I am also grateful for the association with the members of the Center for Petroleum Asset Risk Management (CPARM) research group at the University of Texas at Austin. Their help and support are appreciated.

It is my pleasure to work with graduate students in Dr. Lake's group. I would like to acknowledge Morteza Sayarpour, Wenli Wang, Jong Kim, Anh Nguyen, Babafemi Ogunyomi, Lokendra Jain, Ashwin Venkatraman, Rapheephan Laochamroonvorapongse, Soros Chitsiripanich and Chonpatin Phaiboonpalayoi.

Thanks are also due to General Algebraic Modeling System (GAMS) Development Corporation and Computer Modeling Group (CMG) for providing the software used in this work.

Finally, I want to thank my beloved husband for being extremely supportive along this journey. I am also grateful for the love and support of my daughter, my parents and grandparents. Their sacrifice during my study here is deeply appreciated.

Fei Cao

December, 2014

DEVELOPMENT OF A TWO-PHASE FLOW COUPLED CAPACITANCE RESISTANCE MODEL

Fei Cao, Ph.D.

The University of Texas at Austin, 2014

Supervisor: Larry W. Lake

The Capacitance Resistance Model (CRM) is a reservoir model based on a data-driven approach. It stems from the continuity equation and takes advantage of the usually abundant rate data to achieve a synergy of analytical model and data-driven approach. Minimal information (rates and bottom-hole pressure) is required to inexpensively characterize the reservoir. Important information, such as inter-well connectivity, reservoir compressibility effects, etc., can be easily and readily evaluated. The model also suggests optimal injection schemes in an effort to maximize ultimate oil recovery, and hence can assist real time reservoir analysis to make more informed management decisions.

Nevertheless, an important limitation in the current CRM model is that it only treats the reservoir flow as single-phase flow, which does not favor capturing physics when the saturation change is large, such as for an immature water flood. To overcome this limitation, we develop a two-phase flow coupled CRM model that couples the pressure equation (fluid continuity equation) and the saturation equation (oil mass balance). Through this coupling, the model parameters such as the connectivity, the time constant, temporal oil saturation, etc., are estimated using nonlinear multivariate regression to history match historical production data. Incorporating the physics of two-

phase displacement brings several advantages and benefits to the CRM model, such as the estimation of total mobility change, more accurate prediction of oil production, broader model application range, and better adaptability to complicated field scenarios. Also, the estimated saturation within the drainage volume of each producer can provide insights with respect to the field remaining oil saturation distribution.

Synthetic field case studies are carried out to demonstrate the different capabilities of the coupled CRM model in homogeneous and heterogeneous reservoirs with different geological features. The physical meanings of model parameters are well explained and validated through case studies. The results validate the coupled CRM model and show improved accuracy in model parameters obtained through the history match. The prediction of oil production is also significantly improved compared to the current CRM model. A more reliable oil rate prediction enables further optimization to adjust injection strategies. The coupled CRM model has been shown to be fast and stable. Moreover, sensitivity analyses are conducted to study and understand the impact of the input information (e.g., relative permeability, viscosity) upon the output model parameters (e.g., connectivity, time constants). This analysis also proves that the model parameters from the two-phase coupled model can combine both reservoir compressibility and mobility effects.

Table of Contents

List of Tables

List of Figures

CHAPTER 1: INTRODUCTION

The economic success of oil/gas recovery from hydrocarbon reservoirs ultimately depends on the production rate; hence, the evaluation and prediction of the reservoir/well performance are critical. Continuously, reservoir engineers are engaged in the synthesis of different disciplines including geosciences, physics, chemistry, and mathematics, etc., to better understand and characterize the reservoir behavior. More and more sophisticated technologies and tools have been developed in relevant subjects, such as formation evaluation, reservoir modeling, reservoir simulation, and injection/production optimization and management.

Nevertheless, even though being arduous and careful to characterize the reservoir, reservoir engineers, might still encounter that the consequent reservoir/well performance is not as expected. This is, in general, owing to various uncertainties with respect to the subsurface heterogeneity and an inability to fully characterize these uncertainties. As a result, it is a strategy to apply multiple technologies to achieve synergy, which motivates engineers/researchers to develop alternative reservoir evaluation/prediction methods. The capacitance resistance model (CRM), which will be extensively discussed and studied in this dissertation, is such a model, being able to efficiently provide accurate and meaningful evaluation and prediction to the reservoir/well performance.

1.1 METHODS FOR RESERVOIR PERFORMANCE EVALUATION AND PREDICTION

Before proceeding with the discussion regarding the CRM model, we first review the approaches that are widely used for reservoir performance evaluation and prediction (see Figure 1.1). In general, these methods can be categorized into several classes, such as reservoir simulation, analytical models, and empirical models, etc.

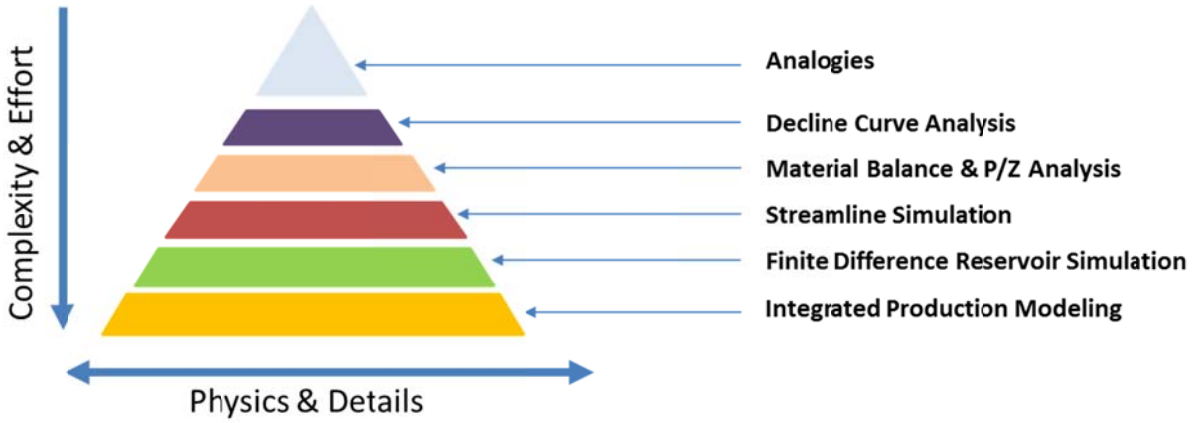

Figure 1.1 General methods for reservoir performance evaluation and prediction (M. J. King and E. Gildin, private communication, 2014).

1.1.1 Reservoir Simulation

Reservoir simulation has been a popular way to estimate reservoir performance as well as to predict future well production rates. Over the years, many reservoir simulators have been developed for reservoirs under different recovery processes, e.g., water flood, gas flood, thermal injection, chemical EOR and hydraulic fracturing.

Traditional reservoir simulations require reservoir geological models consisting of many grid blocks with permeability, porosity, and other properties assigned by block. This is done by means of geostatistical reservoir modeling that often generates many realizations for a specific property with no unique answer. Pressure and saturation equations are then solved numerically for each grid block. As a result, reservoir simulations usually require laborious and complicated procedures with respect to reservoir modeling and history matching. Even so, the forecast might be unreliable owing to various uncertainties associated with the input information (e.g., reservoir geology, fluid/rock properties) and numerical errors (e.g., numerical dispersion, lacking accuracy to capture fingering). Moreover, despite the fact that the numerical techniques for

speeding up a simulation continue to develop; reservoir simulation is, in general, computationally expensive especially for large fields with hundreds of wells.

Streamline simulation provides an alternative to the cell-based traditional reservoir simulations (Datta-Gupta and King, 2007). Streamlines are curves that are tangent to the velocity vectors of the flow. In streamline simulation, streamlines are obtained to be orthogonal to pressure contours, which are solved on an underlying grid that is similar to a traditional reservoir simulation. Fluid is transported along each streamline, which allows a one-dimensional solution along any streamlines, assuming no crossflow among them (Baker, 2001). Therefore, well response is simply the summation of a series of 1D flow simulations. The advantage of streamline simulation lies in its fast computational time as well as its representation of the instantaneous flow field, which can produce data such as drainage regions associated with producers and the flow rate allocations between injector/producer pairs. Nevertheless, one of the key limitations in streamline simulation is the assumption of incompressibility flow to ensure the independence between streamlines; hence it does not favor capturing physics that is transverse to the main direction of flow, such as gravity, diffusion, compressibility, and transverse-thermal effects (Thiele et al. 2010).

1.1.2 Analytical Models

Classic analytical models, such as the macroscopic material balance, have been used to obtain estimation and understanding of the reservoir performance. Macroscopic material balances are sometimes called tank models as they ignore pressure, temperature, and compositional gradients within the system and treat the system as a single homogenous unit (Lake, 1987).

Tank models have many applications including estimating the original oil and gas in place, estimating water influx, and diagnosing production mechanisms. They can be applied to a broad range of reservoir fluids from dry gases to heavy oils (Walsh and Lake, 2003). Nevertheless, the results from macroscopic material balance might not satisfy the accuracy to the desired extent considering the simplifications made in such a complex reservoir system. Also, a tank model does not provide detailed description between wells, which further hinders its application especially in a multi-well system.

1.1.3 Empirical Models

Empirical models (including data-driven models) have been developed to achieve simple correlations through history matching to predict future well performance and determine the ultimate recoverable reserves. An example of traditional empirical methods is the production decline curve analysis (DCA), which is based on empirical observations of production rate decline but not on theoretical derivations. The commonly used trending equations in decline curve analysis are those proposed by Arps (1945).

Besides the traditional empirical models, the data-driven models, which have extensive applications in economics and finance for data analysis, show great potential in optimization of reservoir/well performance (Solomatine et al., 2008; Mahdavi and Khademi, 2012). Data driven models, such as fuzzy logic, neutral network, genetic algorithm, etc., are generally used to analyze data series in a mathematical or stochastic manner. The goal is to find a few shape functions or sinusoidal functions or a small number of eigenvectors that resolve the spatial and temporal properties of the data with sufficient accuracy. Accordingly, the prediction of fluid/oil rate can be possibly achieved by the regression of the existing data.

In general, the advantage of empirical models lies in their simplicity and efficiency. Nevertheless, most empirical models rely exclusively on data information without consideration of reservoir physics. Therefore, they can be distracted by data noise and could not provide an explicit geological/physical meaning to the results.

1.2 INTRODUCTION TO THE CRM MODEL

Based on the discussions above, it is desirable to explore inexpensive approaches that combine data-driven models with reservoir physics to obtain a synergy of both empirical and analytical models. With this motivation, the capacitance resistance model (CRM), a data-driven model based on the continuity equation, was proposed. The CRM model is a comprehensive package that is capable of history matching production data, predicting fluid/oil rates, and optimizing injection schemes. It requires minimum reservoir information (rates and bottom hole pressure) and the model parameters obtained also provide insights to reservoir geological features.

1.2.1 Fundamentals of the CRM Model

The CRM model analogizes the oil reservoir to a resistor-capacitor (RC) electric network to characterize the injector-producer connection and response time (see Figure 1.2). The production rate response is analogous to the voltage across a capacitor in an RC circuit where the battery potential is equivalent to the injection signal.

A fluid continuity equation is established on a reservoir control volume to achieve the contributions from nearby injectors as well as the injector-producer signal response time (time constant) owing to the reservoir/fluids compressibility. The injector-producer

connectivity and the time constant are the two most important parameters obtained from the CRM model using the production/injection rates.

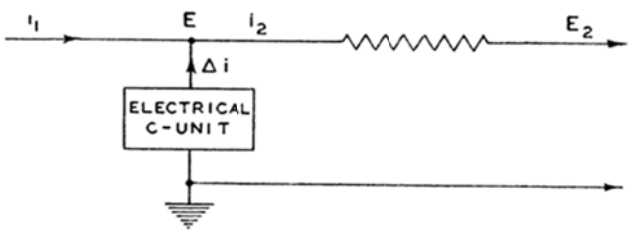

a. An electrical unit (Bruce, 1943)

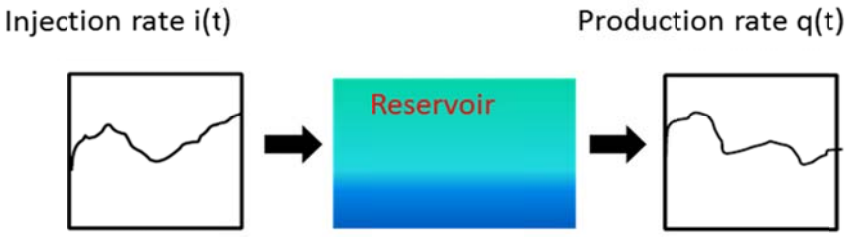

Capacitance---Oil reservoir
Resistance---Rock permeability, fluid viscosity

b. The capacitance resistance model analogy

Figure 1.2 Analogy of the reservoir to electrical units.

Specifically, the connectivity generates information such as the flow rate allocation between injector/producer pairs, from which we are able to quantify the communications between different wells. The time constant approximates the characteristic time of the signal response travelling from injectors to producers, which implies the reservoir compressibility effects. To obtain the connectivity and time constant, a non-linear multivariate regression approach is applied to minimize the difference between the model-estimated rate and the observed rate, which is essentially a data history matching procedure.

The General Algebraic Modeling System (GAMS), which is a high-level modeling system for mathematical programming and optimization, is the platform we use to construct the CRM model. It consists of a language compiler and stable integrated high-performance solvers. It is tailored for complex and large scale modeling applications. The solver for the CRM model is CONOPT, which is a non-linear programming (NLP) solver that is designed to find local optimum for large scale NLP problems.

The computation cost of the CRM model proves to be inexpensive. Because of its efficiency, it is intended for seeking quick solutions to the field dynamics; hence it can assist real time reservoir management and optimization.

From the perspective of reservoir management, there is some particularly useful information obtained from the CRM model.

1) The CRM model generates a well connectivity map, illustrated in Figure 1.3. On this map, the lines indicate which well pairs are connected; whereas line colors imply different intensities of connections. With this information, we are able to gain better understanding of the flood pattern; and therefore manage the injection project effectively in real time. Moreover, the connectivity pattern can also provide insights into reservoir geological features.
2) The injector connectivity can outline the injected water distribution in different directions (see Figure 1.4). Therefore, it is possible to assess the injection efficiency in each injector to adjust injection strategies readily. With the obtained model parameters (connectivity and time constant), we can further predict well performance and optimize injection schemes to maximize the oil production, which serves the ultimate goal of improving oil recovery.

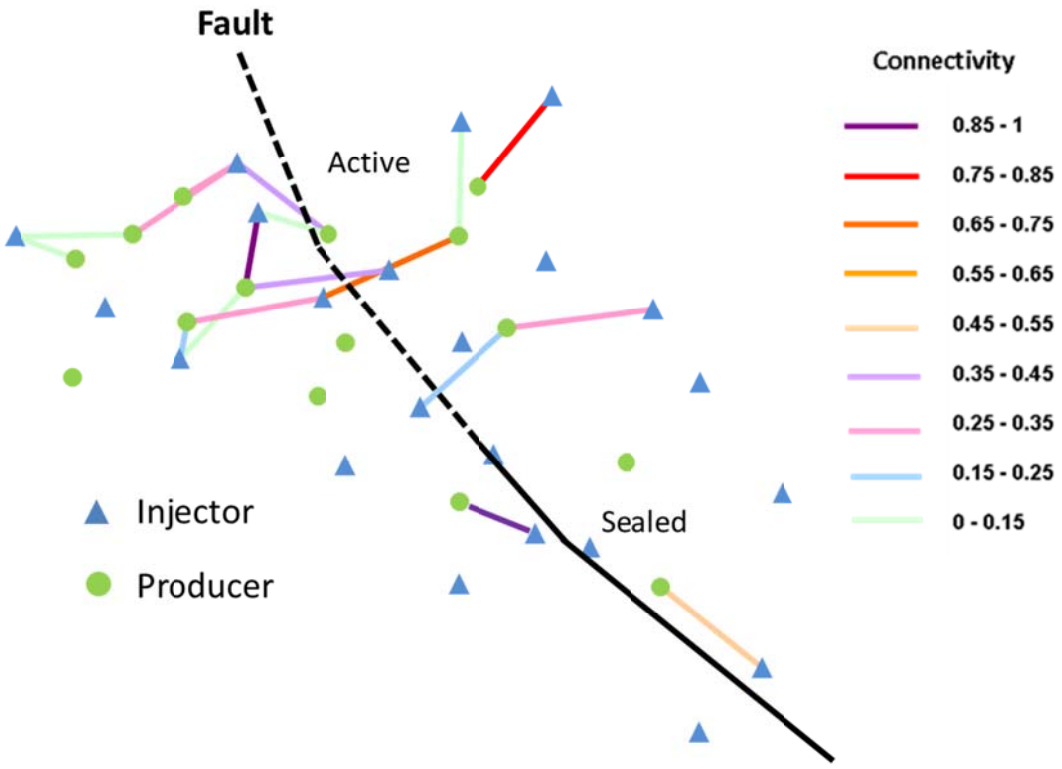

Figure 1.3 Connectivity map from the CRM model.

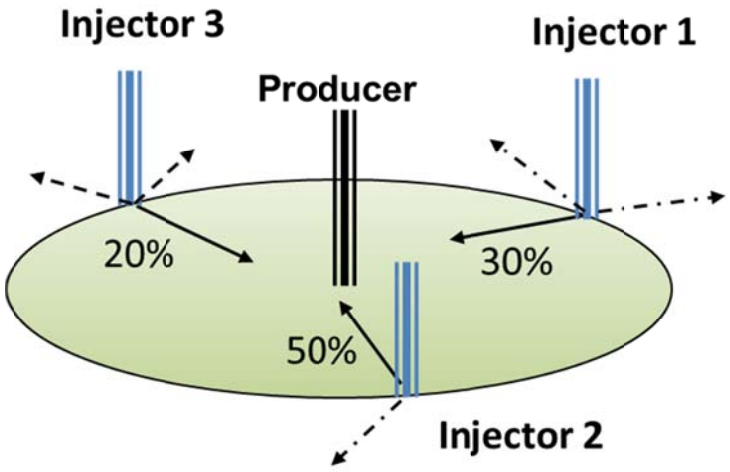

Figure 1.4 Injected water distributions from the CRM model.

1.2.2 Literature Review of the CRM Model

The analogy of flow in an oil reservoir to electrical current flow was proposed by Bruce (1943). He constructed a number of electrical units to physically represent the grid blocks in the reservoir simulation. These electrical units were then wired together to model the reservoir behavior directly based on the similarity between current flow through conductive media and fluid flow through porous media. Later, Wiess et al. (1951) developed a high-speed electronic reservoir analyzer with improved accuracy for predicting the unsteady-state behavior of oil reservoirs. Wahl et al. (1962) applied the resistor-capacitor network (see Figure 1.5), which consisted of 2501 capacitors inter-connected through 4900 resistors, to analyze four reservoirs in Saudi Arabia.

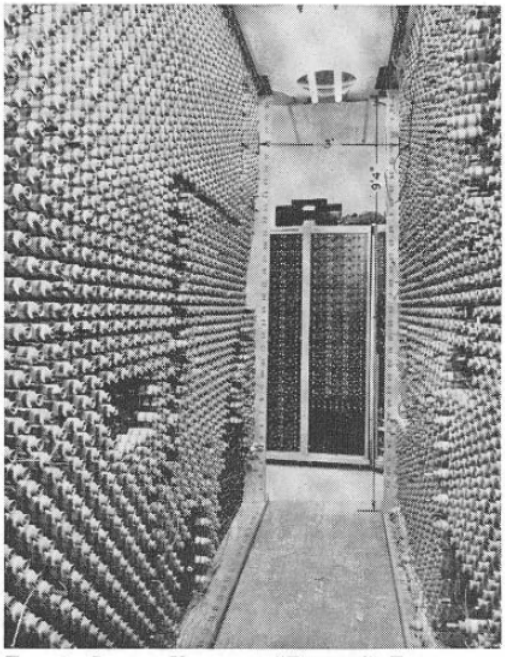

Figure 1.5 View of the resistor-capacitor network (Wahl et al., 1962).

While the early work focused on experimental apparatus design and study using the analogy, a mathematical model that borrows the same resistor-capacitor network

concept was proposed by Lake et al. (2002). Albertoni and Lake (2003) suggested quantifying the communications between wells in a reservoir using only production and injection data. Their research assumed that a production rate is a weighted linear combination of injection rates. Diffusivity filters were used to account for the time lag and attenuation of the changes between injector and producer pairs, especially for large distance and dissipation. However, this work might lead to negative weighting factors between well pairs, which is physically impossible.

Gentil (2005) explored the physical meaning of the regression weights (or inter-well connectivity) as functions of reservoir transmissibility. Based on his research, the weights are the ratios of inverse distance weighted average permeabilities of well pairs associated with each injector. He also incorporated bottom-hole pressure (BHP) fluctuation terms into the model. Furthermore, Gentil proposed an empirical oil fractional flow model to separate the oil production from the total production, which was tested in several numerically simulated fields and then applied to a water flood in Argentina.

Yousef (2005) was the first to mathematically develop the CRM model using material balance. Not only did he propose the concept of connectivity and time constant in the CRM model, he also solved the CRM continuity equation numerically using discretization in time. He extended the CRM model to handle varying BHP's, and successfully addressed the issue of nonphysical weights in the CRM model. He validated the CRM model in both synthetic and field cases, where he found good agreement between the CRM model parameters and the reservoir geological features (Yousef et al., 2006).

Sayarpour (2008) focused on finding a semi-analytical solution to the governing differential equation in the CRM model using super-position in time based on different reservoir control volumes, such as a single reservoir tank, a producer-based drainage

volume, and an injector-producer pair-based volume. These semi-analytical solutions allow rapid estimation of inter-well connectivity. He then combined the CRM model with an oil fractional flow model to match the oil production history, which enables the CRM model to be used for total and oil rate prediction, optimization and reservoir uncertainty quantification. He validated the CRM capabilities with numerical flow simulation and applied the CRM model in several field cases involving water/CO_2 floods.

Weber (2009) used a more powerful optimization software (GAMS) instead of the Microsoft Excel optimization program or the Matlab optimization module to solve for the CRM model parameters and came up with different techniques to clean production data and reduce model parameters, which greatly improved the capability of the CRM model to deal with real field large data sets (Weber et al., 2009).

Wang (2011) developed a new surface subsidence model based on the CRM equations and rock mechanics to predict the average surface location and diagnose the reasons for the subsidence in parts of the Lost Hills oil field in California. She then concluded that high injection rates caused rock damage in the field.

Nguyen (2012) extended the CRM model to primary recovery and water-CO_2 flood. She proposed the integrated CRM model for primary recovery and validated it on several synthetic cases and an Oman field. The application of the CRM model conducted on a west Texas field was also successful and the field was predicted to gain 5372 additional barrels of oil production under the optimized injection strategy.

Laochamroonvorapongse (2013) developed a CRM model considering producer-producer interactions and observed better model parameter accuracy.

Izgec (2009) used the CRM model for transient flow problems, which was validated by comparing to a streamline simulation. The results showed that the CRM model can produce similar inter-well connectivities as a streamline simulation. Also,

Izgec (2010) applied the CRM model with an analytic aquifer model to model differential aquifer influx into each well.

Kaviani et al. (2012) proposed a segmented and compensated capacitance model (CM) to increase the CM tolerance to common field conditions. The segmented CM can be used when unknown BHPs change during the analysis interval. The compensated CM overcomes the requirement to rerun the model after adding a new producer or after shutting-in an existing producer. Kaviani and Jensen (2010) also developed a MPI model, which is similar to the CRM model and applied it to a heavy oil water flooded field.

Salazar-Bustamante et al. (2012) combined the CRM model with decline-curve analysis and successfully predicted the well performance in a reservoir with gas injection. Other applications of the CRM model can be found in those such as Lee, et al., 2011, Parekh and Kabir, 2012, Can and Kabir, 2012, Soroush et al., 2013, Tafti, et al., 2013, with respect to water flooding, gas flooding, etc.

1.2.3 Limitations of the Current CRM Model

An important limitation in the current CRM model is that it neglects the water/oil saturation change and assumes a slightly compressible reservoir system. In other words, the current CRM model is a single-phase flow model in which it is dealing exclusively with the pressure equation. Theoretically, even though the single-phase based model is a good approximation for candidates such as the mature water flood, it does not favor capturing physics when the system has a strong saturation dependency such as for an immature water flood.

In practice, the actual oil field is often complicated in the sense that both new drills and old wells are producing together. While the slightly compressible statement

might be valid for wells with large water cut, it is a poor assumption for those with low water cuts.

Meanwhile, the time constant, a very important parameter for the CRM model, hasn't been be fully studied and discussed in the previous studies. It is currently simplified as a constant with respect to time; whereas it should be a function of total mobility and hence varies with time.

Furthermore, to calculate the oil production from the total production, the current CRM model uses an empirical fractional flow equation (Gentil, 2005), which is only valid at large water cut; whereas an accurate oil rate prediction over the entire range of water cut is essential when optimizing the field injection strategy.

From the data-driven point of view, the single-phase CRM model only uses total production data in a history match to estimate model parameters. However, the abundant oil production data also contain rich information regarding the reservoir behavior, which should be fully used for such a data-driven model.

1.3 INTRODUCTION TO THE COUPLED CRM MODEL

This dissertation aims to upgrade the current CRM model by considering the impact of reservoir two-phase flow. Accordingly, we develop a two-phase coupled CRM model based on the features of immiscible two-phase flow. To realize the coupled CRM model, we construct material balances for both total fluid (both water and oil) and oil, respectively. The total fluid continuity equation is called the pressure equation, which refers to the reservoir compressibility effect. The compressibility effect describes the propagation of pressure wave in the reservoir and it, in a large part, determines the time lag between injection signal and production response. The oil mass balance equation is

called the saturation equation, which refers to the reservoir displacement effect. The displacement effect describes the saturation distribution and evolution in the reservoir, which influences the oil production rate directly and therefore, determines the flood efficiency. Unlike the current CRM model, which does not solve the saturation equation, the coupled CRM model solves the pressure and saturation equations simultaneously at each time step to account for changes in total mobility. We semi-analytically couple the pressure and saturation in a producer-based control volume and use constrained multivariate nonlinear regression to estimate model parameters. The new coupled model is able to not only quantify the inter-well connection but also describe the oil saturation within a producer's drainage volume.

The consideration of the two-phase model can bring benefits as the following:

1) The accuracy of the CRM model should be enhanced by eliminating the assumption of single-phase flow and incorporating the physics of two-phase displacement. The improved accuracy in the consequent connectivity and time constants can lead to better history matches, and hence a better prediction of the total and oil rates.
2) The coupled CRM model can be applied to the entire history of water and gas floods, not being limited to mature water floods (close to incompressible) cases as was the current CRM model, making it more applicable to complicated field scenarios (see Figure 1.6).
3) The time constant in the coupled CRM model reflects the impact of both compressibility and fluid mobility, and hence evolves with the reservoir system dynamics instead of staying constant.
4) The evolution of oil and water saturations within the drainage volume of each producer is well preserved according to the oil material balance, which can

provide information with respect to the remaining oil saturation distribution in the reservoir. Figure 1.7 illustrates such a remaining oil saturation distribution bubble map. This map gives the drainage volume of each producer and the average oil saturation within it at a certain time during the displacement.

5) Based on the relationship between the oil cut produced from a producer and the average oil saturation within the drainage volume, we are able to establish fractional flow curves directly from the coupled model. It enables us to perform accurate prediction of the oil rate and hence better optimize the injection schemes in an effort to maximize field oil production.

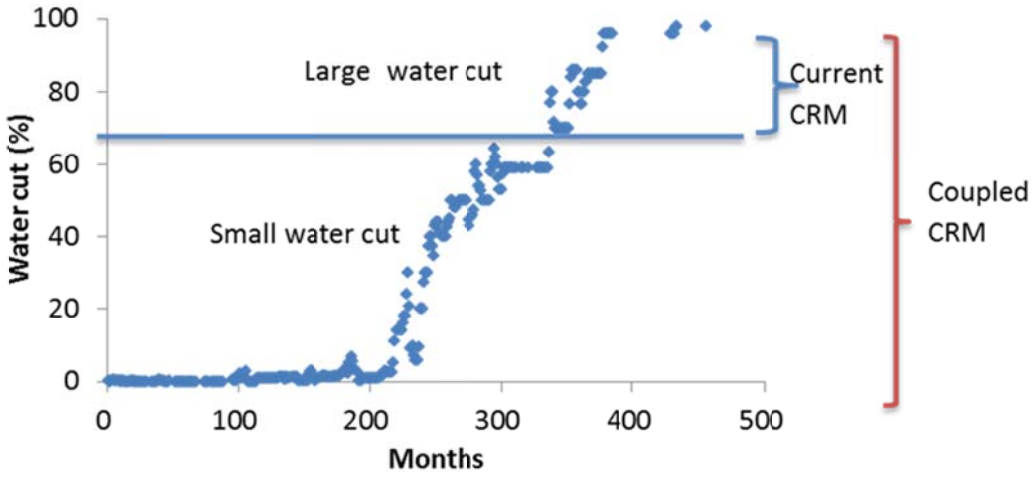

Figure 1.6 Schematic of the water cut range for application of the CRM models.

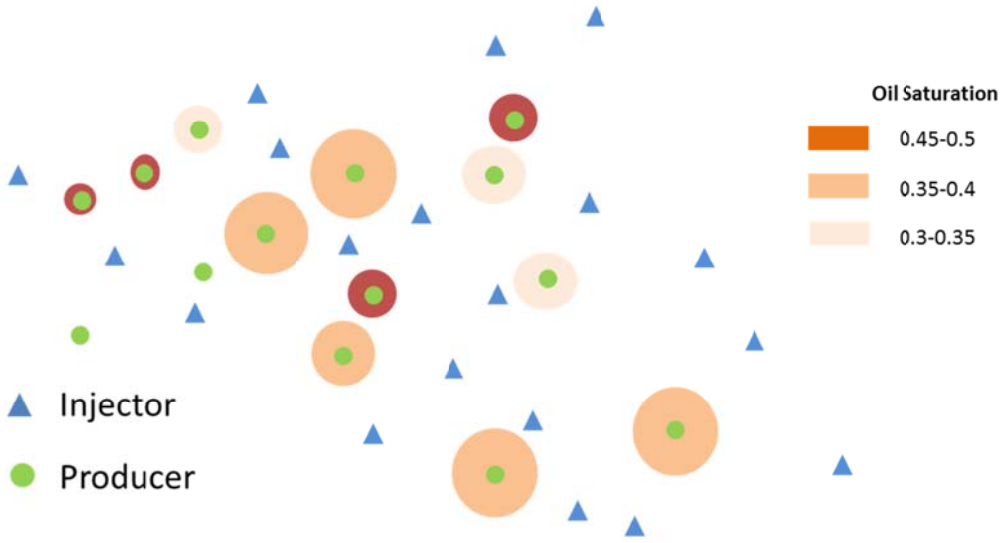

Figure 1.7 Schematic of remaining oil saturation distribution.

In summary, by incorporating the saturation variations to model reservoir two-phase flow, the coupled CRM model can overcome the limitations of previous versions. The coupled CRM model is also expected to improve the quality of oil rate prediction significantly, especially for immature water floods. This work can lead to a more informed workflow of optimizing injection scheme, and serve the goal of improving ultimate oil recovery.

1.4 Chapter Layouts

In this dissertation, Chapter 2 reviews fractional flow models. Fractional flow theories have been developed to describe the two-phase water and oil displacement in the reservoir; thus they have been widely used (but not limited) to evaluate water flood performance and forecast oil production rate. In general, there are two types of fractional flow models: analytical and empirical models. Both are discussed in Chapter 2. We also review the fractional flow model that is currently used in the CRM model.

In Chapter 3, we start with the derivation of the working equations used in the coupled CRM model for history matching. We discuss different options of coupling the pressure and saturation equations. Two kinds of model validation procedures, internal and external validations, are introduced to verify the results obtained from the coupled CRM model. The prediction of fluid rates using the coupled CRM model is more complicated than the current model as the saturation must be updated each time step. The algorithm behind the prediction capability will be discussed in detail. The fractional flow model can be obtained directly from the coupled CRM model and used for oil rate prediction, which is also elaborated in this chapter. Last but not least, we present the optimization ability using the coupled CRM model.

In Chapter 4, we demonstrate different capabilities of the coupled CRM model in synthetic homogeneous and heterogeneous reservoirs with different geological features, which are created in a commercial simulator. In summary, we performed case studies in the following synthetic reservoirs:

1. A homogenous reservoir with a single producer
2. A heterogeneous reservoir with a single producer
3. A five-spot homogeneous reservoir
4. A sealed reservoir
5. A large heterogeneous reservoir with 16 producers and 9 injectors

Production and injection rate data from these synthetic fields are treated as field data to be applied in the coupled CRM model. The application of history match, validation, prediction, and optimization are all performed and discussed.

Chapter 5 conducts sensitivity analysis to study and understand the relationship between the input information (e.g., viscosity, relative permeability, etc.) and the output model parameters such as connectivity and time constant, etc. This is done since we have

introduced new inputs in the coupled CRM model that are previously not required in the current CRM model. This study also proves that the coupled CRM model output parameters can reflect both reservoir compressibility and mobility effects.

Chapter 6 summarizes the technical contributions made in this work. We arrived at several conclusions regarding the coupled CRM model. Future work is also recommended in this chapter.

CHAPTER 2: FRACTIONAL FLOW THEORY

A fractional flow model is important for two-phase flow. Throughout a two-phase immiscible displacement, the water/oil saturation profiles evolve with time. Figure 2.1 illustrates the saturation distribution in a linear system under different displacement stages. During primary recovery, the reservoir system produces mainly oil and the water/oil saturations stay relatively unchanged at the initial condition. After the water flood is initiated, the water/oil saturation profiles change drastically before and after water breakthrough. Typically, a saturation discontinuity (shock) exists and moves until it arrives at the outlet. After water breakthrough, the water/oil saturation profiles are continuous and asymptotically approach residual oil saturation.

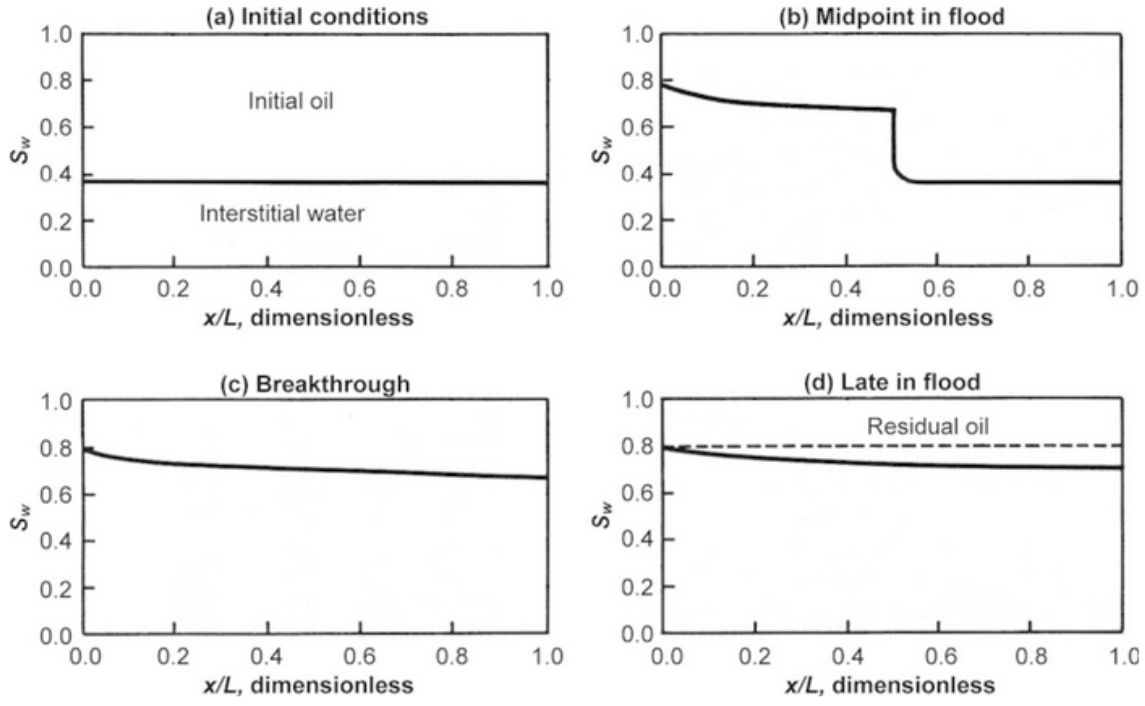

Figure 2.1 The saturation distribution in a homogeneous linear system under the various stages of an water/oil displacement (Willhite, 1986)

Fractional flow theories have been developed to describe the two-phase water and oil displacement in a reservoir; thus, they have been widely used to evaluate water flood performance and forecast oil production rate. They have also been applied in enhanced oil recovery process extensively, such as polymer flooding, alcohol flooding, miscible flooding, steam flooding, and various types of surfactant flooding (Pope, 1980).

In general, there are two types of fractional flow models: analytical and empirical models. Analytical fractional flow models usually stem from Darcy's law and material balance. They take reservoir physics (relative permeability, viscosity, etc.) into consideration and are often expressed as a function of water/oil saturations. For the purpose of reservoir performance estimation and prediction, the empirical fractional flow models are developed, which usually achieve correlations between oil cut and cumulative oil production (or other quantities).

2.1 IMMISCIBLE FRACTIONAL FLOW MODELS

Immiscible displacement occurs when there is no exchange of concentration between phases. The flow of oil and water is a typical example of immiscibility as the oil phase doesn't change when contacted with the water phase (Lake, 1989). Immiscible flood can be described by both analytical and empirical models, which are reviewed in the following sections.

2.1.1 Analytical Fractional Flow Models

2.1.1.1 Buckley and Leverett Model

Buckley and Leverett (1942) proposed the most well-known and classic fractional flow model in the petroleum industry, which characterizes the mechanics of oil being

displaced by an immiscible fluid. They used Darcy's law and relative permeability concepts to describe fluid flow through porous media.

For isothermal immiscible and incompressible flow of oil and water phases in a one dimensional porous medium, the water conservation equation is given as:

$$\frac{\partial S_w}{\partial t_D} + \frac{\partial f_w}{\partial S_w}\frac{\partial S_w}{\partial x_D} = 0 \qquad 2.1$$

where S_w is the water saturation, t_D is the dimensionless time, which is defined to be the cumulative water injection in pore volumes, and x_D is the dimensionless distance, which is the distance normalized by the total length of the one dimensional porous medium, and f_w is the water fractional flow, which has the form of (Leverret and Lewis, 1941):

$$f_w = \frac{1 + \frac{kk_{ro}A}{q\mu_o}\left(\frac{\partial P_{cow}}{\partial x} - \Delta\rho g \sin\alpha\right)}{1 + \frac{k_{ro}\mu_w}{k_{rw}\mu_o}}$$

2.2 where k is the absolute rock permeability, k_{ro} and k_{rw} are the oil and water relative permeabilities, μ_o and μ_w are the oil and water viscosities, q is the volumetric flow rate, A is the cross section area perpendicular to flow, P_{cow} is the capillary pressure, $\Delta\rho$ is the density difference between water and oil phases, g is gravity constant and α is the formation dipping angle.

To obtain a simple analytical solution to Eq. 2.1, Buckley and Leverett (1942) made a key simplification to drop the capillary pressure term P_{cow} in Eq. 2.2. The approximated water fractional flow in a horizontal porous medium is given as:

$$f_w = \frac{1}{1 + \frac{k_{ro}\mu_w}{k_{rw}\mu_o}} \qquad 2.3$$

Substituting Eq. 2.3 into Eq. 2.1 gives a first-order hyperbolic partial differential equation, which can be solved readily to give the following expression:

$$\left(\frac{dx_D}{dt_D}\right)\Bigg|_{S_w} = \frac{df_w}{dS_w} \qquad 2.4$$

Eq. 2.4 is the Buckley and Leverett solution that gives the specific velocity of a constant saturation to be equal to the derivative of the fractional flow curve at that saturation.

Later, Welge (1952) proposed a tangent construction to correct the fractional flow curve f_w at the front, where non-physical solution occurs, and to obtain the average water saturation at breakthrough. Figure 2.2 illustrates a typical fractional flow curve and the tangent construction.

The Buckley-Leverett model combined with the Welge tangent construction has been widely used to evaluate water flood performance. It can be applied to describe the saturation profile at a certain dimensionless time, evaluate water cut change with time, and calculate oil recovery at any time during a water flood. Nevertheless, the Buckley and Leverett model have made many assumptions such as homogenous media, one dimensional flow, incompressible system, negligible gravity and capillarity, negligible dispersion, all of which should be carefully understood prior to application.

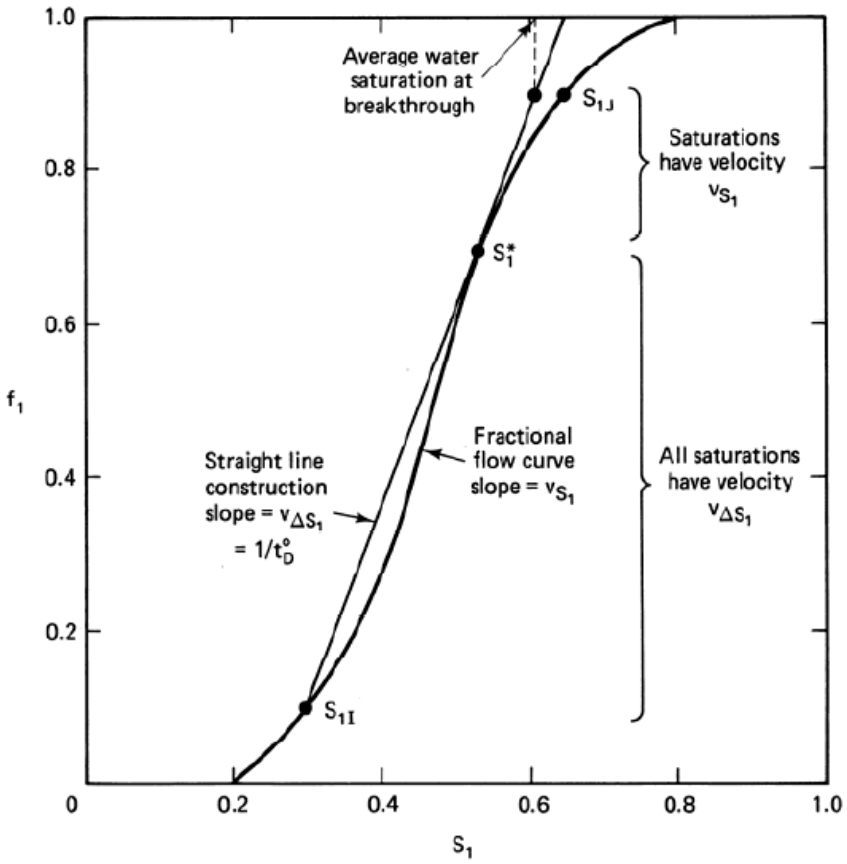

Figure 2.2 Schematic of a water (*i*=1) fractional flow curve and the tangent construction (Lake, 1989).

2.1.1.2 Other Analytical Fractional Flow Models

Besides the Buckley-Leverett model, several other methods have been proposed to consider the impact of vertical variations in permeability and the effect of gravity. Stiles (1949) developed one of the earliest methods, for which the water fractional flow is assumed to be proportional to the permeability-thickness (*kh*) and endpoint mobility ratio. Dykstra and Parsons (1950) proposed a more sophisticated empirical method to account for the initial fluid saturations, mobility ratios and fractional oil recoveries. Their method

simplified the reservoir into several linear layers and assumed no cross flow between layers. Craig (1993) made an effort to summarize and compare different water flood performance prediction models. He classified these models into different categories based on: reservoir heterogeneity, areal sweep effects, numerical methods, displacement mechanisms and empirical approaches.

2.1.2 Empirical Fractional Flow Models

Classic analytical models are loyal to reservoir physics. Nevertheless, they often require estimation of water saturation as a function of time, which is difficult to evaluate for multi-well systems. Therefore, many empirical fractional flow models were developed over the years for the purpose of reservoir performance evaluation and oil production prediction.

In general, there are two types of empirical models.

1. Empirical models based on fractional flow theories in which saturation is preserved. An example is the Ershaghi and Omorigie (1978) model, which assumed that the oil recovery was controlled by a fractional flow curve based on a linear log (kro/krw) vs. Sw relationship. Other similar models were developed by Craft and Hawkins (1959), Lo et al. (1990), Sitorus et al. (2006), etc.
2. Empirical models based on observed trends. For example, Arps (1945) suggested a correlation between natural logarithm of oil cut and oil production rate. Purvis (1985) suggested a linear relationship between (WOR+1) and cumulative oil production. Many other empirical models (Timmermann, 1971) exist.

Gentil Model

The current CRM model is a single-phase model. To separate oil production from the total production, a fractional flow model proposed by Gentil (2005) is used. It is an empirical power law relationship between water oil ratio and the cumulative water injected. According to Gentil, the water cut of a given producer has the form of:

$$f_w = 1 - \frac{1}{1 + aW_i^b} \tag{2.5}$$

where W_i is the cumulative water injected from all injectors that are connected to a producer, a and b are regression parameters that are to be determined by history match.

The advantage of this model is that the water cut is expressed explicitly using the cumulative water injection W_i, which can be controlled and optimized directly in the CRM model. If the water or oil cut is expressed in terms of cumulative oil production, like the empirical models mentioned above, the oil rate prediction/optimization cannot be achieved since the cumulative oil production itself is unknown. Nevertheless, the inherent assumption made in this model is a linear relationship between the natural logs of water oil ratio (WOR) and cumulative water injection, which is usually valid in mature water floods. For the same reason, the application of this fractional flow model is limited to the late time water flood, when well water cut is large.

2.2 MISCIBLE FRACTIONAL FLOW MODELS

Two components are mutually miscible if they mix in all proportions without an interface forming between them (Lake, 1989). In this section, we discuss isothermal miscible displacements using fractional flow theory and with one or more phases present.

Koval Model

The Koval model (1963) was developed to address the issue of viscous figuring in a miscible displacement. Koval modified the viscosity ratio in the fractional flow equation (Leverett and Lewis, 1941) to account for the local heterogeneity and transverse mixing in the following way:

$$F_s = \frac{1}{1 + \frac{1}{K_{val}}\left(\frac{1 - S_s}{S_s}\right)} \tag{2.6}$$

and:

$$K_{val} = H_K E \tag{2.7}$$

$$E = (0.78 + 0.22\left(\frac{\mu_o}{\mu_s}\right)^{1/4})^4 \tag{2.8}$$

where F_s is the solvent fractional flow, S_s is the solvent saturation, K_{val} represents the Koval factor, E is the effective viscosity ratio, H_K is a measure of reservoir heterogeneity, and μ_s and μ_o are the solvent and oil viscosities.

This fractional flow expression (Eq. 2.6) can be applied to oil and solvent in a segregated flow. Eq. 2.6 is also the same as the water fractional flow in a water flood when the oil and water have a straight-line relative permeability. For such a case, the Buckley-Leverett equation may be integrated analytically to give the following expression (Lake, 1989):

$$f_w\big|_{x_D=1} = \begin{cases} 0 & t_D < \dfrac{1}{K_{val}} \\ \dfrac{K_{val} - \sqrt{\dfrac{K_{val}}{t_D}}}{K_{val} - 1} & \dfrac{1}{K_{val}} < t_D < K_{val} \\ 1 & t_D > K_{val} \end{cases} \qquad 2.9$$

where t_D is the dimensionless time, which is defined as $t_D = \dfrac{Cumulative\ injection}{V_p}$.

The derivation of Eq. 2.9 can be found in Appendix A. In Eq. 2.9, the saturation term is eliminated and the Koval approach can then be used for history match during which two parameters, the Koval factor and the pore volume, are estimated.

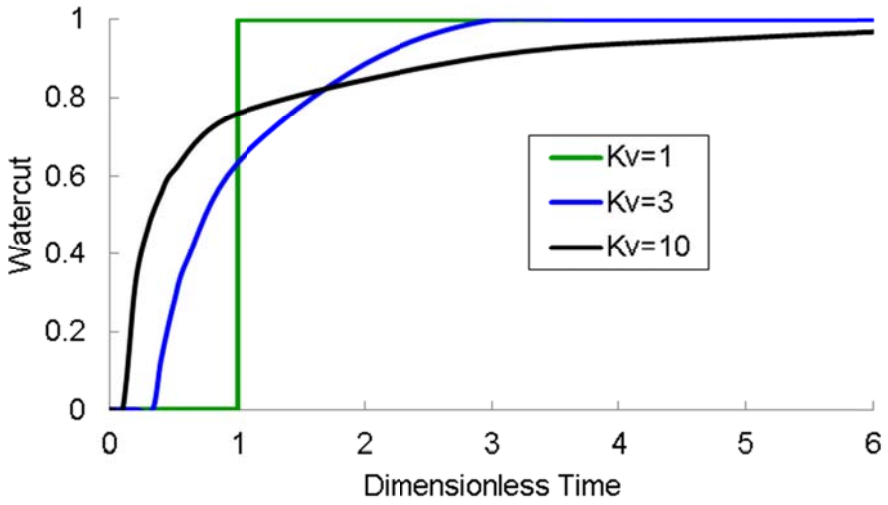

Figure 2.3 Koval method calculated water cut vs. dimensionless time for different Koval factors.

Figure 2.3 illustrates the water cut change with the dimensionless time for different Koval factors. When the Koval factor is 1, the water cut jumps from 0 to 1 after

one pore volume of water is injected, which indicates a piston-like uniform displacement. A large Koval factor usually implies a higher degree of reservoir heterogeneity, therefore lower displacement efficiency.

CHAPTER 3: THE TWO-PHASE FLOW COUPLED CRM MODEL

In this chapter, we present, in detail, the algorithm of the coupled CRM model including constructing the working equations, performing history match using a multivariate regression, validating the model parameters, predicting future productions, and optimizing injection scheme. To better understand the procedure of the coupled CRM model, we give a brief introduction to the current CRM model because it not only establishes the basis, but also shares similar concepts and definitions with the coupled CRM model. We also demonstrate the capabilities and features of the coupled CRM model by considering two-phase flow effects.

3.1 BASIC MATERIAL BALANCE EQUATIONS IN A PRODUCER-BASED DRAINAGE VOLUME

For a water-oil displacement, the mass conservation equations for water and oil in a producer-based control volume are written as:

$$V_b \frac{d\left(\phi\rho_w \overline{S}_w\right)}{dt} = \rho_w i(t) - \rho_w q_w(t) \tag{3.1}$$

$$V_b \frac{d\left(\phi\rho_o \overline{S}_o\right)}{dt} = -\rho_o q_o(t) \tag{3.2}$$

where V_b is the bulk control around a producer, $\overline{S}_o$ and $\overline{S}_w$ are the average oil and water saturations in V_b, ρ_o and ρ_w are oil and water densities evaluated at the average pressure $\overline{P}$ within V_b, ϕ is the average porosity within V_b, and $i(t), q_w(t)$ and $q_o(t)$ are water injection, water production, and oil production rates of the producer under reservoir condition.

Eqs. 3.1-3.2 are the weak forms of the material balance for two-phase immiscible flow of water and oil. To obtain the total fluid material balance, we expand Eqs. 3.1-3.2 using the product rule to give:

$$V_p\left(\frac{d\overline{S}_w}{dt}+\overline{S}_w\left(c_f+c_w\right)\frac{d\overline{P}}{dt}\right)=i\left(t\right)-q_w\left(t\right) \tag{3.3}$$

$$V_p\left(\frac{d\overline{S}_o}{dt}+\overline{S}_o\left(c_f+c_o\right)\frac{d\overline{P}}{dt}\right)=-q_o\left(t\right) \tag{3.4}$$

where V_p is the pore (drainage) volume defined to be $V_p=V_b\phi$, and c_f, c_w and c_o are the pore, water, and oil compressibilities, which are defined as $c_f=\frac{1}{\phi}\frac{d\phi}{d\overline{P}}$, $c_w=\frac{1}{\rho_w}\frac{d\rho_w}{d\overline{P}}$, and $c_o=\frac{1}{\rho_o}\frac{d\rho_o}{d\overline{P}}$.

Eqs. 3.3-3.4 are coupled by the average saturation. Because the summation of water and oil saturations equals 1, combining Eqs. 3.3 and 3.4 gives the total fluid continuity equation as the following:

$$V_p c_t\frac{d\overline{P}}{dt}=i\left(t\right)-q_t\left(t\right) \tag{3.5}$$

where $q_t\left(t\right)$ is the total production rate of the producer under the reservoir condition, and c_t is the total compressibility, which is defined as:

$$c_t=c_f+\overline{S}_w c_w+\overline{S}_o c_o \tag{3.6}$$

Eq. 3.5 is the total fluid continuity equation, which is superficially decoupled from saturation. We refer to it as the "pressure equation" in this dissertation since it describes the pressure propagation effects. The pressure equation implies that the reservoir system is capable of storing/releasing extra fluid because of the rock and fluid compressibilities. If the total compressibility is zero, the production rate would be equal to the injection rate instantaneously. At the other extreme, the time lag between the

injection signal and production response is infinitely large in the case of infinitely large compressibility.

For a two-phase displacement, the material balance equation of either phase (water or oil phase) is a necessary complement to the total fluid continuity equation, Eq. 3.5. Because of our particular interest in oil recovery, we use Eq. 3.4 and refer to it as the "saturation equation" in this dissertation.

We can integrate Eq. 3.5 using a closure relationship between the total production rate and the average reservoir pressure, which is the definition of productivity index (Craft et al. 1959; Lake, 2006):

$$q_t(t) = J_t\left(\overline{P} - P_{wf}\right) \tag{3.7}$$

where J_t is the total productivity index and P_{wf} is the producer's bottom-hole pressure.

A general form of J_t (neglecting the skin) can be expressed by:

$$J_t = \frac{2\pi hk}{\left[\frac{1}{2}\ln\left[\frac{4A}{\gamma C_A r_w^2}\right]\right]}\left[\frac{k_{ro}}{\mu_o} + \frac{k_{rw}}{\mu_w}\right] \tag{3.8}$$

where h is the thickness of the drainage volume, k is the absolute permeability, A is the drainage area, r_w is the wellbore radius, C_A is the Dietz shape factor, γ is the Euler constant, k_{ro} and k_{rw} are oil and water relative permeabilities, and μ_o and μ_w are oil and water viscosities, respectively (Peaceman, 1983).

In Eq. 3.8, the term $\left[\frac{k_{ro}}{\mu_o} + \frac{k_{rw}}{\mu_w}\right]$ is the total relative mobility. We denote it as M_t in this dissertation.

3.2 THE CURRENT CRM MODEL

Before proceeding to the two-phase flow coupled CRM model, it is necessary to introduce the current CRM model briefly. We present the concepts, implementations, and features of the current CRM model in the following subsections.

3.2.1 Working Equations

Because the current CRM model assumes single-phase flow in the reservoir; only the pressure equation (Eq. 3.5) is considered while the saturation equation is neglected.

Meanwhile, the productivity index for single-phase flow can be simplified as:

$$J_t = \frac{2\pi hk}{\mu\left[\frac{1}{2}\ln\left[\frac{4A}{\gamma C_A r_w^2}\right]\right]} \tag{3.9}$$

where J_t is the productivity index for single-phase flow, and μ is the fluid viscosity.

In the above equation, the single-phase flow productivity index is a function of rock properties, fluid properties and well properties but not of pressure or time. Therefore, it is reasonable to treat the productivity index as a constant if there is no dramatic change in reservoir/well conditions for single-phase flow.

Substituting Eq. 3.7 and Eq. 3.9 into Eq. 3.5, we are able to eliminate the average reservoir pressure, $\overline{P}$ to obtain:

$$V_p c_t \frac{d}{dt}\left(\frac{q_t(t)}{J_t} + P_{wf}\right) = i(t) - q_t(t) \tag{3.10}$$

In Eq. 3.10, the primary variable of the pressure equation changes from pressure to production rate, $q_t(t)$. This is done because the CRM model should eventually become an optimization problem in which the difference between the calculated and measured values is minimized to estimate model parameters. The average reservoir pressure data for each producer at each time step are often unavailable, which hinders the

possibility to evaluate the difference between the calculated and observed pressure; whereas, the production rate data are, on the contrary, available and abundant. The optimization problem can be formed readily if we choose to solve for the production rate in the pressure equation.

Assuming constant bottom-hole pressure, the semi-analytical solution to Eq. 3.10 can be obtained using super-position in time (Sayarpour, 2008). We write the final form of the solution as the following:

$$q_{tj}^{k} = q_{tj}^{k-1} e^{\frac{-\Delta t}{\tau_j}} + \left(1 - e^{\frac{-\Delta t}{\tau_j}}\right)\left(\sum_{i}^{n_i} f_{ij} I_i^k\right) \qquad 3.11$$

where q_{tj}^{k} is the total production of producer j at time step k, I_i^k is the water injection rate of injector i at time step k, n_i is the total number of injectors, f_{ij} is the connectivity between the injector *i* and producer *j*, Δt is the time length between the time steps $k-1$ and k, and τ_j is the time constant for producer *j*.

3.2.2 Model Parameters

In Eq. 3.11, f_{ij} and τ_j are model parameters that must be determined. The connectivity f_{ij} represents the fraction of water from injector *i* that contributes to the total production in producer *j*. The summation of connectivity over an injector is less than 1 if injection loss exists and it is greater than 1 if other production support (aquifer, etc.) exists. It is assumed to be constant with respect to time.

The time constant τ_j is another important model parameter and it is defined as:

$$\tau_j = \left(\frac{V_p c_t}{J_t}\right)_j \qquad 3.12$$

By definition, it is a characteristic time for the pressure wave to travel from injectors to a producer. In Eq. 3.12, the time constant is not related to time, and therefore it is also a constant with respect to time.

3.2.3 Nonlinear Multivariate Regression

The connectivity and the time constant mentioned above are estimated using nonlinear multivariate regression. The required objective function is as the following:

$$\min z = \sum_{k=1}^{n_t} \sum_{j=1}^{n_p} (q_{tj}^{k\ cal} - q_{tj}^{k\ obs})^2 \tag{3.13}$$

where $q_{tj}^{k\ obs}$ is the observed production rate data of producer j at time step k, $q_{tj}^{k\ cal}$ is the model-calculated total production rate of producer j at time step k, n_p is the total number of producers, and n_t is the total number of time steps.

This objective function is constrained by:

$$\tau_j, f_{ij} \geq 0 \tag{3.14}$$

$$\sum_{j=1}^{n_p} f_{ij} \leq 1 \quad \text{for any } i \tag{3.15}$$

Eq. 3.14 indicates that the connectivity and the time constant are constrained to be positive. Eq. 3.15 implies a material balance of the injected fluid. The estimation of model parameters by minimizing the objection function is essentially a history matching process.

We mention that $q_{tj}^{k\ obs}$ is usually the allocated production data from well test. There are scenarios when $q_{tj}^{k\ obs}$ is not available and only random well test data are provided. In such a case, Appendix B demonstrates a field case study, where we applied the CRM model to estimate well connetivity using well test data.

3.2.4 Validation, Prediction, and Optimization of Injection Scheme

Normally, one can use a large proportion of the data at hand to perform the history match (data regression) to estimate the model parameters. After that, a validation is necessary to verify the model reliability. We use the model parameters obtained from history match to predict part of the production history using historical injection rates. Comparisons are carried out between the known historical production rates and the CRM model predicted production rates. If the difference is small, the model is considered to be reliable. In this case, prediction can proceed to evaluate the well performance under any future injection scheme. Therefore, we can further optimize the injection strategy to give the maximum oil production. The whole procedure is summarized in Figure 3.1.

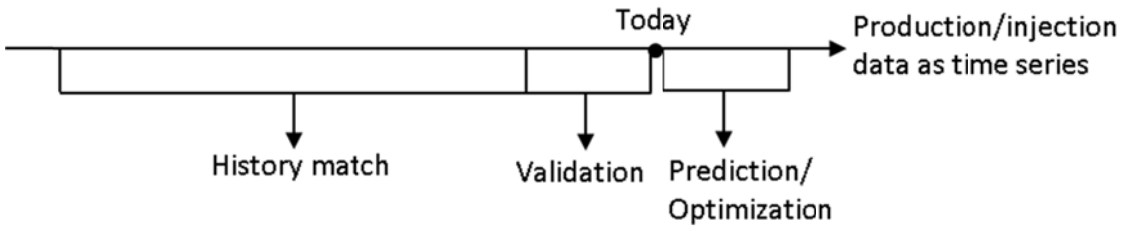

Figure 3.1 Schematic of history match, validation, prediction, and optimization.

Chapter 2 mentioned that an empirical fraction flow model (Gentil, 2005) is used to separate the oil production from the total production. The regression parameters are obtained by history matching the field water cut data. However, in Chapter 4, we will show that the empirical model is not accurate enough for prediction.

3.3 THE COUPLED CRM MODEL

The single-phase flow assumption is only valid when the water flood is mature. For an immature water flood, the current CRM model is no longer accurate because of

the variation in total mobility and the existence of a displacement effect. In such a case, the prediction of oil production using the current CRM model may suffer, which motivates us to develop a two-phase flow coupled CRM model.

3.3.1 Two-Phase Flow Equations

To resolve the limitations caused by neglecting the saturation change in the CRM model, we propose to couple the saturation equation (Eq. 3.4) and the pressure equation (Eq. 3.5) together.

According to Eqs. 3.4, 3.5, and 3.8, we rewrite the pressure and saturation equations in the following matrix form:

$$\begin{pmatrix} V_p c_t & 0 \\ V_p \bar{S}_o \left(c_f + c_o\right) & V_p \end{pmatrix} \begin{pmatrix} \dfrac{d\bar{P}}{dt} \\ \dfrac{d\bar{S}_o}{dt} \end{pmatrix} = \begin{pmatrix} i(t) - J_t \left(\bar{P} - P_{wf}\right) \\ -q_o(t) \end{pmatrix} \tag{3.16}$$

In Eq. 3.16, J_t is the total fluid productivity index for two-phase flow, which is defined in Eq. 3.8. We can rewrite Eq. 3.8 as:

$$J_t = \frac{2\pi hk}{\left[\frac{1}{2}\ln\left[\frac{4A}{\gamma C_A r_w^2}\right]\right]}\left[\frac{k_{ro}}{\mu_o} + \frac{k_{rw}}{\mu_w}\right] = J_t^{'} M_t \tag{3.17}$$

where M_t is the total relative mobility and $J_t^{'}$ is defined as:

$$J_t^{'} = \frac{2\pi hk}{\left[\frac{1}{2}\ln\left[\frac{4A}{\gamma C_A r_w^2}\right]\right]}$$

3.18

In Eq. 3.18, $J_t^{'}$ is a combination of parameters that depend on reservoir and well properties, i.e., absolute permeability, reservoir thickness, and well drainage area.

Therefore, it can be treated as a constant with respect to time unless the reservoir or well condition changes dramatically, i.e. new perforations, etc.

In Eq. 3.17, the total relative mobility M_t depends on saturation through water and oil relative permeabilities. Therefore, a relative permeability model is required to calculate the relative permeability of water and oil at a given saturation. Usually, the relative permeability data are obtained from laboratory experiments, and are fitted with analytical curves. Though no general theoretical expression exists for the relative permeability function, several empirical functions are available (Corey, 1954; Honarpour et al., 1982). We use the following empirical exponential expressions for water and oil relative permeabilities:

$$k_{rw} = k_{rw}^0 \left(\frac{S_w - S_{wr}}{1 - S_{wr} - S_{or}} \right)^{n_1} \tag{3.19}$$

$$k_{ro} = k_{ro}^0 \left(\frac{1 - S_w - S_{or}}{1 - S_{wr} - S_{or}} \right)^{n_2} \tag{3.20}$$

where S_{wr} and S_{or} are irreducible water saturation and residual oil saturation, k_{rw}^0 is the endpoint water relative permeability evaluated at S_{or}, k_{ro}^0 is the endpoint oil relative permeability evaluated at S_{wr}, and n_1 and n_2 are the exponents, which are usually determined by matching the experimental data.

Since the relative permeability data are from core experiments, the fitted curves using Eqs. 3.19-3.20 represent the laboratory or small scale relative permeability models; whereas the coupled CRM model is a model of a large scale. Nevertheless, this disparity is not unique to the coupled CRM model as other models, such as the traditional reservoir simulations, also have similar scale disparities by using the laboratory scale relative permeability.

3.3.2 Coupling of Pressure and Saturation Equations

From Eq. 3.16 and its complementary equations (e.g. Eqs. 3.17, 3.19, 3.20), we observe that the pressure and saturation equations share variables that have either pressure or saturation dependency or both, which are summarized in Table 3.1.

Variable	Relations with pressure or saturation
V_p	$V_P\left(\overline{P}\right)$
c_t	$c_t\left(\overline{P},\overline{S}_o\right)$
c_f and c_o	$c_f\left(\overline{P}\right)$ and $c_o\left(\overline{P}\right)$
μ_w and μ_o	$\mu_w\left(\overline{P}\right)$ and $\mu_o\left(\overline{P}\right)$
k_{rw} and k_{ro}	$k_{rw}\left(S_{o2}\right)$ and $k_{ro}\left(S_{o2}\right)$

S_{o2} is the oil saturation evaluated at the producer.

Table 3.1 Dependencies of variables with respect to saturation and pressure.

As mentioned before, the coupled model is constructed on a producer-based drainage volume. Therefore, variables (except k_{rw} and k_{ro}) in Table 3.1 are estimated using the average saturation and pressure within this drainage volume as illustrated in Figure 3.2.

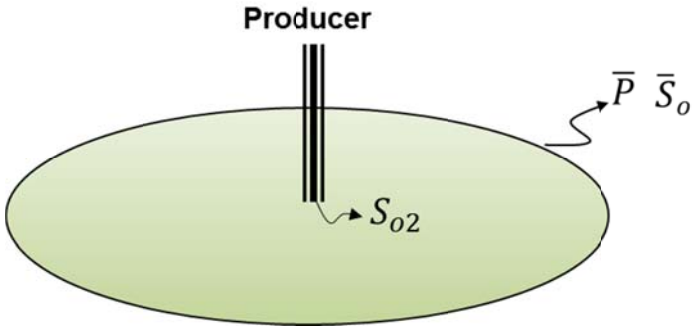

Figure 3.2 Average pressure, average oil saturation and outlet oil saturation within a producer-based drainage volume (Cao et al., 2014).

The pressure and saturation equations could not be solved independently and a coupling is required. Because the changes of variables with respect to pressure are normally small, we neglect the pressure dependency of variables in Table 3.1 in this dissertation. We only focus on the variables' saturation dependencies. The coupling strategy is to first solve the pressure equation and then solve the saturation equation in a produced-based drainage volume (as illustrated in Figure 3.2) at each time step, during which saturation dependent variables in the pressure equation are updated with time. This procedure is elaborated in the following subsections.

3.3.2.1 Solving the Pressure Equation

In this subsection, we derive the semi-analytical solution to the pressure equation. Similar to the current CRM model, we substitute the definition of the productivity index (Eq. 3.7) into the pressure equation (Eq. 3.5) to obtain:

$$V_p c_t \frac{d}{dt}\left(\frac{q_t(t)}{J_t} + P_{wf}\right) = i(t) - q_t(t) \tag{3.10}$$

Superficially, both CRM models arrived at the same equation Eq. 3.10. However, the main difference between the current and coupled CRM models lies in the productivity index used. The current model assumed a single-phase productivity index (Eq. 3.9); whereas the coupled model recovers the two-phase productivity index (Eq. 3.17), which is no longer a constant but varies with saturation and hence changes with time. Consequently, Eq. 3.10 changes from a first order linear ODE in the current CRM model to a first order nonlinear ODE in the coupled CRM model.

Appendix C illustrates the derivation to obtain the semi-analytical solution to Eq. 3.10. We write the final solution to the pressure equation in terms of production rate as the following:

$$q_{tj}^{k} = q_{tj}^{k-1} e^{\frac{-\Delta t}{\tau_j^k}} + \left(1 - e^{\frac{-\Delta t}{\tau_j^k}}\right)\left(\sum_i f_{ij} I_i^k\right) \tag{3.21}$$

where τ_j^k is the time constant at time step k for producer j, which is also defined as:

$$\tau_j^k = \left(\frac{V_p c_t}{J_t}\right)_j^k \tag{3.22}$$

Since the productive index J_t changes with saturation, the resulting time constant τ_j^k also becomes a function of saturation and hence changes with time. We write the full expression of the time constant and rearrange it as the following:

$$\tau_j^k = \frac{\left(\frac{V_p c_t}{J_t^{'}}\right)_j}{\left[\frac{k_{ro}(S_{o2})}{\mu_o} + \frac{k_{rw}(S_{o2})}{\mu_w}\right]_j^k} = \frac{\tau_j^{'}}{M_j^k} \tag{3.23}$$

where $\tau_j^{'}$ is defined as:

$$\tau_j^{'} = \left(\frac{V_p c_t}{J_t^{'}}\right)_j \tag{3.24}$$

In Eq. 3.23, the time constant is grouped into two parts. $\tau_j^{'}$ is a constant with respect to time since $J_t^{'}$ is considered to be a constant (Eq. 3.18) as we have discussed previously. The total relative mobility M_j^k varies with saturation through relative permeabilities and hence changes with time. Therefore, one must update the time constant for each time step depending on the saturation change.

We substitute Eq. 3.24 back to Eq.3.21 and give:

$$q_{tj}^{k} = q_{tj}^{k-1} e^{\frac{-\Delta t}{\tau_j^{'}/M_t^k}} + \left(1 - e^{\frac{-\Delta t}{\tau_j^{'}/M_t^k}}\right)\left(\sum_i f_{ij} I_i^k\right) \tag{3.25}$$

Eq. 3.25 is the working pressure equation used in the coupled CRM model. This equation is to be coupled with the saturation equation since M_t^k must be updated each

time step. There are two unknown parameters: $\tau_j^{'}$ and f_{ij}, which are constants with respect to time and will be determined by the nonlinear regression.

3.3.2.2 Solving the Saturation Equation

We revisit the oil material balance equation (saturation equation), which is given as:

$$V_p\left(\frac{d\overline{S}_o}{dt}+\overline{S}_o\left(c_f+c_o\right)\frac{d\overline{P}}{dt}\right)=-q_o\left(t\right) \tag{3.4}$$

Eliminating the pressure time derivative in Eq. 3.4 leads to a new expression as the following:

$$V_p\frac{d\overline{S}_o}{dt}=-\frac{\overline{S}_o(c_f+c_o)}{c_t}\left(i\left(t\right)-q_t\left(t\right)\right)-q_o\left(t\right) \tag{3.26}$$

Eq. 3.26 implies that the average oil saturation $\overline{S}_o$ change in a producer-based drainage volume (see Figure 3.3) can be caused by either the reservoir compressibility or oil displacement. We can obtain the average oil saturation by solving this equation.

Eq. 3.26 is a first-order nonlinear ordinary differential equation. We mention that the total compressibility c_t is also a function of saturation. However, we use a constant value for c_t considering that the change of c_t with saturation is small. There is a semi-analytical solution available, which is similar to Eq. 3.25. However, the semi-analytical solution is complicated as it is a non-linear expression with exponential terms. Considering that $\overline{S}_o$ usually decreases slowly and continuously with time, we propose to use numerical solutions to Eq.3.26.

Numerically solving $\overline{S}_o$ at time step k can adopt either implicit or explicit solving. The implicit solving is to evaluate $\overline{S}_o^k$ using the saturation at the current time step k, while the explicit solving is to approximate $\overline{S}_o^k$ using the known saturation from

the last time step *k*-1. The implicit solution usually takes more computation time because of the numerical iterations. In this dissertation, we only discuss the explicit solution, which is simple and fast.

Taking the connectivities between the injectors and producers into consideration, the explicit numerical solution to Eq. 3.26 can be given as below:

$$\overline{S}_{oj}^{k} = \overline{S}_{oj}^{k-1} - \frac{\Delta t}{V_{pj}}\left(\frac{\overline{S}_{oj}^{k-1}\left(c_f + c_o\right)}{c_t}\left(\sum_i f_{ij} I_i^k - q_{tj}^k \right) + q_{oj}^k \right) \tag{3.27}$$

where $\overline{S}_{oj}^{k}$ is the average oil saturation within the drainage volume of producer *j* at time step *k*, q_{oj}^{k} is the oil production rate of producer *j* at time step *k*, and V_{pj} is the pore volume of producer *j*. We mention that $\overline{S}_{oj}^{k-1}$ equals the average initial saturation of producer *j*, $\overline{S}_{ij}$, at time step *k* =1.

There are two unknown parameters: $\overline{S}_{ij}$ and f_{ij} in Eq. 3.27. The initial saturation $\overline{S}_{ij}$ will be obtained by the nonlinear regression; whereas f_{ij} is determined by the pressure equation, Eq. 3.25. Therefore, it must be coupled with the pressure equation. The combination of Eq. 3.27 and Eq. 3.25 makes it a fully coupled CRM model.

3.3.2.3 Solving the Saturation Equation in a Simplified Manner

Solving the saturation equation fully as given by Eq. 3.27 is a rigorous way. Nevertheless, the major impact to oil saturation change is the oil production rather than the compressible effect (Lake, 1989). Therefore, we simplify the saturation equation by neglecting the compressibility contribution. As a result, the saturation equation becomes:

$$V_p \frac{d\overline{S}_o}{dt} = -q_o(t) \tag{3.28}$$

The numerical solution to Eq.3.28 is given as:

$$\overline{S}_{oj}^{k} = \overline{S}_{oj}^{k-1} - \frac{\Delta t}{V_{pj}} q_{oj}^{k} \tag{3.29}$$

where $\overline{S}_{oj}^{k-1}$ equals to average initial saturation of producer j, $\overline{S}_{ij}$, at time step k =1.

The only unknown parameter in Eq. 3.29 is the initial oil saturation $\overline{S}_{ij}$, which will be determined by regression. Unlike Eq. 3.27, which requires f_{ij} from the pressure equation, solving Eq. 3.29 makes a simplified-coupled CRM model since no feedback is needed from the pressure equation.

In the context of this paper, we refer to the solving of saturation equation using Eq. 3.29 as the simplified-coupled CRM model. We will demonstrate that using the simplified-coupled CRM model leads to a slight difference from using the fully-coupled CRM model in Chapter 4.

3.3.2.4 Updating the Saturation-Dependent Variables in the Pressure Equation

As discussed, we can obtain the oil saturation through solving the saturation equation. Meanwhile, the total relative mobility M_t^k in the pressure equation can be updated using the oil saturation obtained.

The total relative mobility M_t^k relates to saturation through relative permeabilities, k_{rw} and k_{ro}, in the pressure equation. However, the relative permeability is a function of the outlet oil saturation, S_{o2}, around the producer, rather than the average oil saturation. Therefore, we must build a relationship between the outlet and the average oil saturations. We propose using the Welge (1952) equation, which has the form of (Lake, 1989):

$$S_{o2} = \overline{S}_o + Q_i \left(1 - f_w \Big|_{x_D=1}\right) \tag{3.30}$$

where Q_i is the cumulative water injection in pore volumes since the initiation of the water injection, which is defined as: $Q_i = \frac{\sum_k \sum_i f_{ij} I_i^k}{V_p}$ in a multiwall system, and $f_w\big|_{x_D=1}$ is the water cut at the outlet (producer), which can be readily evaluated from the production data, i.e., $1 - \frac{q_o}{q_t}$.

To estimate Q_i in Eq. 3.30, the pore volume, V_p, must be known beforehand. There are two options to evaluate the pore volume. The first approach is to treat the pore volume as a model parameter, similar to the connectivity and the time constant whose values are determined by the nonlinear regression. Another method is to obtain the pore volume by explicitly inverting the Koval (1963) fractional flow equation to achieve a relationship between water cut and dimensionless time as shown in Eq. 3.31.

$$f_w\big|_{x_D=1} = \begin{cases} 0 & t_D < \dfrac{1}{K_{val}} \\ \dfrac{K_{val} - \sqrt{\dfrac{K_{val}}{t_D}}}{K_{val} - 1} & \dfrac{1}{K_{val}} < t_D < K_{val} \\ 1 & t_D > K_{val} \end{cases} \qquad 3.31$$

where t_D is the dimensionless time, which is defined as $t_D = \frac{Cumulative\ injection}{V_p}$.

The producer drainage volume V_p can be obtained through nonlinear regression. Therefore, using the Welge equation with the estimated producer drainage volume from the Koval approach, we can calculate the outlet oil saturation using the average oil saturation to evaluate the relative permeability.

3.3.2.5 History Match with Nonlinear Multivariate Regression

The history match is essentially a nonlinear multivariate regression procedure to obtain the optimized model parameters by solving the pressure and saturation equations in the coupled CRM model. As discussed before, we have two options to couple the pressure and saturation equations:

1. Fully-coupled option: couple the pressure equation Eq. 3.25 with the saturation equation Eq. 3.27.
2. Simplified-coupled option: couple the pressure equation Eq. 3.25 with the simplified saturation equations Eq. 3.29.

The Fully-Coupled Option

For the fully-coupled option, we require information such as oil/water viscosities, oil/water/pore compressibilities, and oil/water relative permeability curves, besides production and injection data. We assume constant values for viscosity and compressibility with respect to pressure.

Figure 3.3 illustrates the fully-coupled option. Initially, we make a guessed value of f_{ij}, $\tau_j^{'}$ and $\overline{S}_{ij}$, which are used to evaluate the average oil saturation, $\overline{S}_o$. The average oil saturation is then transferred into the outlet oil saturation, S_{o2}, using the Welge equation accordingly. As a result, the time constants, τ_j, can then be updated, which ensures the incorporation of the saturation change. Finally, we calculate the production rate using Eq. 3.25 with the updated time constants. The same procedure is repeated to advance to the next time step.

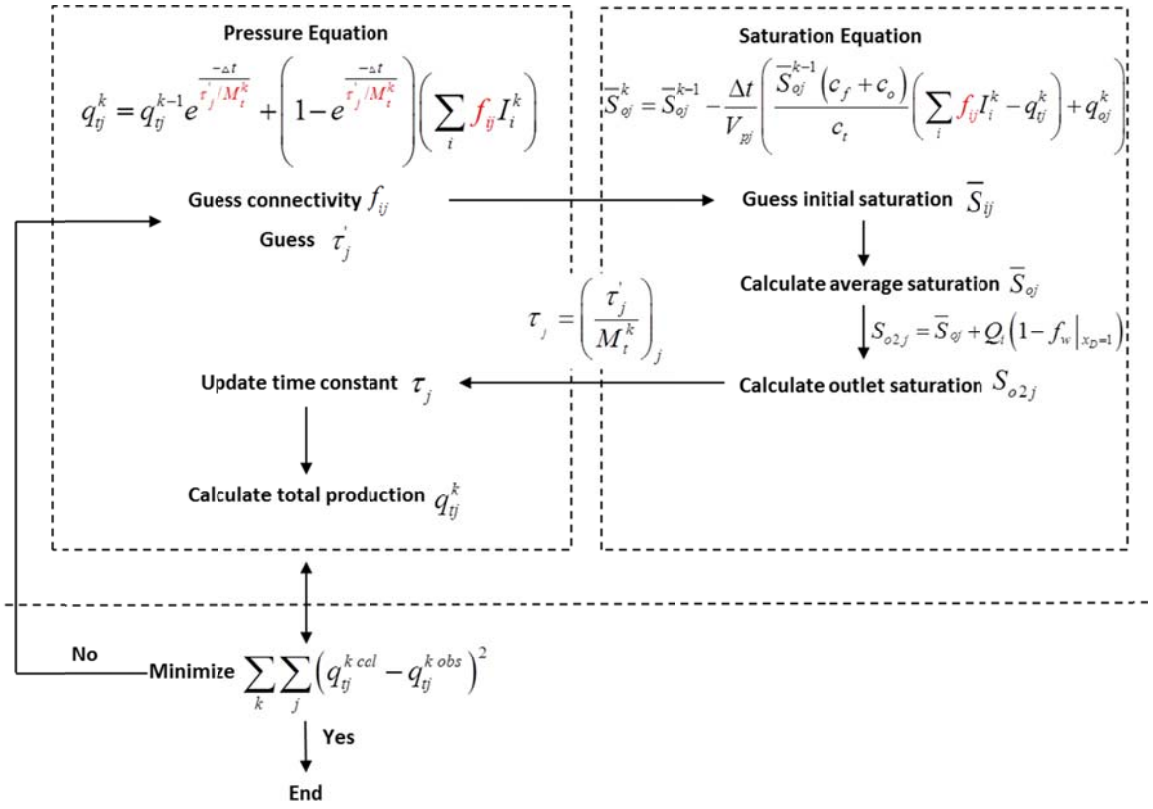

Figure 3.3 Flowchart of the fully-coupled option.

After the production rate at each time step is obtained, a multivariable nonlinear regression then follows to decide if the difference between the calculated and observed production rates is the minimum (see Figure 3.3). If it is not the minimum, the guessed value of f_{ij}, τ_j' and $\bar{S}_{ij}$ will be updated until the minimum difference is found.

This regression problem is presented as the following. The objective function of the coupled CRM model is:

$$\min z = \sum_{k=1}^{n_t} \sum_{j=1}^{n_p} \left[(q_{tj}^{k\ obs} - q_{tj}^{k\ cal})^2 \right] \qquad 3.32$$

where $q_{tj}^{k\ obs}$ is the observed total fluid production rate at time step k for producer j, and $q_{tj}^{k\ cal}$ is the calculated total fluid production rate at time step k for producer j, n_t and n_p are the total number of time steps and producers, respectively.

This objective function is constrained by:

$$\sum_j f_{ij} \le 1 \quad \text{for any } i \tag{3.33}$$

and:

$$S_{or} < \overline{S}_{ij} < 1 - S_{wr} \tag{3.34}$$

$$S_{or} < \overline{S}_{oj} < 1 - S_{wr} \tag{3.35}$$

$$S_{or} < S_{o2j} < 1 - S_{wr} \tag{3.36}$$

and:

$$f_{ij} > 0 \; and \; \tau_j^{'} > 0 \tag{3.37}$$

Eq. 3.32 states that the objective is to minimize the squared differences between the calculated and the measured production rates. The constraint from Eq. 3.33 indicates a material balance of injected water, in which the summation of the injection contribution from a particular injector to different producers should be equal to the total injection from that injector. It also allows for lost injection since the sum can be less than 1. The connectivities in Eq. 3.33 are summed over the producer index j, which requires solving for the model parameters for all producers at the same time. The constraints in Eqs. 3.34-3.36 restrict the range of the initial average, temporal average and outlet oil saturation to be between the residual oil saturation and the original oil saturation. The constraint from Eq. 3.37 is used to guarantee non-negative solutions to f_{ij} and $\tau_j^{'}$.

Similar to the current CRM model, the CONOPT solver in GAMS is used to solve the regression problem described by Eqs. 3.32-3.37.

The Simplified-Coupled Option

For the simplified-coupled option, we require less information than the fully-coupled option since we neglect the reservoir and fluid compressibilities. Except for production and injection data, we need oil/water viscosities and oil/water relative permeabilities. We also consider viscosity to be constant with respect to pressure.

Figure 3.4 illustrates the simplified-coupled option. In the simplified-coupled case, the average saturation of each time step can be calculated using the initial guess of initial saturation and the oil production data. As a result, the time constant can be updated with the saturation obtained and the guessed value of $\tau_j^{'}$. One can then calculate the total production rate using the updated time constant together with guessed value of connectivity.

The same regression procedure (Eqs. 3.32-3.37) as the fully-coupled option then follows to decide if the guessed values should be updated to achieve the minimum difference between the calculated and the observed production rates. We observe that no feedback from the pressure equation is needed in the saturation equation, hence the name "simplified-coupled" option.

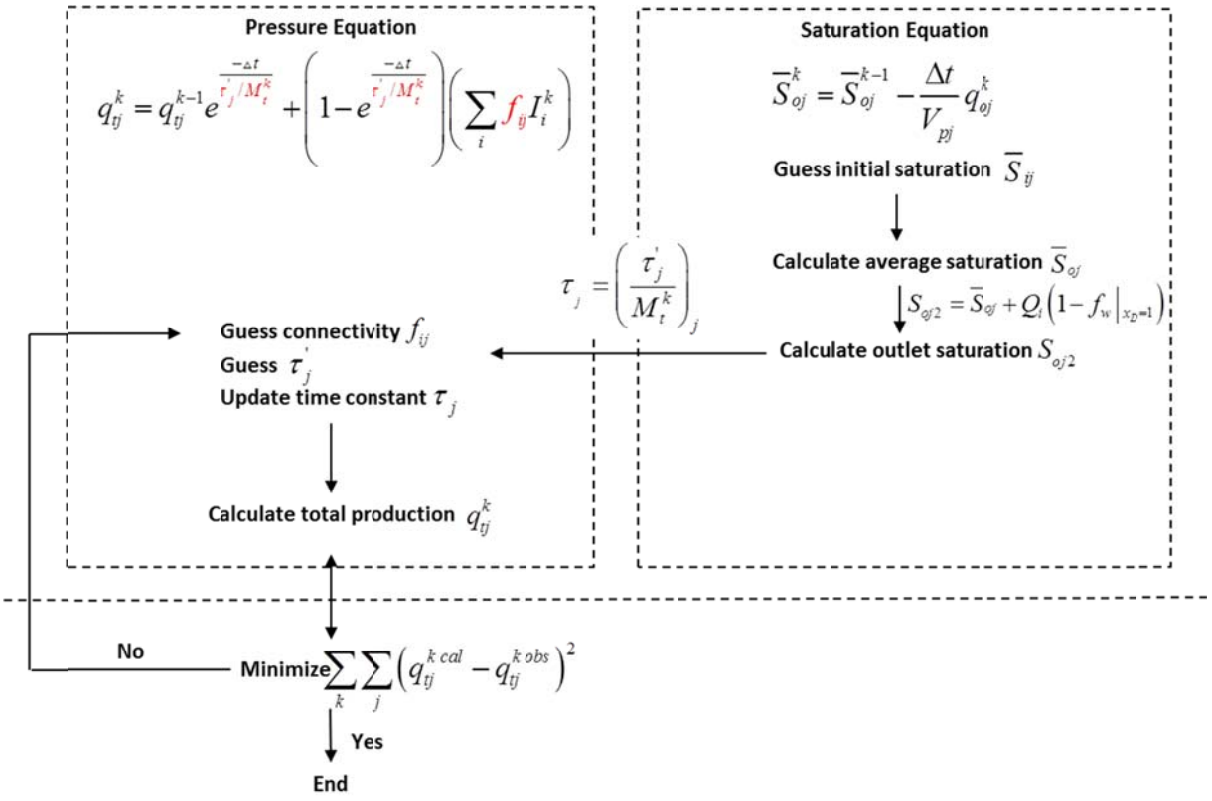

Figure 3.4 Flowchart of the simplified-coupled option.

From the fully-coupled option to the simplified-coupled option, the computational complexity and requirement for information are reduced. The fully-coupled solving needs more information and is expected to take more computational time; while the simplified-coupled case is easier to solve, though it may sacrifice some accuracy as we ignored the compressibility. Nevertheless, solution accuracy and computation efficiency are often two incompatible aspects in numerical models. It is practitioner's decision to choose which one they prefer.

3.4 VALIDATION, PREDICTION AND OPTIMIZATION OF INJECTION SCHEME

After history matching production data using the nonlinear regression, it is important to validate the model parameters obtained. If the parameter quality proves to be good, we can proceed to predict total/oil production rates and further perform optimization of injection scheme.

3.4.1Validation

In the coupled CRM model, we obtain three important parameters, i.e., the well connectivities, the time constants, and the water/oil saturations, within a chosen time horizon through history match. The quality of model parameters obtained lays the foundation for further applications such as prediction and optimization. Therefore, it is very important to develop validation procedures to evaluate whether the model parameters are reliable to the degree for the intended purpose or application. We propose two different types of validations in the coupled CRM model. They are internal and external validations.

3.4.1.1 Internal Validation

An internal validation is to verify the reliability of the coupled CRM model with itself. It is essentially a retro prediction process that is embedded within the coupled CRM model. Figure 3.5 shows the procedure of an internal validation.

For an internal validation, the validation time window usually follows the history match time window immediately. We use the model parameters obtained from history match to predict the production rate under historical injection rates within the validation window. Comparisons are then carried out between the known historical production rates

and the CRM model predicted production rates. If the difference is small, the model is considered to be reliable. In this way, we are also able to check if we have built the model correctly.

Here, we mention that the algorithm for predicting production rates in the internal validation is actually the same as the "prediction" algorithm, which will be discussed in detail in the subsection 3.4.2. In other words, the "internal validation" and "prediction" are technically the same but only for different purposes.

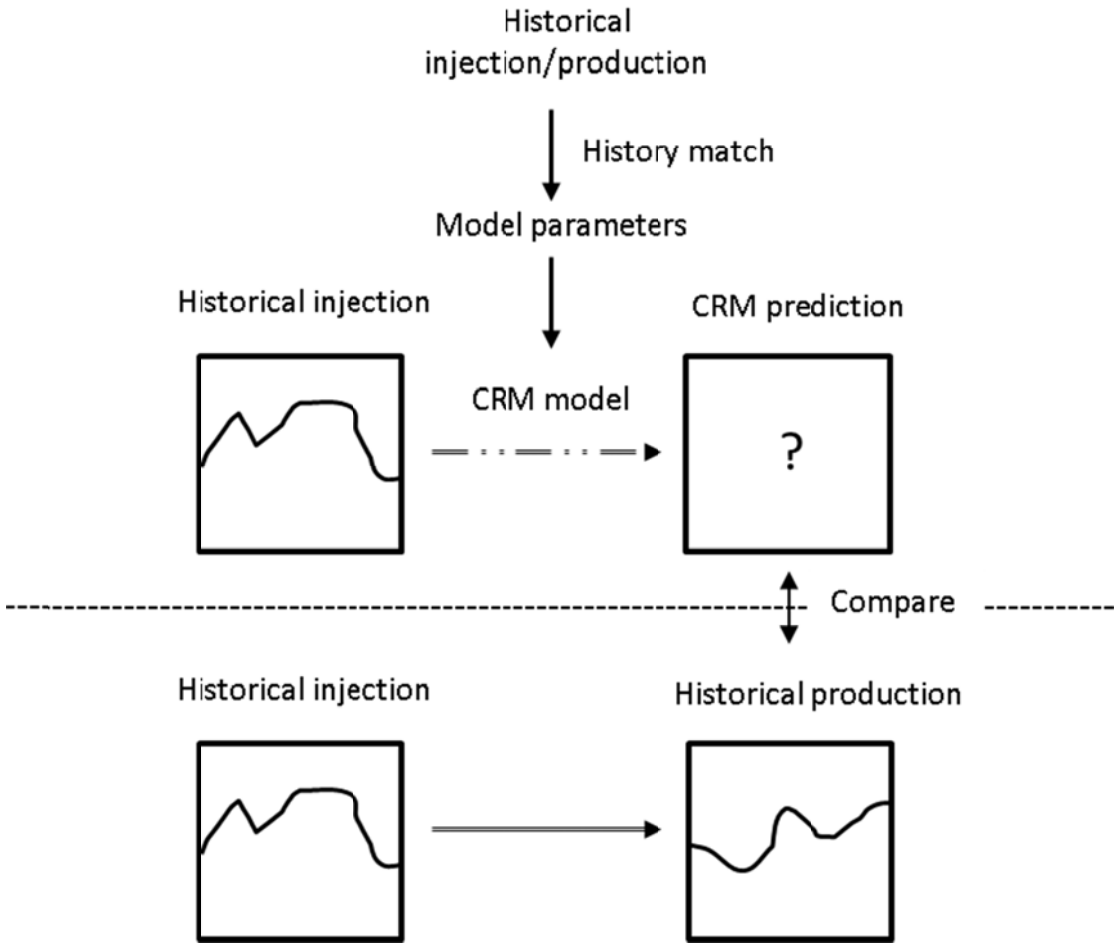

Figure 3.5 Internal validation of the coupled CRM model.

3.4.1.2 External Validation

Unlike an internal validation in which the CRM model itself is involved, an external validation uses a reliable independent procedure to provide the same (or similar) model parameters as those from the coupled CRM model (see Figure 3.6). By comparing the counterparts, we are able to validate the results from the coupled CRM model.

In this dissertation, we use traditional reservoir simulation to perform the external validation for the coupled CRM model. However, reservoir simulation doesn't generate the same parameters as the coupled CRM model readily. For example, there is no time constant concept in the traditional reservoir simulation. Also, there exists a difference in the modeling scale between the coupled CRM model and reservoir simulation. Specifically, the CRM model has a unique modeling scale that is equivalent to a producer-based drainage volume; whereas the reservoir simulation's modeling scale depends on the grid block size, which is usually much smaller than a producer's drainage volume. Because of these issues, we must not only come up with model parameters that are equivalent to those from the coupled CRM model, but also scale up them if necessary. Therefore, the external validation is a semi-quantitatively procedure that we expect the model parameters to be not exactly the same but very close since they are evaluated by different methods under different modeling scales. Figure 3.6 shows the procedure of an external validation.

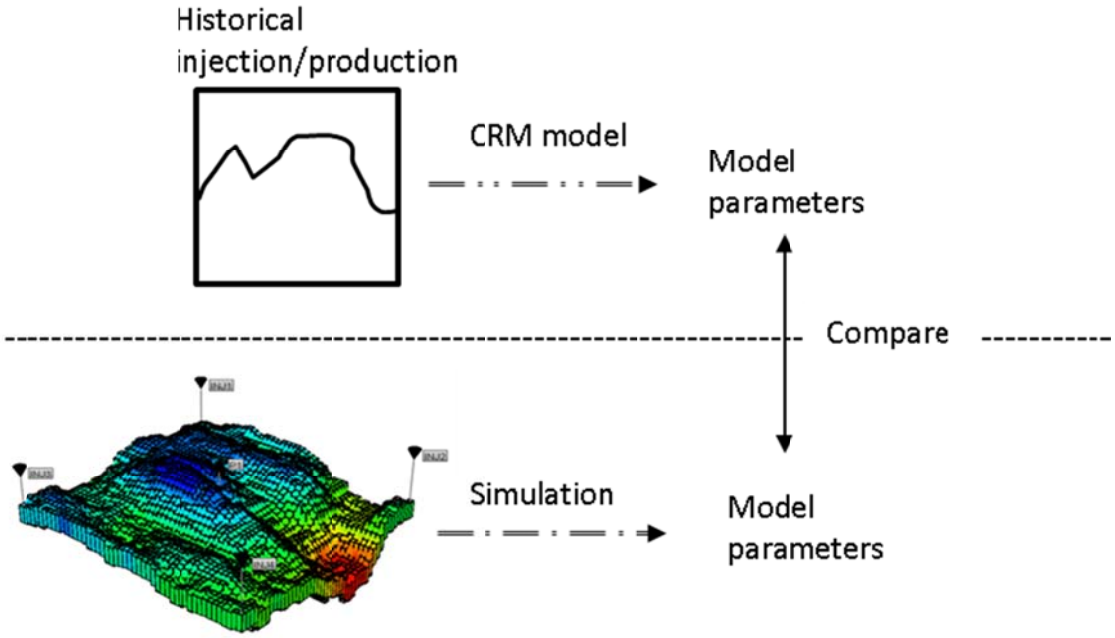

Figure 3.6 External validation of the coupled CRM model.

3.4.2 Prediction

Prediction is a crucial capability as it provides evaluation of well performance under future injection schemes. Accurate prediction of both future total and oil production rates is the most important step to optimize injection strategies.

Prediction of fluid rates in the coupled CRM is more complicated than in the current CRM model. In the current CRM model, we only need to know the connectivity and the time constant, both of which are constant with respect to time, to calculate total production rate. Oil production rates are then estimated using a separate fractional flow model.

The coupled CRM model, as a two-phase flow model, is more advantageous in predicting both total and oil rates. In the coupled CRM model, the saturation must be

evaluated first before estimating the total production rate at each future time step. As explained in the previous history match section that the average oil saturation at each time step is obtained by solving the oil material balance equation, we can then take advantage of the oil production data at hand to generate a relationship between the oil (or water) fraction, i.e., $\frac{q_o}{q_t}$ (or $\frac{q_w}{q_t}$.), and the average saturation, $\overline{S}_o$ (or $\overline{S}_w$). As a result, we are able to construct fractional flow curves directly (see Figure 3.7).

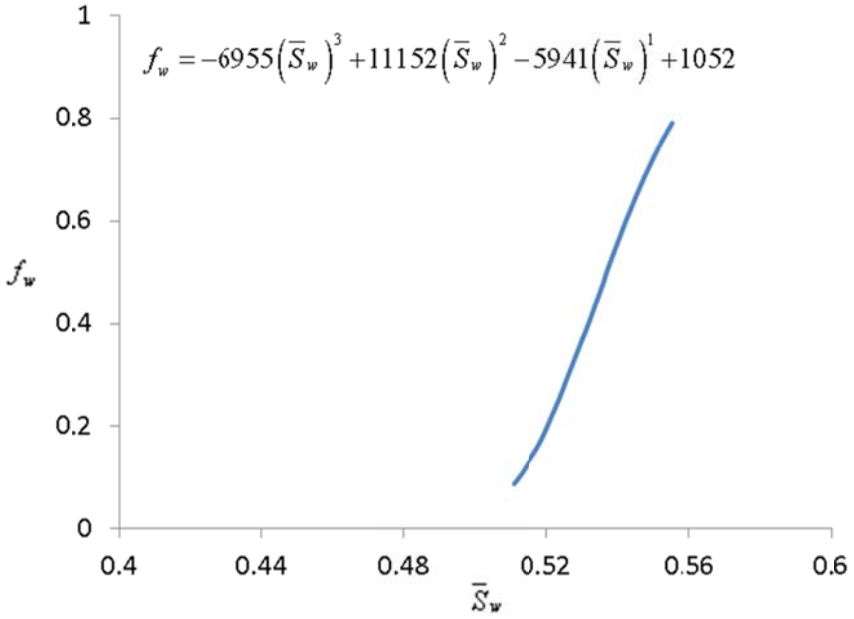

Figure 3.7 An example of a fitting fractional flow curve from the historical data for the coupled CRM model.

Before proceeding, it is worth mentioning that the saturation in Figure 3.7 is the average saturation within a producer's drainage volume instead of the outlet saturation that we usually use in the fractional flow theory. As mentioned before, the outlet oil saturation, or the oil saturation evaluated at the producer, is calculated from the average oil saturation using Welge equation since it can't be measured or calculated directly. Any

inaccuracy in the average saturation or any violations in the assumptions made in the Welge equation can consequently cause errors in the outlet saturation. On the contrary, the average oil saturation is the hard data that comes directly from oil material balance. For this reason, we determine to use the average oil (or water) saturation in the fractional flow model for prediction to reduce unnecessary errors and predict oil rate more accurately.

Nevertheless, the fractional flow curve in Figure 3.7 is built over the history match time window, therefore an extrapolation is needed to extend it to a future time window. For each future time step, a prediction algorithm is designed in the coupled CRM model to obtain total fluid rate and oil rate sequentially. Figure 3.8 illustrates the algorithm used for prediction. We assume k is a time step when all the quantities including oil/total rates, water cut and the average water saturation are known, while k+1 is the next time step to be predicted.

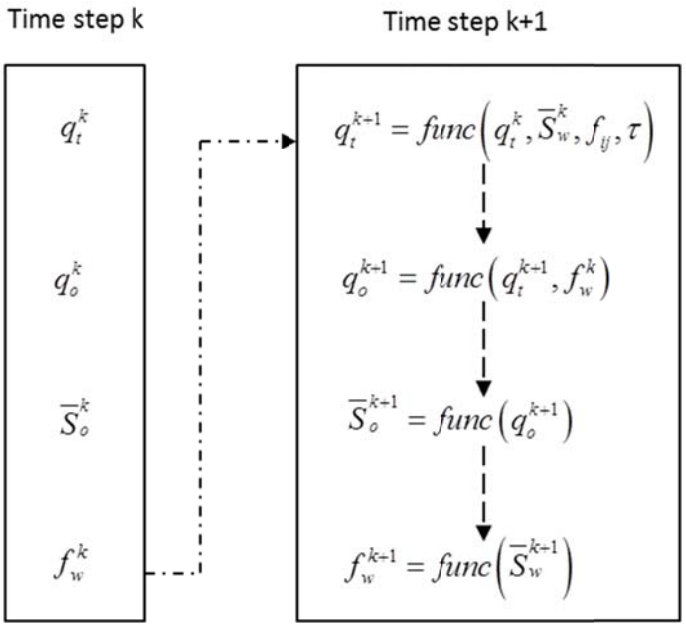

Figure 3.8 Prediction algorithm in the coupled CRM model.

Total production rate, q_t^{k+1}, to be predicted, is a function of total production rate, q_t^k from last time step k and the outlet oil saturation, S_{o2}^{k+1}, at current time step k+1. We estimate q_t^{k+1} using the explicit saturation S_{o2}^k considering that saturation usually changes slowly. After total production q_t^{k+1} is obtained, oil rate q_o^{k+1} can be evaluated explicitly using the water cut f_w^k for the same reason that the change of water cut is also slowly and continuously. Using the oil material balance equation, we can further update the average oil saturation $\overline{S}_o^{k+1}$, hence the average water saturation $\overline{S}_w^{k+1}$. As we have discussed that we have achieved a relationship between the average water saturation and water cut, a new water cut f_w^{k+1} can be obtained accordingly by extrapolating this fractional flow curve. The last step is to update the outlet oil saturation S_{o2}^{k+1} using $\overline{S}_w^{k+1}$ (or $\overline{S}_o^{k+1}$) and f_w^{k+1} obtained. Up until now, all the quantities in time step k+1 are updated. The same procedure is repeated to advance to the next time step.

There is also an implicit prediction algorithm that can be adopted in the coupled CRM model. It involves evaluating production rate at time step k+1 using other unknown variables evaluated at time k+1. Specifically, after we obtained all the quantities at time step k+1 following the procedures we described above, we recalculate q_t^{k+1} using the updated outlet saturation, S_{o2}^{k+1}. The oil rate q_o^{k+1} is also re-evaluated using the current water cut, f_w^{k+1}. Consequently, new values of $\overline{S}_o^{k+1}$, f_w^{k+1} and S_{o2}^{k+1} can be obtained sequentially. The iteration for time step k+1 will terminate when the saturation and water cut values converge. The same procedure is repeated to the next time step. As a result, it is more sophisticated as it requires iterations within each time step to solve for the saturation and water cut implicitly and hence more time-consuming.

In this dissertation, we mainly use the first algorithm since we have found that the accuracy is good enough for the prediction purpose.

3.4.3 Optimization of Injection Scheme

The capability of predicting well performance under a specific injection scheme enables us to optimize the future injection strategy in an effort to maximize the oil production. In other words, the optimization is essentially the process to find the injection scheme that gives the most oil production.

There are several different optimization objective functions that can be adopted in the coupled CRM model. For example, we can maximize the net present value by considering the injection cost and oil price, or we can minimize the field total water production by maintaining the same total field injection, etc. In this dissertation, we discuss maximizing the field total oil production while retaining the same total field injection.

The decision variables (the quantities to be optimized) in this problem are the injection rates of injectors, which should be constrained within a certain range considering the injection facility limitations. Moreover, there are also different injection optimization strategies to adopt. One can maintain constant injection rate in each injector over the future time horizon. This injection scheme is simple itself as an optimization problem since there are only a small number of parameters to be determined. And it is also easy to follow practically in the field. Another approach is to change the injection rates in each injector periodically. In this way, we might obtain more oil production by constantly stimulating the system. However, it would increase the complexity of the optimization problem. In this dissertation, we keep the injection rates constant considering that we only optimization for a short time in the case study.

Following the discussions above, the optimization of injection scheme in the coupled CRM model again becomes a regression problem with an objective function as:

$$\max z = \sum_{k=1}^{n_t^{opt}} \sum_{j=1}^{n_p} \left[q_{oj}^{k} \right] \tag{3.38}$$

And this objective function subjects to:

$$\sum_{k=1}^{n_t^{opt}} \sum_{i=1}^{n_i} I_i^k = I_{total} \tag{3.39}$$

and:

$$I_{lower} < I_i^k < I_{upper} \tag{3.40}$$

where q_{oj}^{k} is the oil production rate at a future time step k for producer j, n_t^{opt} and n_p are the total number of time steps for optimization and the total number of producers, respectively, and I_{upper} and I_{lower} are the injection upper and lower limits, respectively .

Eq. 3.38 is the objective function that aims to optimize the field total oil production over the optimization time window. Eq. 3.39 implies that the field total injection during the optimization time is fixed. Eq. 3.40 states the injection rate of each injector at each time step should be bounded between the injection upper and lower limits.

CHAPTER 4: SYNTHETIC RESERVOIR STUDIES

The coupled CRM model has come up with new model parameters to describe two-phase flow, such as the time-varying time constants and the remaining oil saturation. It is important to systematically verify these parameters in an effort to test the validity of the coupled CRM model as a whole. In this chapter, we design synthetic case studies in a commercial reservoir simulator (CMG) to validate the coupled CRM model parameters and also demonstrate its capabilities, such as history match, prediction and optimization of injection scheme.

We apply the coupled CRM model to five synthetic reservoirs. Each case study highlights different characteristics of the coupled model. We briefly summarize all the cases as follows:

1). A homogeneous reservoir with a single producer

We design this case to show the validity of the coupled CRM model in a homogenous reservoir. We first demonstrate the history match capability of the coupled CRM model and then validate the model parameters obtained by comparing them with reservoir simulation results.

2). A heterogeneous reservoir with a single producer

A real reservoir is often heterogeneous. Variability of rock and fluid properties is a reality that must be dealt with in any reservoir modeling. We perform a history match in this heterogeneous reservoir and validate the model parameters through reservoir simulation results. The impact of reservoir heterogeneity to the coupled CRM model is also studied and discussed.

3). A five-spot homogeneous reservoir

We focus on the fractional flow models in this case. Three different fractional flow models including Gentil model, Koval model, and the coupled CRM model are discussed. We apply these models to different stages of a water flood (mature and immature water floods) to analyze their advantages and limitations.

4). A sealed reservoir

In this case, the reservoir is constructed with more geological features. We add an impermeable seal, which separates the reservoir into two compartments. We are interested in comparing results between the current and the coupled CRM models. Moreover, an optimization of injection scheme is also performed to maximize oil production using the coupled CRM model.

5). A heterogeneous reservoir with 16 producers and 9 injectors

The last case study features a heterogeneous reservoir with a fluvial channel deposition environment. Permeability varies spatially in the reservoir while the main directions of heterogeneity are along northwest and southeast. We apply the coupled CRM model to this field with 16 producers and 9 injectors. Both fully-coupled and simplified-coupled schemes are used and the results are then compared and discussed.

4.1 VALIDATION USING RESERVOIR SIMULATION

Synthetic reservoirs serve as ideal candidates for model validation since every aspect in the reservoir is known. We mentioned two types of validation procedures, internal and external validations, in Chapter 3. The internal validation relies on the CRM model itself for verification; whereas the external validation uses an independent procedure to validate model parameters.

We use a commercial reservoir simulator (CMG) to validate the coupled CRM model externally. Model parameters, such as time constants and saturations, are estimated using CMG and are further compared with those from the coupled CRM model. In the following sections, we explain how one can obtain time constant and saturation from a reservoir simulation.

4.1.1 Time Constant

In physics and engineering, the time constant is the parameter characterizing the response to a step input of a first-order linear time-invariant (LTI) system (Lipták, 2005). A first-order LTI system is the one that can be modeled by a single first-order differential equation in time. Examples include the simplest single-stage electrical resistor-capacitor (RC) circuit (see Figure 4.1). To determine the time constant in the time domain, the usual approach is to stimulate the system with a step input (Wie, 1998). Physically, the time constant represents the time it takes for the system's step response to reach 63.2% of its final (asymptotic) value. Figure 4.2 is a schematic illustration of the voltage curve of a charging capacitor in a RC circuit. The vertical axis shows the voltage across the capacitor as a percentage of the applied voltage to the RC circuit and τ represents the RC time constant.

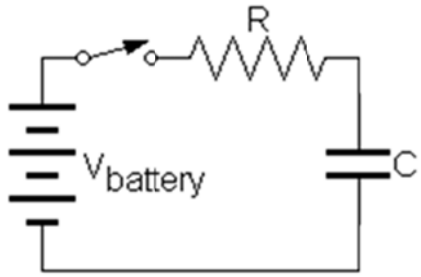

Figure 4.1 Schematic of a single-stage electrical resistor-capacitor circuit.

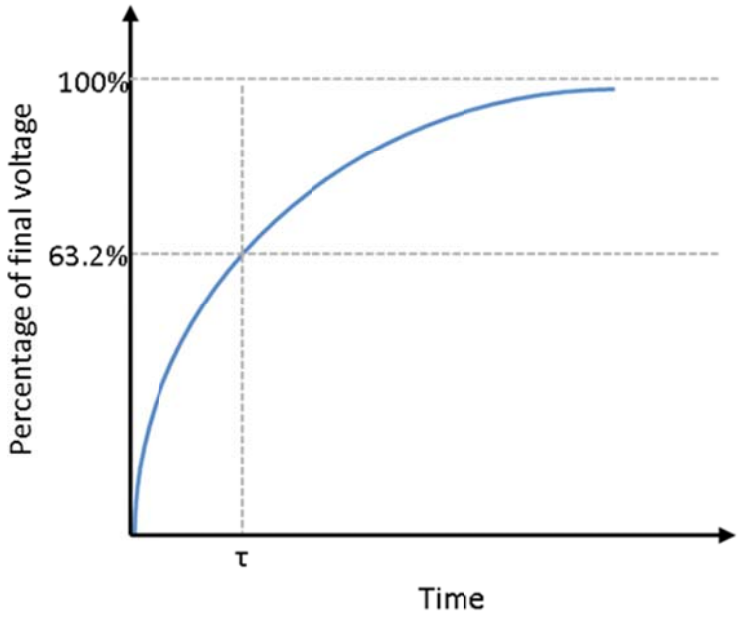

Figure 4.2 Schematic of the time constant in a RC circuit.

The reservoir system is similar to a RC circuit in that it is also a first-order LTI system. Therefore, we can use the well-established concept of time constant in a first-order LTI system to find the time constant from a reservoir simulation. Namely, we introduce an injection pulse, which is a sudden change in injection rates, to explore the time constant. The pulse test consists of changing the injectors' flow rate and measuring the time it takes for the producers to respond (see Figure 4.3).

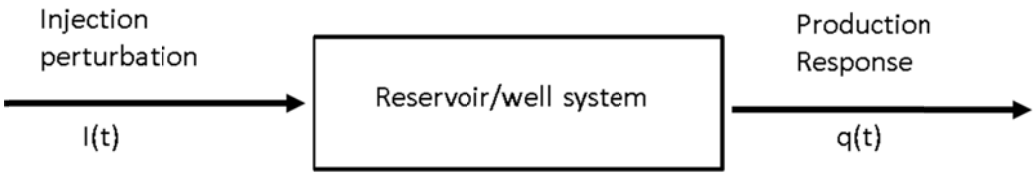

Figure 4.3 Pulse test in the reservoir simulation.

Figure 4.4 shows a typical injection perturbation and the production response. The injection rates can be discontinuous while the production rate is continuous because of the compressibility of the reservoir.

In Figure 4.4, the injection perturbation starts at the 7th month and lasts for 15 months. We observe that the production responds to this perturbation immediately at the 7th month and rises afterwards until the 16th month when it stabilizes. We define the full production response to be the rate that is equal to the injection pulse rate. In this case, it takes 4 months for the production rates to reach 63.2% of the full response. As a result, the time constant for the producer in this example is 4 months.

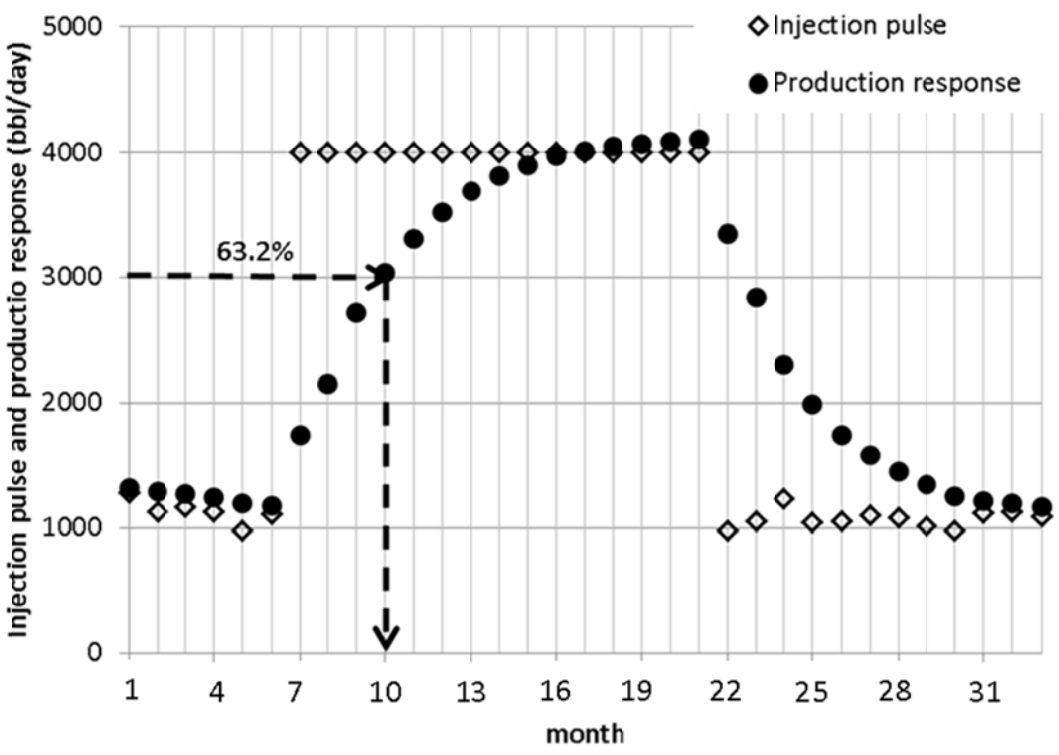

Figure 4.4 An example of injection perturbation and production response.

The time constant obtained from the injection rate pulse test is similar to the CRM time constant. However, it is not the exact equivalence to the time constant in the CRM model. Therefore, the comparison of time constants is semi-quantitative; we expect the value of time constants from the two methods to be close but not exactly the same.

4.1.2 Saturation

As mentioned in Chapter 3, the average oil saturation within a producer-based drainage volume can be evaluated from the coupled CRM model. In the reservoir simulation, each grid block has an oil saturation value. Consequently, we must calculate the average oil saturation of grid blocks that represent a producer's drainage volume in a reservoir simulation and compare it with the coupled CRM model. However, it is often difficult to identify the drainage volume controlled by a certain producer in a reservoir simulation with many producers. For this reason, we design cases with only one producer in the reservoir so that the entire reservoir represents the drainage volume. This way, we can compare saturation easily. As for the outlet oil saturation, which is the oil saturation measured at the well, it is the average oil saturation of the grid blocks where the producer is located.

4.2 CASE 1: A HOMOGENEOUS RESERVOIR WITH A SINGLE PRODUCER

The first case study is an illustration of the validity of the coupled CRM model in a homogeneous reservoir. We demonstrate the coupled CRM model history match capability first and then compare the obtained model parameters to those from a reservoir simulation to validate the coupled model externally.

4.2.1 General Reservoir Information

The simulated reservoir is a two-dimensional homogeneous reservoir (see Figure 4.5). A horizontal permeability of 200 md and a porosity of 0.2 are assigned to all grid blocks. Key reservoir and fluid parameters of this field are summarized in Table 4.1.

Parameters	Value
Number of grid blocks	33×33×1
Grid block sizes (ft)	80×80×65
Porosity	0.2
Horizontal permeability (md)	200
Vertical permeability (md)	20
Oil compressibility (psi^{-1})	3×10^{-5}
Water compressibility (psi^{-1})	1×10^{-6}
Rock compressibility (psi^{-1})	1×10^{-6}
Water relative permeability	$k_{rw}^{o}\left(\frac{S_w - S_{wr}}{1 - S_{wr} - S_{or}}\right)^2$
Oil relative permeability	$k_{ro}^{o}\left(\frac{1 - S_w - S_{or}}{1 - S_{wr} - S_{or}}\right)^2$
Irreducible water saturation	0.3
Residual oil saturation	0.4
End-point water relative permeability	0.3
End-point oil relative permeability	1
Water viscosity (cp)	0.72
Oil viscosity (cp)	3.25
Initial reservoir pressure (psi)	1250

Table 4.1 Key reservoir and fluid parameters of case 1.

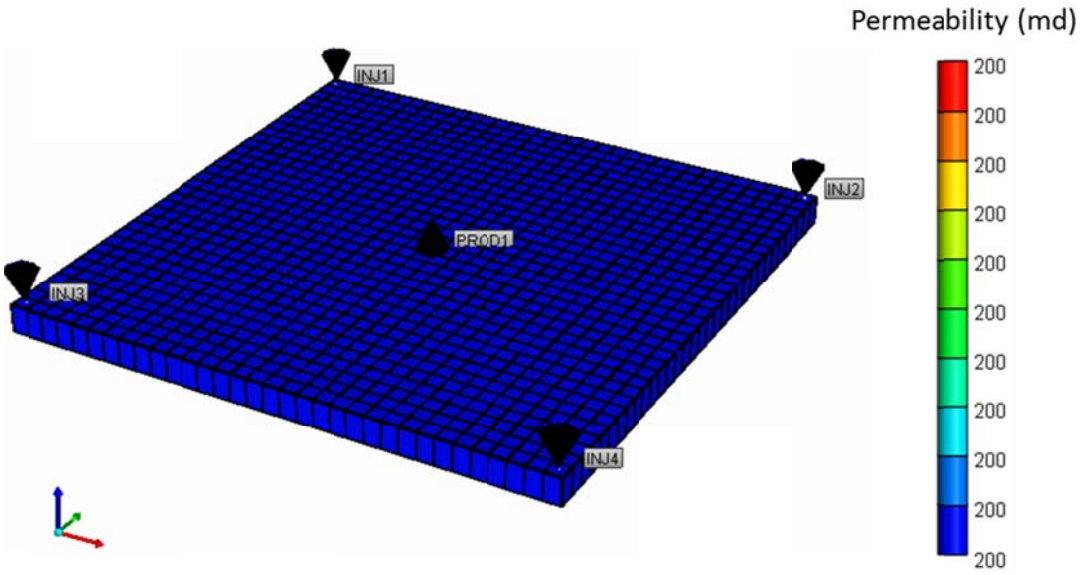

Figure 4.5 Permeability distributions in case 1.

This synthetic field consists of 4 injectors and 1 producer (see Figure 4.5). The distance between an injector-producer pair is 1800 ft. The producer is vertically completed over the entire thickness of the reservoir and is operating under a constant bottom-hole pressure constraint of 250 psi.

The injection rates are fluctuating monthly as shown in Figure 4.6. In this case, the lack of injection in the first 12 months represents primary recovery. Secondary water injection then follows and continues throughout the remainder of the simulation. The total simulation time is 383 months with one month per time step. The production and injection data are monthly data. These data are noise free.

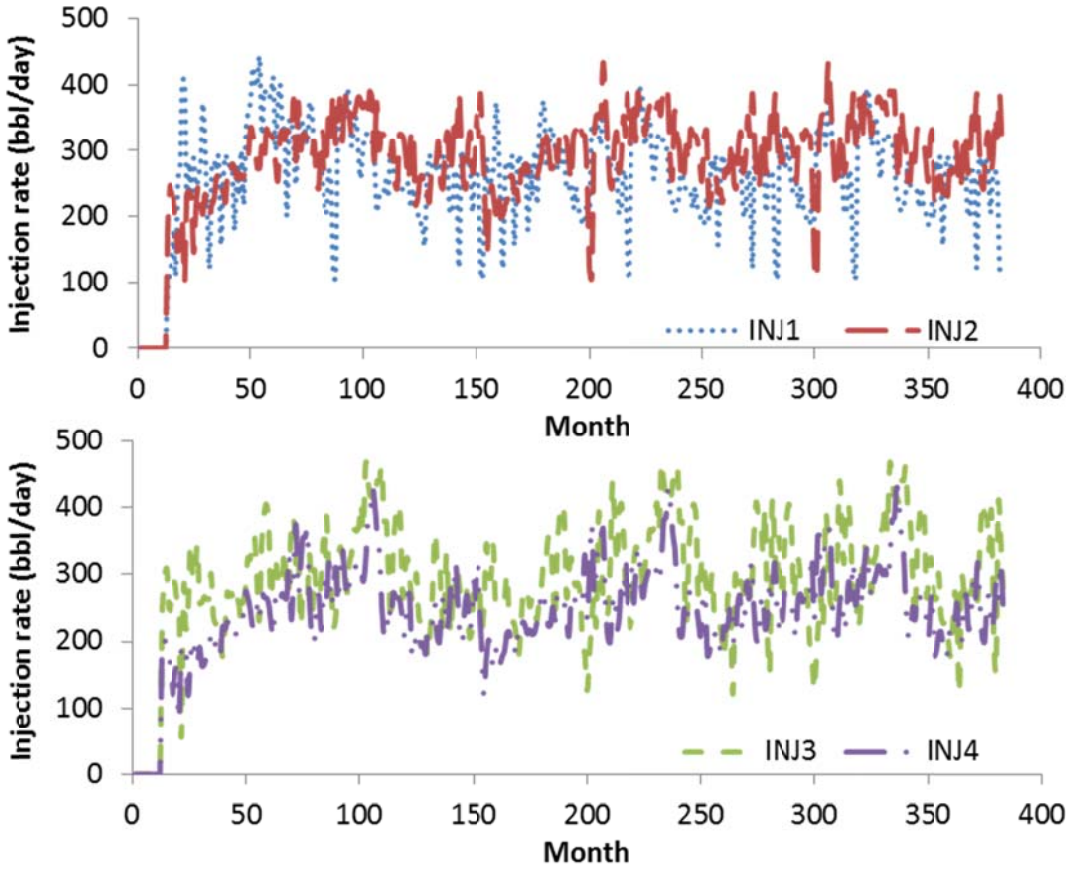

Figure 4.6 Varying injection rates of the four injectors in case 1.

Figure 4.7 gives the simulated total and oil rates of the producer. Fast declines in oil production rates are observed during the primary depletion. After injection is initiated, the reservoir pressure started to rise. As a result, the producer regained its productivity as shown by the increasing production rates. After 7 years of water flood, the oil production rates dropped drastically after water breakthrough. From then on, the water cut increased gradually and eventually reached 0.97 at the end of the simulation.

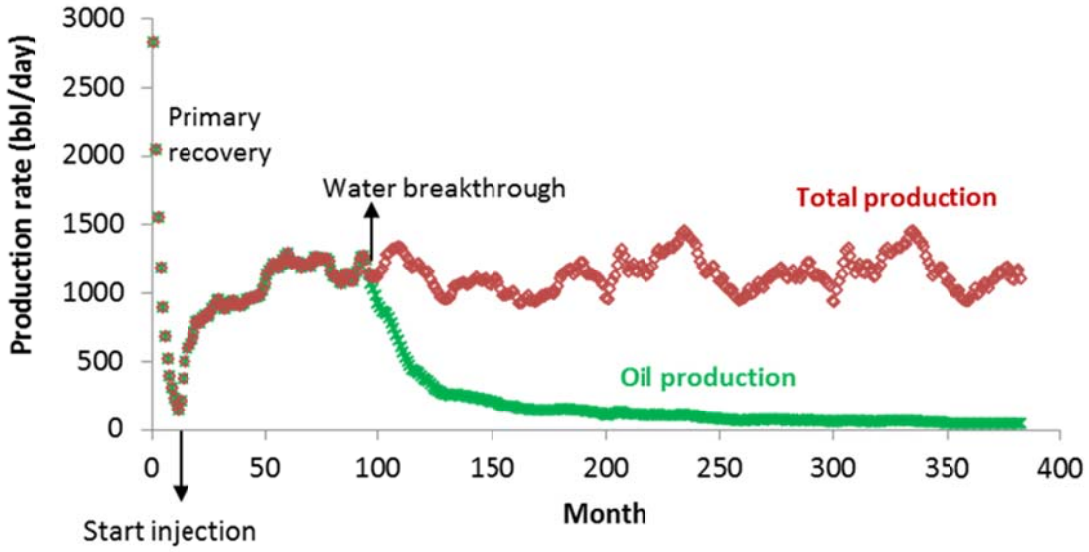

Figure 4.7 The total and oil production history of the single producer in case 1.

4.2.2 Application of the Coupled CRM Model

4.2.2.1 The Coupled CRM Inputs

The production and injection rates from the reservoir simulation results are treated as field data and used in the coupled CRM model. In this case, we applied the simplified-coupled scheme and all required inputs for the coupled CRM model are summarized in Table 4.2.

Input		Value
Rate		Injection/production data
Reservoir/fluid properties	μ_w (cp)	0.72
	μ_o (cp)	3.25
	k_{rw}	$k_{rw}^{o}\left(\frac{S_w - S_{wr}}{1 - S_{wr} - S_{or}}\right)^2$
	k_{ro}	$k_{ro}^{o}\left(\frac{1 - S_w - S_{or}}{1 - S_{wr} - S_{or}}\right)^2$
	S_{wr}	0.3
	S_{or}	0.4
	k_{rw}^{0}	0.3
	k_{ro}^{0}	1

Table 4.2 The coupled CRM inputs in case 1.

4.2.2.2 History Match

The time window for history match is from the 100th to the 350th month (see Figure 4.8). This time window covers from small to large water cut regimes, which represents a complete water flood.

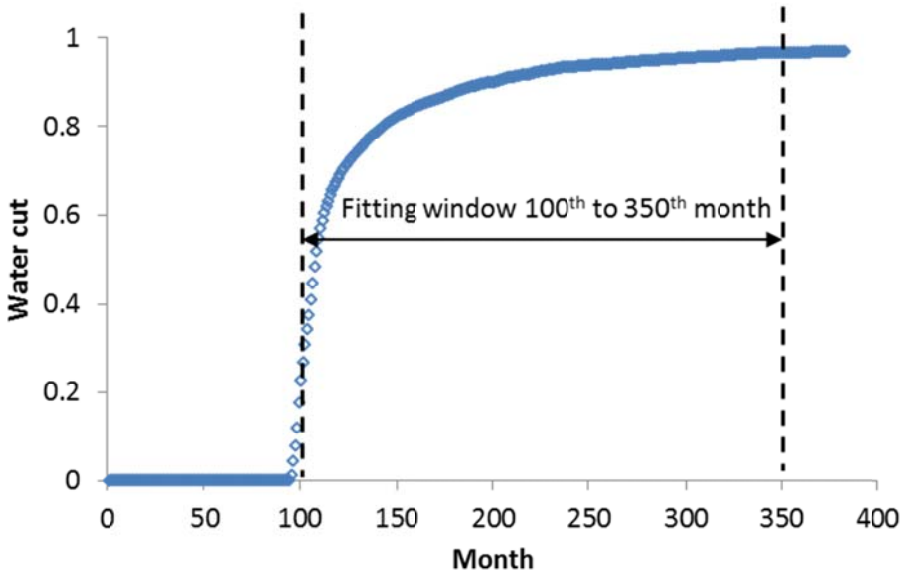

Figure 4.8 History match time window in case 1.

The total production history match results are in Figure 4.9. We use the coefficient of determination (or R^2) to indicate the goodness of fit, which is defined as the following:

$$R^2 = 1 - \frac{\sum_i (y_i - f_i)^2}{\sum_i (y_i - \bar{y})^2} \qquad 4.1$$

where y_i is the observed value, f_i is the modelled value, and $\bar{y}$ is the mean of the observed data.

The coefficient of determination is a statistical measure that will give information about how well a model approximates the real data. An R^2 of 1 indicates that the regression line perfectly fits the data.

In this case, R^2 has a value of 0.99 indicating a good history match. The subsequent CRM model parameters, such as the connectivity and time constants, are

adjusted to attain the history match. Therefore, a good quality in total production fits is the first step to ensure reliable estimation of model parameters.

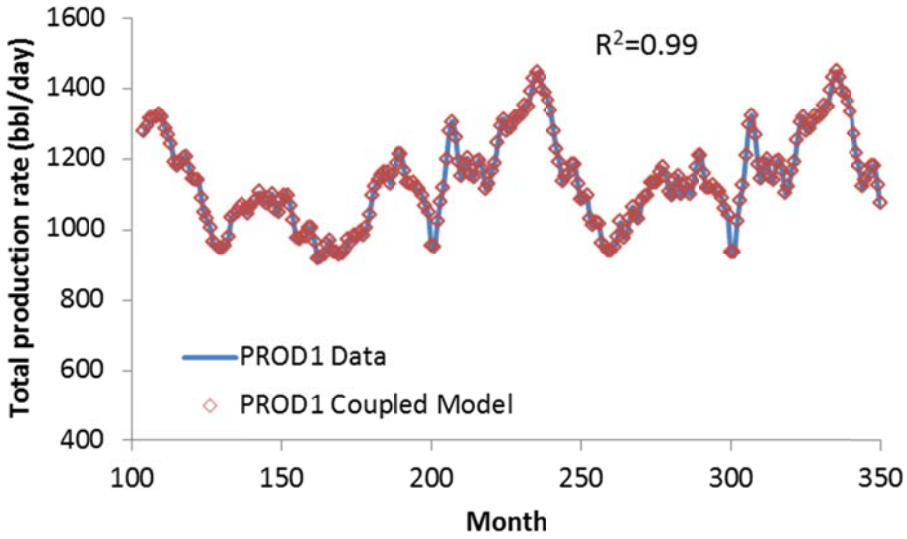

Figure 4.9 The total production history match in case 1.

The well pair connectivity map is in Figure 4.10. Since there is only one producer and no possible injection loss in the reservoir, every barrel of water injected from the injectors will entirely contribute to the production. Therefore, the connectivity is 1 amongst all injector-producer pairs.

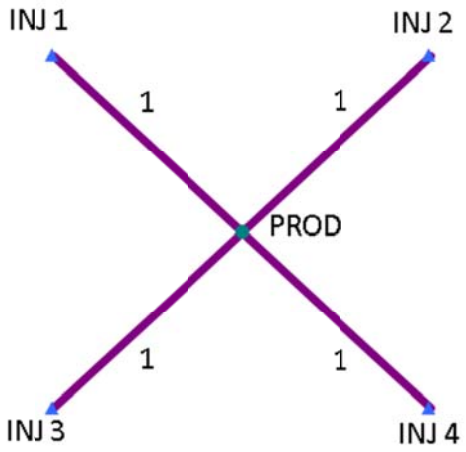

Figure 4.10 Connectivity map obtained in case 1.

Unlike the current CRM model, the time constants from the coupled CRM model change with time reflecting the saturation change. Figure 4.11 gives the coupled CRM model time constant at each month within the history match window. In general, the average time constant at small water cuts is about 127 days, while it is around 94 days at large water cuts according to the coupled CRM model.

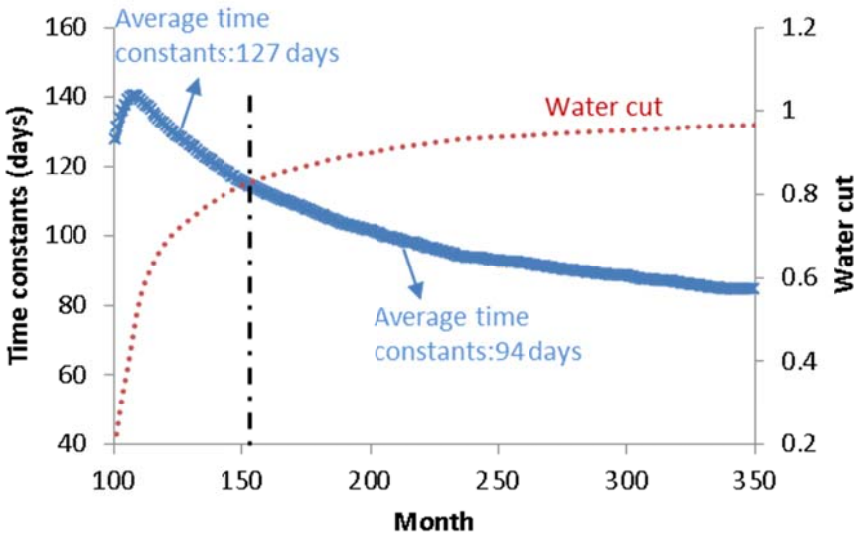

Figure 4.11 Time constants obtained in case 1.

The coupled CRM model is also able to capture the average oil saturation evolution within the drainage volume around the producer. The average and outlet oil saturations of producer 1 are in Figure 4.12. In general, the figure shows a reasonable trend that the outlet oil saturation is larger than the average oil saturation at early time when the water cut is small; whereas they approaches each other in a mature water flood stage.

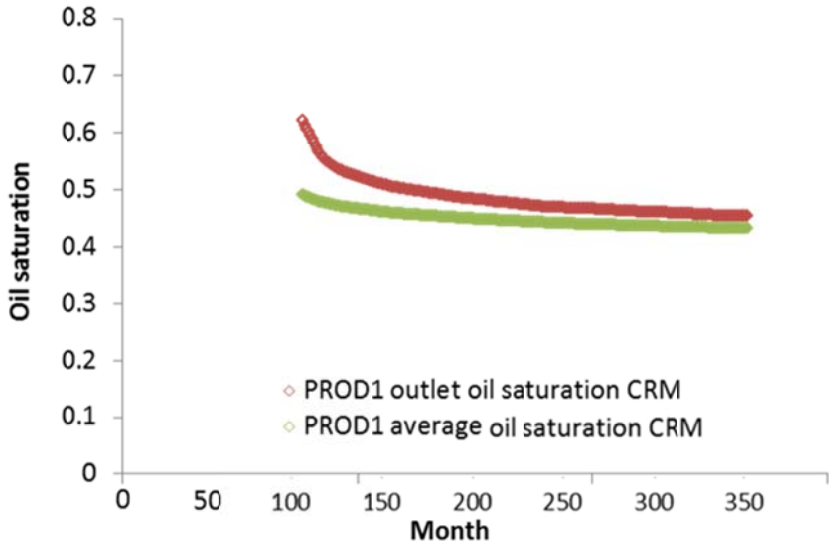

Figure 4.12 The average and outlet oil saturations in case 1.

4.2.2.3 Validation

Time Constant

In Figure 4.11, the coupled CRM model indicates that time constants are large at early time and small at late time. To verify this trend, we design two injection pulse tests,

which are introduced at early and late times of water flood, respectively, to evaluate the time constant.

Table 4.3 lists the general information of the three injection pulse tests. The first injection pulse is introduced at early time when the producer's water cut is 0.56 and the total injection pulse is 15 months long at 4000 bbl/day (see Figure 4.13). In the second pulse test, we conduct the pulse test at smaller pulse intensity of 2000 bbl/day for 15 months to see if the time constant is affected by the strength of the pulse. The third injection pulse, which is 4000 bbl/day and lasts for 10 months, is introduced at late time when the water cut is as large as 0.96 (see Figure 4.14).

The production responses to the three injection pulse tests are shown in Figures 4.13-4.15.

	Time introduced	**Producer water cut (when pulse is introduced)**	**Pulse rate in each injector (bbl/day)**	**Pulse duration in each injector (months)**
Pulse test 1	115^{th} month	0.56	1000	15
Pulse test 2	115^{th} month	0.56	500	15
Pulse test 3	336^{th} month	0.96	1000	10

Table 4.3 Injection pulse tests conducted in case 1.

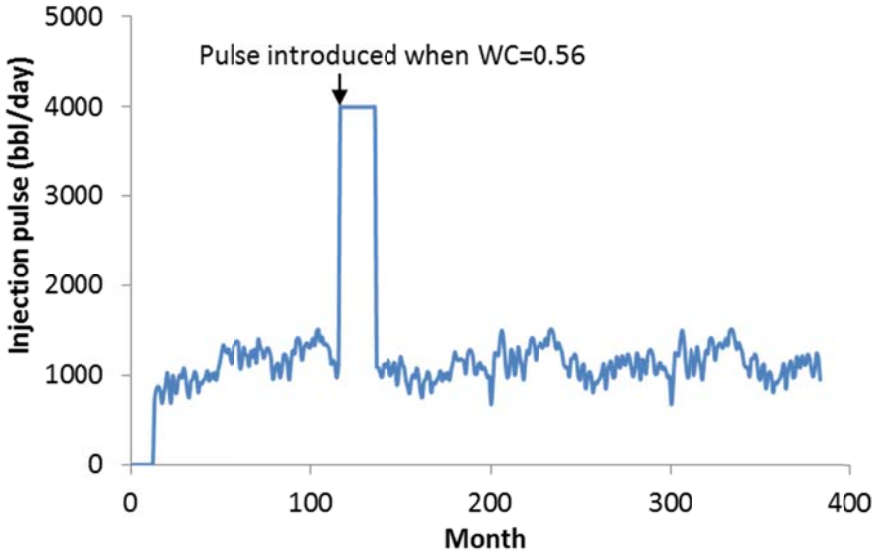

Figure 4.13 Injection pulse tests introduced at early time in case 1.

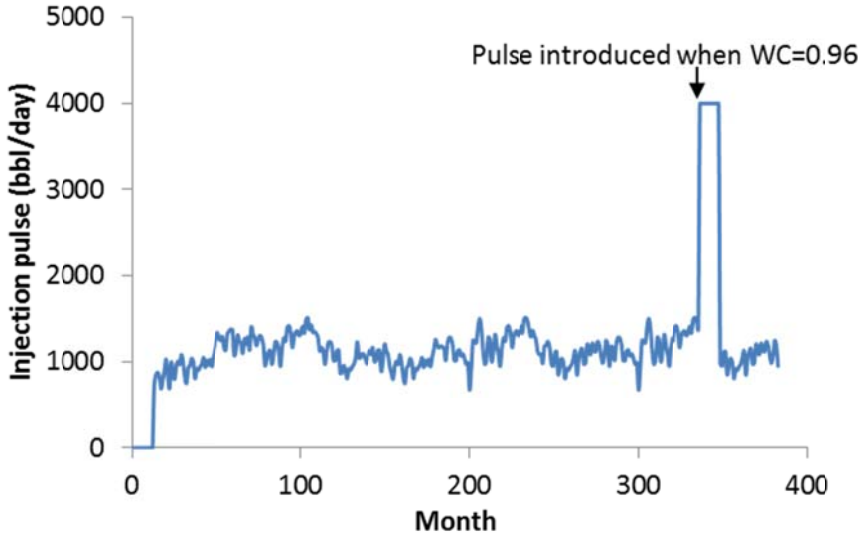

Figure 4.14 Injection pulse tests introduced at late time in case 1.

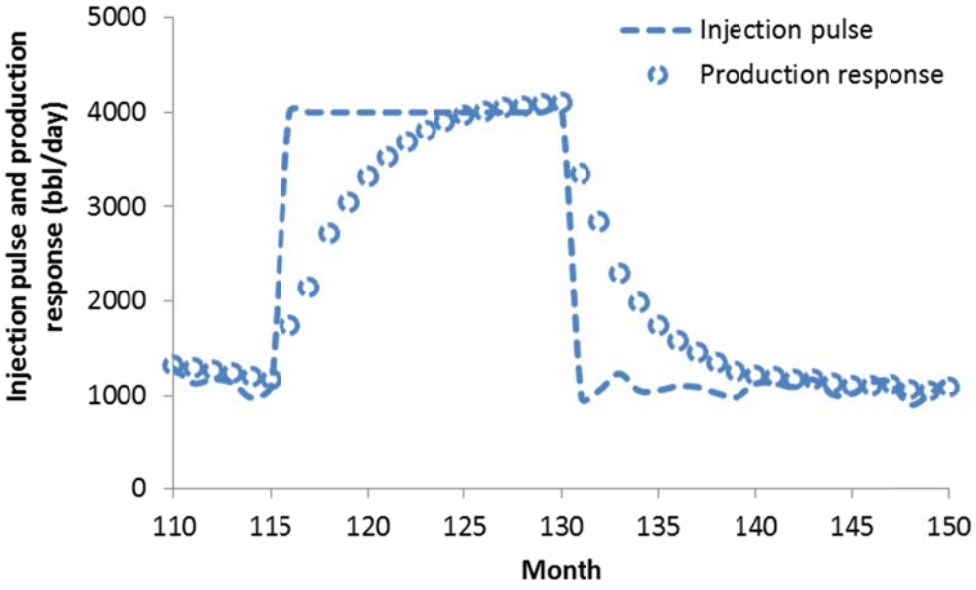

Figure 4.15 Production responses to injection pulse test 1 in case 1.

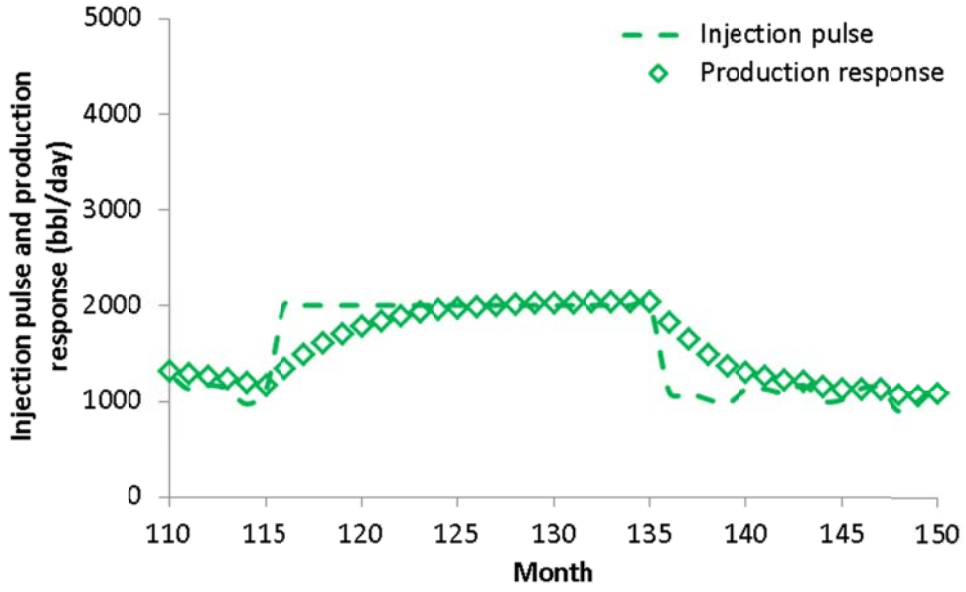

Figure 4.16 Production responses to injection pulse test 2 in case 1.

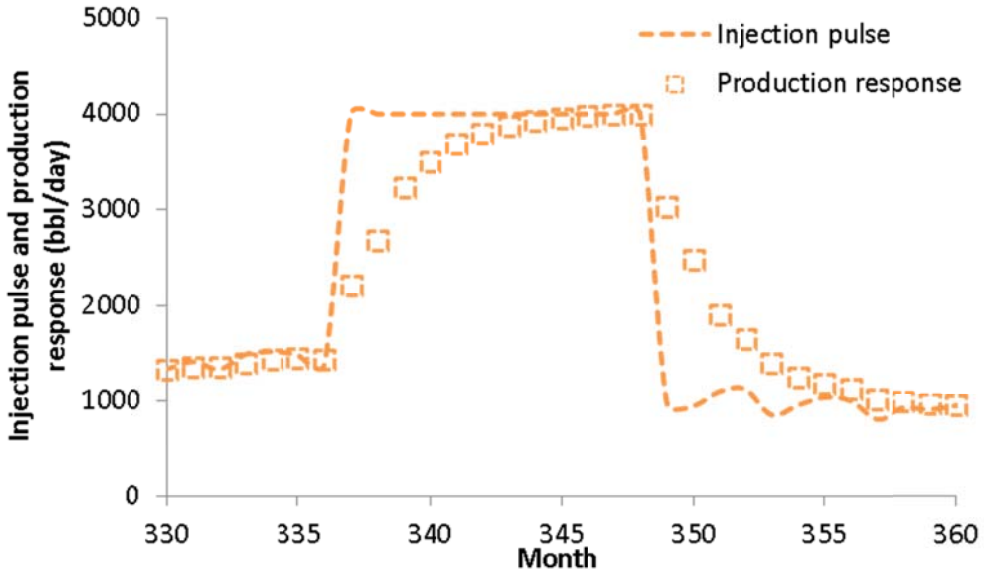

Figure 4.17 Production responses to injection pulse test 3 in case 1.

To find out the time constant, we normalize the production response as a percentage of the full response, which is defined to be the production response that is equal to the injection pulse rate. Figure 4.18 shows the normalized production response for pulse tests 1 and 2. According to Figure 4.18, it takes 119 days for the producer to reach the 63.2% production response. Therefore, the time constant is 119 days at the time when the injection pulse test is introduced regardless of the strength of the injection signal.

In the late time pulse test, it takes 270 days to reach a full production response (see Figure 4.19). The 63.2% production response corresponds to 79 days. Thus, the time constant at late time is 79 days.

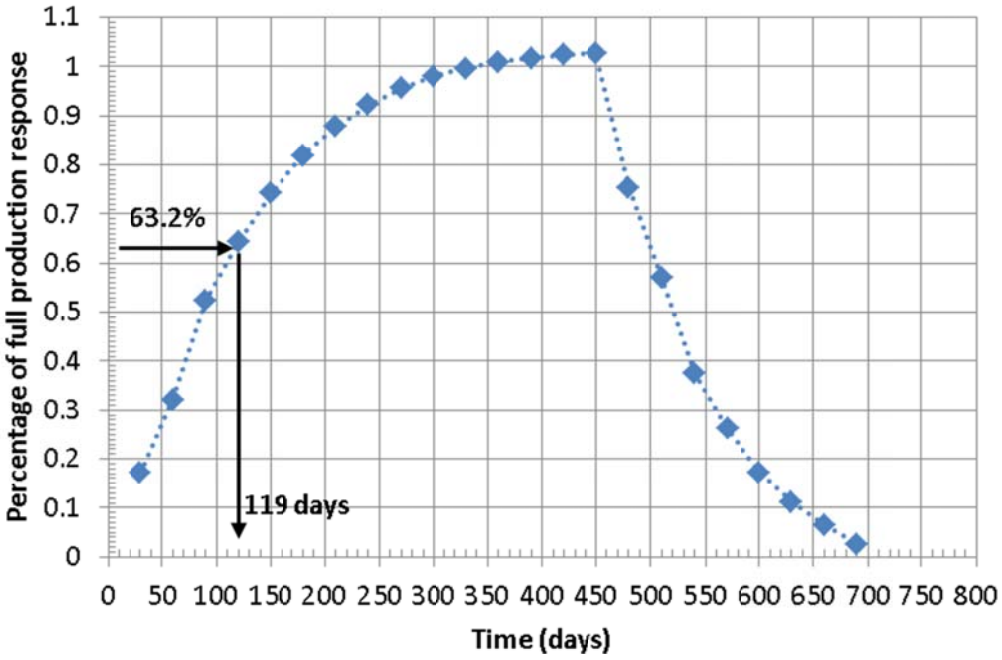

Figure 4.18 Normalized production responses vs. time at early time in case 1.

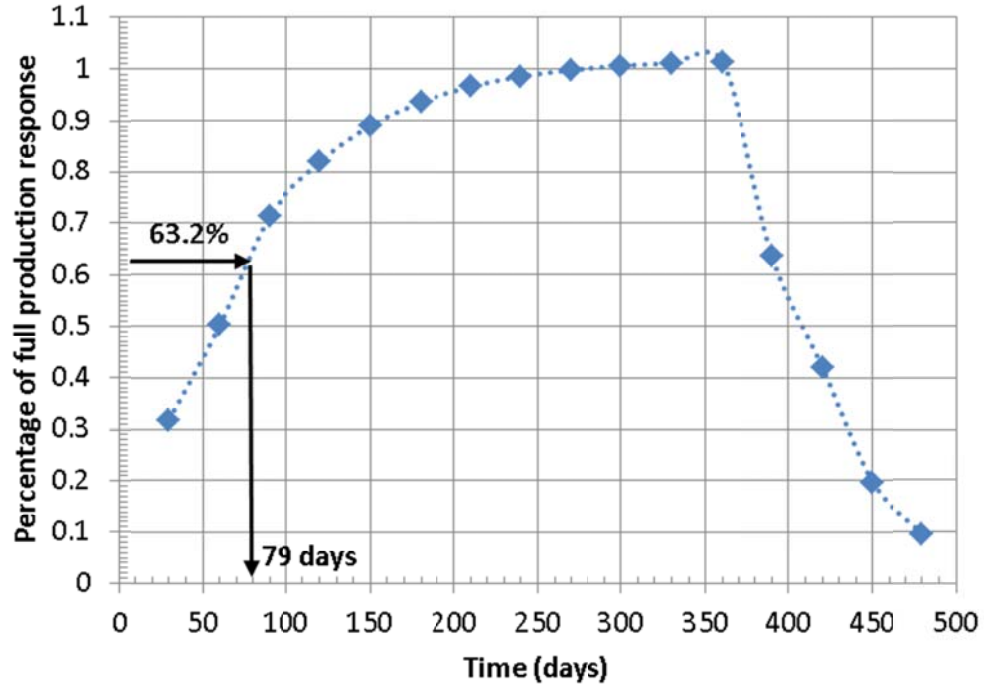

Figure 4.19 Normalized production responses vs. time at late time in case 1.

As shown in Figure 4.11, we can obtain the coupled CRM model time constant at any given time. To compare with the simulation results, we take the value of time constant at the time when injection pulses are imposed, which is the 115^{th} and the 336^{th} month, respectively.

Table 4.4 summarizes the time constants from the coupled CRM model and reservoir simulation. Both methods show the trend of time constants decreasing with time. In each water flood stage, they come up with consistent time constant results even though the time constant values are not exactly the same.

	The Coupled CRM	Reservoir Simulation
Time constant at early time (days)	130	118
Time constant at late time (days)	84	79

Table 4.4 Time constants from the coupled CRM and reservoir simulation in case 1.

Saturation

In a reservoir simulation, the saturation equation is solved on each grid block and consequently each cell has a saturation value. Figure 4.20 shows an oil saturation distribution after 20 years of water flooding from the reservoir simulation. In this case, the drainage volume of producer 1 is the whole reservoir. Thus, we take the average value of oil saturation in all grid blocks and use it to represent the average saturation within the drainage volume of the producer. The outlet saturation is the oil saturation of the grid block where the producer is located.

Figure 4.21 shows the saturation from both the coupled CRM model and reservoir simulation. The average saturation from the coupled CRM model matches the simulation results very well in the fitting window. As discussed previously, the average oil saturation from the coupled CRM model is calculated from oil material balance and therefore is not a fitting result. Figure 4.21 also presents that the CRM outlet oil saturation matches the simulated oil saturation profile satisfactorily in this homogeneous case.

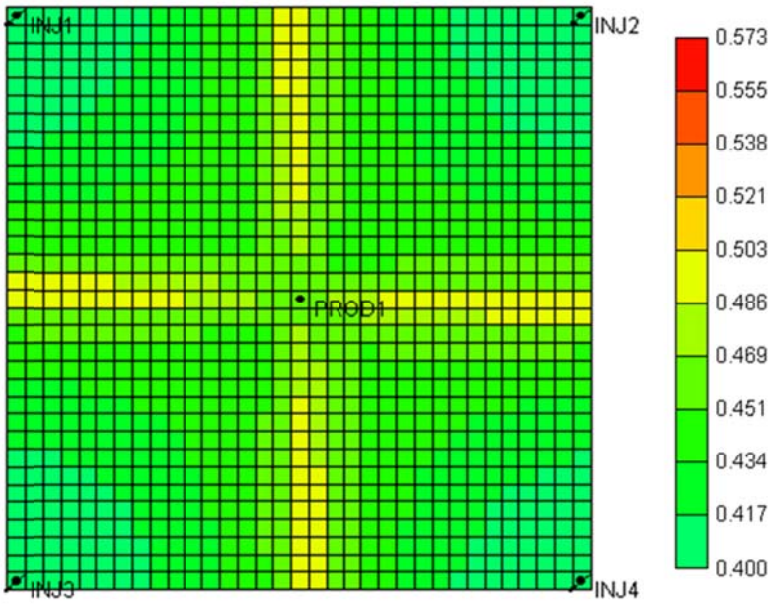

Figure 4.20 Oil saturation distribution after 20 years of water flooding in case 1.

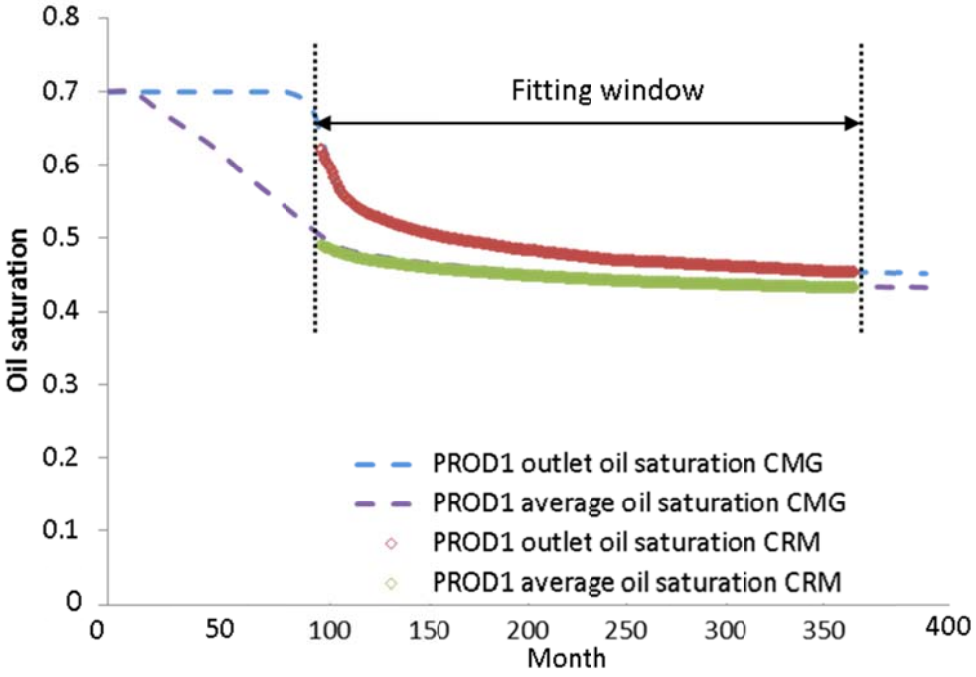

Figure 4.21 Average and outlet oil saturations from the coupled CRM model and reservoir simulation in case 1.

4.2.3 Summary

In case 1, we focus on demonstrating the history match capability of the coupled CRM model and validating the obtained model parameters using a commercial reservoir simulator. The results show that the coupled CRM is able to capture well pair connectivities and describe time-varying time constants and saturation. The time constants and saturation from the CRM model agree well with the reservoir simulation results in this homogeneous case.

4.3 CASE 2: A HETEROGENEOUS RESERVOIR WITH A SINGLE PRODUCER

A real reservoir is, in general, heterogeneous. This means that petrophysical properties, such as permeability, porosity and fluid saturation, will vary spatially. Variability of rock and fluid properties is a reality that must be dealt with in reservoir modeling and performance prediction. In this second case study, the impact of reservoir heterogeneity on the coupled CRM model is studied. Through the application of the coupled CRM model, its validity is further tested in the presence of reservoir heterogeneity.

4.3.1 General Reservoir Information

The data set we use to create the permeability field is the Stanford V dataset (Mao and Journel, 1999). It is a complete 3D dataset representing a clastic reservoir made up of meandering fluvial channels with crevasse splays and levies in a mud background. This dataset provides a quasi-exhaustive sampling of petrophysical properties over multiple layers. An open-source computer package (Stanford geostatistical modeling software or SGEMS) is used to perform sequential Gaussian simulation (Nowak and Verly, 2005) to generate different permeability realizations. In this case study, we only take a part of the permeability data (see Figure 4.22) and use them in the reservoir simulator to create a two-dimensional heterogeneous reservoir with varying depth (see Figure 4.23). Key reservoir and fluid parameters of this field are summarized in Table 4.5.

The synthetic field has 4 injectors and 1 producer. The producer is vertically completed and is operating under a constant bottom-hole pressure constraint of 250 psi. Similar to the previous case study, there is no injection in the first 12 months. A secondary water injection then follows after a year of depletion and continues till the end

of the simulation. The total simulation time is 283 months with one month per time step. The production and injection data are monthly data. These data are noise free.

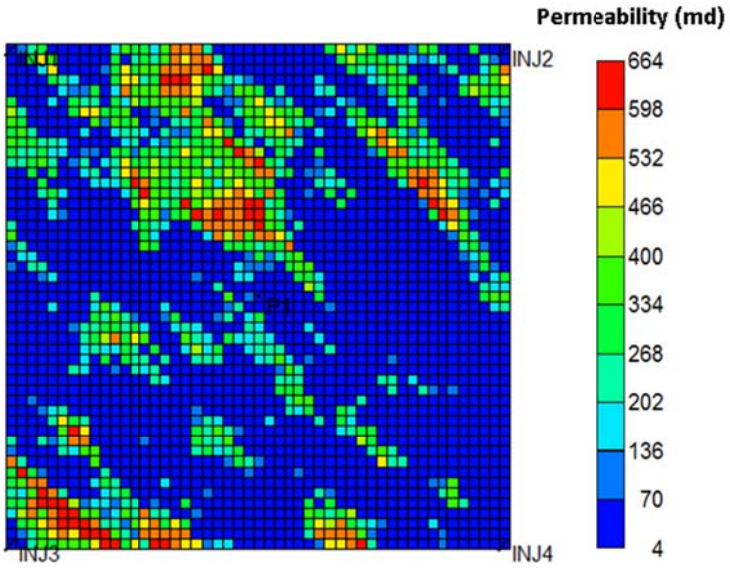

Figure 4.22 Reservoir permeability distributions in case 2.

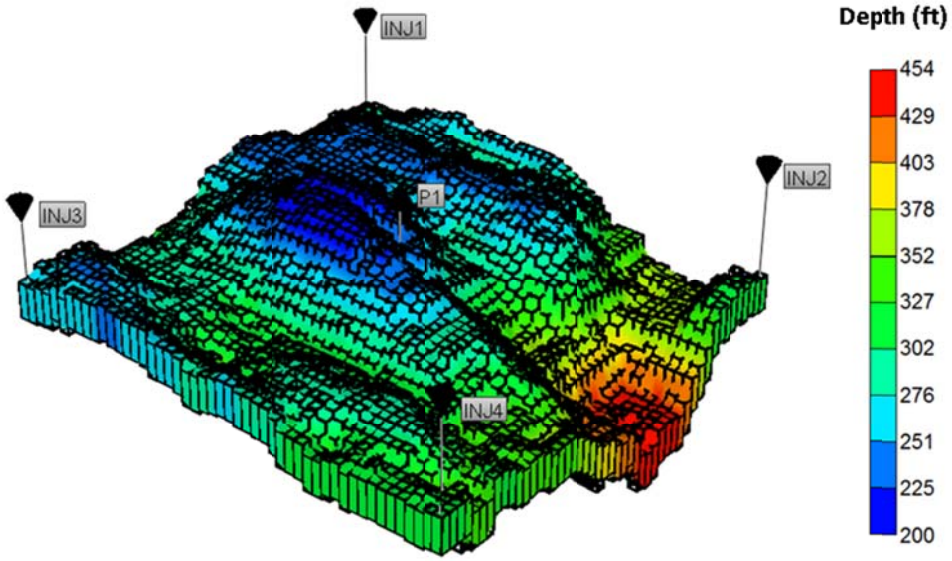

Figure 4.23 Reservoir depths in case 2.

Parameters	Value
Number of grid blocks	49×49×1
Grid sizes (ft)	40×40×50
Porosity	0.2
Oil compressibility (psi^{-1})	5×10^{-5}
Water compressibility (psi^{-1})	1×10^{-6}
Rock compressibility (psi^{-1})	1×10^{-6}
Water relative permeability	$k_{rw}^{o}\left(\frac{S_w - S_{wr}}{1 - S_{wr} - S_{or}}\right)^2$
Oil relative permeability	$k_{ro}^{o}\left(\frac{1 - S_w - S_{or}}{1 - S_{wr} - S_{or}}\right)^2$
Irreducible water saturation	0.3
Residual oil saturation	0.4
End-point water relative permeability	0.3
End-point oil relative permeability	1
Water viscosity (cp)	0.72
Oil viscosity (cp)	3.25
Initial reservoir pressure (psi)	2000

Table 4.5 Key reservoir and fluid parameters in case 2.

4.3.2 Application of the Coupled CRM Model

4.3.2.1 The Coupled CRM Inputs

In case 2, we use the fully-coupled scheme in the coupled CRM model. Besides the production and injection data, other required inputs are summarized in Table 4.6.

Input		Value
Reservoir/fluid properties	μ_w (cp)	0.72
	μ_o (cp)	3.25
	k_{rw}	$k_{rw}^o \left(\frac{S_w - S_{wr}}{1 - S_{wr} - S_{or}} \right)^2$
	k_{ro}	$k_{ro}^o \left(\frac{1 - S_w - S_{or}}{1 - S_{wr} - S_{or}} \right)^2$
	S_{wr}	0.3
	S_{or}	0.4
	k_{rw}^o	0.3
	k_{ro}^o	1
	c_f (psi^{-1})	1×10^{-6}
	c_w (psi^{-1})	1×10^{-6}
	c_o (psi^{-1})	5×10^{-5}
	c_t (psi^{-1})	2.65×10^{-6}

Table 4.6 The coupled CRM model inputs in case 2.

4.3.2.2 History Match

The time window for the history match is from the 55th to the 250th month (see Figure 4.24), which starts immediately after water breakthrough and ends when the producer's water cut reaches 0.95.

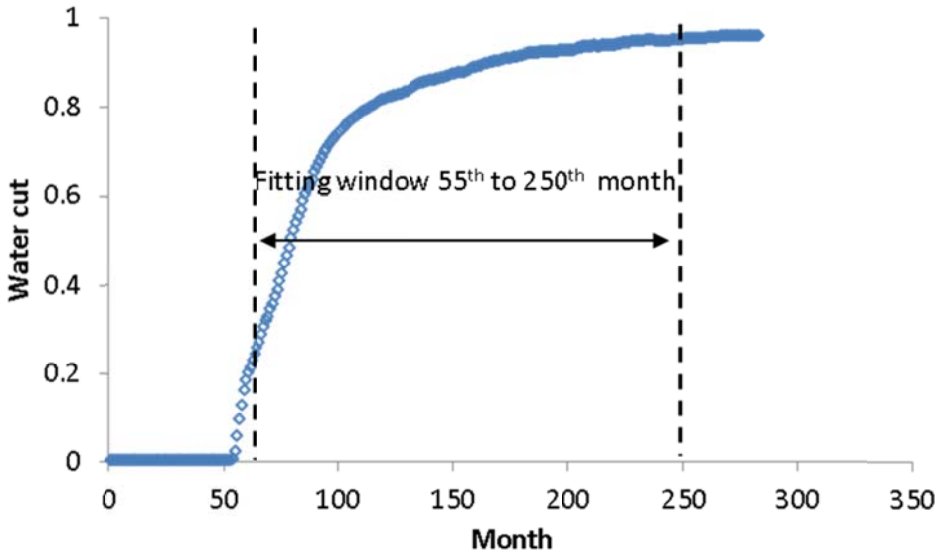

Figure 4.24 The history match time window used in case 2.

Figure 4.25 gives the history match results of the total production rates of the producer. The calculated total production rate matches the observed data satisfactorily with errors less than 2%. The coefficient of determination is 0.99 indicating an excellent fit. The reservoir is bounded and there is no injection loss possible. Therefore, similar to the previous case study, the connective is 1 between all the injector-producer pairs, as expected (see Figure 4.26).

Figure 4.27 gives the time-varying time constants that reflect the saturation impact. The average time constant is 126 days when water cut is smaller than 0.8. When well water cut reaches above 0.8, the time constant continues to decrease because of smaller total reservoir compressibility and larger total fluid mobility. The average time constant is about 95 days at the late time.

The average oil saturation of producer 1 within its drainage volume is in Figure 4.28, which also gives the outlet oil saturation. In general, the outlet oil saturation is

larger than the average oil saturation in early time when water cut is small. In mature water floods, the outlet and average oil saturations approach each other.

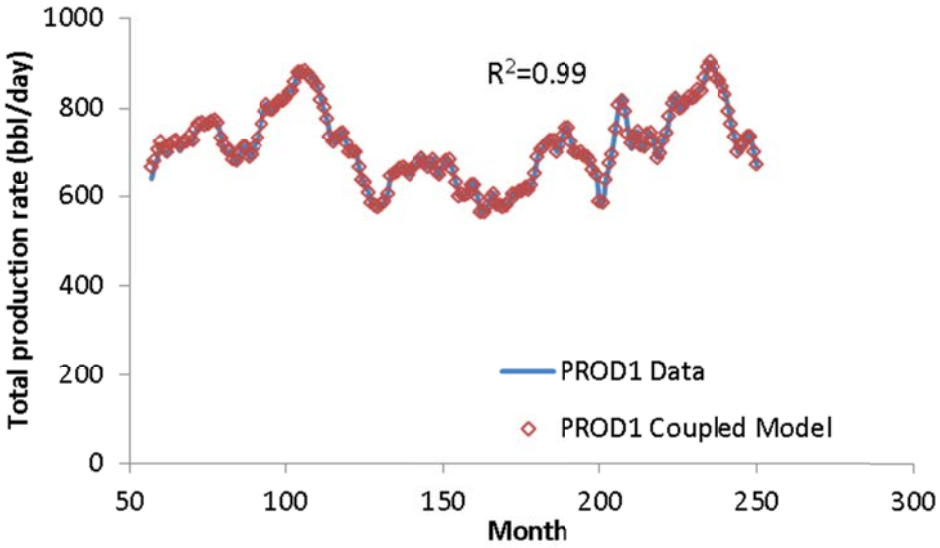

Figure 4.25 The total production history match in case 2.

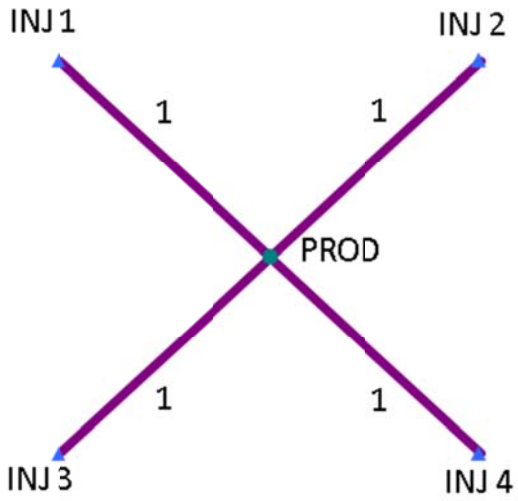

Figure 4.26 Connectivity map obtained in case 2.

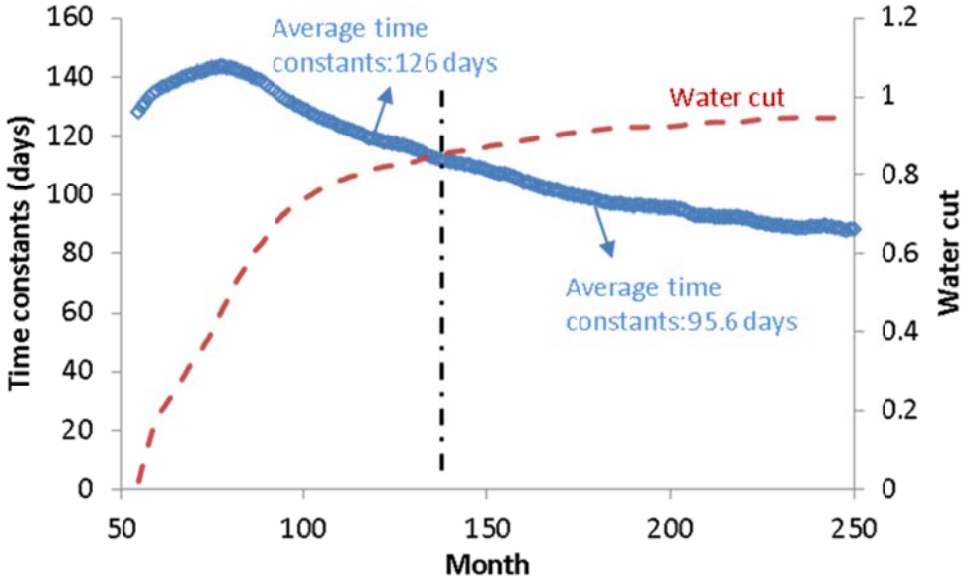

Figure 4.27 Time constants obtained in case 2.

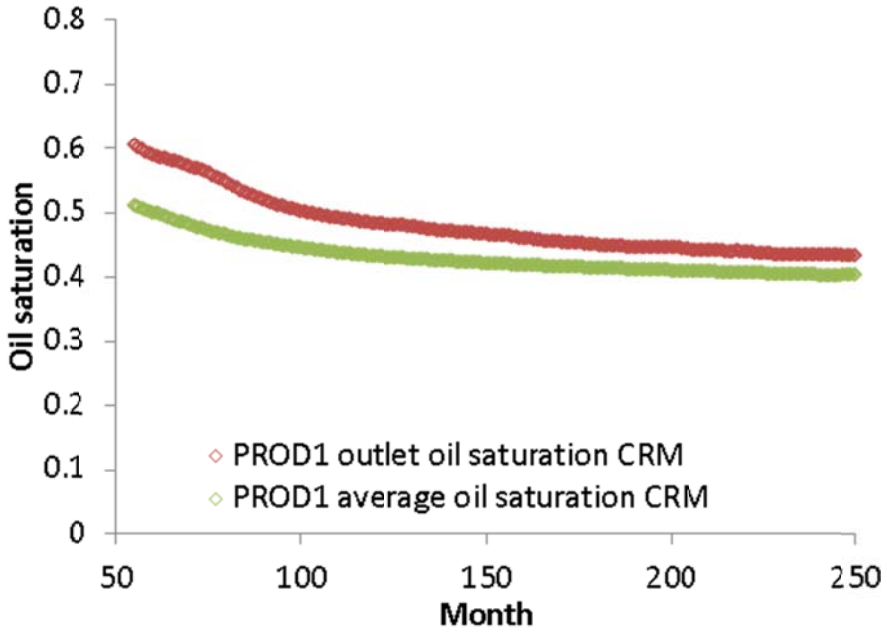

Figure 4.28 Average and outlet oil saturations obtained in case 2.

4.3.2.3 Validation

Time Constant

Table 4.7 summarizes the two injection pulse tests that are performed in the reservoir simulation. The first injection pulse is introduced when the water cut at the producer is 0.15. The production response is shown in Figure 4.29 and the time constant is 126 days when the production response reaches 63.2% of the full response.

A second injection pulse is introduced when the water cut at the producer is 0.95. The production response is in Figure 4.30. It takes 81 days for the production to reach 63.2% of the full response. Therefore the time constant is 81 days.

	Time introduced	**Producer water cut (when pulse is introduced)**	**Pulse rate in each injector (bbl/day)**	**Pulse duration in each injector (months)**
Pulse test 1	61^{th} month	15%	1000	15
Pulse test 2	217^{th} month	95%	1000	15

Table 4.7 Injection pulse tests conducted in case 2.

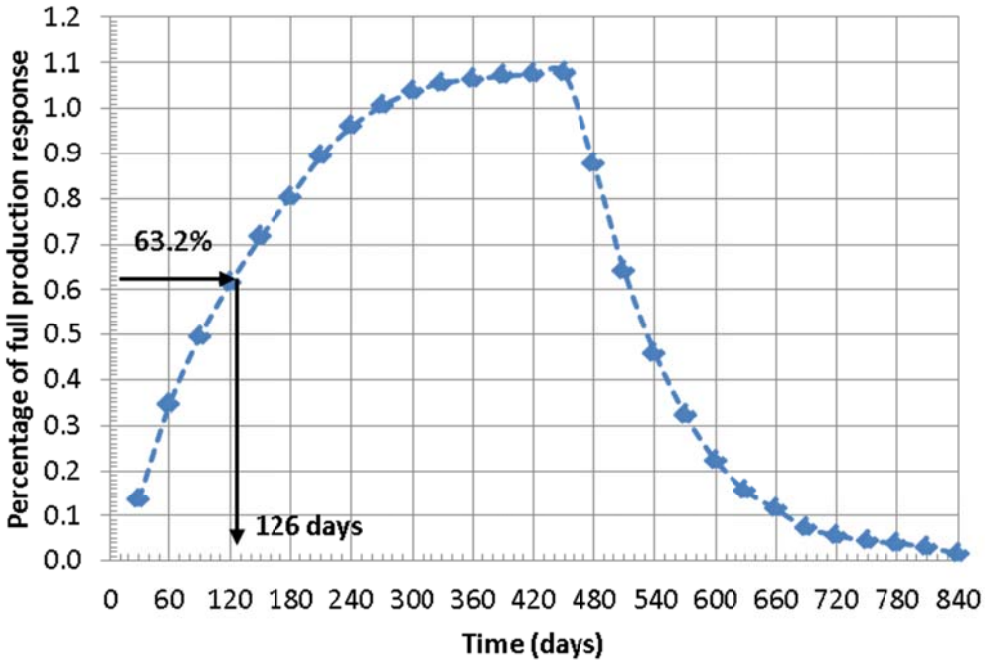

Figure 4.29 Normalized production response vs. time at early time in case 2.

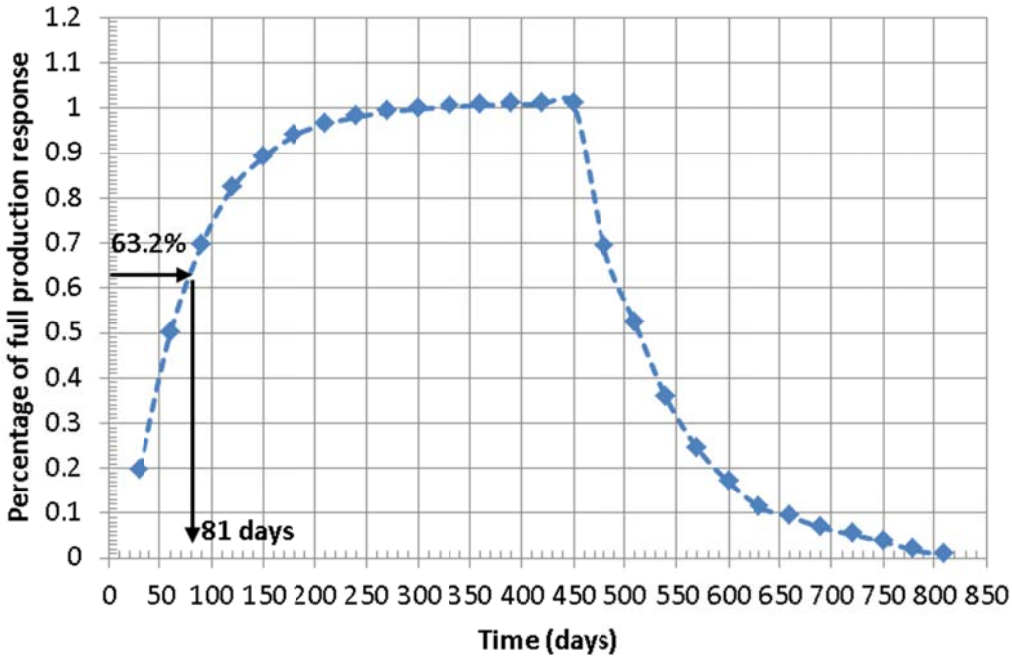

Figure 4.30 Normalized production response vs. time at late time in case 2.

Table 4.8 summarizes the time constants from the coupled CRM model and the reservoir simulation. The CRM time constants are taken at the 61th and the 217th month, respectively, when injection pulse tests are carried out. Overall, the time constants agree very well with each other in both early and late time.

There is no obvious impact to the time constant caused by reservoir heterogeneity in this case. This is because the effects of reservoir heterogeneity are contained in the production response, which is the input of the coupled CRM model. Since time constants are estimated by history matching the production rates, they should also contain the information of heterogeneity indirectly.

	The Coupled CRM	Reservoir Simulation
Time constant at early time (days)	134	126
Time constant at late time (days)	90	81

Table 4.8 Time constants from the coupled CRM and reservoir simulation in case 2.

Saturation

Figure 4.31 shows the average oil saturation from the coupled CRM model and reservoir simulation. One can observe a discrepancy between the two curves; whereas they should agree with each other as in case 1. We also observe that the two curves are almost parallel to each other. This difference is caused by the reservoir heterogeneity.

Heterogeneity can lead to non-uniform fluid displacement front leaving behind area un-swept in a water-oil displacement. Figure 4.33 shows the evolution of the oil saturation distribution with time from the reservoir simulation. We observe that some

portions of the reservoir in the east and west directions were at the original oil saturation even after a fairly long time of displacement. Therefore, we recognize the circled areas in Figure 4.33 to be the un-swept region as the oil saturation stayed intact after 22 years of water flood. If we discount these un-swept regions and re-evaluate field average oil saturation (see Figure 4.31) in reservoir simulation, the new average oil saturation are very close to the CRM estimated average oil saturation, which indicates that the CRM average oil saturation is the effective oil saturation in a heterogeneous case. This is because the coupled CRM model is based on oil material balance using the oil production rate. The bypass oil is trapped in the reservoir and is not contributing to the oil production. Consequently, it is not captured by the coupled CRM model. Figure 4.32 is the outlet oil saturation from the coupled CRM model, which shows a slight mismatch since the outlet saturation is calculated from the average oil saturation.

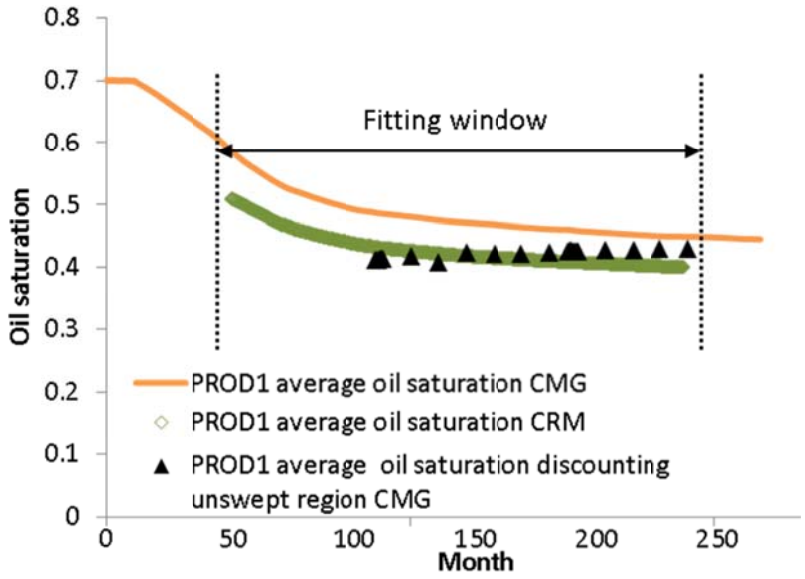

Figure 4.31 The average oil saturation from coupled CRM model and reservoir simulation in case 2.

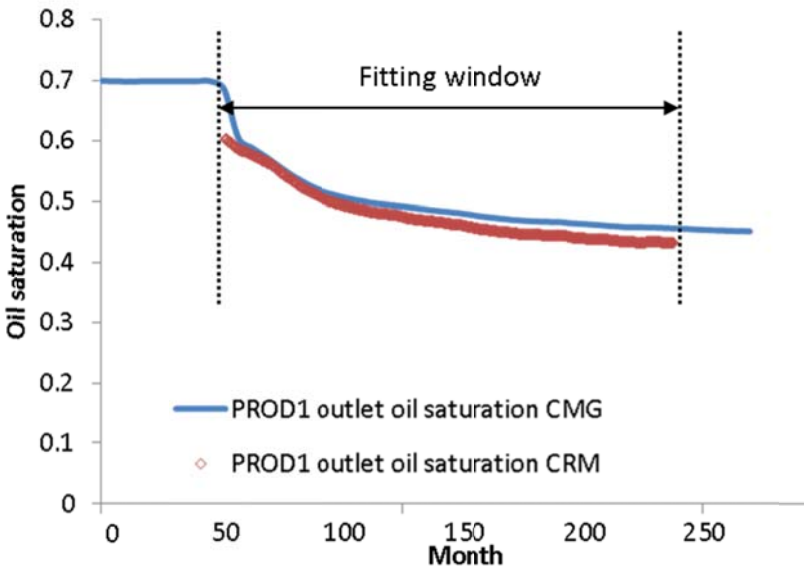

Figure 4.32 The outlet oil saturation from the coupled CRM model and reservoir simulation in case 2.

4.3.3 Summary

In case 2, we applied the coupled CRM model to a heterogeneous reservoir. The time constants obtained are in good agreement with the simulation results, which further confirmed that the time constant should vary with time. There is no obvious impact to the time constant caused by reservoir heterogeneity as the time constants contain the information of heterogeneity indirectly through the production response.

The average oil saturation from the coupled CRM model is the effective average oil saturation because it is calculated from oil material balance, which is confirmed by comparing the CRM average saturation with the reservoir simulation average saturation discounting un-swept regions.

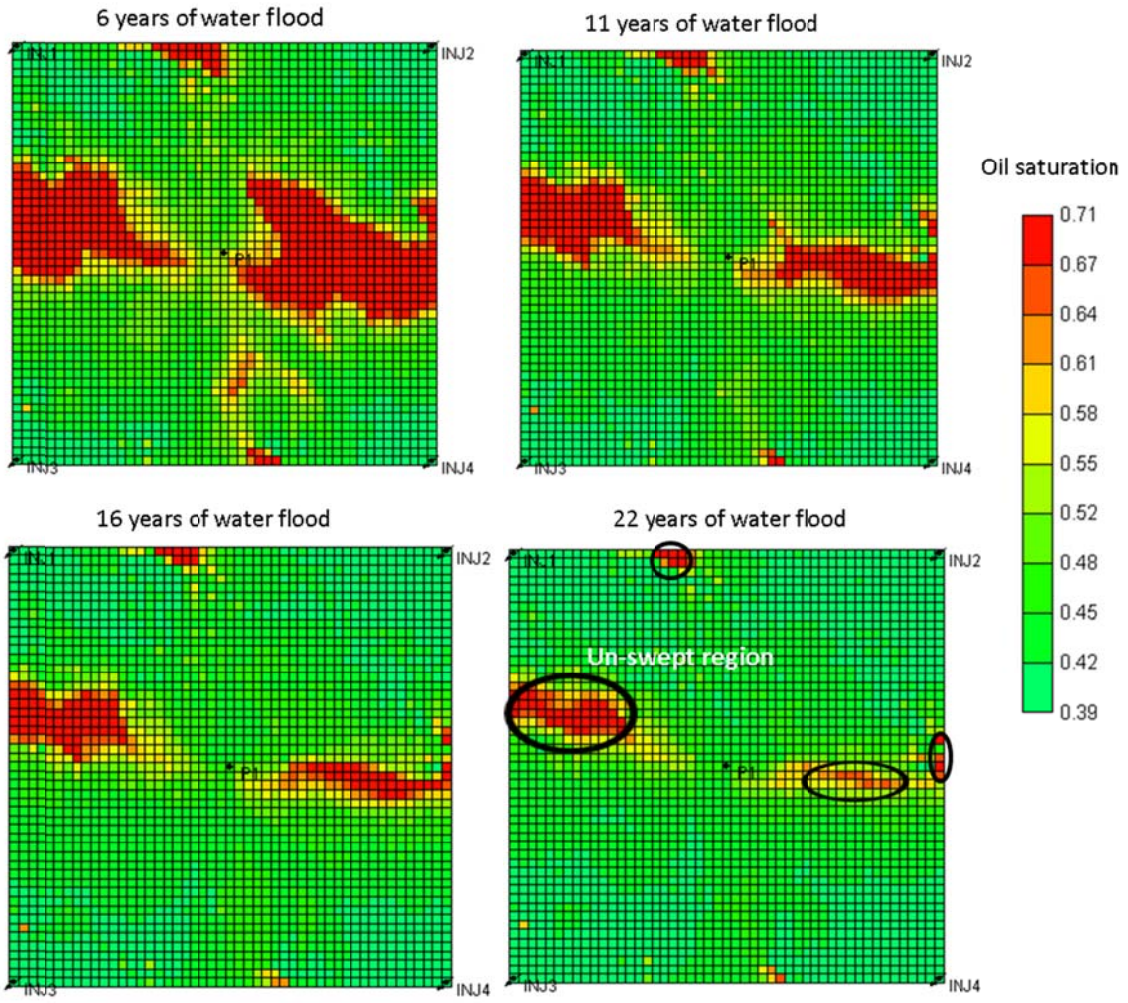

Figure 4.33 Oil saturation distributions at different stages of water flood in case 2.

4.4 CASE 3: A FIVE SPOT HOMOGENEOUS RESERVOIR

One of the advantages of the CRM model is its capability of optimizing water injection to maximize oil production. To suggest injection scheme in the future, the CRM model should be able to predict both the total and oil production rates accurately. The third case study is dedicated to a comparison among three fractional flow models (Gentil model, Koval model, and the coupled CRM model) and their applications in both mature

and immature water floods. Advantages and limitations of these fractional flow models are analyzed and discussed.

4.4.1 General Reservoir Information

This case is a five-layer homogeneous reservoir. Key reservoir and fluid parameters are summarized in Table 4.9. There are 5 injectors and 4 producers under a five-spot injection pattern (see Figure 4.34) in this field. All producers are vertically completed through all layers and are operating under a constant bottom-hole pressure constraint of 250 psi. Figures 4.35 and 4.36 show the injection rates and production responses, respectively. All producers behave similarly since the reservoir is homogeneous and the well pattern is symmetric. The numerical simulation extends to 283 months, with one month for each time step.

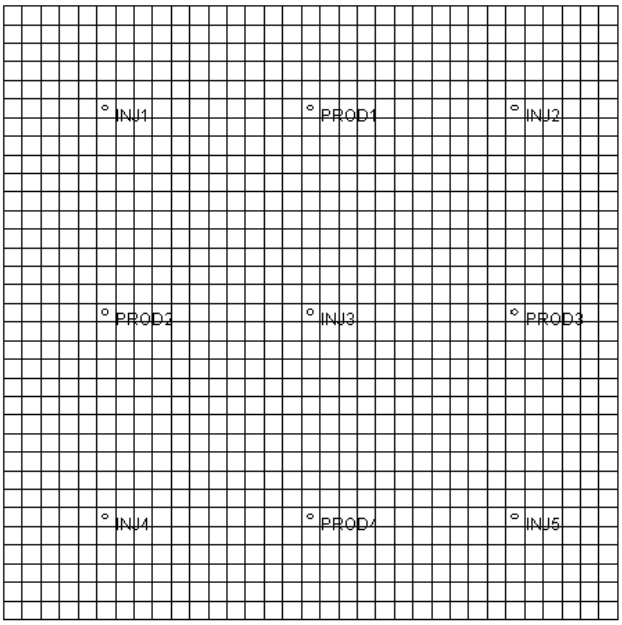

Figure 4.34 Well locations in case 3.

Parameters	Value
Number of grid blocks	33×33×5
Grid block sizes (ft)	77.5×77.5×70
Permeability (md)	200
Porosity	0.2
Oil compressibility (psi^{-1})	3×10^{-5}
Water compressibility (psi^{-1})	1×10^{-6}
Rock compressibility (psi^{-1})	1×10^{-6}
Water relative permeability	$k_{rw}^{o}\left(\frac{S_w - S_{wr}}{1 - S_{wr} - S_{or}}\right)^2$
Oil relative permeability	$k_{ro}^{o}\left(\frac{1 - S_w - S_{or}}{1 - S_{wr} - S_{or}}\right)^2$
Irreducible water saturation	0.3
Residual oil saturation	0.4
End-point water relative permeability	0.3
End-point oil relative permeability	1
Water viscosity (cp)	0.72
Oil viscosity (cp)	1.63
Initial reservoir pressure (psi)	1250

Table 4.9 Key reservoir and fluid parameters in case 3.

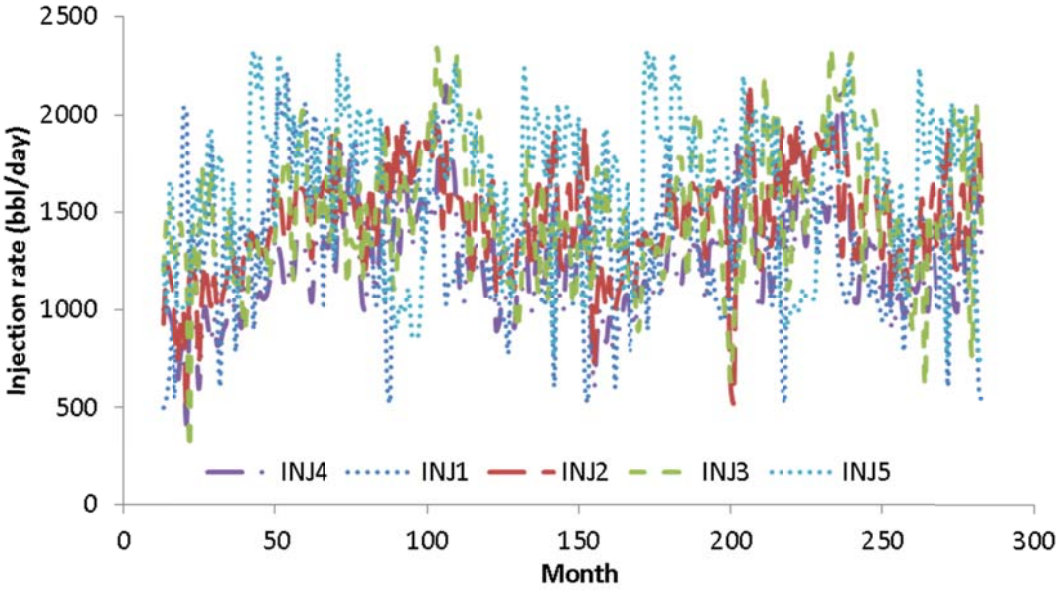

Figure 4.35 Injection rates in case 3.

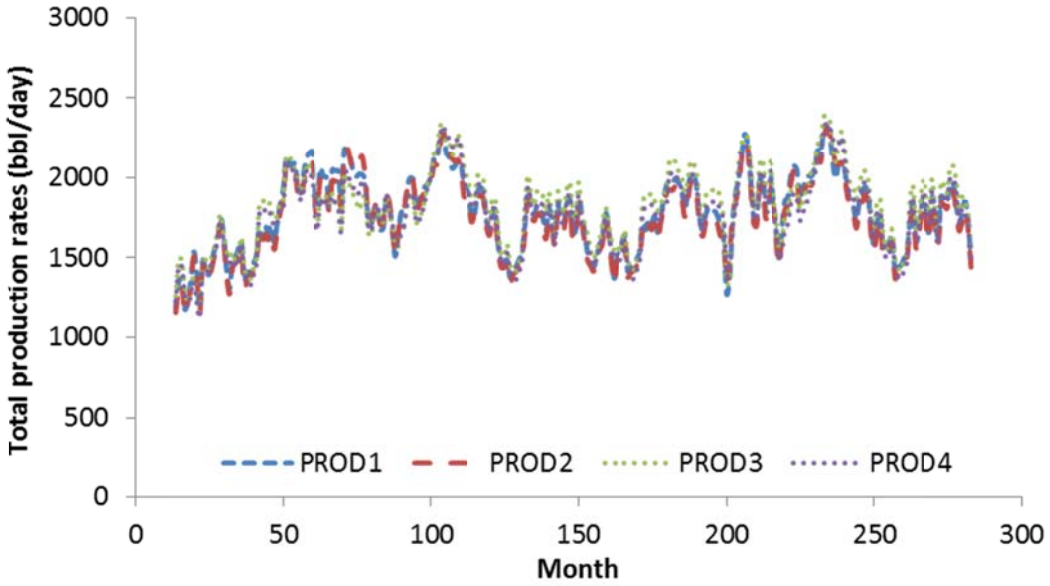

Figure 4.36 Total production responses in case 3.

4.4.2 Application of the Fractional Flow Models

We discuss the application of three fractional flow models including Gentil model, Koval model, and the coupled CRM model. Two time windows, which represent different stages of water flood, are selected for application since the flow characteristics are distinct under different displacement phases (see Figure 4.37).

In the mature water flood, the reservoir system turns less compressible and the fluid flow can be approximated as single-phase flow. The water cut is usually large and approaching one asymptotically (see Figure 4.37). Most empirical fractional flow models are suitable in this mature water flood region. However, immature water flood usually implies a strong two-phase flow region, when the water/oil saturation change is significant. The oil production rate is usually large at this stage and most empirical fractional flow models suffer by not considering the saturation impact.

For the purpose of comparison, we select the same time window to construct fractional flow models and further use them for prediction (see Table 4.10).

	Time window for constructing fractional flow model (month)	**Prediction window (month)**
Mature water flood	75-115	116-125
Immature water flood	150-250	251-275

Table 4.10 Summary of time windows for fractional flow models in case 3.

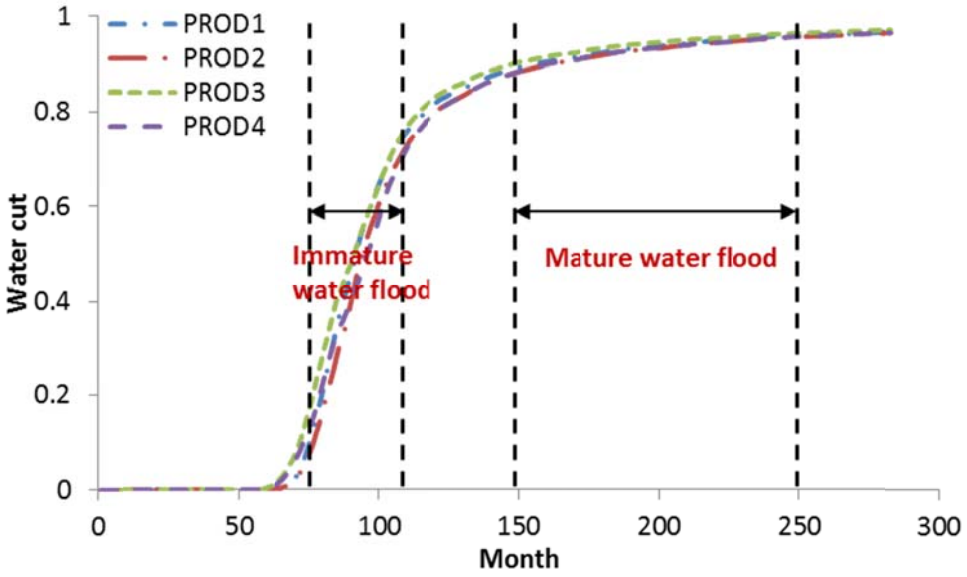

Figure 4.37 Time windows to apply the fractional flow models in case 3.

4.4.2.1 Gentil Model

The fractional flow model proposed by Gentil (2005) is used in the current CRM model to separate oil production from the total production. It is an empirical power law relationship between water-oil ratio and the cumulative water injected. According to Gentil, the water cut of a given producer has the form of:

$$f_w = 1 - \frac{1}{1 + aW_i^b} \qquad 4.2$$

where a and b are regression parameters that are to be determined by history match, and W_i is the cumulative water injected from all injectors that are connected to a producer, which is defined as:. $W_i = \sum_i f_{ij} I_i$.

The inherent assumption in the Gentil model is a linear relationship between the natural logs of water oil ratio (WOR) and cumulative water injection.

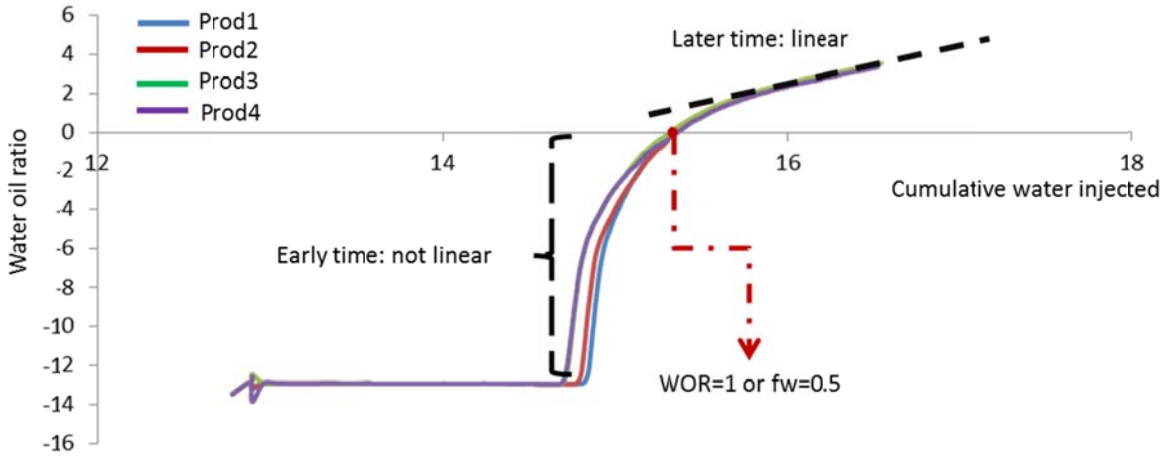

Figure 4.38 Natural logs of cumulative water injection vs. water oil ratio in case 3.

Figure 4.38 shows the natural log of cumulative water injection and water-oil ratio for each producer in this synthetic five-spot case. At early time, there is no linear relationship existing between the natural logs of cumulative water injected and water-oil ratio. The linearity doesn't appear until the water cut exceed 0.7, which limits this model to be only ideal for the mature water flood region.

In the following section, we demonstrate the application of the Gentil model in both mature and immature water flood windows mentioned above. Prior to the application of the fractional flow model, the current CRM model is used first to achieve connectivities f_{ij} between well pairs in the history match window (see Table 4.10); hence the cumulative injection W_i in Eq. 4.2 can be evaluated.

Mature Water Flood

Since all producers behave similarly in this field, we only discuss the results of producer 1. Figure 4.39 shows the oil production history match and prediction results of producer 1, both of which are satisfactory at this mature water flood stage. Figure 4.40

confirms that the relationship between the natural logs of cumulative water injection and water-oil ratio is linear as fitted. The average relative errors in oil rate prediction are below 5% in all producers (see Figure 4.41).

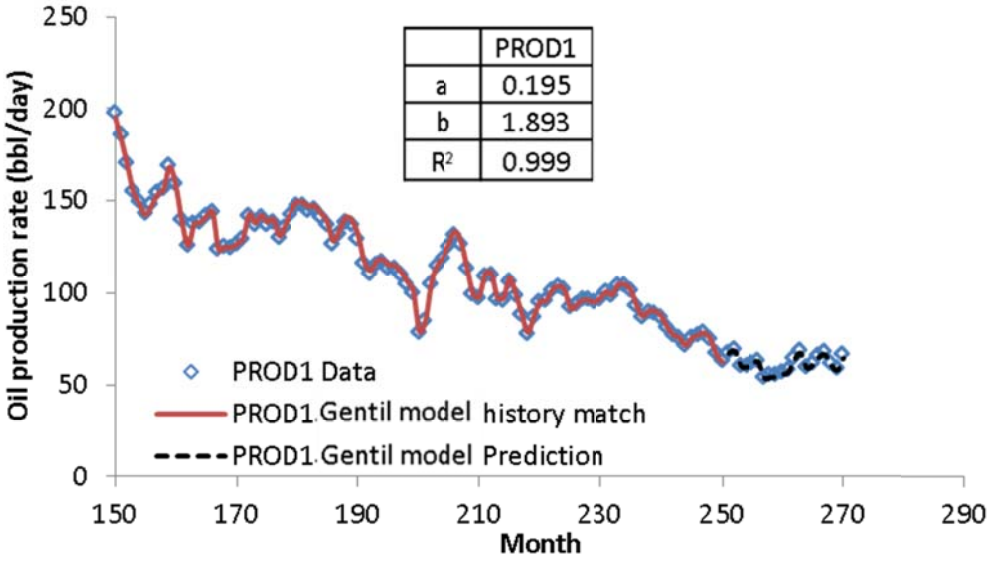

Figure 4.39 History match and prediction results of producer 1 using Gentil model in the mature flood time window in case 3.

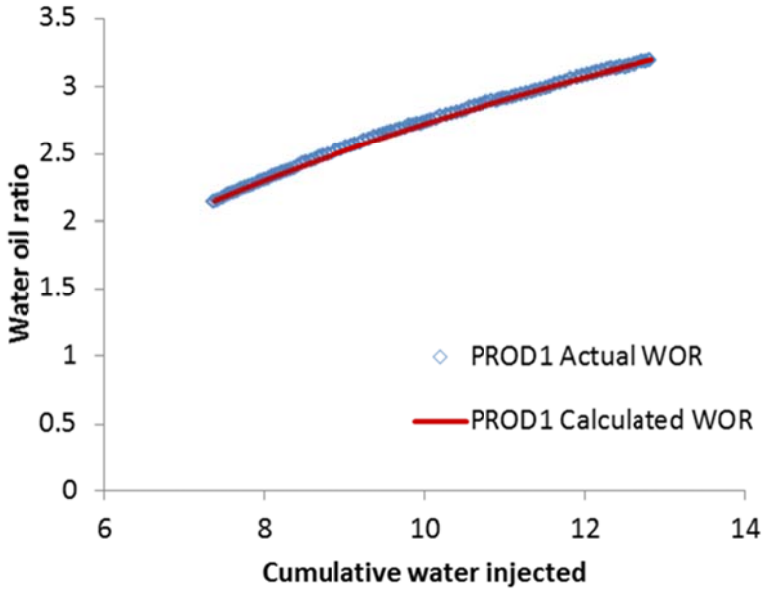

Figure 4.40 Actual and calculated cumulative water injected vs. WOR of producer 1 using Gentil model in the mature flood time window in case 3.

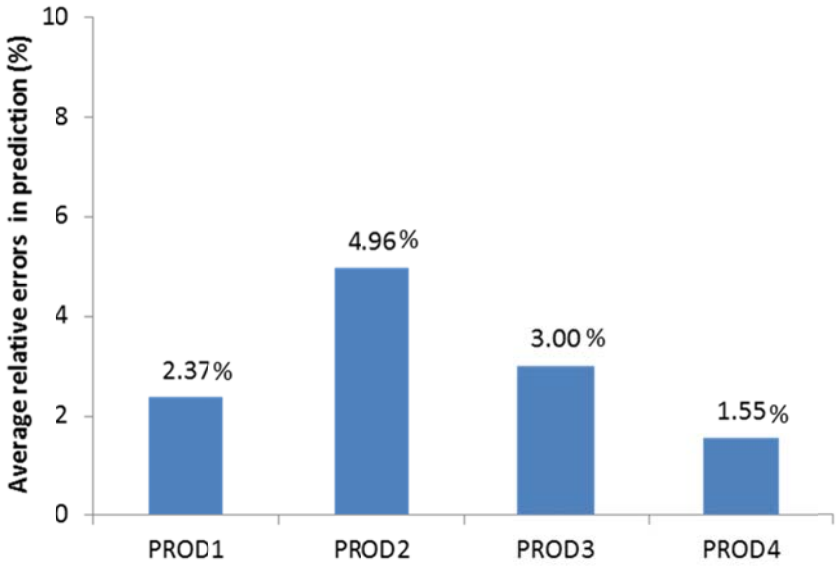

Figure 4.41 Average relative errors in oil rate prediction using Gentil model in the mature flood time window in case 3.

Immature Water Flood

Figure 4.42 gives the oil production history match and prediction results of producer 1 in an immature water flood. The fits of oil production are acceptable since we have minimized the difference between the calculated and observed rates, even though the model attempts to fit the relationship between the natural logs of cumulative water injected and WOR with a straight line while the actual correlation is nonlinear (see Figure 4.43). However, the model's failure to capture the nonlinearity results in an inaccurate prediction. Figure 4.44 shows the oil rates prediction quality is not satisfactory with average relative errors around 20% in producers 3 and 4, and 30% in producers 1 and 2. With these large errors, the model is not suitable for optimization purpose any more.

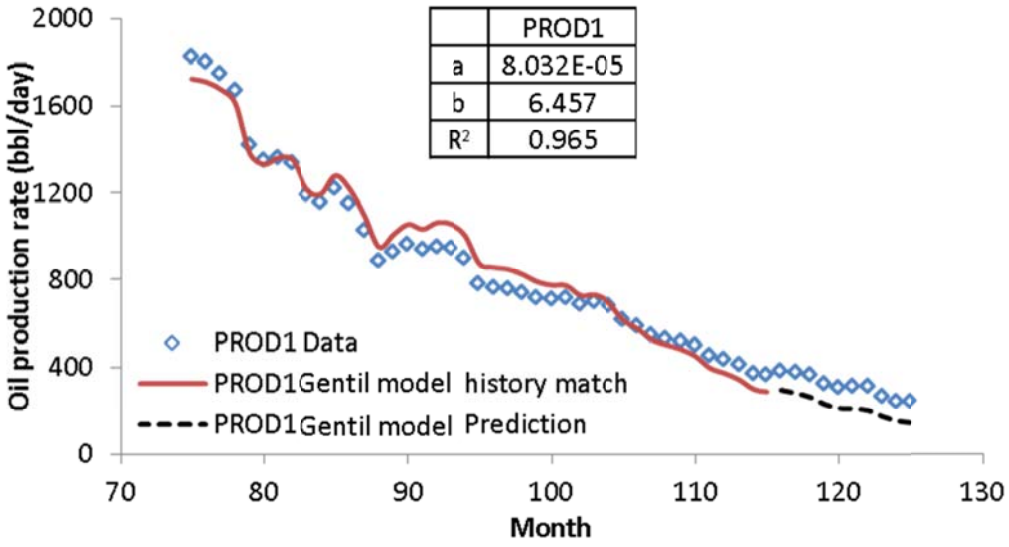

Figure 4.42 History match and prediction results of producer 1 using Gentil model in the immature flood time window in case 3.

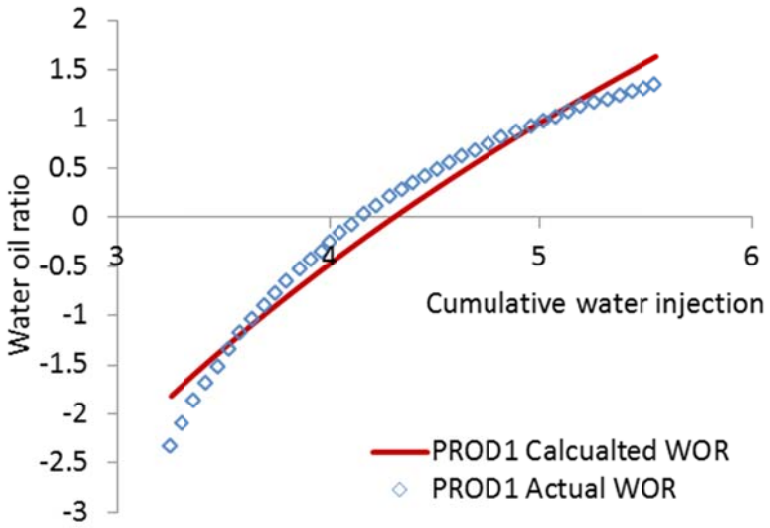

Figure 4.43 Actual and calculated cumulative water injected vs. WOR of producer 1using Gentil model in the immature flood time window in case 3.

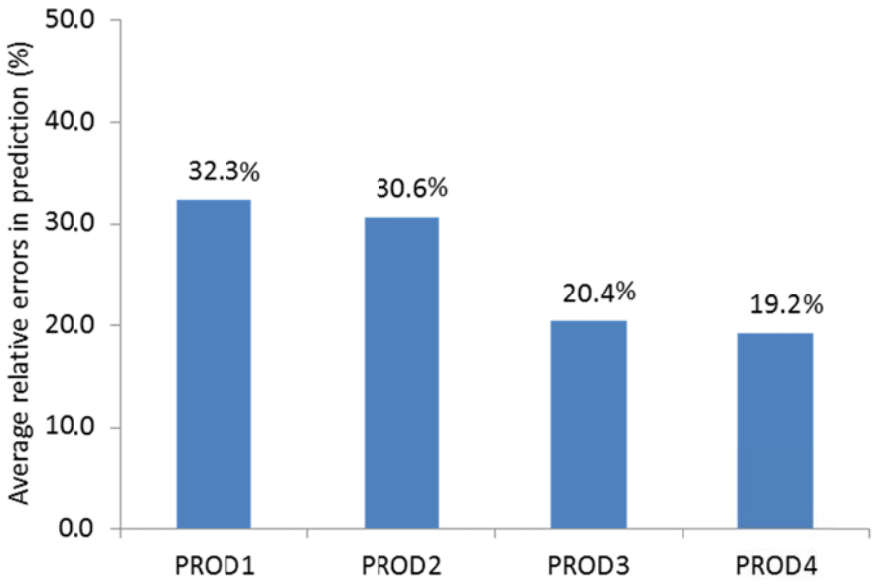

Figure 4.44 Average relative errors in oil rate prediction using Gentil model in the immature flood time window in case 3.

4.4.2.2 Koval Model

In Chapter 2, we have reviewed the Koval fractional flow theory, which is developed to address the issue of viscous figuring in a miscible displacement. We also mentioned that the Koval fractional flow expression is the same as the Buckley-Leverett water fractional flow expression in a water flood when the oil and water phases have straight-line relative permeabilities. For such a case, the Buckley-Leverett equation may be integrated analytically to give the following expression (Lake, 1989):

$$f_w\big|_{x_D=1} = \begin{cases} 0 & t_D < \dfrac{1}{K_{val}} \\ \dfrac{K_{val} - \sqrt{\dfrac{K_{val}}{t_D}}}{K_{val} - 1} & \dfrac{1}{K_{val}} < t_D < K_{val} \\ 1 & t_D > K_{val} \end{cases} \qquad 4.3$$

where t_D is the dimensionless time, which is defined as: $t_D = \dfrac{\sum_k \sum_i f_{ij} I_i}{V_p}$.

In Eq. 4.3, the saturation term is eliminated and the Koval approach can be used for water cut history match during which two parameters, the Koval factor and the pore volume, are estimated. The Koval method can be a powerful predictive tool when combined with the CRM model as the CRM model can quantify the injection contribution ($f_{ij} I_i$) to each producer at each time step.

In the following section, we demonstrate using the Koval approach to history match water cut data and predict future oil production rate. Prior to the application, the current model CRM model is used first to achieve connectivities (f_{ij}) between well pairs so that t_D in Eq. 4.3 can be estimated.

Mature Water Flood

In Figure 4.45, we observe that the Koval water cut curve approaches an abrupt end with water cut equaling 1; whereas the actual water cut approaches one asymptotically. As a result, the Koval-predicted water cut is 1 and, consequently, there is no oil production. This case reveals a limitation of the Koval approach, which is the inaccuracy when applied to a mature water flood as the Koval-predicted water cut is 1 at this stage.

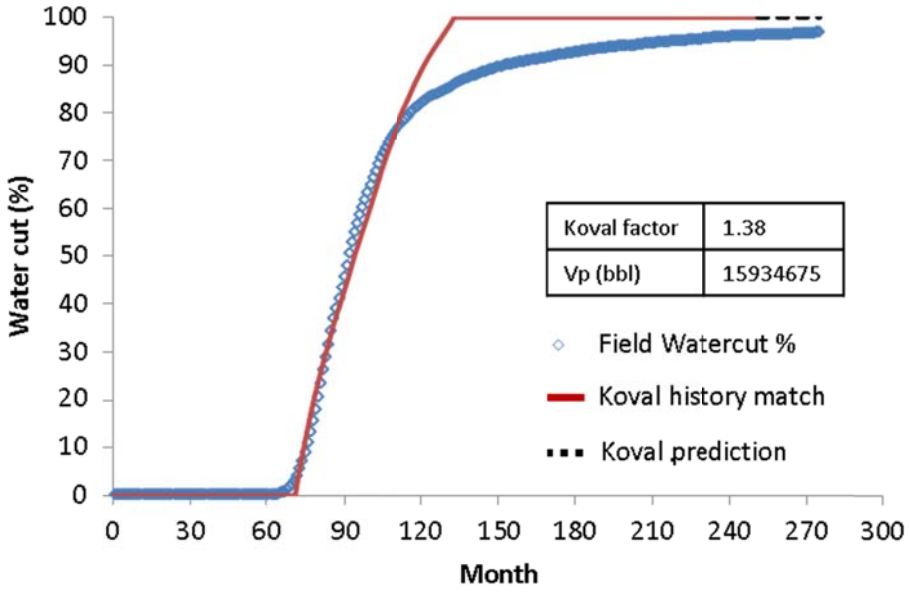

Figure 4.45 History match and prediction results of producer 1 using Koval model in the mature flood time window in case 3.

Immature Water Flood

In an immature water flood, the Koval water cut history match quality improves (see Figure 4.46). Nevertheless, an over-prediction trend is observed, resulting in lower

oil production rates as shown in Figure 4.47. Overall, the Koval prediction quality is acceptable with average errors below 11.5% in all producers (see Figure 4.48).

Figure 4.49 implies that if we can push the history match time window back to an earlier time, both the history match and the prediction quality are excellent. In other words, the Koval approach can give good results if it is applied to an early stage water flood when the producer water cut is relatively small.

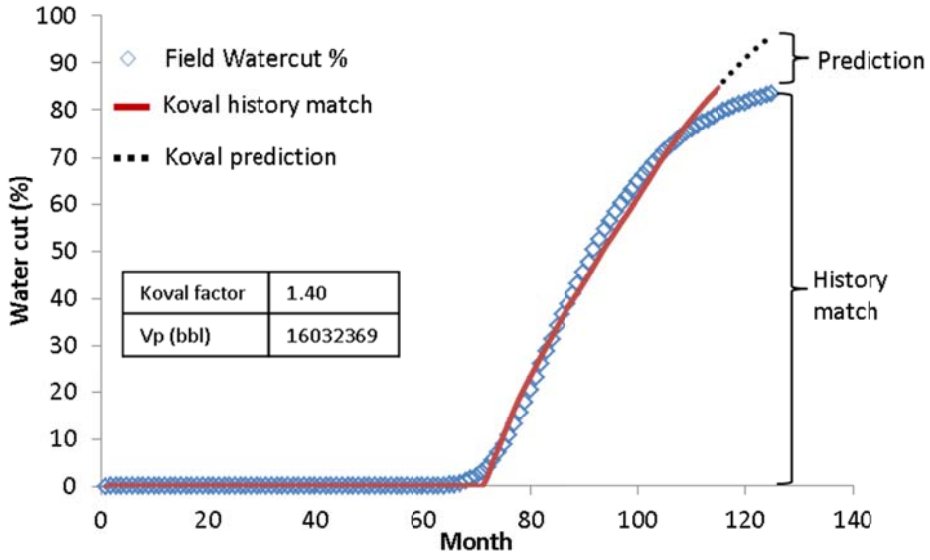

Figure 4.46 History match and prediction results of producer 1 using Koval model in the immature flood time window in case 3

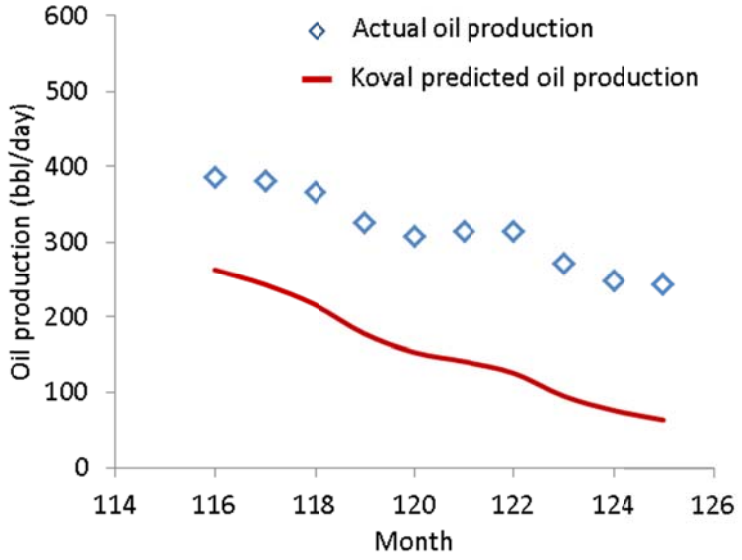

Figure 4.47 Oil rate prediction of producer 1 using Koval method in the immature flood time window in case 3.

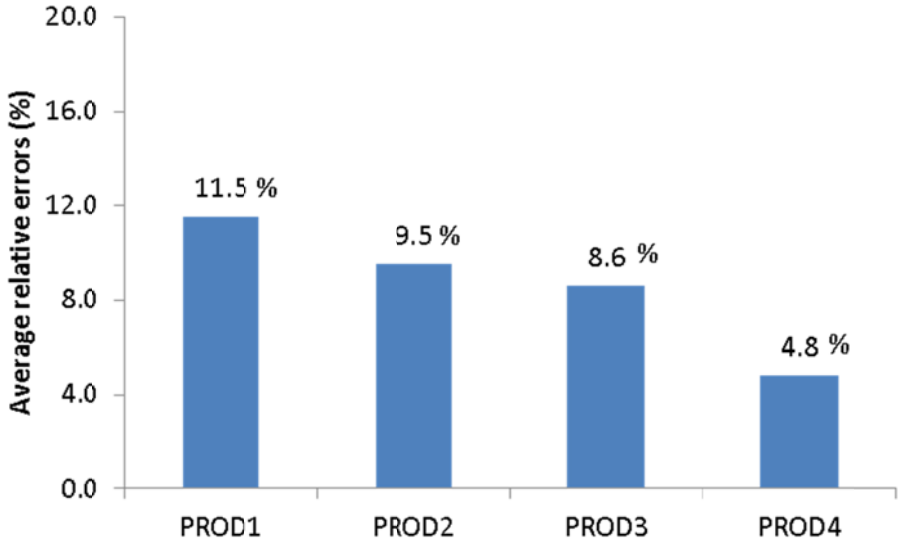

Figure 4.48 Average relative errors in oil rate prediction using Koval model in the immature flood time window in case 3.

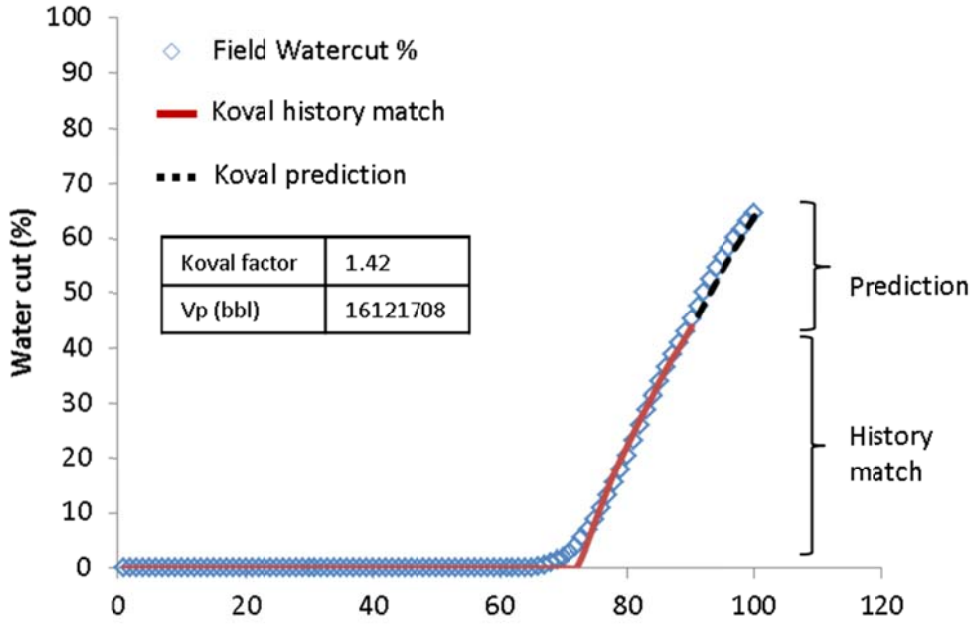

Figure 4.49 History match and prediction results of producer 1 using Koval model in an earlier immature flood time window in case 3.

4.4.2.3 The Coupled CRM Model Fractional Flow Model

The fractional flow models mentioned above follow a history match procedure during which model parameters are achieved. And these model parameters are further used for oil rate prediction.

For the coupled CRM model, the fractional flow curve is constructed directly using the average oil saturation and the historical water cut data. We fit the curve with a regression model and extrapolate it for prediction.

Mature Water Flood

The fractional flow curve of producer 1 within the history match window is in Figure 4.50. We observe that both the average water saturation and water cut are limited in a narrow range in the mature water flood stage. The curve is fitted with a polynomial function, which can be extrapolated for prediction (see Figure 4.51). Overall, the average relative errors in oil rate prediction are below 4% in all producers indicating an excellent prediction quality (see Figure 4.52).

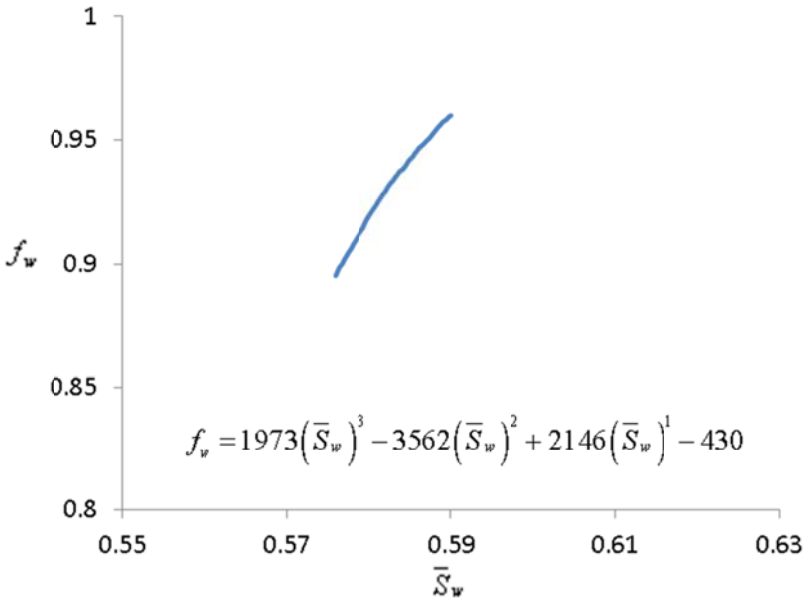

Figure 4.50 Fractional flow curve of producer 1 from the coupled CRM model in the mature flood time window in case 3.

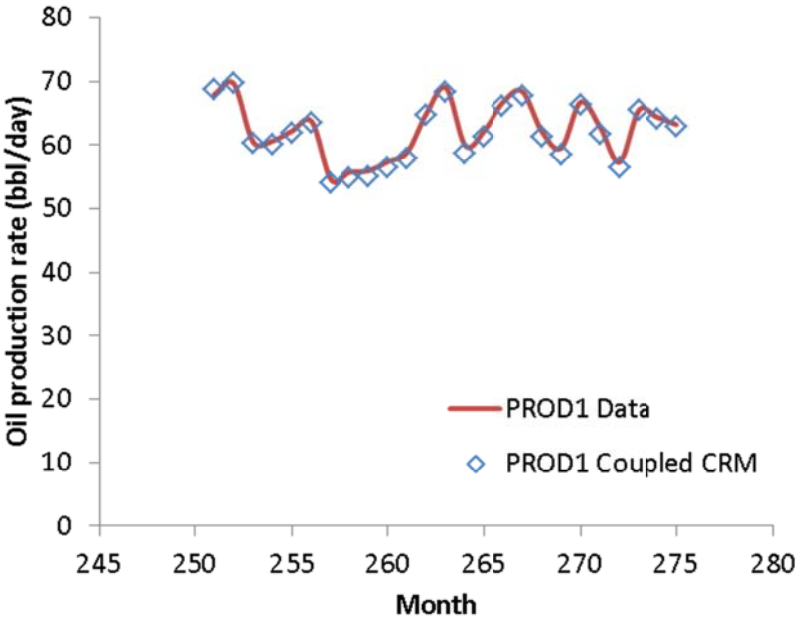

Figure 4.51 Oil rate prediction of producer 1 using the coupled CRM model in the mature flood time window in case 3.

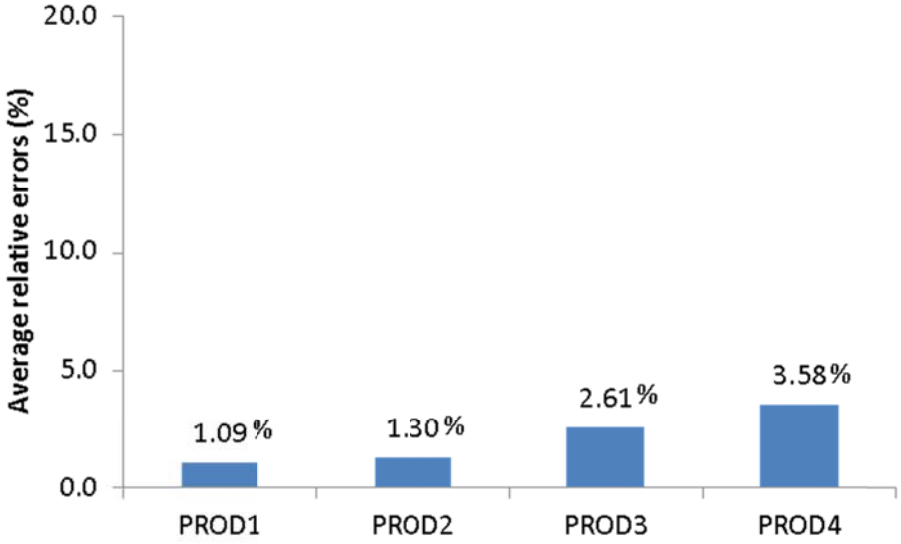

Figure 4.52 Average relative errors in oil rate prediction using the coupled CRM model in the mature flood time window in case 3.

Immature Water Flood

In the immature water flood stage, the fractional flow curve is elongated since the water saturation change is large (see Figure 4.53). The oil rate prediction results of producer 1 are excellent (see Figure 4.54). Figure 4.55 shows that the average relative error is less than 5.2% in producer 1, and is only 1.1% in producer 3. The improvement in the accuracy is significant compared to the Gentil model and Koval approach results at early time.

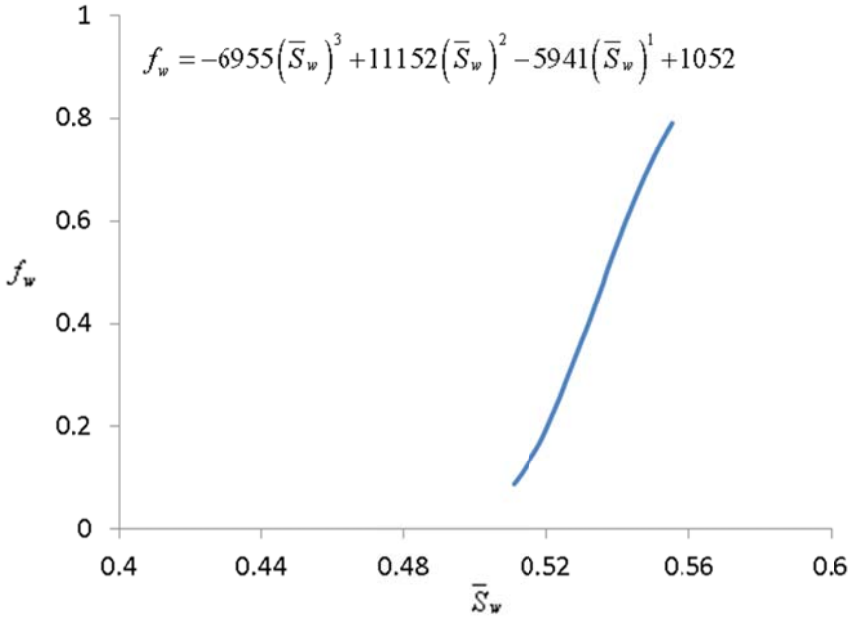

Figure 4.53 Fractional flow curve of producer 1 from the coupled CRM model in the immature flood time window in case 3.

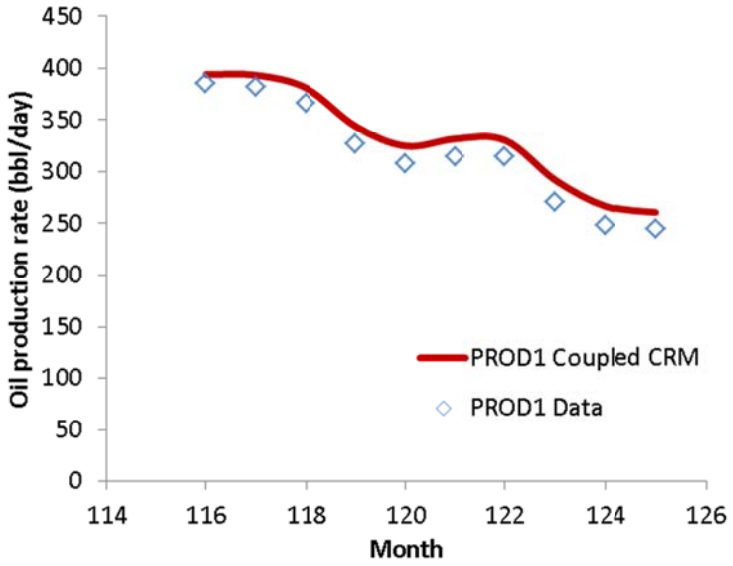

Figure 4.54 Oil rate predictions using the coupled CRM model in the immature flood time window in case 3.

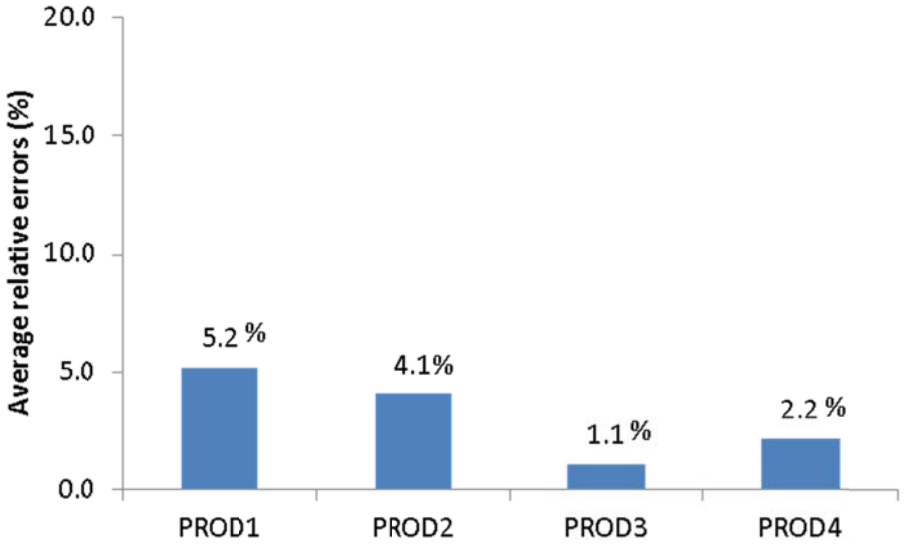

Figure 4.55 Average relative errors in oil rate prediction using the coupled CRM model in the immature flood time window in case 3.

4.4.3 Summary

In this case study, we have discussed three fractional flow models including: Gentil model, Koval model, and the coupled CRM fractional flow model. The first two fractional flow models follow a history match procedure during which model parameters are achieved, which are further used for oil rate prediction. For the coupled CRM model, the fractional flow curve is constructed directly using the average oil saturation and the historical water cut data. We fit the curve with a regression model and extrapolate it for prediction.

Figures 4.56 and 4.57 summarize the oil rates prediction errors using these fractional flow models at different stages (mature and immature) of a water flood. In the mature water flood, the Koval model lost its prediction capability as the Koval-predicted water cut is 1; whereas the Gentil model works as good as the coupled CRM model. Nevertheless, the coupled CRM gives the best prediction quality among the three fractional flow models.

In an immature water flood, the Gentil model generates large errors in oil rate prediction, which hinders its further application for injection optimization. While the Koval approach prediction is acceptable, the coupled CRM model gives excellent results.

This case demonstrates that the coupled CRM fractional flow model works satisfactorily regardless of the displacement phases.

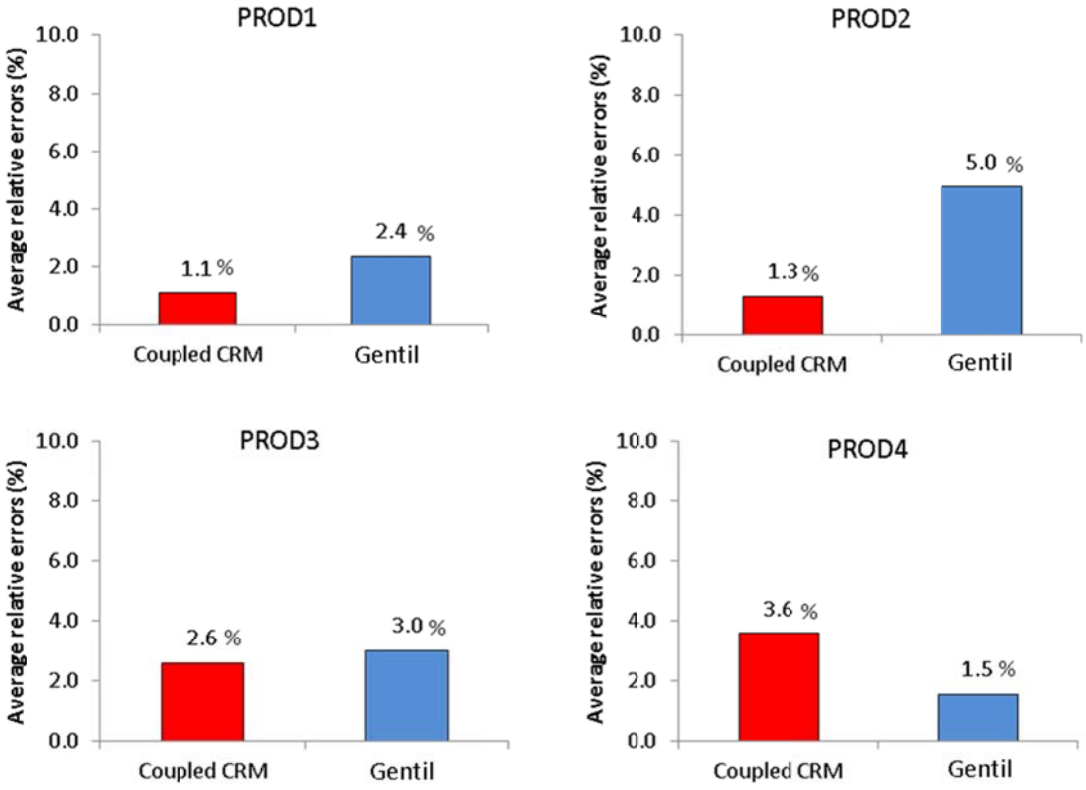

Figure 4.56 Comparison of average relative errors in oil rate prediction in the mature water flood in case 3.

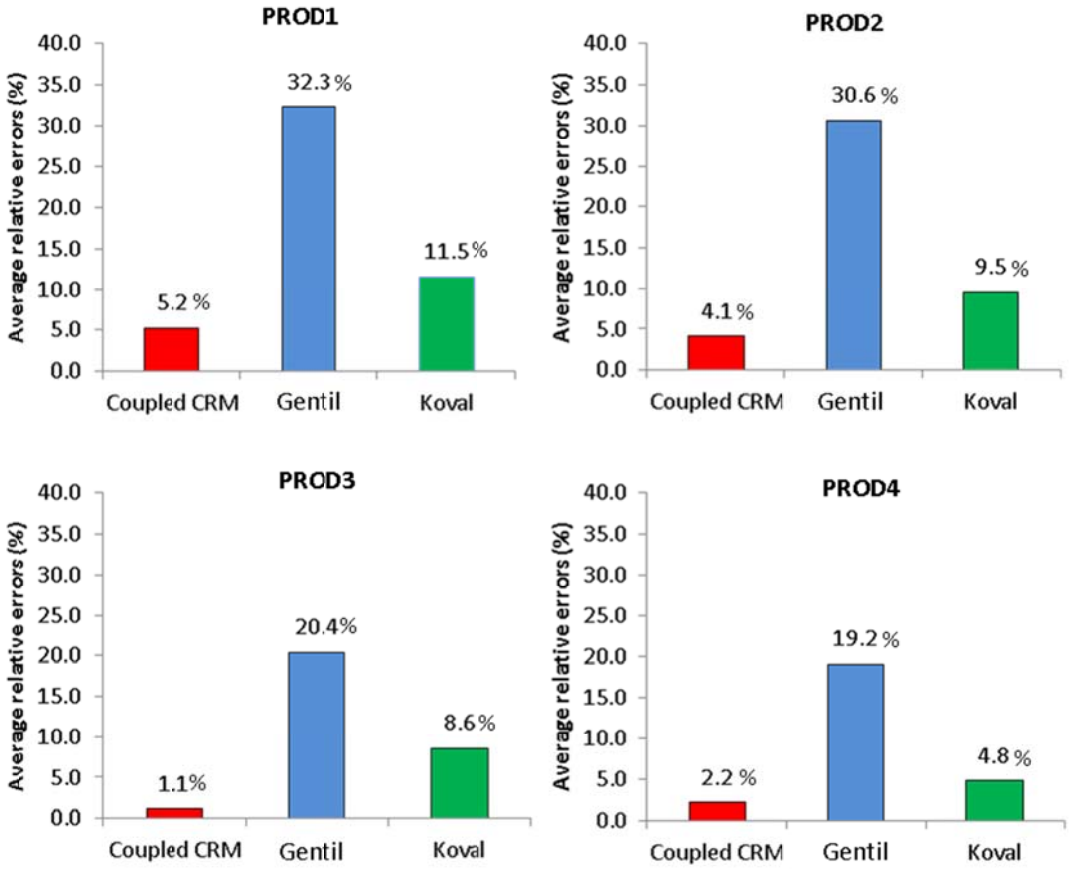

Figure 4.57 Comparison of average relative errors oil rate prediction in the immature water flood in case 3.

4.5 CASE 4: A SEALED RESERVOIR

We continue to test the coupled CRM model in a sealed reservoir to see if the model can capture this geological feature. Previously, we have mentioned the benefits of introducing the coupled CRM model. To justify our claims, we compare the coupled and current CRM models under different displacement stages. The performance of both models in history match and validation are discussed. Moreover, an optimization of injection scheme is performed to maximize oil production using the coupled CRM model.

4.5.1 General Reservoir Information

This synthetic field is the same as the previous five-spot homogenous reservoir (case 3) in every aspect except the permeability distribution. There is a 1 md low-permeability region, which separates the reservoir into two compartments (see Figure 4.58). Other key parameters of this field can be found in Table 4.9.

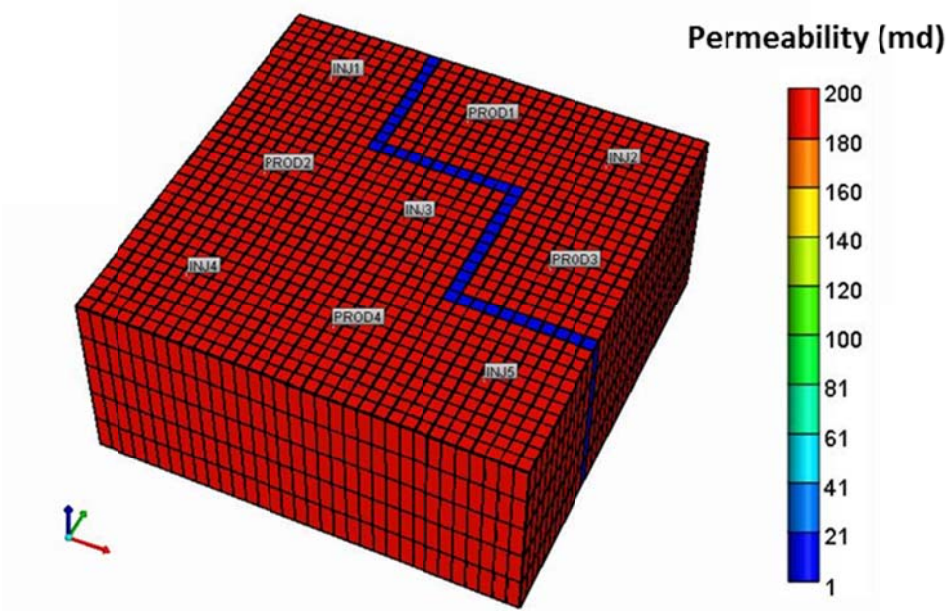

Figure 4.58 Permeability distributions in case 4.

Figure 4.59 shows the simulated water cuts of the four producers in this field. We observe that water cuts fall into two groups. Since producers 2 and 4 are supported by 4 injectors, water breaks through early in these two wells and water cuts increase steeply afterwards. On the contrary, producers 3 and 4 are only supported by injector 2; therefore the displacement takes longer time and the water cuts rise gradually.

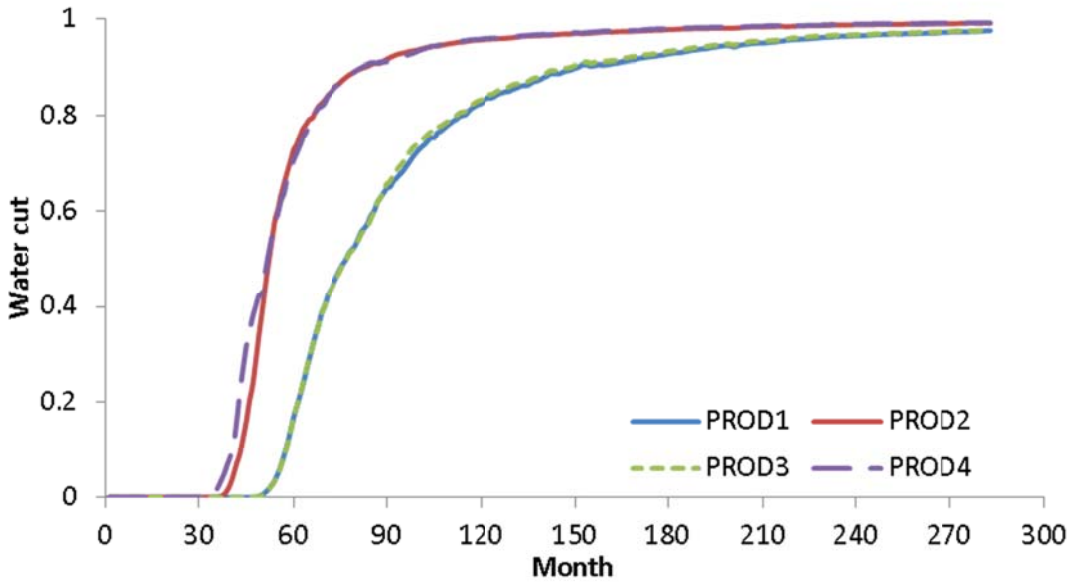

Figure 4.59 The simulated water cuts in case 4.

4.5.2 Application of the Coupled and Current CRM Models

As mentioned before, the reservoir flow characteristics are distinct under different water-oil displacement phases. The reservoir system is less compressible and the fluid flow can be approximated as single-phase flow in a mature water flood; whereas immature water flood usually implies a strong two-phase flow region, when the water/oil saturation change is significant. We have claimed that the coupled CRM model is more favorable in capturing physics when the saturation change can't be neglected, such as an immature water flood. In this case study, we apply both coupled and current models in mature and immature water floods to demonstrate the necessity and benefits of a two-phase coupled CRM model.

For the purpose of comparison, we use the same history match and validation time windows (see Table 4.11) to apply both CRM models. We also performed water injection scheme optimization using the coupled CRM model in the time window in Table 4.11.

	History match window (month)	**Validation window (month)**	**Prediction window (month)**
Mature water flood	60-260	261-280	281-292
Immature water flood	55-95	96-105	106-117

Table 4.11 Summary of time windows for coupled and current CRM models in case 4.

The inputs for the current CRM model are the simulated injection and production rates. The input for the coupled CRM model can be found in Appendix D and we use a simplified-coupled scheme in this case.

4.5.2.1 Mature Water Flood

History Match

We use the coefficient of determination (R^2) to compare the total production history match quality in all producers (see Table 4.12). Both models give positive R^2 values that are greater than 0.95, indicating excellent fit qualities.

	PROD1	PROD2	PROD3	PROD4
Coupled CRM fit quality (R^2)	0.983	0.998	0.990	0.998
Current CRM fit quality (R^2)	0.950	0.956	0.957	0.992

Table 4.12 The coefficient of determination (R^2) in all producers in the mature water flood in case 4.

The estimated connectivities between well pairs are in Figure 4.60, where lines indicate connection and color differentiates the intensity of the connectivity. We observe that both models capture the key geology feature by showing no connection between wells across the seal. The coupled CRM model gives symmetric connectivity patterns, which is in a good agreement with the symmetric field geology; whereas the connectivity pattern is not symmetric according to the current CRM model. The current CRM model also indicates that there is no connection between injector 1 and producer 4, which is questionable since there is no fluid barrier between this well pair.

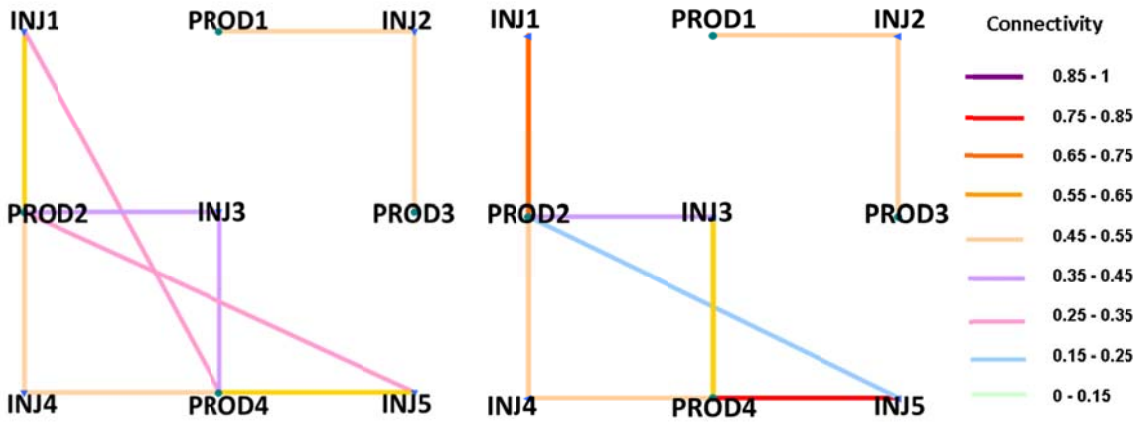

a) Coupled CRM model b) Current CRM model

Figure 4.60 Connectivity obtained in the mature water flood in case 4.

In the coupled model, the time constants are a function of saturation (see Figure 4.61); whereas they are constants with respect to time in the current CRM model (se Figure 4.62). To verify the time constants obtained, we perform injection pulse test at the 230th month in reservoir simulation. Table 4.13 summarizes the results. In general, both coupled and current models agree with the simulation results at this mature water flood time window. However, the current CRM model over-estimates the time constant in producer 2 to be 45 days while it should be around 28 days.

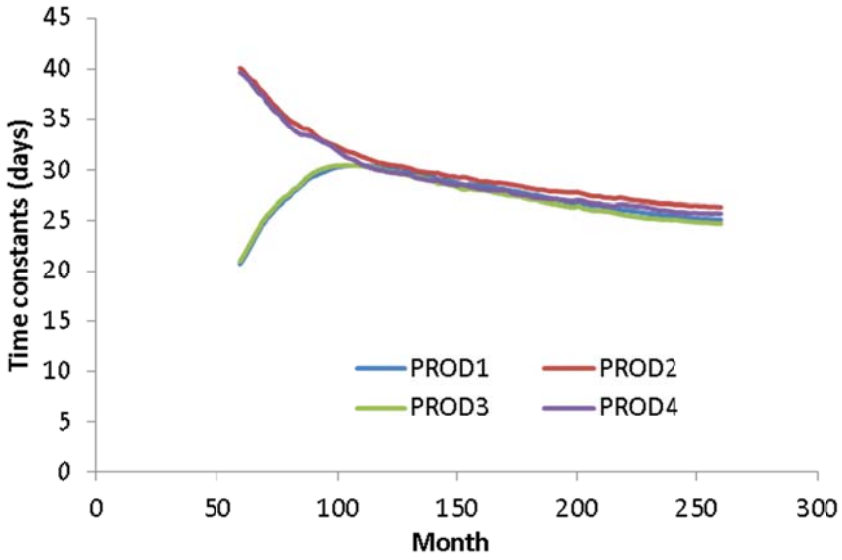

Figure 4.61 Evolution of the time constants using the couple CRM model in the mature water flood in case 4.

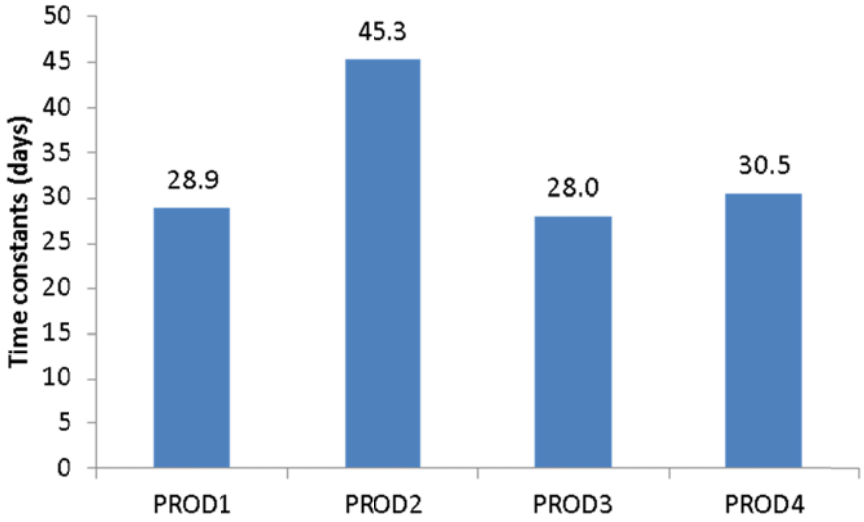

Figure 4.62 Time constants obtained from the current CRM in the mature water flood in case 4.

	PROD1	**PROD2**	**PROD3**	**PROD4**
Reservoir simulation time constants (days)	27.17	28.68	26.95	27.81
Coupled CRM time constants (days)	25.72	26.85	25.24	26.26
Current CRM time constants (days)	28.89	45.26	28.01	30.49

Table 4.13 Time constants at the 230th month from the coupled CRM model, current CRM model and reservoir simulation in case 4.

There is no saturation result from the current CRM model since it is a single-phase flow model; whereas the coupled CRM provides the evolution of saturation with time. Figure 4.63 gives the outlet and average oil saturation of each producer obtained from the coupled CRM model. We find that the outlet oil saturations of producers 2 and 4 match the CMG results satisfactorily.

However, it shows an over-estimation in outlet oil saturation in producers 1 and 3. This is owing to the relatively severe gravity segregation among reservoir layers in the reservoir simulation, which is caused by the slow recovery of producers 1 and 3. The top layer where the producers 1 and 3 are located shows much smaller oil saturation change over time compared to the lower layers. Taking the average saturation of all layers over which producers 1 and 3 are perforated gives a very coarse estimates of the outlet saturation. Consequently, it is difficult to obtain representative outlet saturation in this case to compare with the CRM results.

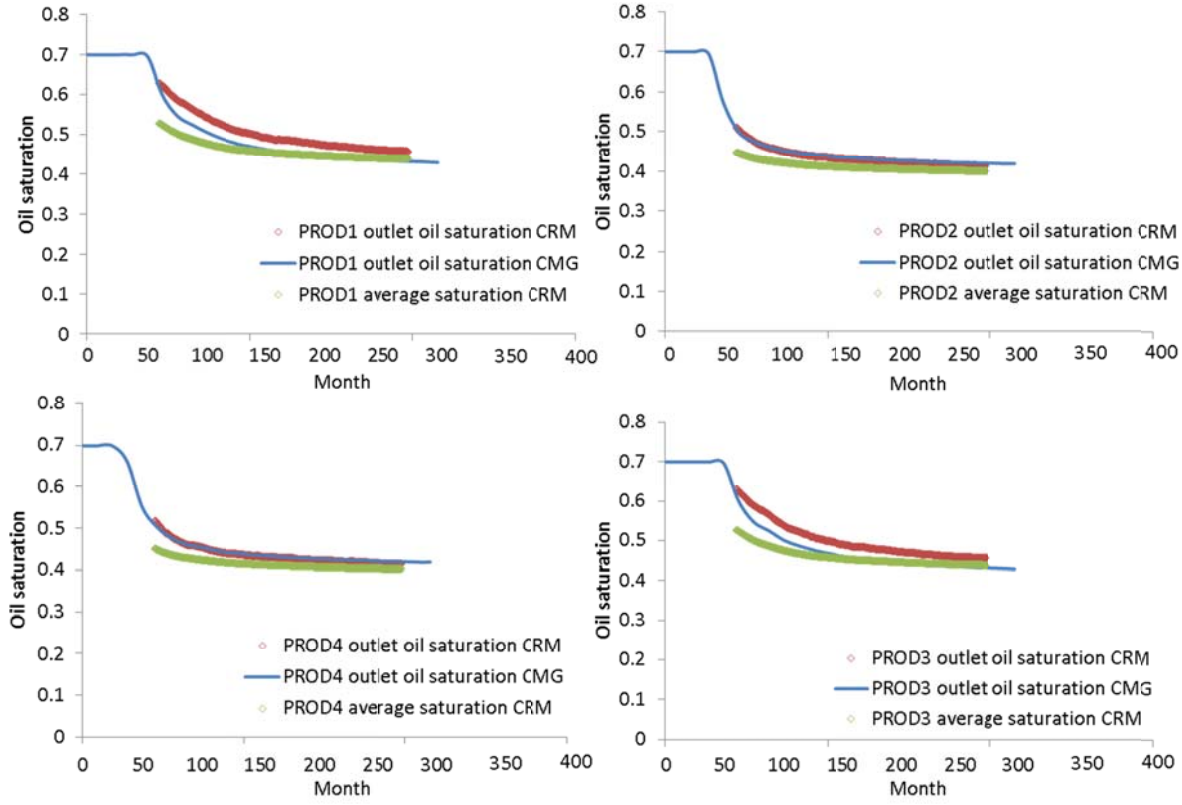

Figure 4.63 The outlet and average oil saturations for each producer using the coupled CRM model in the mature water flood in case 4.

Validation

Following the internal validation procedure that is discussed in Chapter 3, we validate both coupled and current CRM models in this section. Both total and oil production rates are predicted under the historical injection schemes in the validation time window (from the 261^{th} to the 280^{th} month).

In Figure 4.64, both CRM models performed excellently in the prediction of total production rates. In general, the coupled CRM has smaller average relative errors; especially in producers 2 and 3 (see Figure 4.65).

The average relative errors of oil rate prediction in each producer are in Figure 4.66. The prediction qualities are about the same in producers 2 and 4 using both models; whereas the coupled CRM model is more accurate in producers 1 and 3 (see Figure 4.67).

This case mimics a practical scenario that producers of different maturity are producing together. The current CRM is accurate for producers with large water cut, however it is less suitable for low water cut wells. By considering saturation change, the coupled CRM model is not limited by the maturity of producers and therefore is more applicable to complicated field cases.

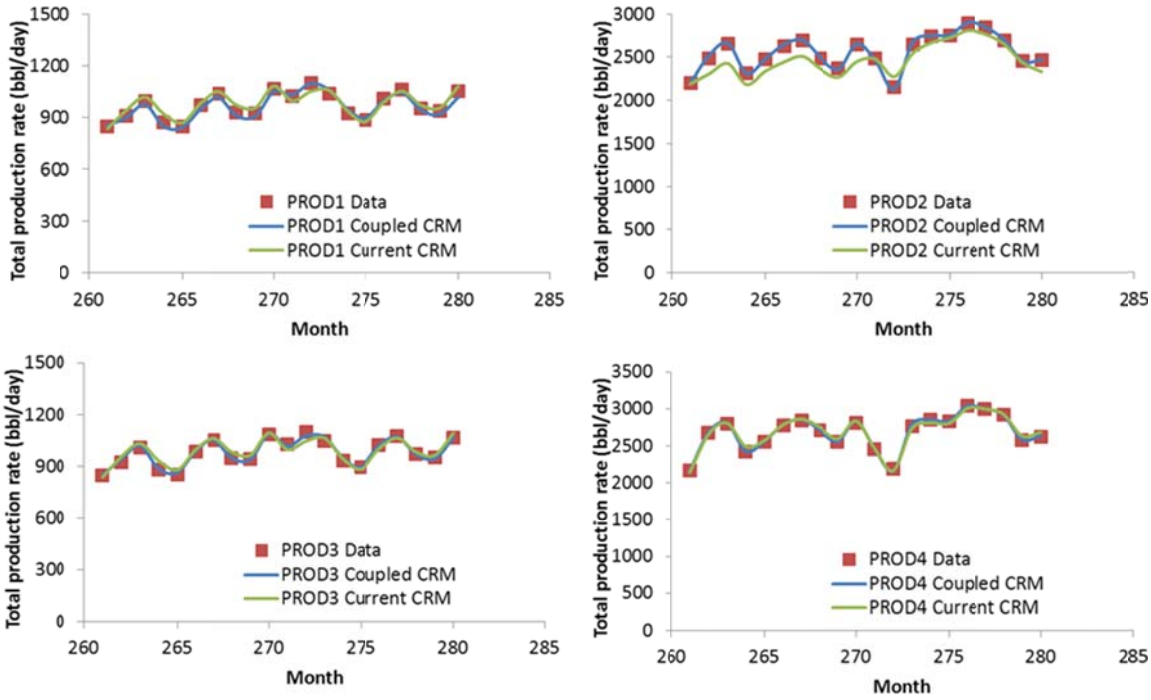

Figure 4.64 Validation of total production rate using the coupled and current CRM models in a mature water flood in case 4.

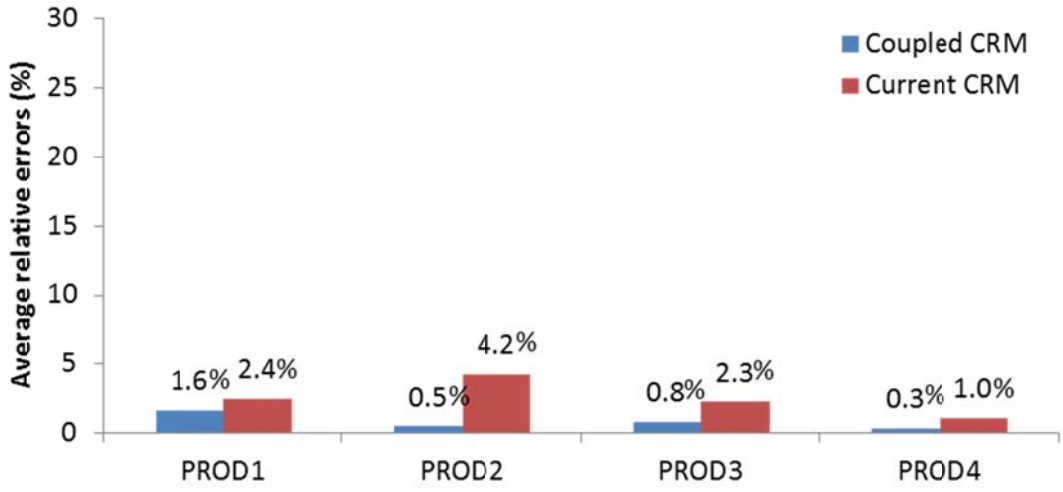

Figure 4.65 Average relative errors in total production rate validation using the coupled and current CRM models in a mature water flood in case 4.

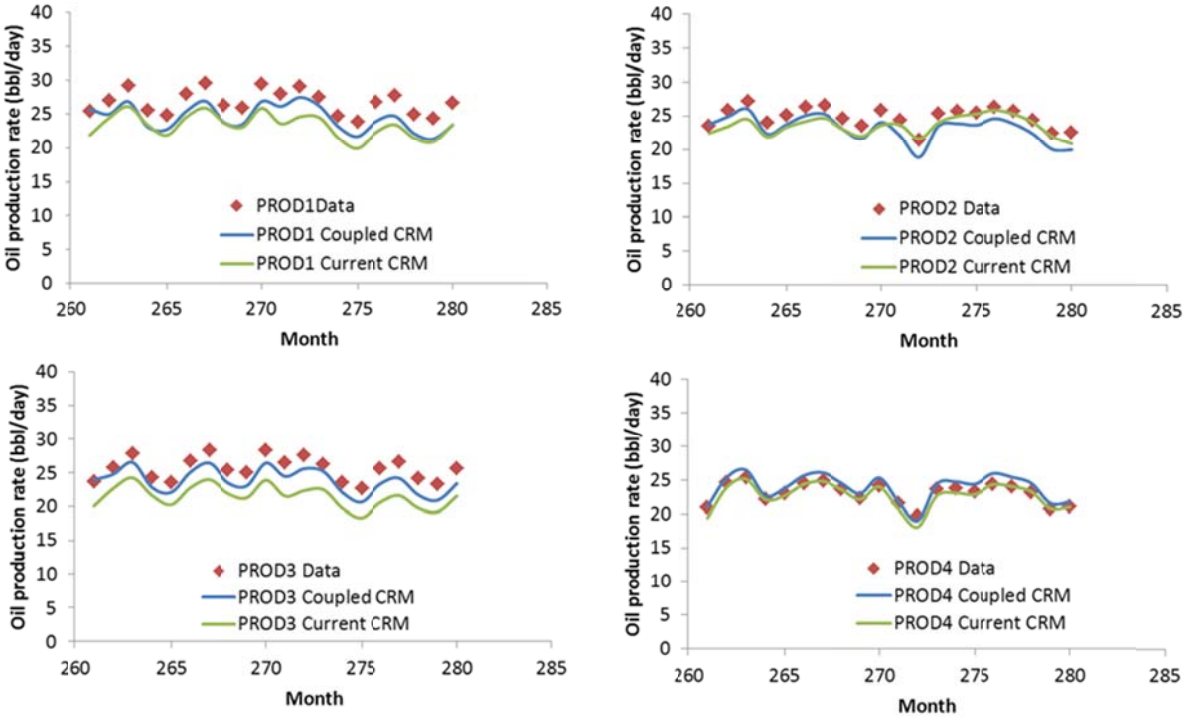

Figure 4.66 Validation of oil production rate using the coupled and current CRM models in a mature water flood in case 4.

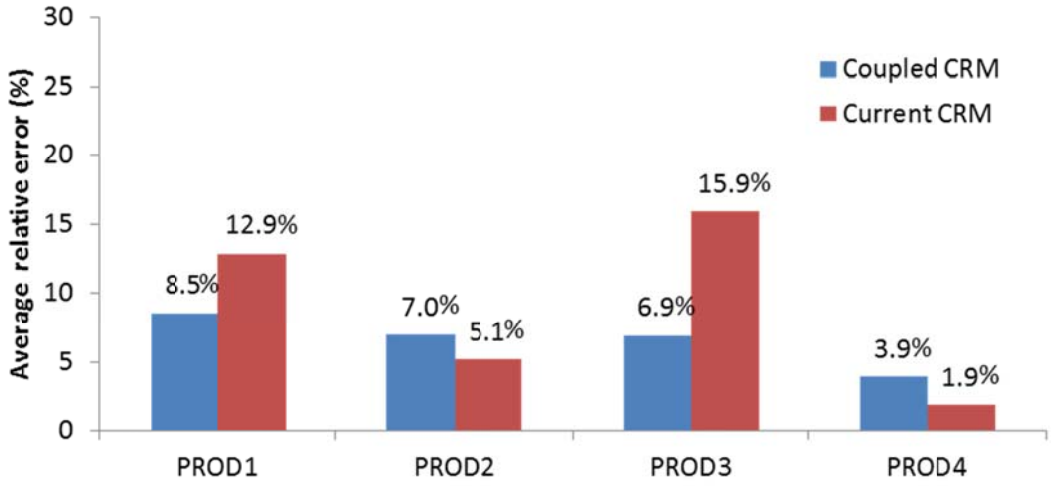

Figure 4.67 Average relative errors in oil production rate validation using the coupled and current CRM models in a mature water flood in case 4.

Optimization of Injection Scheme

In this section, we demonstrate the optimization capability of the coupled CRM model. The injection optimization time window is from the 281th to the 294th month. The field total injection stays the same as the historical total injection (see Table 4.14) during this time frame. The injection rate is bounded between 2200 bbl/day and 500 bbl/day, which are the largest and smallest historical injection rates, respectively.

The optimization results suggest that the maximum oil production would occur if we increase the injection rates of injectors 1, 2 and 3 to 2200 bbl/day and reduce the injection rates of injectors 4 and 5 to 600 bbl/day (see Figure 4.68). The historical injection scheme in Figure 4.68 is the average injection rates in each injector since the historical injection rates vary with time. With this optimized injection scheme, one can obtain an additional 3365.6 barrel of oil in one year, which is a 8% increase over the historical oil recovery (see Figure 4.69).

	Historical injection scheme	**Optimized injection scheme**
Field total injection (bbl)	3007575	3007575
Field total oil production (bbl)	42334	45700
Improved oil recovery	8%	

Table 4.14 Summary of water injection and oil recovery under historical and optimized injection schemes in the mature water flood in case 4.

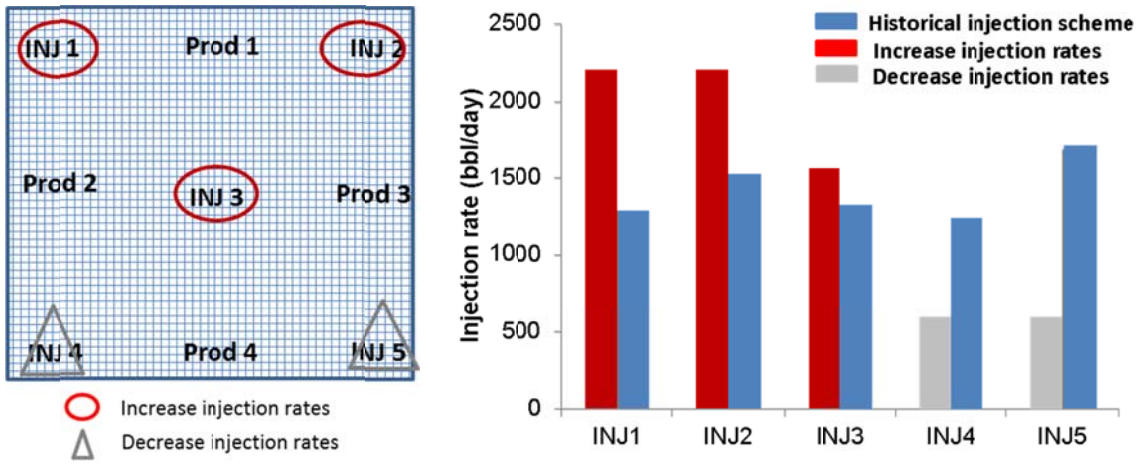

Figure 4.68 The historical and optimized injection scheme using the coupled CRM model in a mature water flood in case 4.

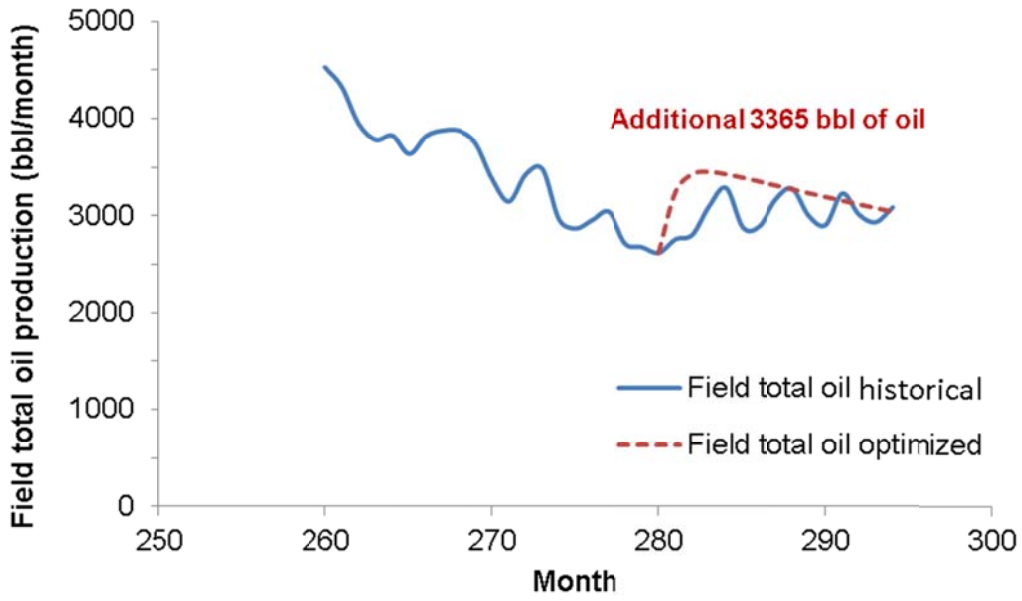

Figure 4.69 Optimized oil production rate in a mature water flood using the coupled CRM model in case 4.

4.5.2.2 Immature Water Flood

Table 4.15 shows the total production history match quality of the coupled and current CRM models in the immature water flood time window. Overall, both models give good fits with large R^2 values. Nevertheless, the coupled CRM model performs better especially in producers 1 and 3.

	PROD1	**PROD2**	**PROD3**	**PROD4**
Coupled CRM fitting quality (R^2)	0.923	0.985	0.920	0.991
Current CRM fitting quality (R^2)	0.873	0.913	0.824	0.982

Table 4.15 The coefficient of determination (R^2) in all producers in an immature water flood in case 4.

Figure 4.70 gives well connectivities. Again, both models show no well connection across the seal. The coupled CRM connectivity map display symmetry connection pattern. The current model suggests no connectivity between injector 1 and producer 4 again, which remains questionable.

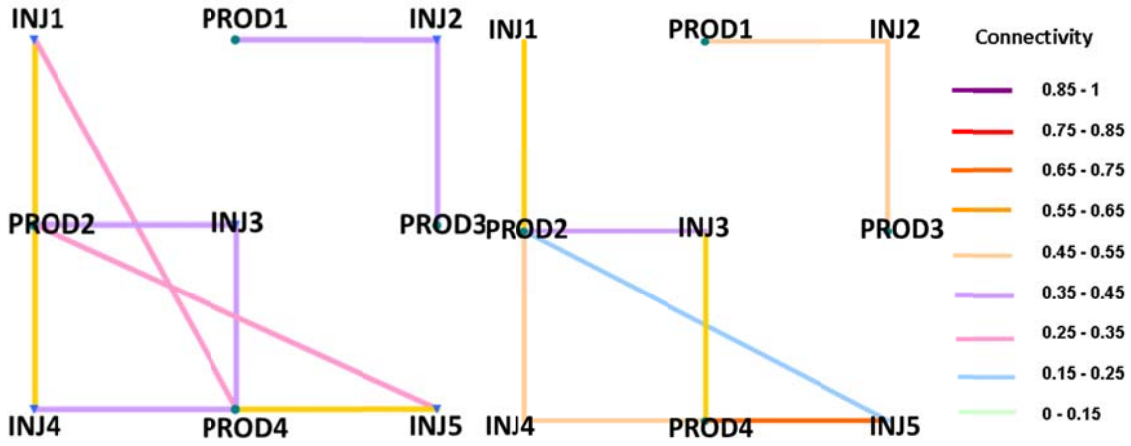

a) Coupled CRM model b) Current CRM model

Figure 4.70 Connectivity obtained in an immature water flood in case 4.

Time constants are in Figures 4.71 and 4.72. Similar to the previous case, we perform an injection pulse test at 61th month to explore the time constant from reservoir simulation to compare with CRM models. Table 4.16 indicates that the current CRM model over-estimates the time constants in producers 1, 2 and 3; whereas the coupled CRM model time constants agree with the simulation time constants excellently.

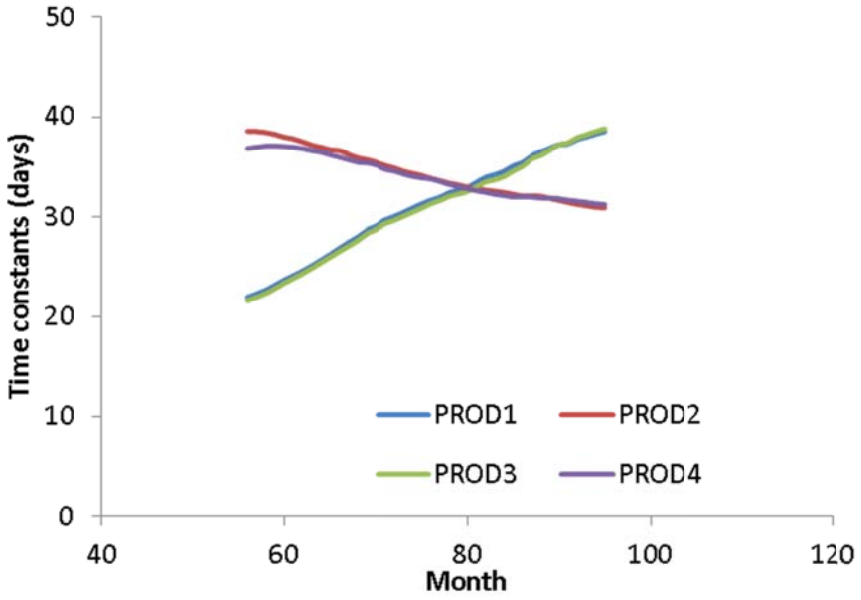

Figure 4.71 Evolution of time constants using the coupled CRM model in an immature water flood in case 4.

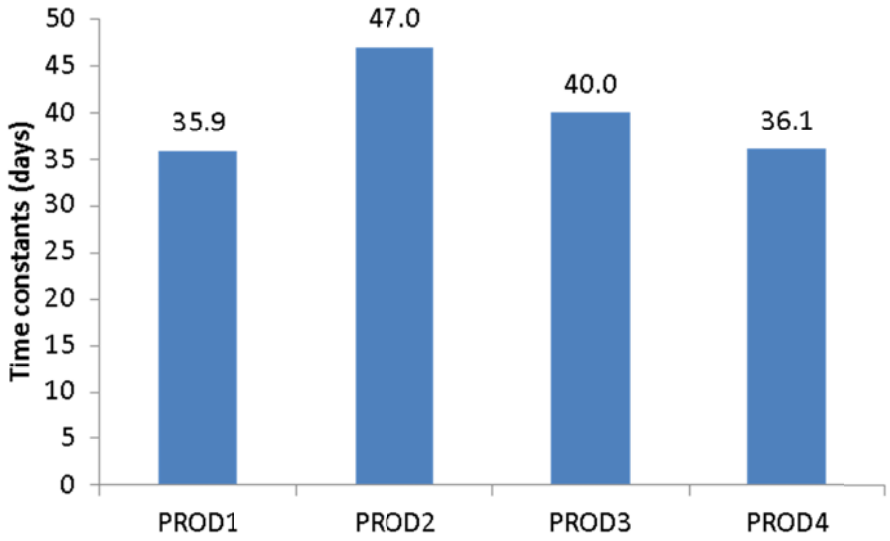

Figure 4.72 Time constants obtained using the current CRM model in an immature water flood in case 4.

	PROD1	**PROD2**	**PROD3**	**PROD4**
Reservoir simulation time constants (days)	27.37	38.29	27.73	38.70
Coupled CRM time constants (days)	25.16	37.22	24.91	36.70
Current CRM time constants (days)	35.90	46.98	39.99	36.07

Table 4.16 Time constants at the 61th month from the coupled CRM, current CRM and reservoir simulation in case 4.

Validation

Figures 4.73 presents the total production rate validation results. We observe that both CRM models can predict total production rates accurately with small average relative errors (see Figure 4.74) in both mature and immature water floods.

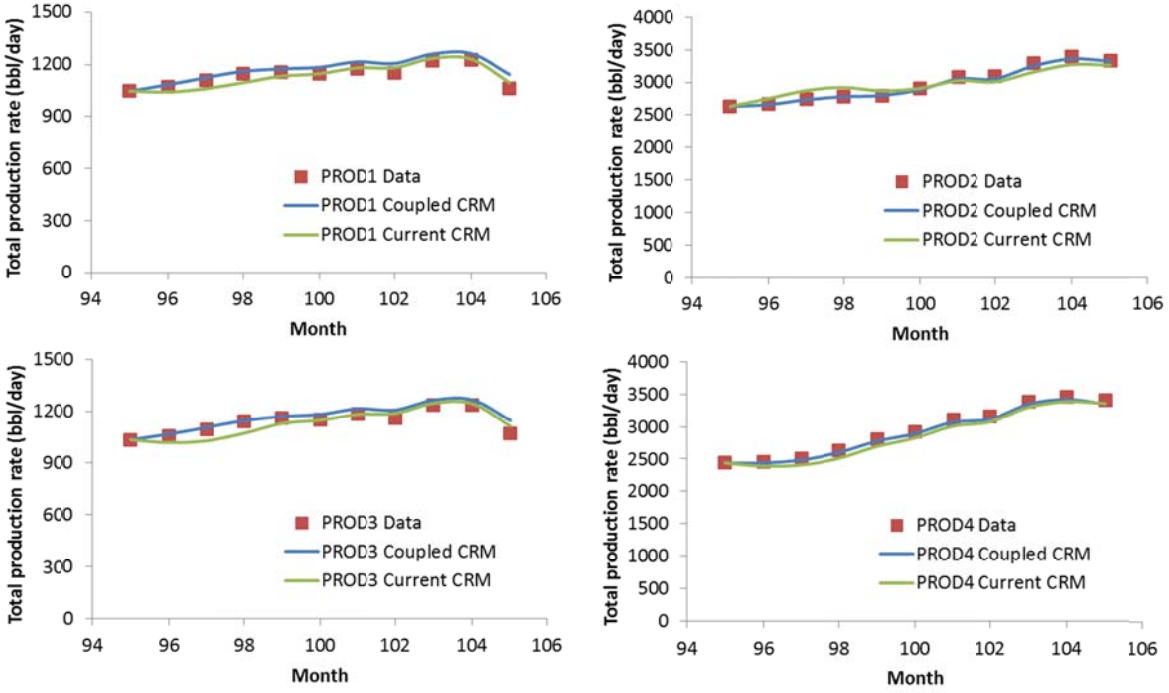

Figure 4.73 Validation of total production rate of an immature water flood using the coupled and current CRM models in case 4.

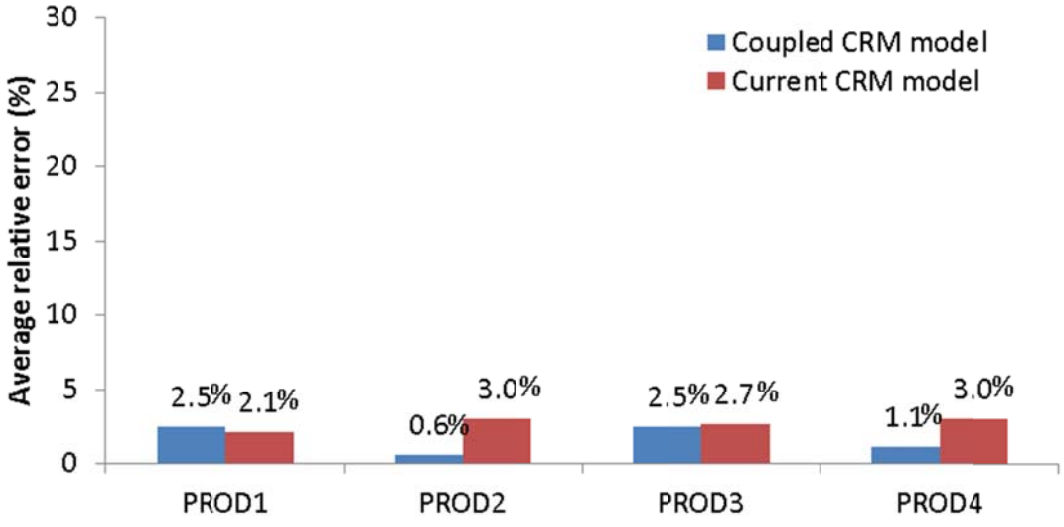

Figure 4.74 Average relative errors in total production rate validation using the coupled and current CRM models in an immature water flood in case 4.

Significant improvement occurs in oil rate prediction using the coupled CRM model (see Figure 4.75). It reduces the prediction errors to be less than 7.6%; while the errors are up to 23% when using the current CRM model. With such a large error in validation, the current CRM model is less reliable for further application in optimizing the injection scheme.

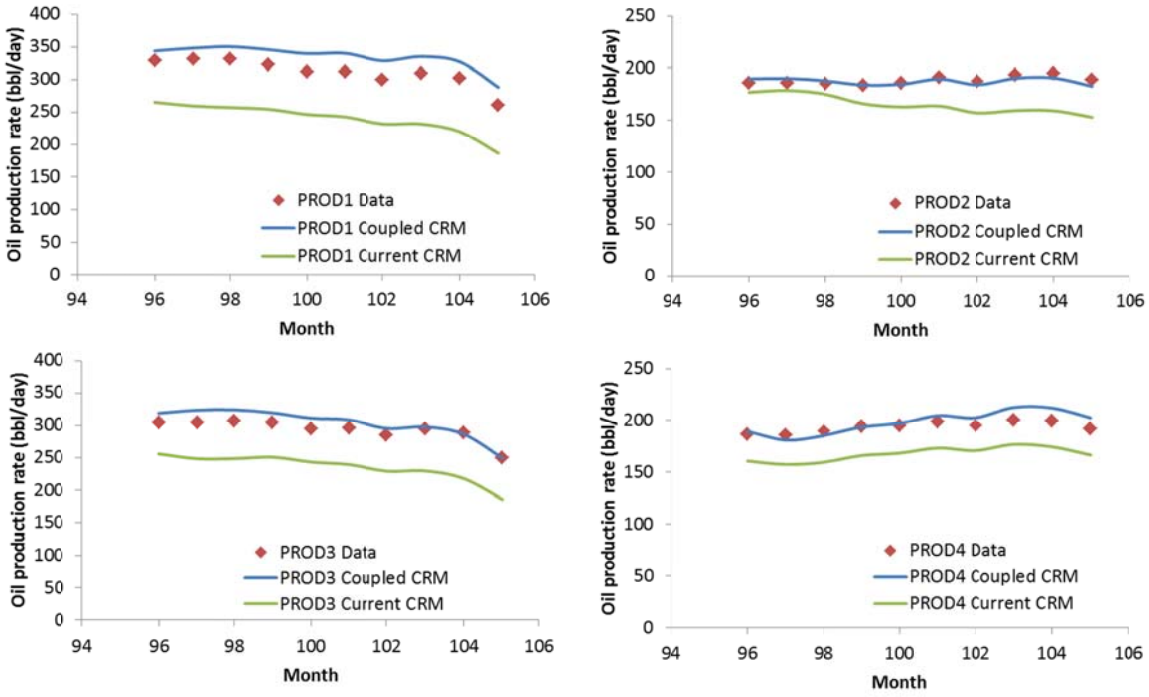

Figure 4.75 Validation of oil production rate in an immature water flood using the coupled and current CRM models in case 4.

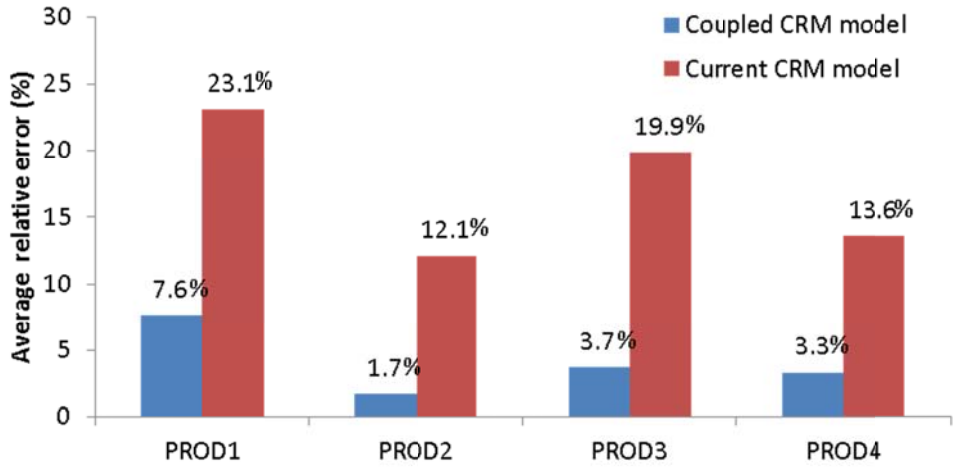

Figure 4.76 Average relative errors in oil production rate validation using the coupled and current CRM models in an immature water flood in case 4.

Optimization of Injection Scheme

The optimization time window extends from the 105th to the 114th month during which the field total injection is constrained to be the same as the historical injection (see Table 4.17). The injection rate is bounded between 2200 bbl/day and 500 bbl/day, which are the largest and smallest historical injection rates, respectively.

Optimization suggests to adjust the injection strategy such that the injection rates of injectors 1, 2 and 5 should be increased to 2200 bbl/day and the injection rates of injectors 3 and 4 should be reduced to 1000 bbl/day and 600 bbl/day, respectively (see Figure 4.77). The optimized injection scheme can give additional 35693 bbl of oil in one year (see Figure 4.78), which is a 12% increase over the historical oil production (see Table 4.17).

	Historical injection scheme	Optimized injection scheme
Field total injection (bbl)	2465214	2465214
Field total oil production (bbl)	299755	335449
Improved oil recovery	12%	

Table 4.17 Summary of water injection and oil recovery under historical and optimized injection schemes in the immature water flood in case 4.

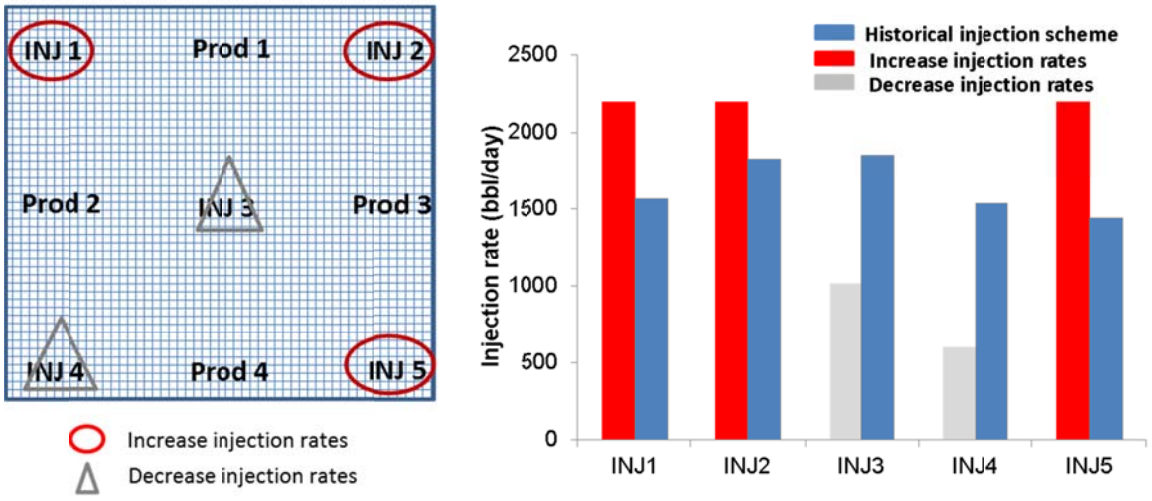

Figure 4.77 The historical and optimized injection scheme using the coupled CRM model in an immature water flood in case 4.

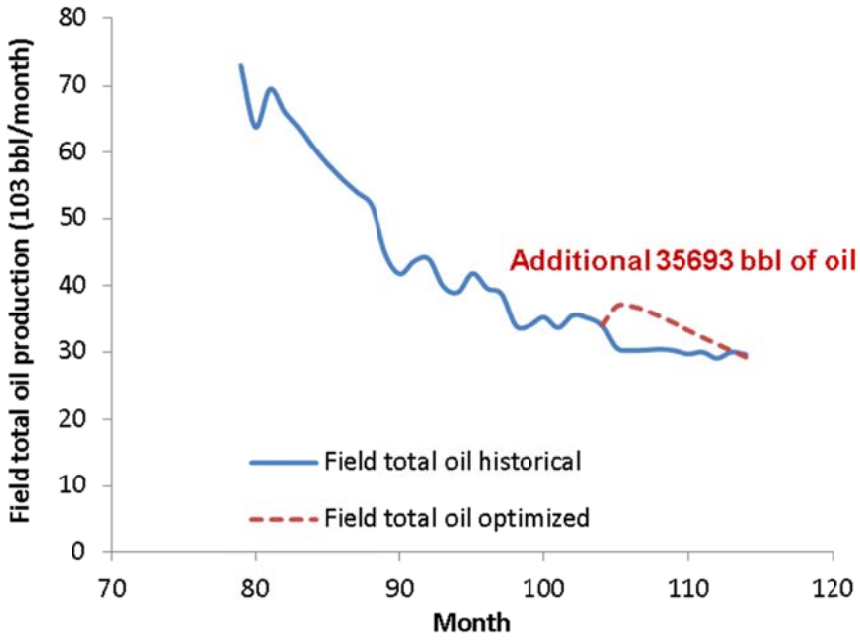

Figure 4.78 Optimization of oil production rate in an immature water flood using the coupled CRM model in case 4.

4.5.3 Summary

The coupled and current CRM models are tested using synthetic data from a heterogeneous reservoir with a seal. Two time windows (mature and immature water floods) are chosen for application. The results show that all estimated model parameters in both time windows are in a good agreement with simulated values. The coupled CRM model significantly improves the accuracy of predicting oil production rate, especially in an immature water flood, compared to the current CRM model. An improved accurate oil validation enables us to further optimize the injection rate. The optimized injection scheme is able give 8% additional oil production in a synthetic mature water flood and 12% additional oil production in an immature water flood.

4.6 CASE 5: A HETEROGENEOUS RESERVOIR WITH 16 PRODUCERS AND 9 INJECTORS

In the last case study, we feature a highly heterogeneous reservoir in a fluvial channel deposition environment. Permeability varies spatially in the reservoir while the main directions of heterogeneity are along northwest and southeast directions. We test the coupled CRM model in this field with 16 producers and 9 injectors. An alternative way of connectivity presentation is demonstrated in this case. Both fully-coupled and simplified-coupled schemes are applied and the results are then compared and discussed.

4.6.1 General Reservoir Information

The data set we use to create the permeability field is the Stanford V dataset, which is the same as case 2. The geostatistical modeling software SGEMS is applied to perform the sequential Gaussian simulation to generate permeability and reservoir depth realizations, which are then assigned in the reservoir simulation. This reservoir has totally 5 layers. Each layer has a different permeability distribution (see Figure 4.79). The fluvial channels are along the northwest and southeast directions throughout all layers. The depth of each grid also varies (see Figure 4.80). Porosity is fixed at the value of 0.2. Other key reservoir and fluid parameters of this field are summarized in Table 4.18. There are 9 injectors and 16 producers in this synthetic field and wells locations are shown in Figure 4.81.

Figure 4.82 is the simulated water cuts in all producers. It shows that producer water cuts behave differently owing to the reservoir heterogeneity. We observe most wells have water breakthrough time around the 20^{th} month. The exceptions are producers 11 and 13, whose water breakthrough time is much later at the 42^{th} month and the 55^{th} month, respectively.

Parameters	Value
Number of grid blocks	49×49×5
Grid block sizes (ft)	40×40×40
Porosity	0.2
Oil compressibility (psi^{-1})	5×10^{-5}
Water compressibility (psi^{-1})	1×10^{-6}
Rock compressibility (psi^{-1})	1×10^{-6}
Water relative permeability	$k_{rw}^{o}\left(\frac{S_w - S_{wr}}{1 - S_{wr} - S_{or}}\right)^2$
Oil relative permeability	$k_{ro}^{o}\left(\frac{1 - S_w - S_{or}}{1 - S_{wr} - S_{or}}\right)^2$
Irreducible water saturation	0.3
Residual oil saturation	0.4
End-point water relative permeability	0.3
End-point oil relative permeability	1
Water viscosity (cp)	0.5
Oil viscosity (cp)	1.66
Initial reservoir pressure (psi)	1250

Table 4.18 Key reservoir and fluid parameters of case 5

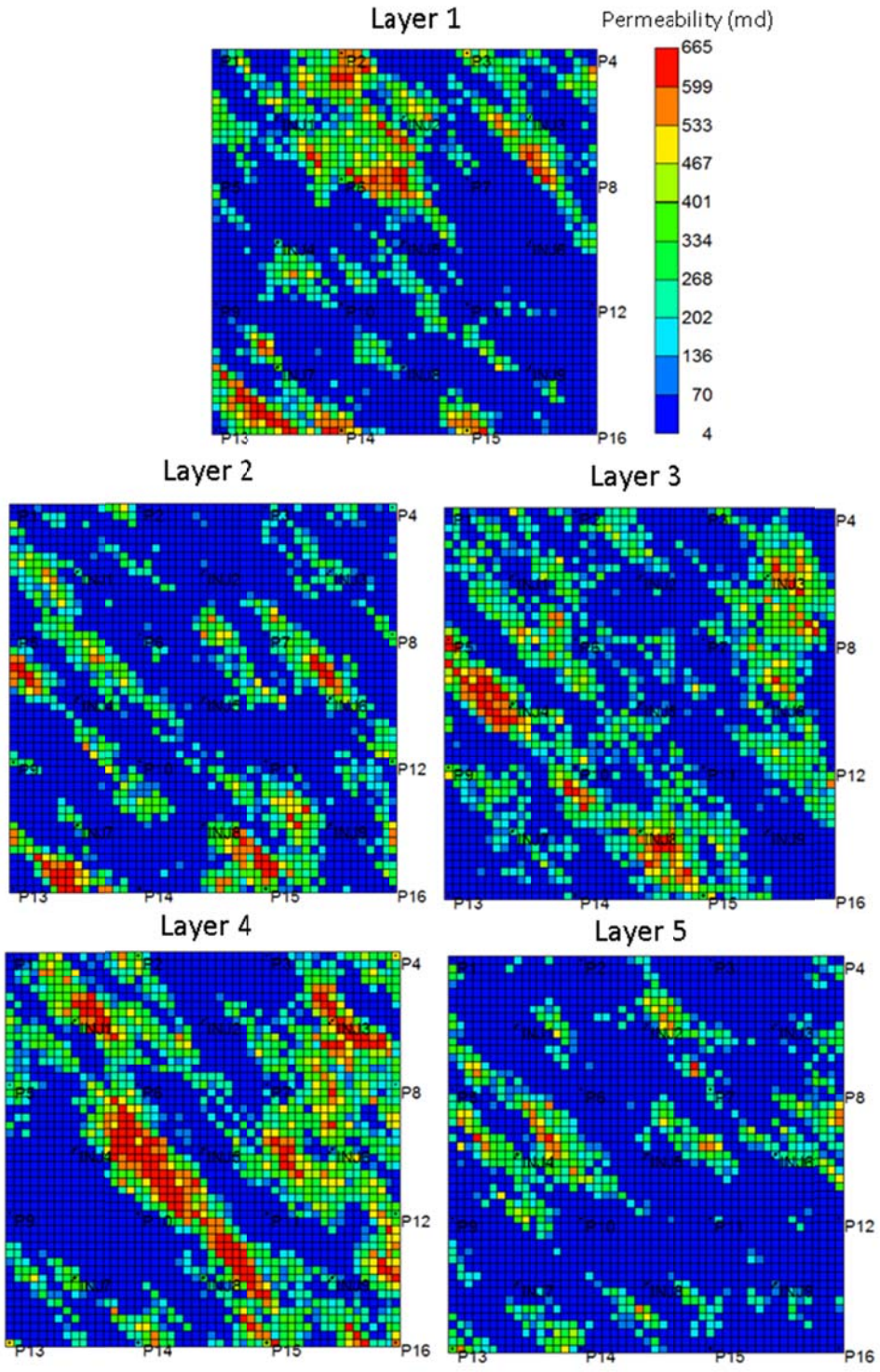

Figure 4.79 Reservoir permeability distributions in case 5.

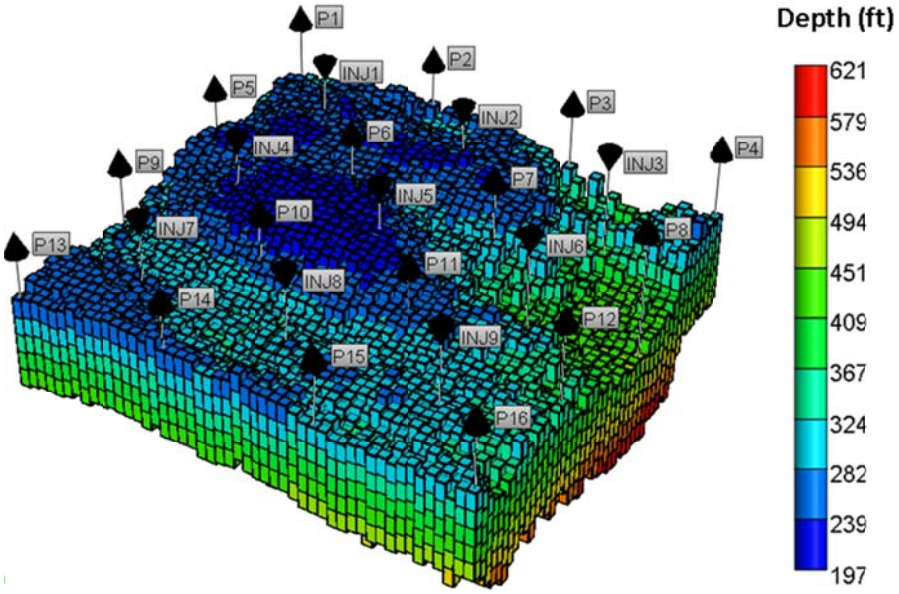

Figure 4.80 Reservoir depths in case 5.

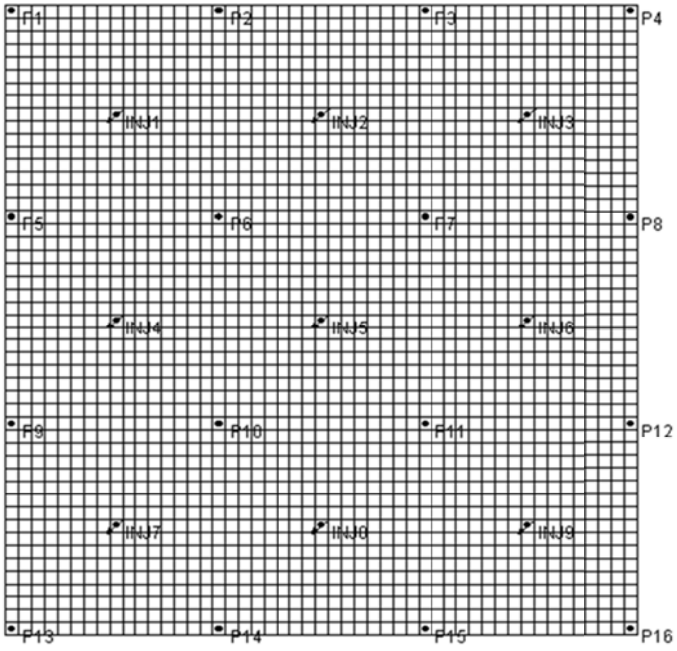

Figure 4.81 Well locations in case 5.

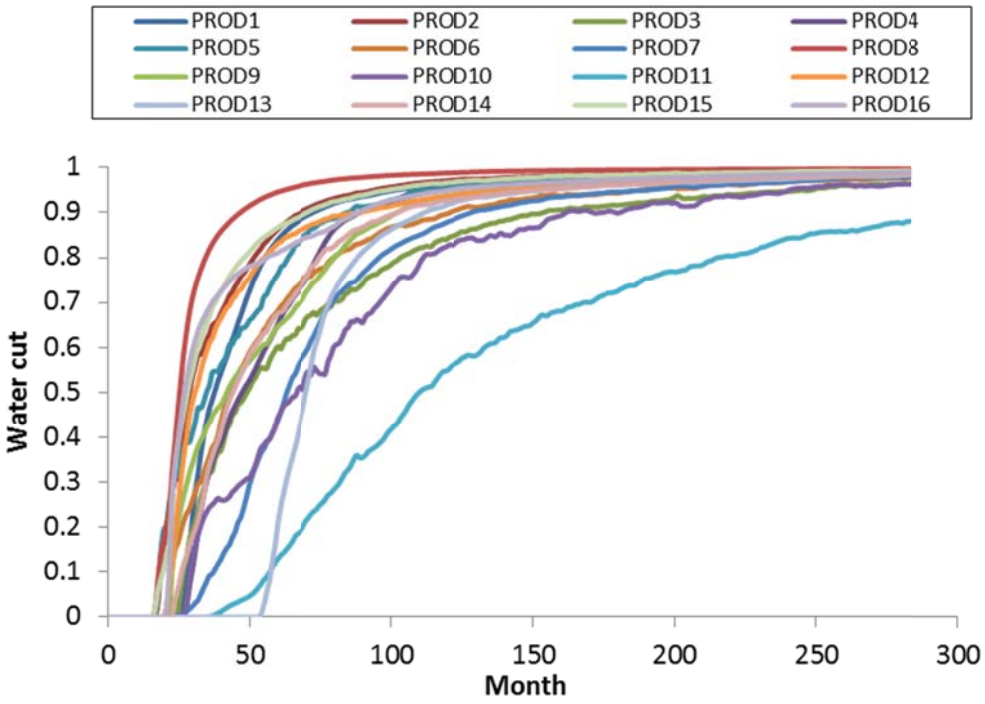

Figure 4.82 The simulated water cuts in case 5.

4.6.2 History Match Using Fully-Coupled and Simplified-Coupled Schemes

In this case, we applied both the fully-coupled and simplified-coupled CRM models to compare the model parameters obtained as well as the computation time under the two different schemes.

4.6.2.1 History Match Inputs

Besides the injection and production data, the required inputs for the fully-coupled scheme are summarized in Table 4.19. The simplified-coupled scheme uses the same inputs as the fully-coupled scheme except that compressibilities are not required. The history match time window extends from the 60th to the 250th month.

Input		Value
Reservoir/fluid properties	μ_w (cp)	0.5
	μ_o (cp)	1.66
	k_{rw}	$k_{rw}^{o}\left(\frac{S_w - S_{wr}}{1 - S_{wr} - S_{or}}\right)^2$
	k_{ro}	$k_{ro}^{o}\left(\frac{1 - S_w - S_{or}}{1 - S_{wr} - S_{or}}\right)^2$
	S_{wr}	0.3
	S_{or}	0.4
	k_{rw}^{o}	0.3
	k_{ro}^{o}	1
	c_f (psi^{-1})	1×10^{-6}
	c_w (psi^{-1})	1×10^{-6}
	c_o (psi^{-1})	5×10^{-5}
	c_t (psi^{-1})	2.65×10^{-6}

Table 4.19 The coupled CRM inputs for fully-coupled scheme in case 5.

4.6.2.2 The Total Production Fits

To present the history match quality under the two different schemes, we summarize the coefficient of determination (R^2) in all producers in Figure 4.83. Both schemes show positive and large R^2 values, indicating excellent total production fits. Overall, the fully-coupled CRM model gives a slightly better history match quality than the simplified-coupled CRM model except for producers 4 and 11. We also observe that the producers 11 and 13 have poor fits regardless of the model schemes used.

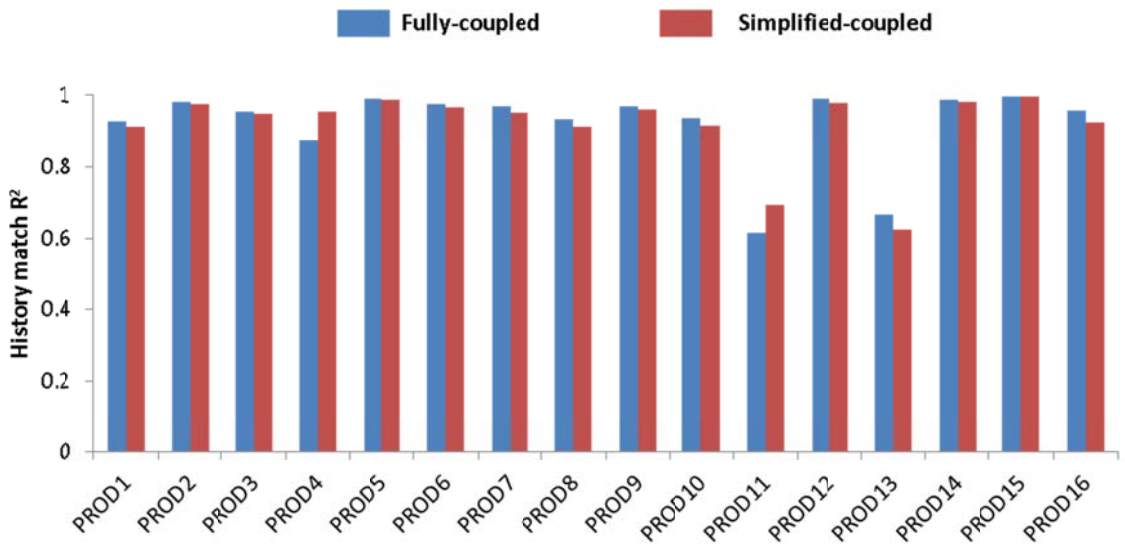

Figure 4.83 The total production history match fitting quality using the fully-coupled and simplified-coupled CRM models in case 5.

4.6.2.3 Connectivity

High permeability stripes along northwest and southeast directions serve as geological references to validate the coupled CRM model as we also expect a similar trend to be seen on the connectivity map.

Figure 4.84 is a typical connectivity map that we have shown many times in this dissertation. This map provides the fraction of water contribution from an injector to its adjacent producers. The summation of connectivity from a particular injector should be 1 if there is no injection loss. This map is particularly helpful from the perspective of water flood operation and management, since we are able to understand the injected water allocation among producers and therefore can adjust the injection schemes accordingly. Nevertheless, we do not observe an obvious trend showing strong connectivity along the channel directions from this map.

To further study the heterogeneity in the reservoir, we present an alternative connectivity map, which treats the connectivities as vectors in Figure 4.84 and further decomposes them into components along and orthogonal to the channel direction. The resulting connectivity map is shown in Figure 4.85. According to this map, 71% of injected water of injector 3 contributes to the production along the channel direction; whereas the remainder 29% of water is directed in the orthogonal direction, which is less favorable for fluid flow owing to the low reservoir permeability. The sum of the two orthogonal connectivities in a particular injector is still 1 (if no injection loss) to ensure a material balance on the injected water. From this new map, one can observe that the injected water mainly follows the channel direction, which is in a good agreement with the field permeability distributions. We also notice some injectors (such as injectors 1, 6, and 9) mainly contribute orthogonally to the channel direction, which can be a result of subjection to the local heterogeneity. In this case, we found that the new connectivity map is more helpful to study the reservoir heterogeneity and provide insights about the geological features of the reservoir.

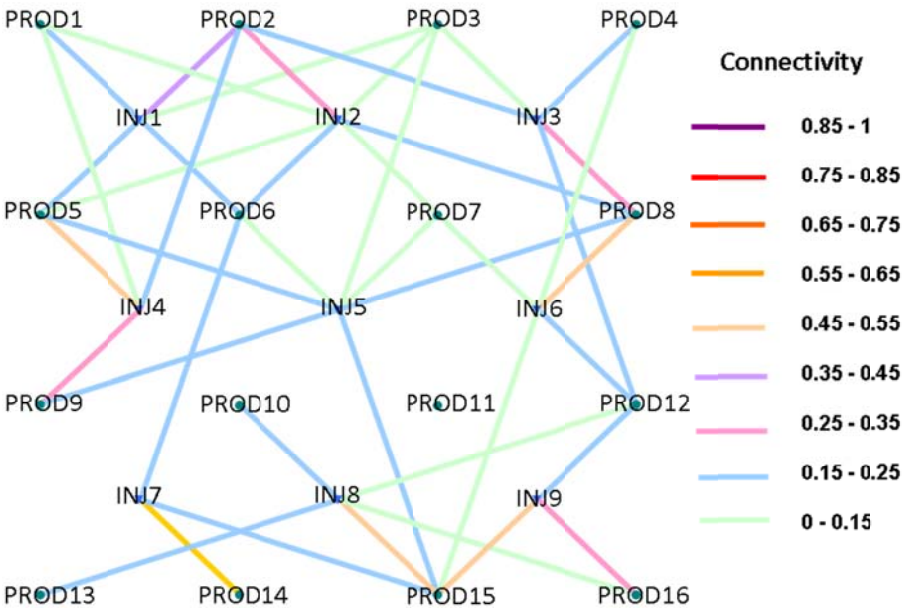

Figure 4.84 Connectivity obtained using the fully-coupled CRM model in case 5.

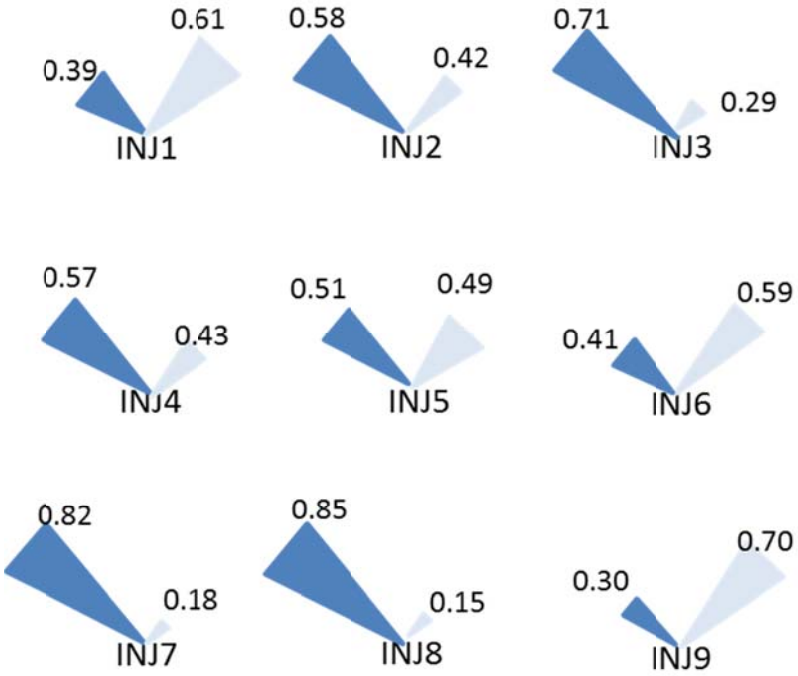

Figure 4.85 Connectivity vector map obtained using the fully-coupled CRM model in case 5.

Figure 4.86 compares the connectivities obtained using the two schemes. From a qualitative perspective, the two connectivity maps are, in a large part, similar. For example, both schemes show that producer 11 is not supported by any injectors. To quantify the difference, we summarize the injection contributions along and orthogonal to the channel direction in Tables 4.20 and 4.21. The table shows that injectors 3, 5, 7 and 8 have slightly different injected water allocations with the two schemes used, while the results in other injectors are very consistent.

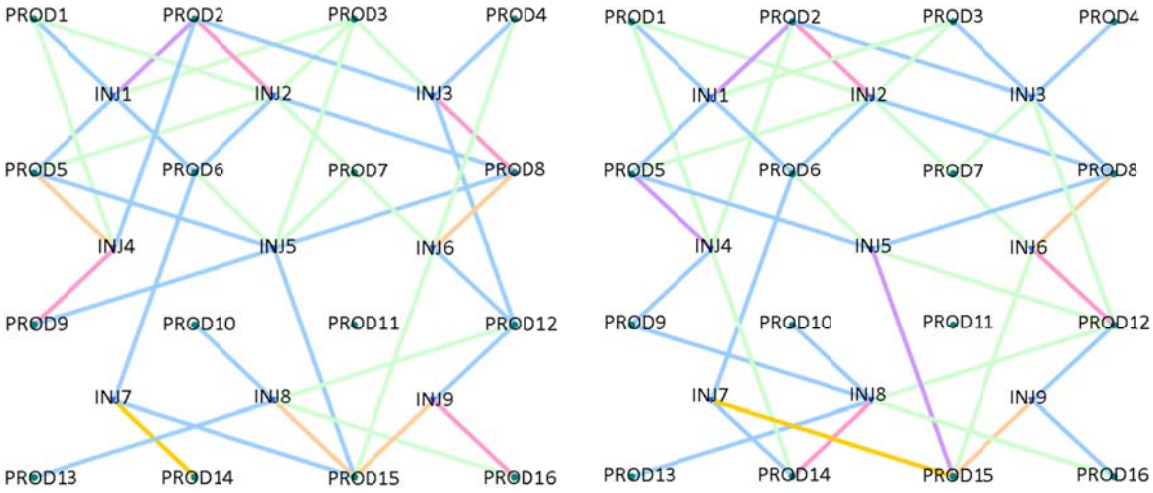

a) Fully-coupled CRM model b). Simplified-coupled CRM model

Figure 4.86 The connectivity maps obtained from the fully-coupled and simplified-coupled CRM model in case 5.

	Northwest and southeast (channel)	Northeast and southwest
INJ1	39%	61%
INJ2	58%	42%
INJ3	71%	29%
INJ4	57%	43%
INJ5	50%	50%
INJ6	41%	59%
INJ7	82%	18%
INJ8	85%	15%
INJ9	26%	74%

Table 4.20 Injection distributions along and orthogonal to the channel direction obtained from the fully-coupled CRM model in case 5.

	Northwest and southeast (channel)	Northeast and southwest
INJ1	40%	60%
INJ2	59%	41%
INJ3	58%	42%
INJ4	62%	38%
INJ5	62%	38%
INJ6	40%	60%
INJ7	66%	34%
INJ8	48%	52%
INJ9	25%	75%

Table 4.21 Injection distributions along and orthogonal to the channel direction obtained from the simplified-coupled CRM model in case 5.

4.6.2.4 Time Constants

The fully-coupled CRM model time constants are in Figure 4.87. The time constants vary between 15 and 37 days among producers depending on their associated drainage volumes and total fluid mobilities. Producers 11 and 13 are missing from Figure 4.87. Their time constants are greater than 300 days, which implies that the injection contribution is very small and therefore the main production mechanism in these two producers is pressure depletion. Figure 4.88 compares the average time constants with time obtained under the two schemes. In general, the fully-coupled scheme gives slightly larger time constants than the simplified scheme.

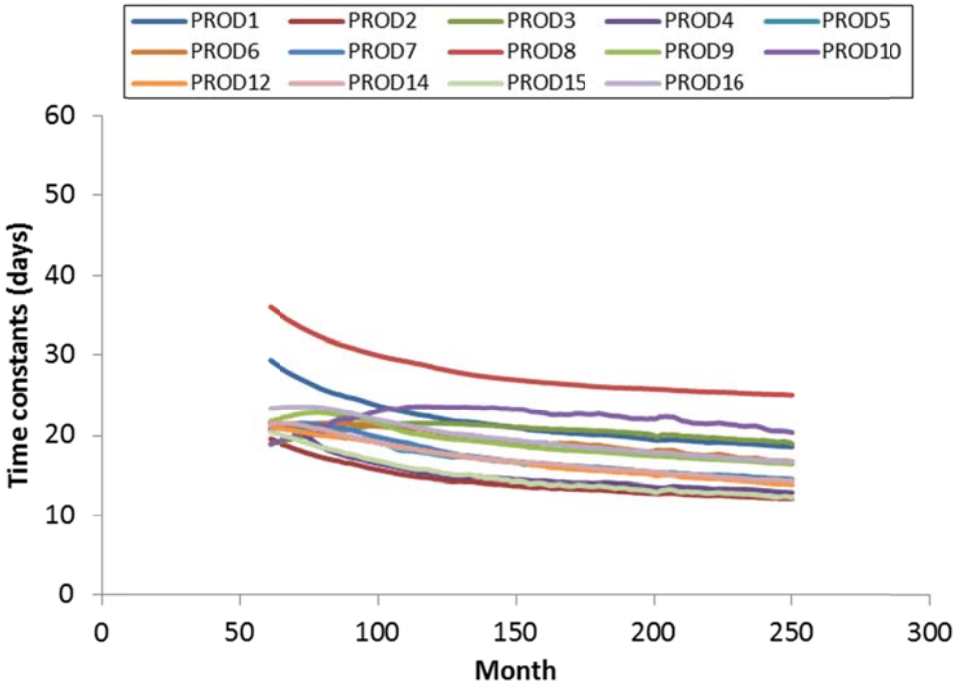

Figure 4.87 Time constants obtained using the fully-coupled CRM model in case 5.

Figure 4.88 Average time constants with time for each producer using the fully and simplified coupled schemes in case 5.

4.6.2.5 Saturation

We present the saturation results in some producers using the fully-coupled CRM model (see Figure 4.89). For comparison, we summarized the initial (the 60th month) average oil saturation and the remaining average oil saturation in the last month (the 260th month) of the history match widow using the two schemes in Tables 4.22 and 4.23. In general, the two approaches give consistent saturation results.

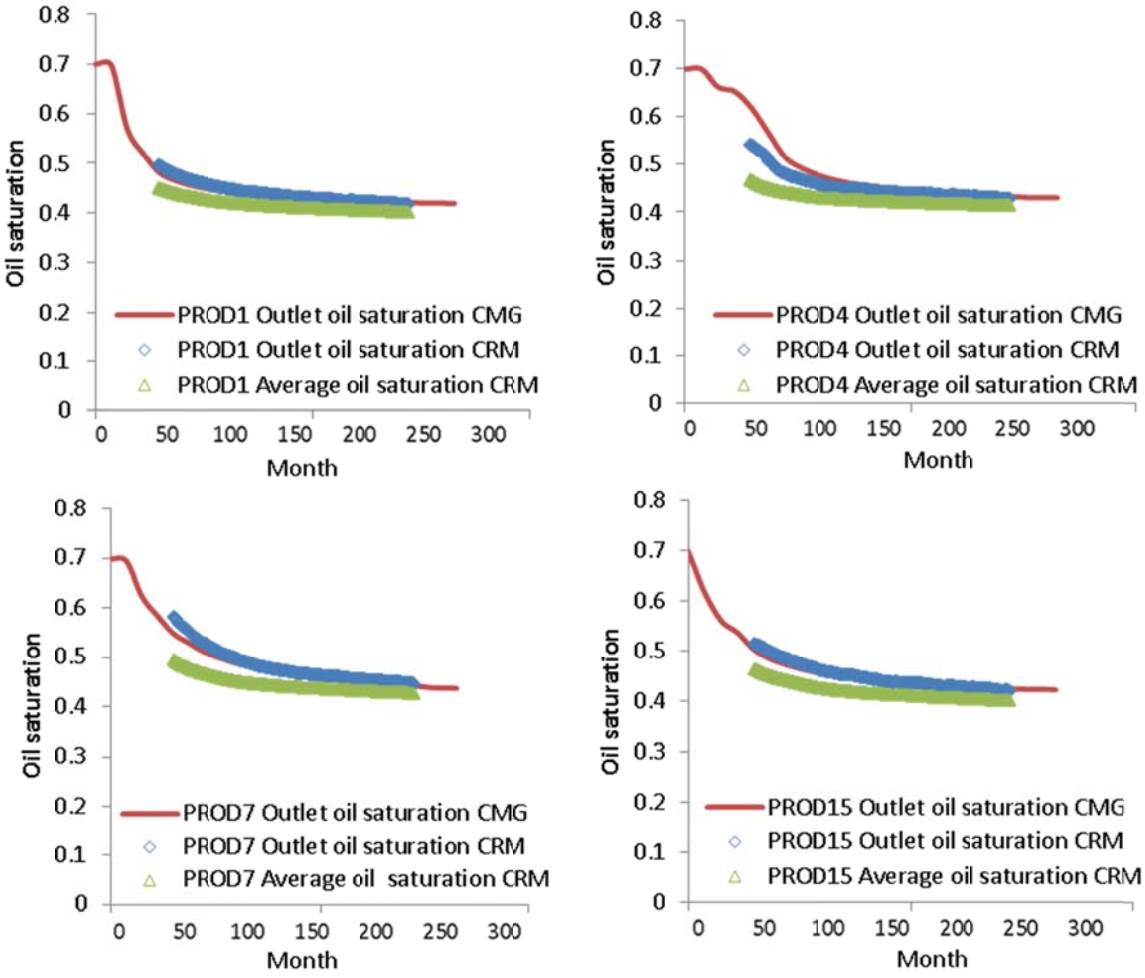

Figure 4.89 Oil saturation obtained using the fully-coupled CRM model in case 5.

Well number	Initial oil saturation at the 60th month	
	Fully-coupled CRM	Simplified-coupled CRM
PROD1	0.4908	0.5070
PROD2	0.4554	0.4537
PROD3	0.4559	0.4873
PROD4	0.4605	0.4586
PROD5	0.4718	0.4662
PROD6	0.5176	0.4982
PROD7	0.4939	0.4704
PROD8	0.5376	0.5367
PROD9	0.5115	0.5105
PROD10	0.5026	0.4907
PROD11	0.5830	0.5404
PROD12	0.4811	0.4762
PROD13	0.5736	0.5676
PROD14	0.4929	0.4733
PROD15	0.4649	0.4649
PROD16	0.5056	0.4786

Table 4.22 The initial average oil saturation at the 60th month using the fully-coupled and simplified-coupled CRM model in case 5.

Well number	Remaining oil saturation at the 250th month	
	Fully-coupled CRM	Simplified-coupled CRM
PROD1	0.4001	0.4001
PROD2	0.4016	0.4018
PROD3	0.4400	0.4587
PROD4	0.4201	0.4119
PROD5	0.4271	0.4257
PROD6	0.4314	0.4396
PROD7	0.4163	0.4236
PROD8	0.4000	0.4000
PROD9	0.4323	0.4364
PROD10	0.4602	0.4621
PROD11	0.4849	0.4823
PROD12	0.4050	0.4050
PROD13	0.4027	0.4028
PROD14	0.4135	0.4197
PROD15	0.4001	0.4001
PROD16	0.4200	0.4271

Table 4.23 The remaining average oil saturation at the 250th month using the fully-coupled and simplified-coupled CRM models in case 5.

4.6.2.6 Computation Time

Finally, the computation time of the simplified and fully coupled options is in Figure 4.90. Even though both cases take only minutes to run, the simplified-coupled case is about three times faster than the fully-coupled case. While it is true that the fully-coupled model costs more time, this case doesn't lead to a general conclusion that the fully-coupled case is three times slower than the simplified-coupled option. The

computation time can vary depending on the size of the field, number of wells and the length of the history match window, etc.

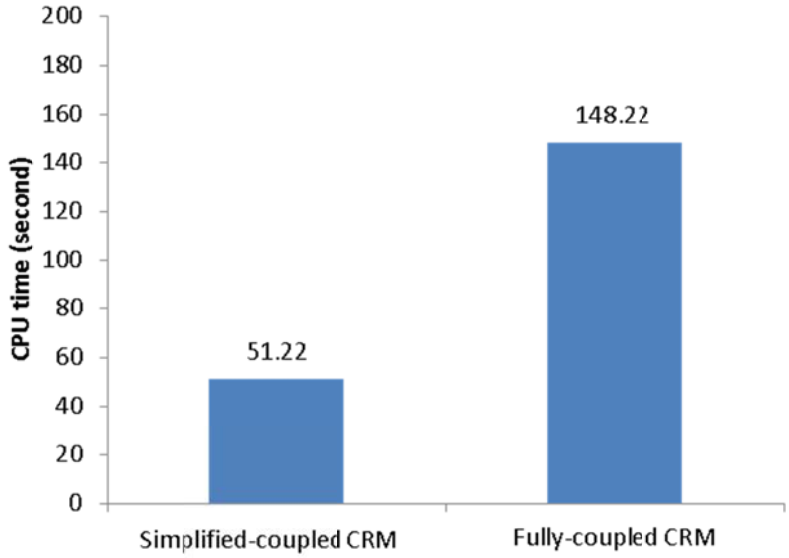

Figure 4.90 Comparison of CPU time of the fully-coupled and simplified-coupled schemes in case 5

4.6.3 Summary

The coupled CRM model is tested in a highly heterogeneous reservoir. Both fully-coupled and simplified-coupled schemes are applied. We observe that the model parameters obtained are slightly different since the compressibility has been neglected in the saturation equation in the simplified-coupled scheme. The fully-coupled model cost three times more computation time compared to the simplified-coupled model in this case. We also find that the connectivity vector map is more helpful to study the reservoir heterogeneity and provide insights towards the geological features of the reservoir.

CHAPTER 5: SENSITIVITY STUDY

As demonstrated in the previous chapters, the coupled CRM model can capture the two-phase flow effects. Extra reservoir/fluid information is required as inputs to accomplish this goal in the coupled CRM model, which includes oil/water viscosities, oil/water relative permeabilities, and pore/fluid compressibilities. To study and understand the relationship between these extra inputs and the CRM model outputs (model parameters such as the connectivity and the time constant, etc.), we perform sensitivity analysis in this chapter.

There are numerous approaches (Saltelli et al., 2008) to performing a sensitivity analysis. In this chapter, we adopt the changing-one-factor-at-a-time (OFAT) method, which is the simplest and most common approach, to find out what impact a specific factor produces on outputs. The OFAT procedure is comprised of changing one input variable while keeping others at their baseline (nominal) values and then returning the variable to its nominal value to repeat for each of the other inputs in the same way. Sensitivity may then be measured by monitoring changes in the output. Changing one variable at a time increases the comparability of the results and minimizes the chances of computer program crashes, more likely when several input factors are changed simultaneously. Nevertheless, because OFAT does not take into account the simultaneous variation of input variables, it limits its capability to detect the presence of interactions between input variables.

5.1 EFFECT OF MOBILITY AND COMPRESSIBILITY

In this chapter, we explore the coupled CRM model sensitivity concerning two aspects: mobility and compressibility effects. The mobility effect can influence the

saturation distribution and evolution in the reservoir, and therefore impacts the oil production rate and the flood efficiency. The compressibility effect describes the propagation of pressure wave in the reservoir and hence determines the time lag between injection signal and production response.

All factors considered in the sensitivity study in this chapter are summarized in Figure 5.1. The mobility effect includes oil and water relative permeabilities and oil-water viscosity ratio. Commonly used empirical relative permeability models separate the endpoint relative permeability and exponents explicitly, which will be discussed separately.

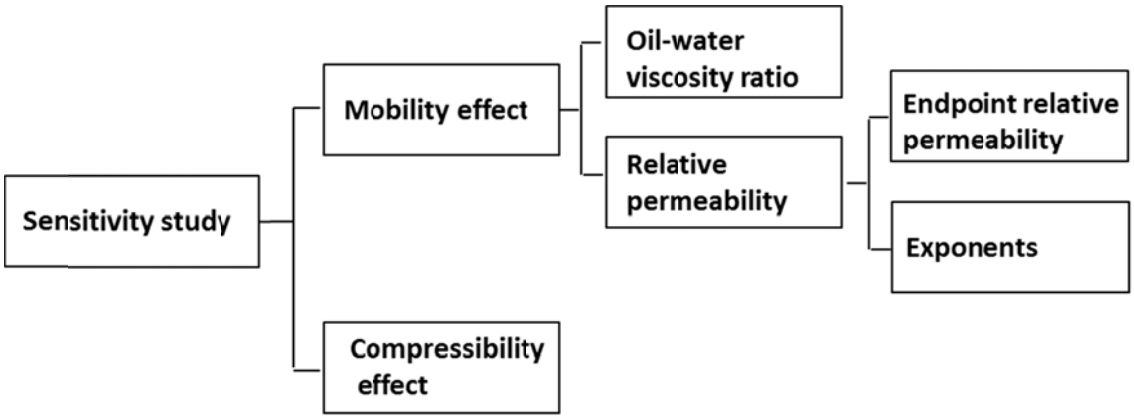

Figure 5.1 Effects considered in the sensitivity study.

5.1.1 Effect of Mobility Change

Neglecting the capillary pressure and gravity effect, the water fractional flow in a water-oil immiscible displacement has the form of (Buckley and Leverett, 1942):

$$f_w = \frac{1}{1+\frac{k_{ro}\mu_w}{k_{rw}\mu_o}} \qquad 5.1$$

We introduce the commonly used empirical relative permeability exponential expressions (Corey, 1954):

$$k_{rw} = k_{rw}^{0}\left(\frac{S_w - S_{wr}}{1 - S_{wr} - S_{or}}\right)^{n_1} \tag{5.2}$$

$$k_{ro} = k_{ro}^{0}\left(\frac{1 - S_w - S_{or}}{1 - S_{wr} - S_{or}}\right)^{n_2} \tag{5.3}$$

where k_{rw}^{0} and k_{ro}^{0} represent the water and oil relative permeability end-points, respectively, which is the relative permeability evaluated at the saturation when the other phase becomes immobile (see Figure 5.2), and n_1 and n_2 represent the water and oil relative permeability exponents, which are obtained by fitting the experimental data. The relative permeability exponents control how fast the relative permeability curves decline or increase with saturations in the model.

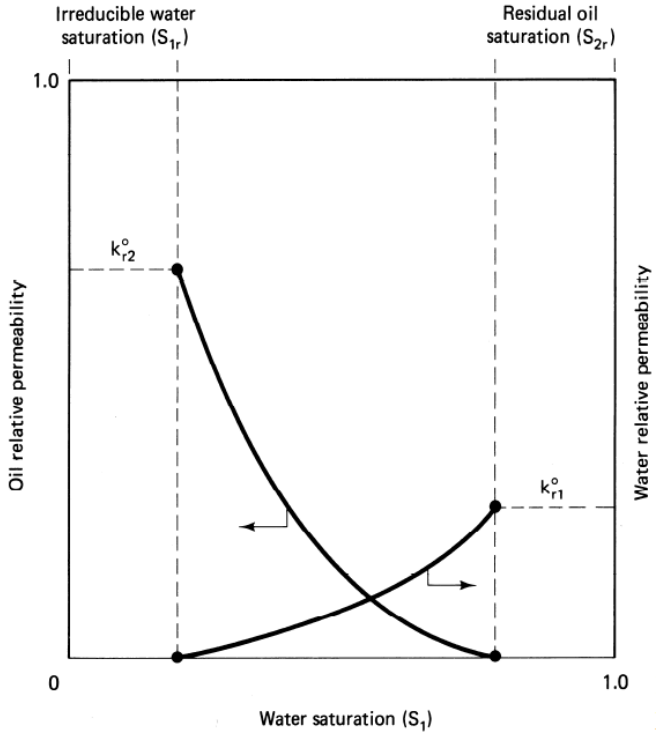

Figure 5.2 Schematic of oil-water relative permeabilities (Lake, 1989).

Substituting Eqs. 5.2-5.3 into Eq. 5.1, we obtain:

$$f_w = \frac{1}{1+\frac{(1-S)^{n_2}}{M^o S^{n_1}}} \tag{5.4}$$

where M^0 is the endpoint water-oil mobility ratio, which is defined as:

$$M^0 = \frac{k_{rw}^0 \mu_o}{k_{ro}^0 \mu_w} \tag{5.5}$$

and S is the reduced water saturation given as:

$$S = \frac{S_w - S_{wr}}{1 - S_{wr} - S_{or}} \tag{5.6}$$

Figure 5.3 illustrates how end-point water-oil mobility ratio M^0 affects the shape of the fractional flow curves and the displacement efficiency. Large end-point mobility ratio can cause unstable flood front and viscous fingering during the displacement. Decreasing the end-point mobility ratio can increase vertical and areal sweep efficiency. In fact, most EOR processes rely, to some extent, on lowering the mobility ratio between the displacing and displaced fluids.

We mention that changing oil-water viscosity ratio (μ_o / μ_w) or water-oil relative permeability endpoint ratio (k_{rw}^0 / k_{ro}^0) can achieve the same purpose of changing the mobility ratio, while the corresponding mechanisms are completely different.

As a whole, the fractional flow curve is uniquely determined as a function of saturation through the relative permeability relations and the oil-water viscosity ratio.

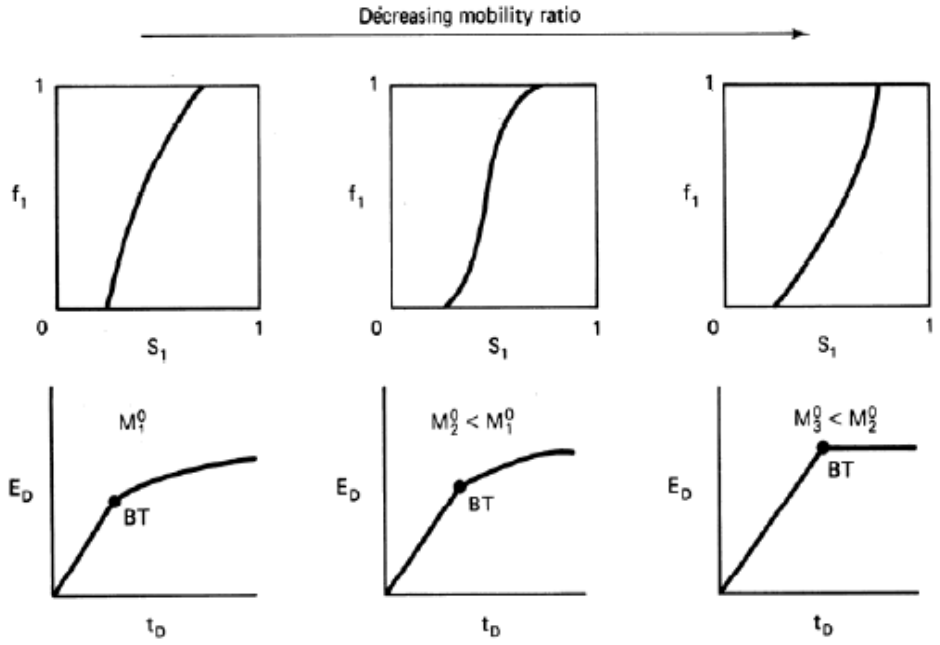

Figure 5.3 Schematic illustration of the effect of end-point mobility ratio on displacement efficiency (Lake, 1989).

5.1.2 Effect of Compressibility Change

Reservoir pore and fluid are compressible. In a one-dimensional flow, it is found that fluid compressibility can spread out the Buckley-Leverett shock front (Lake, 1989) However, the effect is not pronounced until the compressibility is significantly large (see Figure 5.4).

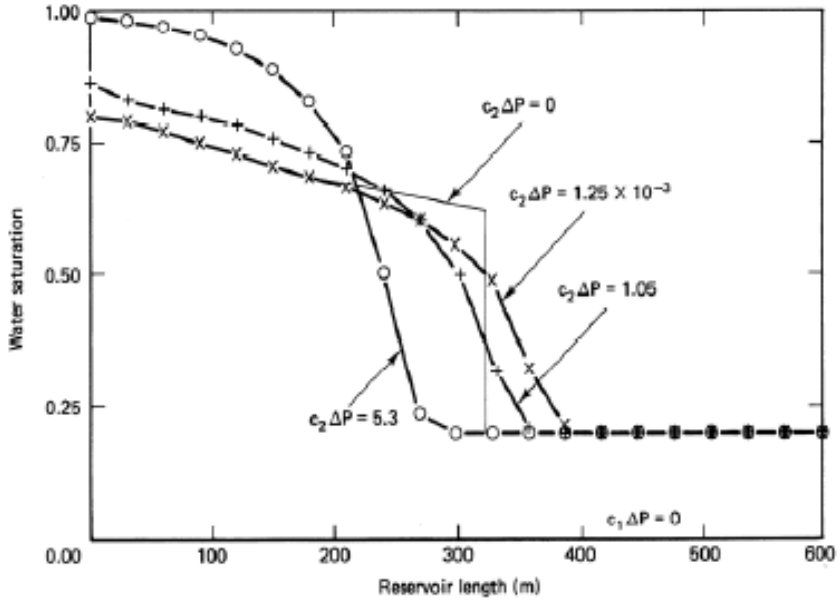

Figure 5.4 Water saturation profiles for one-dimensional water floods at a certain time under different oil compressibilities (adapted from Samizo, 1982).

In general, compressibility determines the time lag between injection signal and production response. Large compressibility will cause a large time lag as the reservoir system is able to store/release more fluid for the same pressure change. Consequently, more time must be taken for the producer to respond to the injection signal. At the extreme case when the compressibility is zero, the production reacts to the injection signal instantaneously without a time lag as the reservoir system has no capability of storing/releasing any extra fluid.

5.2 SENSITIVITY CASE STUDIES

A homogenous synthetic reservoir (see Figure 5.5), which is the same as the five-spot reservoir that we have mentioned in Chapter 4, is used for the following analysis and discussions. We use a synthetic reservoir because it enables us to change any

reservoir/fluid properties of interest and obtain a production response accordingly. Furthermore, the reservoir should be homogeneous to avoid any complication caused by reservoir heterogeneity, which ensures that the effects in the outputs are caused by the variable of interest unambiguously. Table 5.1 summarizes the reservoir/fluid properties that are most relevant to this sensitivity analysis. Other information in this field can be found in Table 4.9.

Parameters	**Value**
c_o (psi^{-1})	3×10^{-5}
c_w (psi^{-1})	1×10^{-6}
c_f (psi^{-1})	1×10^{-6}
k_{rw}	$k_{rw}^{o}\left(\frac{S_w - S_{wr}}{1 - S_{wr} - S_{or}}\right)^{n_1}$
k_{ro}	$k_{ro}^{o}\left(\frac{1 - S_w - S_{or}}{1 - S_{wr} - S_{or}}\right)^{n_2}$
n_1	2
n_2	2
S_{wr}	0.3
S_{or}	0.4
k_{rw}^{o}	0.3
k_{ro}^{o}	1
μ_w (cp)	0.72
μ_o (cp)	1.63

Table 5.1 Reservoir/fluid parameters.

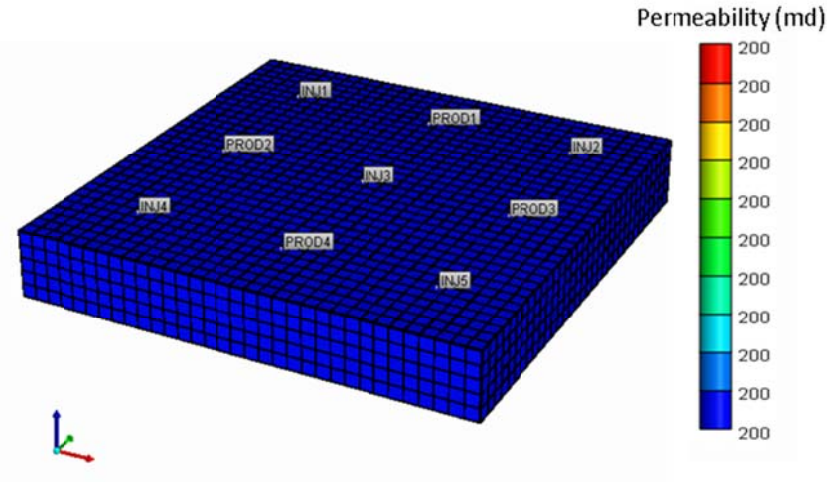

Figure 5.5 A synthetic homogeneous reservoir used for sensitivity study.

Based on the discussion above, we perform sensitivity analysis with respect to the changes of four parameters in this reservoir:

1) Oil-water viscosity ratio
2) Water-oil relative permeability endpoint ratio
3) Oil/water relative permeability exponents
4) Oil compressibility

The procedure to conduct the sensitivity study is described in Figure 5.6. Each time, one of the properties mentioned above is changed. We then perform a reservoir simulation (CMG) run using the changed value of the property of interest to obtain the production response. There are 4 producers in the reservoir. To avoid repetition, we only take the performance of producer 1 for analysis as the other producers behave similarly.

Using the injection rates, the corresponding simulated production rates and the new value of property of interest, a coupled CRM model run can be made. The history match time window is fixed from the 75^{th} to the 250^{th} month in all the sensitivity case studies we carry out. Afterwards, we can obtain the coupled CRM outputs. Meanwhile,

we analyze the impacts this particular property produced on the outputs (connectivity, time constant, and saturation).

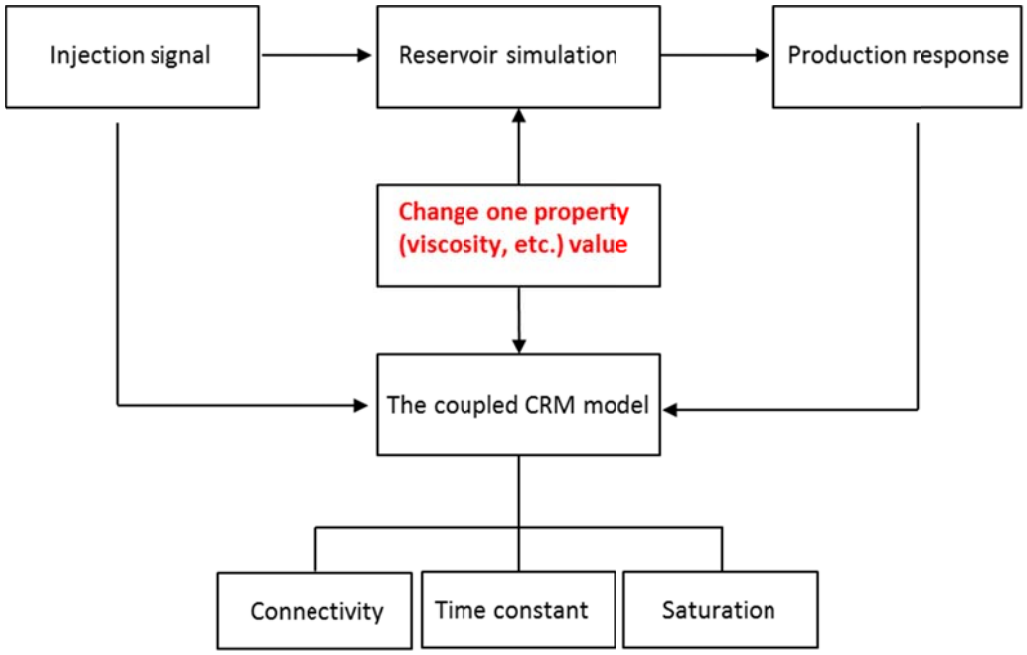

Figure 5.6 Schematic of the procedures to conduct sensitivity analysis.

5.2.1 Changing the Oil-Water Viscosity Ratio

In this section, we discuss the impact of oil-water viscosity ratio on the coupled CRM model output parameters. Table 5.2 summarizes the water/oil viscosity data used for the sensitivity study. The water viscosity is kept the same at 0.72cp; while oil viscosity varies so that the oil-water viscosity ratio changes accordingly.

	μ_w (cp)	μ_o (cp)	μ_o / μ_w
Case 1	0.72	1.63	2.3
Case 2	0.72	16.3	22.6
Case 3	0.72	32.6	45.3

Table 5.2 Viscosity data in the sensitivity analysis.

We conduct three separate reservoir simulation (CMG) runs using the above viscosities. Figure 5.7 shows the simulated water cut of producer 1. We notice that early water breakthrough occurs in the case of large oil-water viscosity ratio, which leads to a small oil recovery as indicated in Figure 5.8.

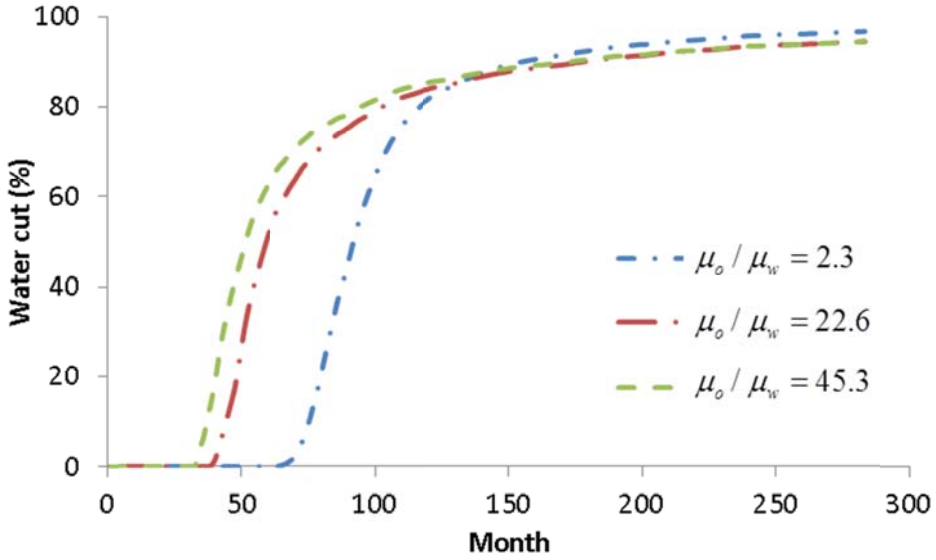

Figure 5.7 The simulated water cuts of producer 1 under different oil-water viscosity ratios.

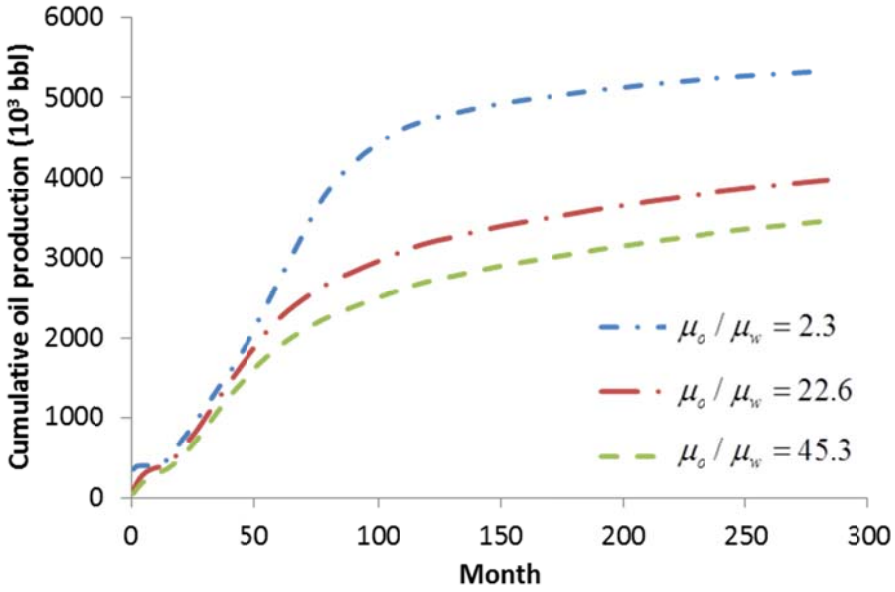

Figure 5.8 The simulated oil recovery of producer 1 under different oil-water viscosity ratios.

Using injection data and the corresponding simulated production data, three coupled CRM runs are performed with the viscosity inputs in Table 5.2. We discuss the model parameters obtained in the following sections.

5.2.1.1 Connectivity

The connectivity obtained using the coupled CRM model in case 1 (oil-water viscosity ratio 2.3) is shown in Figure 5.9. A near symmetric connectivity map is observed, which is valid since the reservoir is homogeneous and the well pattern is symmetric. Table 5.3 shows the connectivity values obtained.

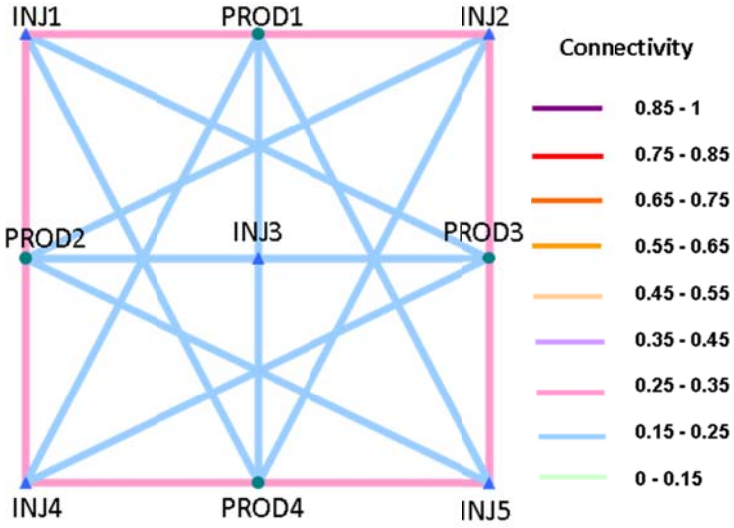

Figure 5.9 Connectivity map for the case of $\mu_o / \mu_w = 2.3$ using the coupled CRM model.

	PROD1	**PROD2**	**PROD3**	**PROD4**
INJ1	0.33	0.34	0.16	0.17
INJ2	0.32	0.16	0.34	0.18
INJ3	0.25	0.25	0.25	0.25
INJ4	0.17	0.34	0.16	0.33
INJ5	0.18	0.17	0.33	0.32

Table 5.3 Connectivity matrix for the case of $\mu_o / \mu_w = 2.3$ using the coupled CRM model

We use connectivities obtained from case 1 as a base case and compute the relative change in connectivities obtained from cases 2 and 3. The relative connectivity change is defined as the absolute difference in connectivity between the target case and the base case divided by the magnitude of the base case connectivity. The base case is chosen purely for the purpose of comparison. There is no implication that the results in the base case are better than other cases.

Tables 5.4-5.5 present the relative connectivity change in case 2 and case 3 compared to case 1. If one takes the average value of the relative change among all well pairs, case 2 gives a 4.07% average relative change while it is 6.73% in case 3. Both changes are small.

	PROD1	**PROD2**	**PROD3**	**PROD4**	**Average change compared to base case**
INJ1	2.68%	3.43%	5.95%	6.51%	4.07%
INJ2	2.35%	7.98%	1.74%	0.49%	
INJ3	2.14%	4.00%	2.25%	3.88%	
INJ4	2.05%	0.21%	6.91%	2.04%	
INJ5	8.78%	8.61%	4.06%	5.28%	

Table 5.4 Relative connectivity change of case 2 ($\mu_o / \mu_w = 22.6$) compared to case 1($\mu_o / \mu_w = 2.3$)

	PROD1	**PROD2**	**PROD3**	**PROD4**	**Average change compared to base case**
INJ1	5.16%	7.23%	13.07%	12.25%	6.73%
INJ2	4.32%	15.56%	4.12%	1.89%	
INJ3	2.66%	4.81%	2.67%	4.78%	
INJ4	6.65%	2.60%	2.82%	0.61%	
INJ5	13.46%	14.75%	6.76%	8.38%	

Table 5.5 Relative connectivity change of case 3 ($\mu_o / \mu_w = 45.3$) compared to case 1($\mu_o / \mu_w = 2.3$)

5.2.1.2 Time Constant

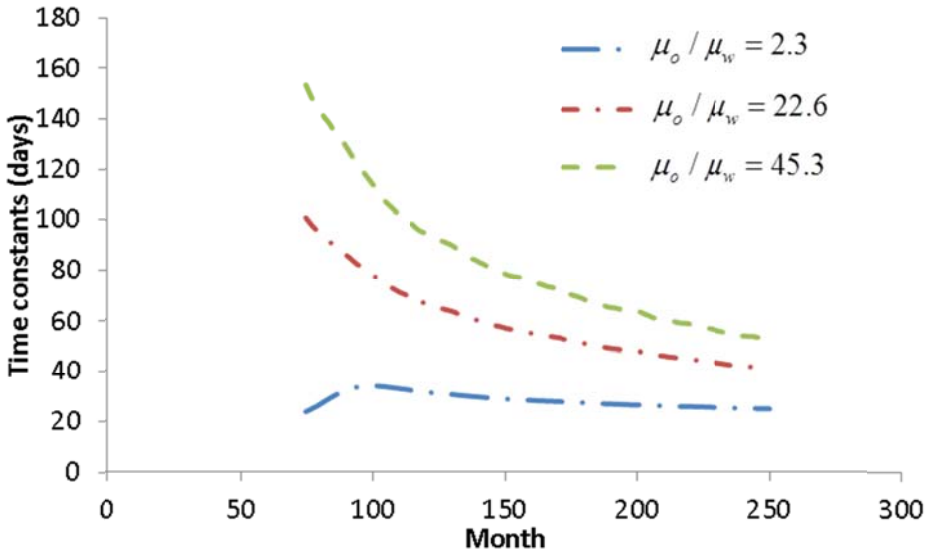

Figure 5.10 Time constants obtained using the coupled CRM model under different viscosity ratios.

Figure 5.10 gives the time constant results with different viscosity ratios. We observe a trend that the time constants increase with the increase of oil-water viscosity ratio. Figure 5.10 also shows that the difference in time constants becomes small at late time (mature water flood) as it is mainly water flowing in this production phase and water viscosity is the same for all three cases.

5.2.1.3 Average Oil Saturation

Figure 5.11 shows the average oil saturation evolution in producer 1. Case 1 ($\mu_o / \mu_w = 2.3$) has the smallest average oil saturation compared to the other two cases, which is an indication that oil has been displaced by water more efficiently within the producer's drainage volume; whereas, there are still much oil remained if the viscosity ratio is large.

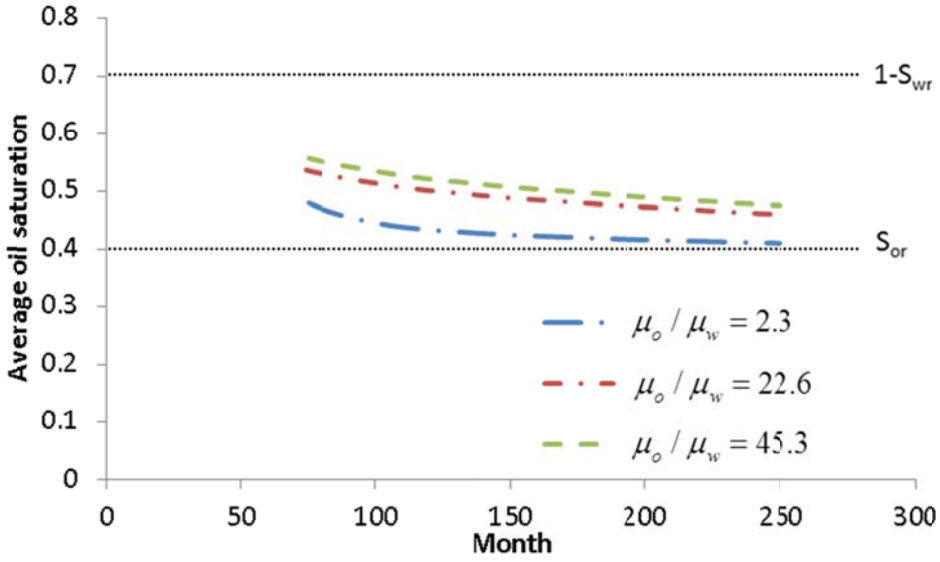

Figure 5.11 The average oil saturation obtained using the coupled CRM model under different viscosity ratios.

5.2.2 Changing Relative Permeability Exponent

We explore three sets of relative permeability exponents in this sensitivity study as shown in Figure 5.12. We keep the relative permeability exponents the same for water and oil phases for the purpose of increasing the comparability of the results. The water and oil endpoint relative permeabilities are fixed to be 1 and 0.3, respectively.

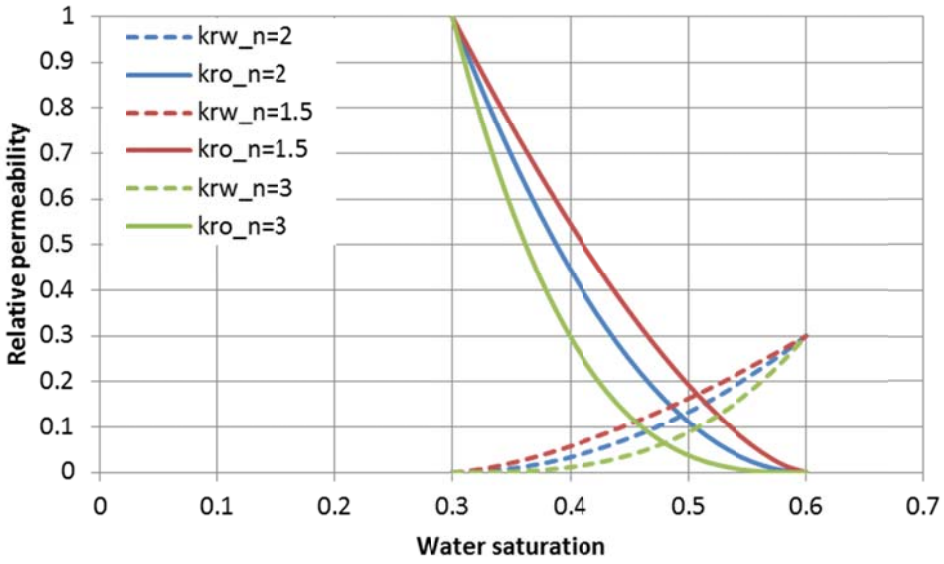

Figure 5.12 Relative permeability curves used in the sensitivity analysis.

Figure 5.13 shows the simulated water cuts in producer 1 from the three separate reservoir simulation runs. The water cuts behave differently that the large exponents case has steeper water cut curve compared to the other cases, resulting in smaller oil production rates (see Figure 5.14). On the contrary, the water cuts rise gradually and oil rates are relatively large when exponents are small. Also, the large exponent case has water breakthrough time slightly later than the other two cases, though the difference is not pronounced.

The coupled CRM model requires relative permeabilities as inputs. We conducted three CRM runs with different relative permeability inputs shown in Figure 5.12. The results are discussed in the following sections.

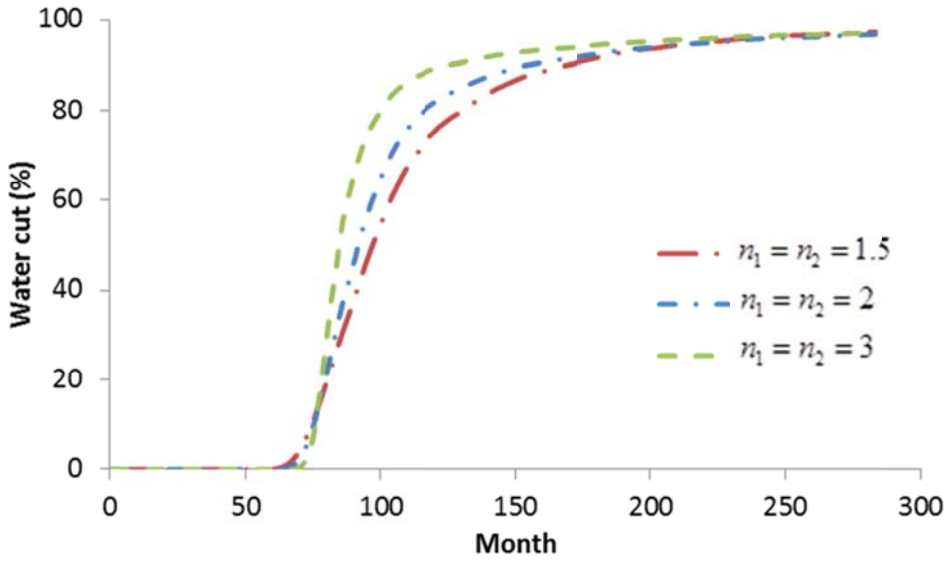

Figure 5.13 The simulated water cuts of producer 1 under different relative permeability exponents.

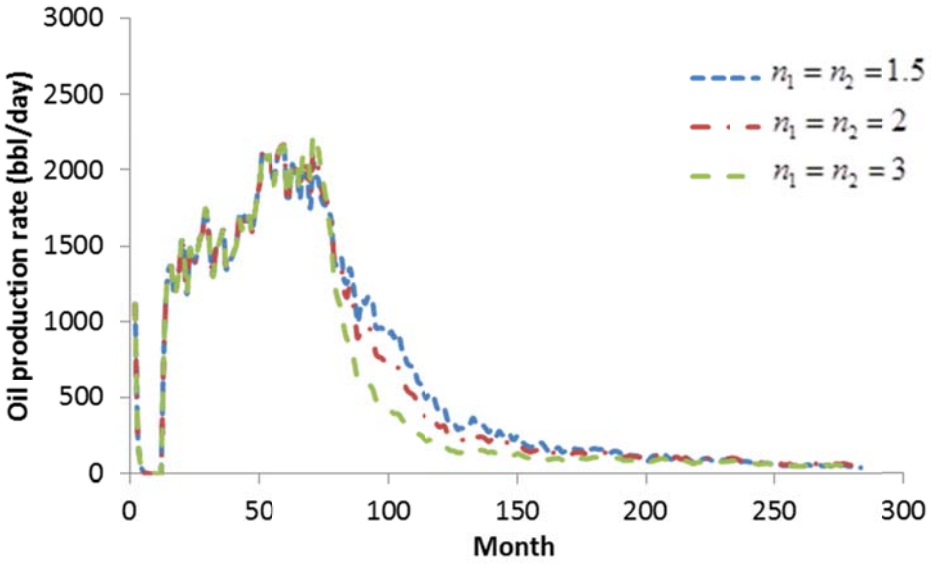

Figure 5.14 The simulated oil production rates of producer 1 under different relative permeability exponents.

5.2.2.1 Connectivity

The connectivity obtained when water/oil relative permeability exponents are equal to 2 is in Figure 5.15. Table 5.6 gives the connectivity values. Similar to the previous case, we observe a near symmetric connectivity map.

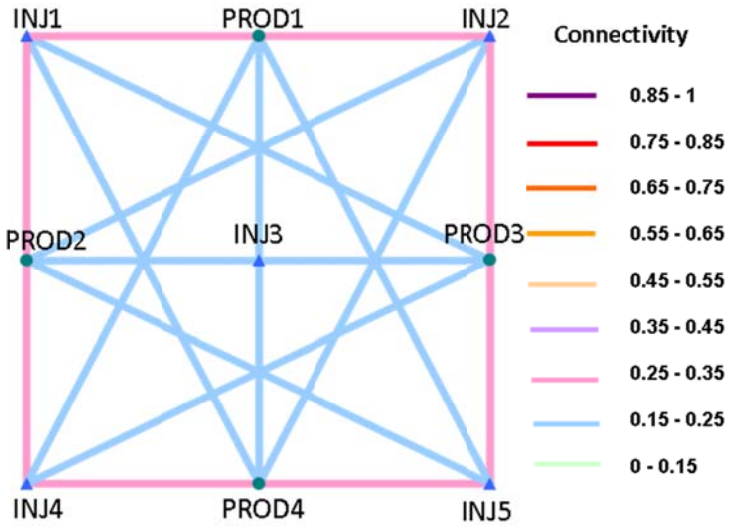

Figure 5.15 Connectivity map for the case of exponents *n*=2 using the coupled CRM model.

	PROD1	**PROD2**	**PROD3**	**PROD4**
INJ1	0.33	0.33	0.17	0.17
INJ2	0.32	0.17	0.33	0.18
INJ3	0.26	0.25	0.24	0.25
INJ4	0.17	0.33	0.17	0.33
INJ5	0.17	0.17	0.34	0.32

Table 5.6 Connectivity matrix for the case of exponents *n*=2 using the coupled CRM model.

Tables 5.7-5.8 present the relative change in connectivity compared to the above case when *n*=2. The average relative changes in the case of exponents equal to 1.5 and 3 are 1.41% and 2.6%, respectively. Again, the connectivity only change slightly when we range the relative permeability exponents.

	PROD1	**PROD2**	**PROD3**	**PROD4**	**Average change compared to base case**
INJ1	0.80%	1.27%	2.33%	1.89%	1.41%
INJ2	2.22%	0.80%	0.17%	3.03%	
INJ3	1.30%	0.20%	1.08%	0.05%	
INJ4	3.30%	0.87%	1.54%	1.57%	
INJ5	0.74%	1.58%	1.06%	2.30%	

Table 5.7 Relative connectivity change of exponents n=1.5 compared to exponents n=2.

	PROD1	**PROD2**	**PROD3**	**PROD4**	**Average change compared to base case**
INJ1	2.96%	3.20%	4.00%	8.14%	2.60%
INJ2	0.10%	9.47%	3.39%	2.84%	
INJ3	1.62%	0.50%	0.18%	2.35%	
INJ4	0.70%	1.18%	0.74%	1.20%	
INJ5	4.93%	1.27%	0.44%	2.89%	

Table 5.8 Relative connectivity change of exponents n=3 compared to exponents n=2.

5.2.2.2 Time Constant

Figure 5.16 gives the time constants obtained from the coupled CRM model. It shows the time constants increase with the increase in the exponents. We also notice that the difference in time constants becomes small at late time (mature water flood) among the three cases. This can be explained using the relative permeability curves (Figure 5.12), which shows the relative permeabilities of either phase (water or oil) under different exponents are close when the saturation approaches the irreducible oil saturation. Therefore, the total fluid mobility values are similar among the three cases, resulting in similar time constants.

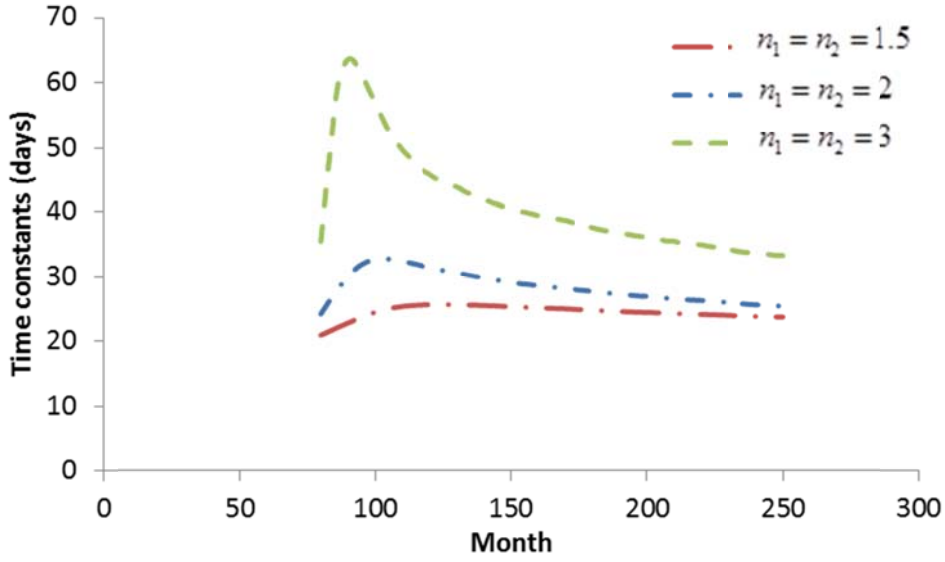

Figure 5.16 Time constants obtained using the coupled CRM model under different relative permeability exponents.

5.2.2.3 Average Oil Saturation

The average oil saturation change in producer 1 is shown in Figure 5.17. In Figure 5.17, the small exponents (n_1=n_2=1.5) case has the smallest average oil saturation indicating that efficient water-oil displacement; whereas, there are large portion of oil remained in the case of large value exponents (n_1=n_2=3) case, implying low sweep efficiency.

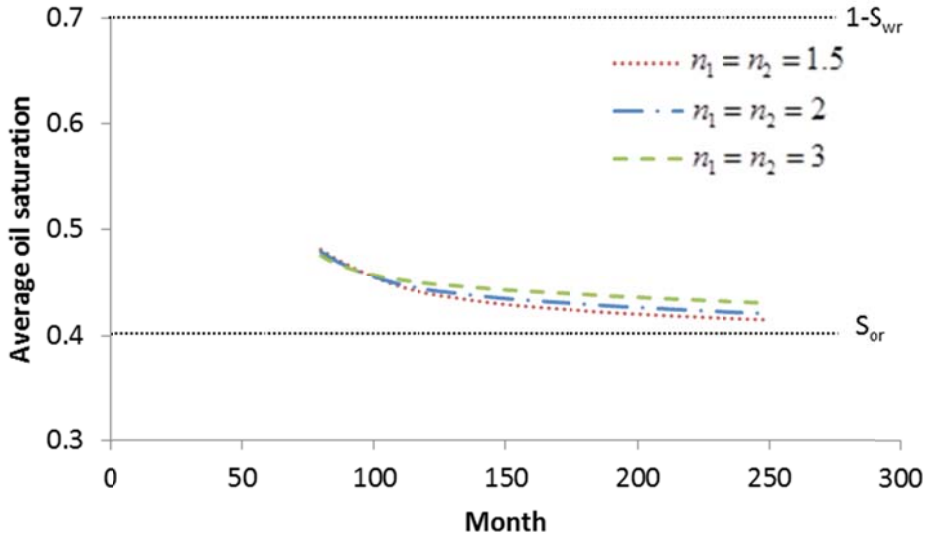

Figure 5.17 Average oil saturation obtained using the coupled CRM model under different relative permeability exponents.

5.2.3 Changing Relative Permeability Endpoint Ratio

In this sensitivity study, we fix the water and oil relative permeability exponents to be 2. The endpoint oil relative permeability is kept at 1. We test three scenarios when the water relative permeability endpoint equals to 0.1, 0.3 and 0.6, respectively. Therefore the water-oil relative permeability endpoint ratio ranges from 0.1, 0.3 and 0.6

accordingly. Figure 5.18 shows the relative permeability models used in this sensitivity study.

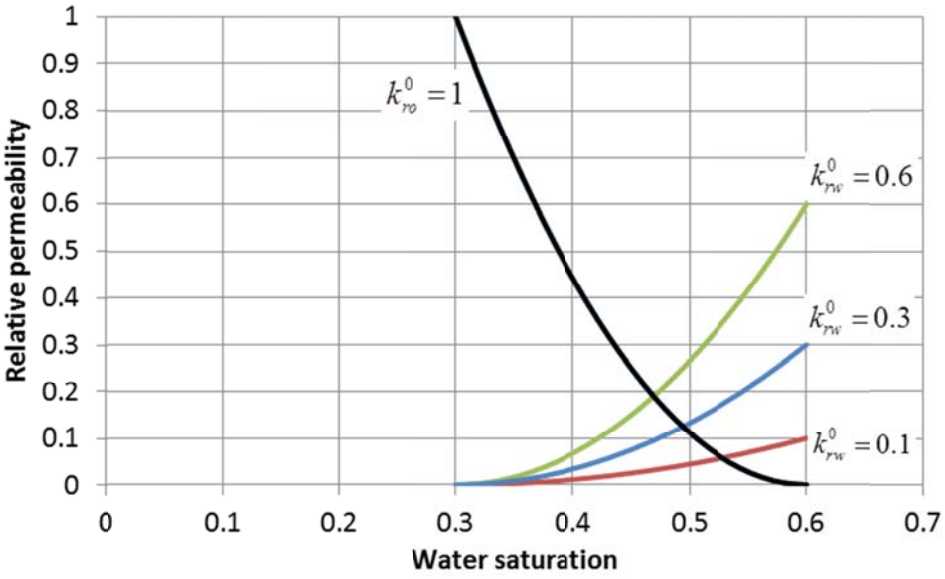

Figure 5.18 Relative permeability models with different water endpoints.

We performed three reservoir simulation runs using different water relative permeability endpoints in Figure 5.18 while all other inputs are the same. The results are shown in Figures 5.19 and 5.20. In case of large endpoint ratio (0.6), we observe early water breakthrough and gradually increasing water cuts in producer 1. On the contrary, small endpoint ratio (0.1) case gives a steep water cut curve with late water breakthrough.

We conduct three coupled CRM runs with different relative permeability inputs in Figure 5.18 to see how relative permeability endpoint ratio affects the output parameters.

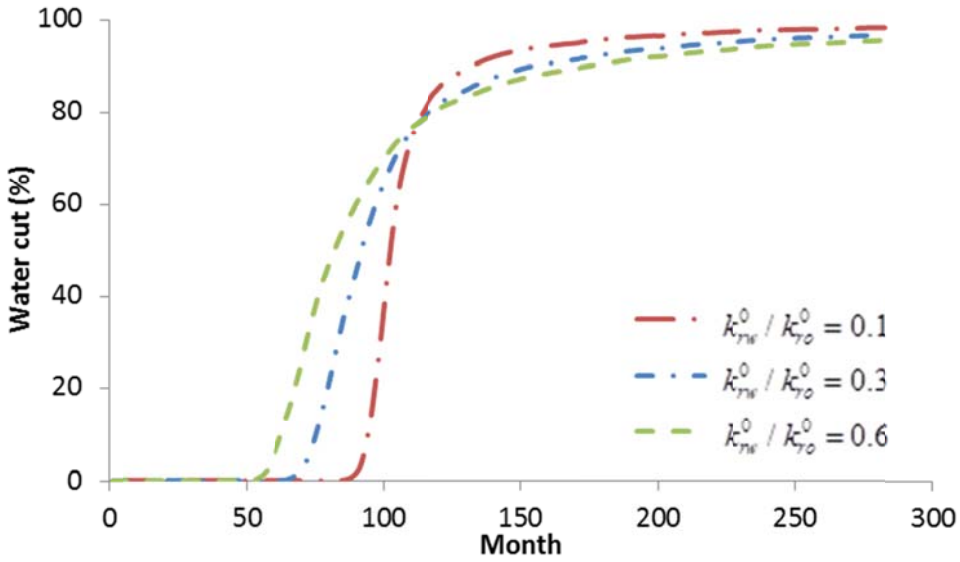

Figure 5.19 The simulated water cuts of producer 1 under different water-oil endpoint ratios.

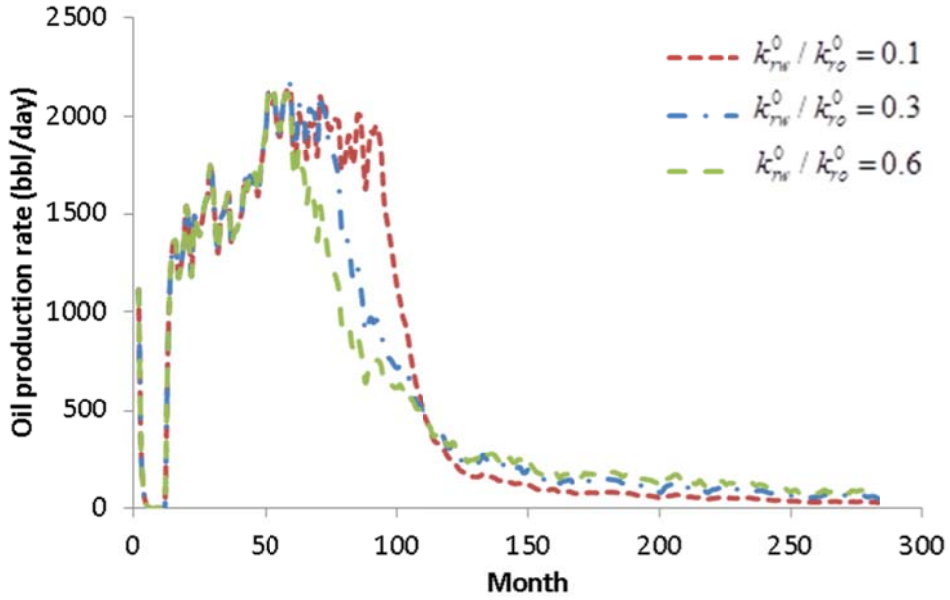

Figure 5.20 The simulated oil production rates of producer 1 under different water-oil endpoint ratios.

5.2.3.1 Connectivity

The connectivity obtained when $k_{rw}^0 / k_{ro}^0 = 0.3$ is shown in Figure 5.21 and Table 5.9. We use this case as the base case. Tables 5.10-5.11 show the relative change of connectivity in the other two cases compared to the base case. The average relative changes in the case of water-oil endpoint ratios equal to 0.1 and 0.6 are 9.78% and 1.58%, respectively. In general, the change in connectivity is small when water-oil relative permeability endpoint ratio changes.

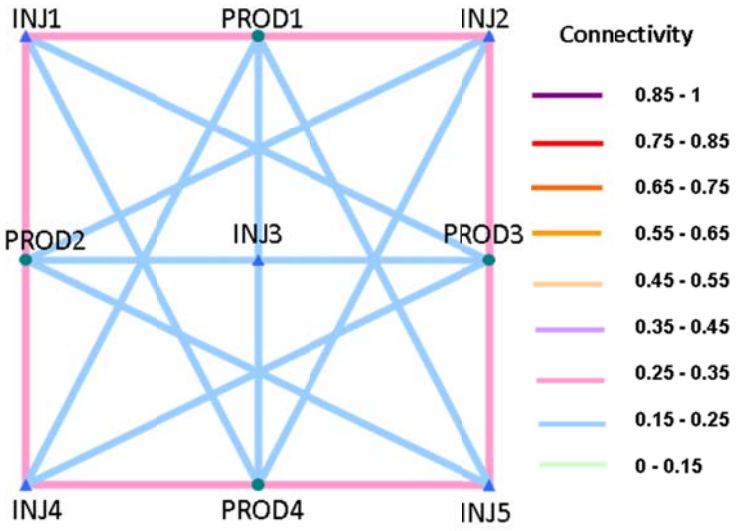

Figure 5.21 Connectivity map for the case of $k_{rw}^0 / k_{ro}^0 = 0.3$ using the coupled CRM model.

	PROD1	PROD2	PROD3	PROD4
INJ1	0.33	0.34	0.16	0.17
INJ2	0.32	0.16	0.34	0.18
INJ3	0.25	0.25	0.25	0.25
INJ4	0.17	0.34	0.16	0.33
INJ5	0.18	0.17	0.33	0.32

Table 5.9 Connectivity matrix for the case of $k_{rw}^0 / k_{ro}^0 = 0.3$ using the coupled CRM model.

	PROD1	PROD2	PROD3	PROD4	Average change compared to base case
INJ1	7.23%	7.45%	12.25%	16.67%	9.78%
INJ2	8.13%	20.88%	13.40%	19.24%	
INJ3	0.03%	2.47%	2.20%	0.34%	
INJ4	17.61%	7.57%	19.48%	11.87%	
INJ5	10.75%	8.08%	1.87%	8.12%	

Table 5.10 Relative connectivity change of water-oil endpoint ratio 0.1 compared to water-oil endpoint ratio 0.3.

	PROD1	PROD2	PROD3	PROD4	Average change compared to base case
INJ1	0.15%	1.61%	4.15%	0.66%	1.58%
INJ2	0.82%	2.54%	1.67%	2.12%	
INJ3	0.55%	2.56%	3.87%	0.60%	
INJ4	0.02%	0.17%	0.73%	0.54%	
INJ5	0.79%	4.02%	3.17%	0.87%	

Table 5.11 Relative connectivity change of water-oil endpoint ratio 0.6 compared to water-oil endpoint ratio 0.3.

5.2.3.2 Time Constant

In Figure 5.22, according to the coupled CRM model, time constants decrease with the increase of water-oil endpoint ratios. Also, it shows the difference in time constants among the three cases at late time (mature water flood) becomes slightly larger compared to those at early time (immature water flood). If we revisit the relative permeability curves in Figure 5.18, we observe that the difference in the relative permeability of water phase under different endpoints intensifies when saturation is close to the irreducible oil saturation. Consequently, the total fluid mobility among the three cases varies the most at late time and hence a larger difference in time constants is observed.

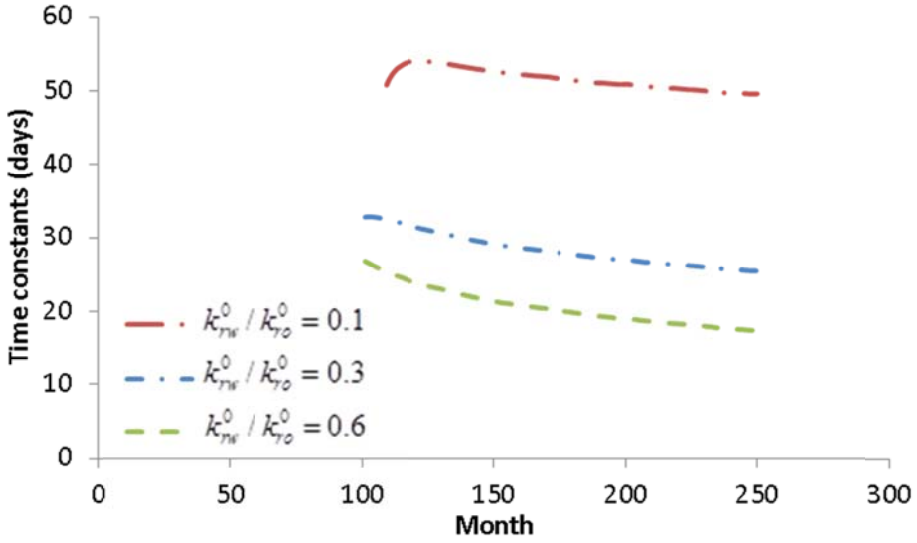

Figure 5.22 Time constants obtained using the coupled CRM model under different relative permeability endpoint ratios.

5.2.3.3 Average Oil Saturation

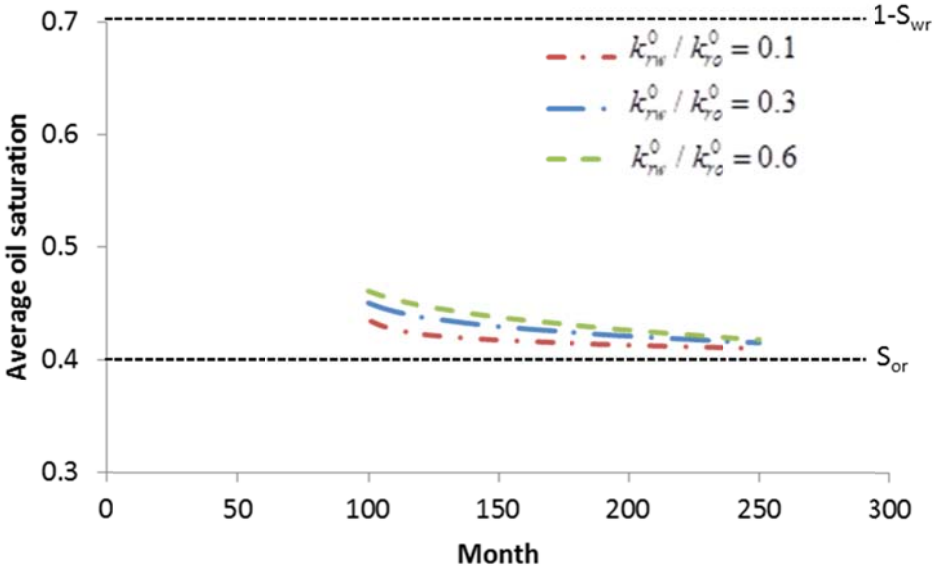

Figure 5.23 Average oil saturation obtained using the coupled CRM model under different relative permeability endpoint ratios.

Figure 5.23 gives the average oil saturation change in producer 1. It shows the small water-oil endpoint ratio case has small remaining oil saturation. Large remaining oil saturation occurs when water-oil endpoint ratio is large.

5.2.4 Changing the Compressibility

In this last sensitivity study, we exam what effects compressibility can produce on the output parameters in the coupled CRM model. We performed three cases with different oil compressibilities (see Table 5.12). The water and pore compressibilities are fixed considering that they are usually very small. We range the value of oil compressibility from 1×10^{-5} psi^{-1} to 10×10^{-5} psi^{-1}.

	c_w (psi^{-1})	c_f (psi^{-1})	c_o (psi^{-1})
Case 1	1×10^{-6}	1×10^{-6}	1×10^{-5}
Case 2			3×10^{-5}
Case 3			10×10^{-5}

Table 5.12 Compressibility data used in the sensitivity study.

Figures 5.24-5.26 show the reservoir simulation results corresponding to the three different oil compressibility cases. We observe that in the primary recovery phase, the large oil compressibility case released the most total fluid as the total compressibility is also large (see Figure 5.24). The smaller the oil compressibility, the smaller the total production rates are.

In the secondary recovery, the total production rates are close for all three cases. Nevertheless, different production time lags are observed in Figure 5.25. The production

rates profile is smoother in the case of large oil compressibility. As mentioned before, the compressibility effect is negligible on the water fractional flow. Figure 5.26 shows that the water cuts in the three cases are nearly the same.

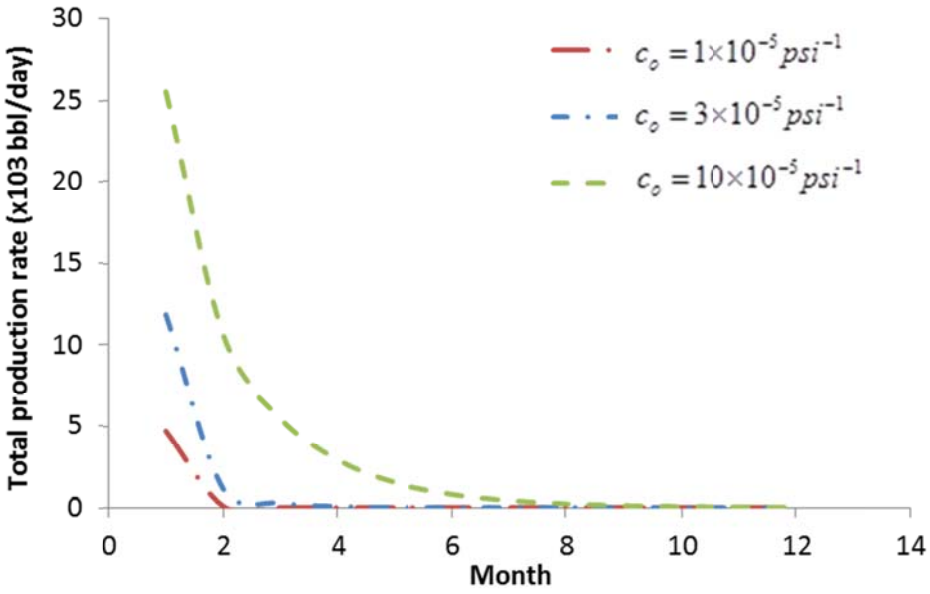

Figure 5.24 The simulated primary production rates of producer 1 under different oil compressibilities.

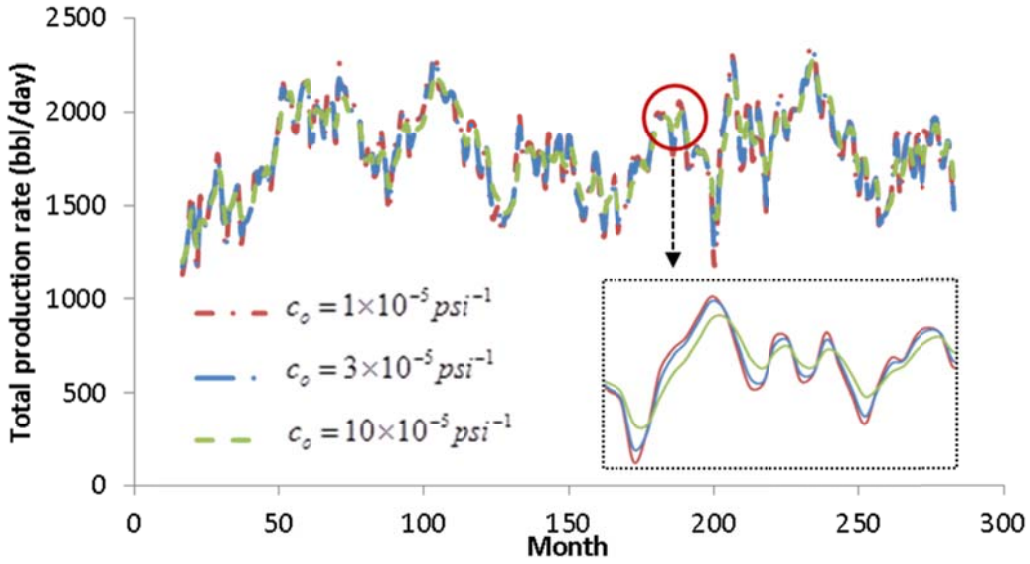

Figure 5.25 The simulated secondary recovery production rates of producer 1 under different oil compressibilities.

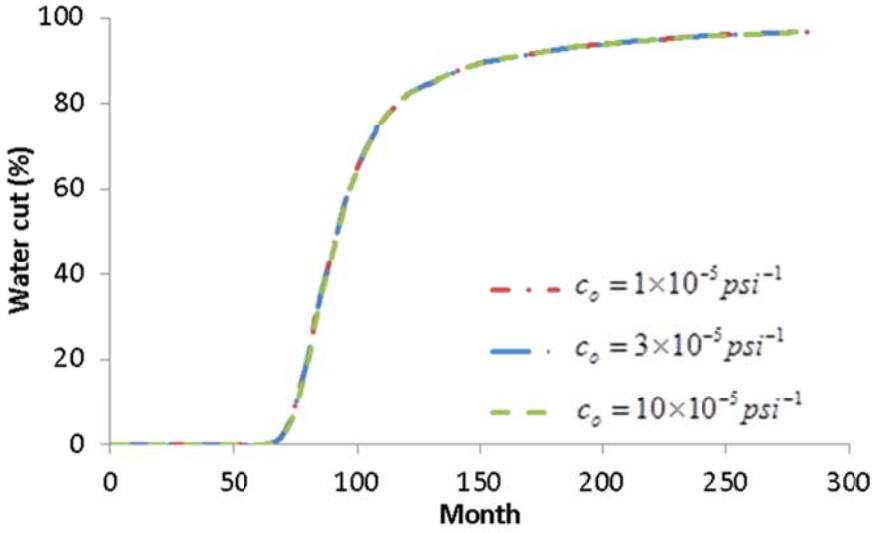

Figure 5.26 The simulated water cuts of producer 1 under different oil compressibilities.

The coupled CRM model requires water/oil/pore compressibilities as inputs. We conduct the coupled CRM runs with the compressibility inputs in Table 5.15. The results are discussed as the following.

5.2.4.1 Connectivity

The connectivities obtained for $c_o = 1\times10^{-5}\ psi^{-1}$ is in Figure 5.27. Table 5.6 shows the connectivity values. Similar to the previous cases, we observe a near symmetric connectivity pattern.

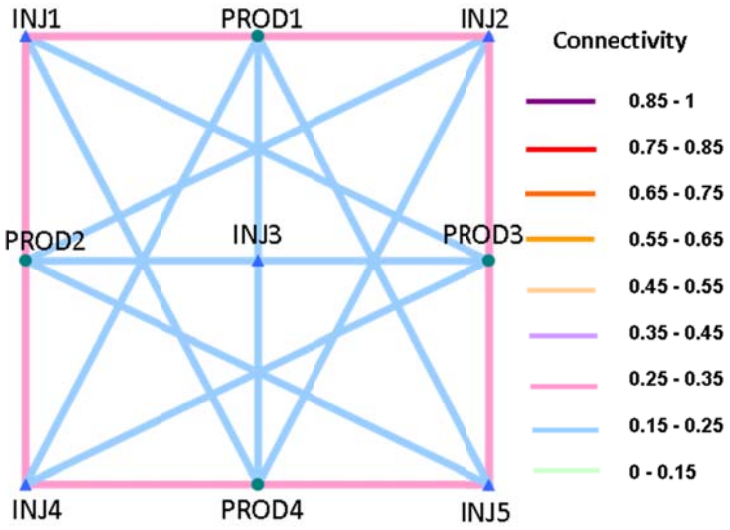

Figure 5.27 Connectivity map for the case of $c_o = 1\times10^{-5}\ psi^{-1}$ using the coupled CRM model.

	PROD1	PROD2	PROD3	PROD4
INJ1	0.32	0.32	0.18	0.18
INJ2	0.32	0.18	0.32	0.18
INJ3	0.25	0.25	0.24	0.25
INJ4	0.18	0.32	0.18	0.32
INJ5	0.18	0.17	0.34	0.31

Table 5.13 Connectivity matrix for the case of $c_o = 1\times10^{-5}\ psi^{-1}$ using the coupled CRM model.

Tables 5.14-5.15 summarize the relative change in connectivity in the other two cases with larger oil compressibilities. The average relative change in connectivity of case 2 ($c_o = 3\times10^{-5}\ psi^{-1}$) is 3.77%. Case 3 ($c_o = 10\times10^{-5}\ psi^{-1}$) gives a 8.42% average relative change in connectivity, which is slightly higher than case 2.

	PROD1	**PROD2**	**PROD3**	**PROD4**	**Average change compared to base case**
INJ1	2.27%	4.53%	8.11%	4.47%	3.77%
INJ2	0.50%	11.14%	6.88%	2.16%	
INJ3	0.44%	2.53%	3.60%	1.41%	
INJ4	4.13%	4.91%	10.24%	2.95%	
INJ5	1.22%	0.82%	1.35%	1.71%	

Table 5.14 Relative connectivity change of case 2 ($c_o = 3\times10^{-5}\ psi^{-1}$) compared to case 1($c_o = 1\times10^{-5}\ psi^{-1}$)

	PROD1	**PROD2**	**PROD3**	**PROD4**	**Average change compared to base case**
INJ1	8.21%	10.22%	17.60%	16.46%	8.42%
INJ2	3.77%	20.79%	9.78%	3.55%	
INJ3	2.11%	0.58%	0.29%	3.00%	
INJ4	12.66%	8.19%	13.55%	6.14%	
INJ5	11.13%	9.36%	4.61%	6.49%	

Table 5.15 Relative connectivity change of case 3 ($c_o = 10\times10^{-5}\ psi^{-1}$) compared to case 1($c_o = 1\times10^{-5}\ psi^{-1}$)

5.2.4.2 Time Constant

Figure 5.28 gives the time constants of the three different oil compressibility cases using the coupled CRM model. According to the coupled model, the case with largest oil compressibility gives the largest time constant; while smaller compressibility cases have smaller time constants.

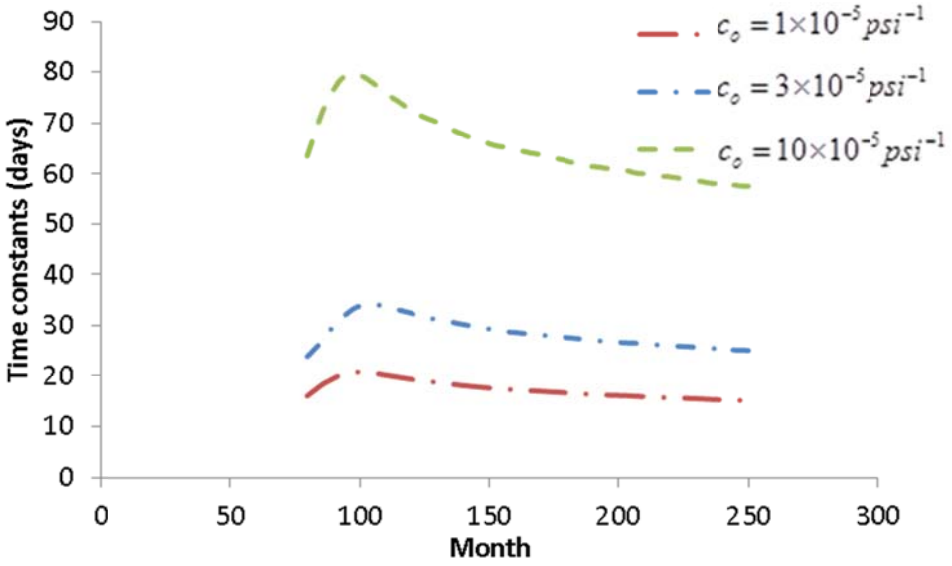

Figure 5.28 Time constants obtained using the coupled CRM model under different oil compressibilities.

5.2.4.3 Average Oil Saturation

Figure 5.29 shows the average oil saturation change in producer 1. As we mentioned before, compressibility has negligible effect on the fractional flow. Figure 5.29 confirms that the three cases have similar average oil saturation profiles. And the remaining oil saturations at the end of the fitting window are nearly the same.

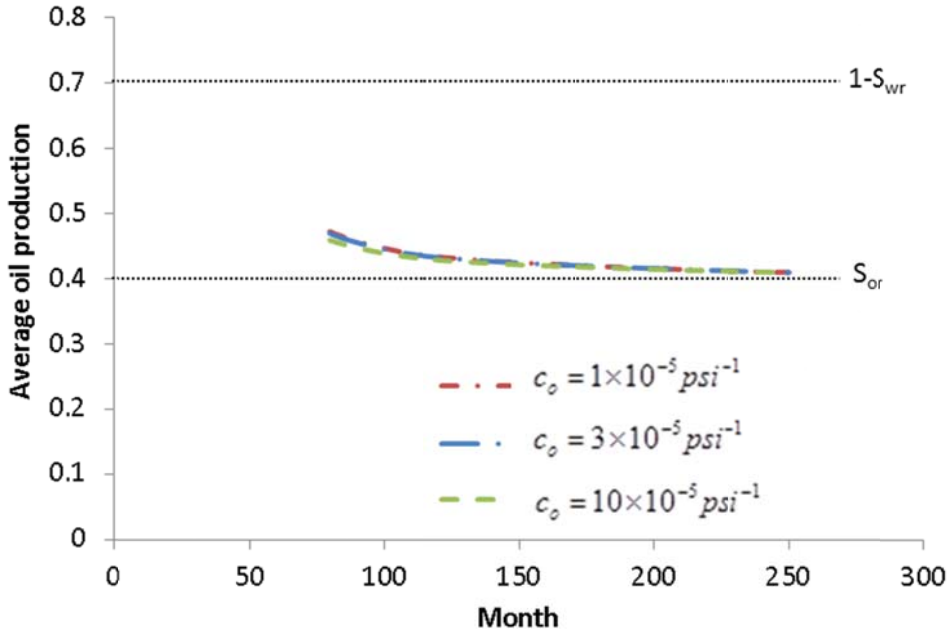

Figure 5.29 Average oil saturation obtained using the coupled CRM model under different oil compressiblities.

5.3 SENSITIVITY STUDY SUMMARY

5.3.1 Connectivity

All the four sensitivity studies have shown that the inter-well connection obtained by the coupled CRM model varies only slightly with changes in mobility and compressibility effects. This means that the connectivity is not sensitive to the mobility and compressibility change. On the contrary, it is reminiscent of the studies in Chapter 4 that the connectivity could change drastically under different field geology cases such as sealed reservoirs, heterogeneous reservoirs, etc. Hence, we conclude that connectivity is weakly related to both mobility and compressibility and is, in a large part, determined by the reservoir permeability distributions.

5.3.2 Time Constant

The time constant in the coupled CRM model is defined as the following:

$$\tau_j^k = \frac{\left(\frac{V_p c_t}{J_t^{'}}\right)_j}{\left[\frac{k_{ro}\left(S_{o2}\right)}{\mu_o} + \frac{k_{rw}\left(S_{o2}\right)}{\mu_w}\right]_j^k} \tag{5.7}$$

The time constant is a measurement of reservoir system compressibility as well as total fluid mobility. Large time constants occur when a reservoir has large compressibility or small total fluid mobility.

In the sensitivity case study, it shows that large time constants are obtained under the following scenarios:

1): Large oil-water viscosity ratio;

2): Large relative permeability exponents;

3): Small water-oil relative permeability endpoint ratio;

4): Large oil phase compressibility

These results are consistent with the definition of the time constant in the coupled CRM model. Therefore, the sensitivity study proves that the time constant from the coupled CRM model is a comprehensive parameter that reflects both reservoir compressibility and mobility effects. However, the current CRM model could not achieve a variable time constant reflecting the changes of mobility with time.

Nevertheless, though time constant implies information regarding total fluid mobility according to Eq. 5.7, it doesn't suggest displacement efficiency, which is relevant to oil production. Specifically, while a small time constant implies a large total fluid mobility, it may be caused by the fast flowing of an unwanted fluid phase.

5.3.3 Saturation

In the sensitivity studies using the coupled CRM model, we found that the following scenarios are favorable for oil being displaced by water (giving small remaining average oil saturations):

1: Small oil-water viscosity ratio;

2: Small relative permeability exponents;

3: Small water-oil relative permeability endpoint ratio;

These CRM results are consistent with the water-oil fractional flow theories that the remaining oil saturation is usually small when the displacement takes place in an efficient way.

Meanwhile, we observe that the remaining oil saturation is almost unaffected by changing the reservoir compressibility, which is also consistent with the illustrations in Figure 5.4 given by Lake (1989).

In summary, we conclude that the coupled CRM model output parameters follow reasonable change with respect to the change of inputs. They reflect both reservoir compressibility and mobility effects, whereas model parameters in the single-phase current CRM model can only imply compressibility effect.

CHAPTER 6: CONCLUSIONS AND FUTURE WORK

The CRM model is a simple and quick tool that only uses production and injection data to characterize well connectivity. The current CRM model is limited to mature water floods since saturation change is ignored in the model. However, there are circumstances when saturation change should not be neglected, such as in an immature water flood. This dissertation is dedicated to developing a coupled CRM model that couples the pressure and saturation equations together to account for the saturation impact. As a result, we can resolve the limitation in the current CRM model and broaden the application of the model. In this chapter, we summarize the technical contributions of this work, and make conclusions and recommendations.

6.1 TECHNICAL CONTRIBUTIONS

The working equations (the pressure and saturation equations) in the coupled CRM model were derived from the continuity equation and oil material balance on a producer-based drainage volume. Unlike the current CRM model where a constant single-phase productivity index is assumed, we recover the productivity index corresponding to the two-phase reservoir flow in our work. As a result, the time constant now depends on time and reflects the saturation impact. The time-varying time constant changes the ordinary differential pressure equations' linearity from a linear ODE to a non-linear ODE. The saturation equation is also non-linear. We obtained a semi-analytical solution for the pressure equation and a numerical solution for the saturation equation. The semi-analytical pressure solution is derived by performing discretization in time assuming that injection rate and time constant stay unchanged over each time step.

The explicit numerical saturation solution is achieved under the assumption that the saturation usually changes continuously and slowly.

Two coupling options to solve the pressure and saturation equations simultaneously are proposed and designed. The fully-coupled option engages both the pressure and saturation equations at each time step. The simplified-coupled option solves the pressure and saturation equations together in a simplified manner by neglecting the compressibility contribution in the saturation equation. After the equation coupling, a multivariate non-linear regression problem is then solved to minimize the difference between the calculated and observed production rate, and therefore estimate model parameters (connectivity, time constant and initial saturation). The regression solver we choose is CONOPT in GAMS, which is a non-linear programming (NLP) solver that is designed to find local optimum for large scale NLP problems.

Prediction capability has been designed in the coupled CRM model to evaluate well performance under future injection schemes. Prediction of total fluid rates in the coupled CRM is more complicated than the existing CRM model since saturation is involved. Two prediction algorithms, explicit and implicit algorithms, are introduced and discussed. We have implemented the explicit algorithm in the coupled CRM model since the accuracy is good to the desired degree. While prediction of total rates requires more efforts, the oil prediction is simple and straightforward. This is because the coupled CRM model is a two-phase flow model and we can readily obtain the oil saturation change with time. The fractional flow curve is constructed directly using the average oil saturation and the historical water cut data. Extrapolation of this fractional flow curve enables prediction of oil rates.

We developed validation procedures to evaluate whether the model parameters are reliable. Two different kinds of validation are demonstrated and discussed. They are

internal and external validations. An internal validation verifies the reliability of the coupled CRM model by predicting part of the production history under historical injection rates using the model parameters obtained from history match. Through the comparisons between the known historical production rates and the predicted production rates, we are able to check if the model is correct. External validation uses a reliable independent procedure to obtain the same (or similar) model parameters as those from the coupled CRM model. By comparing the counterparts, we are able to validate the results from the CRM model.

Once all model parameters are estimated and validated, the coupled CRM model described above is ready to find an optimal injection strategy to maximize the field's total oil production over a future specified time horizon. There are several different optimization objectives and strategies. In this dissertation, we discussed the implement of an optimization procedure to maximize the field total oil production while retaining a constant injection rate in each injector. Each injector has a different injection rate.

We test the coupled CRM model in synthetic homogeneous and heterogeneous reservoirs to illustrate the implemented capabilities (history match, prediction, validation and optimization), discuss model parameters (connectivity, time constant, and saturation) obtained, as well we validate these model parameters. We also compare the results of the coupled and the current CRM models to show the difference after taking saturation into account. We applied three fractional flow models to the same field case at two displacement stages (immature and mature water floods) to discuss their advantages and limitations. Meanwhile, we explore the coupled model sensitivity to fluid viscosity ratio, compressibility and oil-water relative permeability, respectively, in a synthetic homogeneous reservoir. These sensitivity studies help us to understand the relationship between the inputs and the outputs in the coupled CRM model.

6.2 CONCLUSIONS

1. The coupled CRM model successfully incorporated the saturation impact. By solving the pressure and saturation equation simultaneously, the saturation change at each time step is now reflected in the model. Consequently, the coupled model and the model parameters obtained are more accurate than the existing CRM model by honoring the two-phase water oil displacement physics.
2. Case studies have shown that the application of this two-phase model is not limited to mature water floods; it can be used in immature water floods with a significant improvement in the model parameter accuracy. Therefore, the coupled CRM model expands the application and adaptability of the existing CRM model.
3. The model parameters obtained from the coupled CRM model are reasonable and correct. The connectivity between wells reflects the geological features (seals, channels, etc.) that have been set up in the simulation cases. The time constant corresponds reasonably with the numerical simulation results. Moreover, the coupled model estimated the saturation change within the producer's drainage volume, which is also validated through reservoir simulation.
4. The time constant in the CRM model should be a function of total compressibility and fluid mobility since it is a time-varying quantity that is determined by the two-phase flow dynamics. Both the coupled CRM model and synthetic case studies show large time constant at early time and small time constants at late time during a water flood displacement. While it is possible to assume unchanged value for time constant in mature water flood when the saturation variation is small, saturation change should not be neglected in the early stage of water flooding. Therefore, the coupled CRM is recommended for the application in the case of an immature water flood.

5. The coupled CRM can describe the saturation change within a producer's drainage volume, which provides insight to the displacement efficiency. The sensitivity case studies have shown that small average oil saturation from the coupled CRM model often indicates an efficient displacement and vice versa.
6. The sensitivity study proves that connectivity is weakly related to both reservoir mobility and compressibility effects and is, in large part, determined by the reservoir permeability distributions.
7. Through sensitivity study, we conclude that the time constant from the coupled CRM model reflects both reservoir compressibility and mobility effects; whereas it can only imply compressibility effect in the single-phase CRM model.
8. The fractional flow model obtained from the coupled CRM model is accurate to predict future oil production rate in both mature and immature water floods. Since the coupled CRM model is a two-phase flow model, saturation change can be evaluated readily. The fractional flow curve is constructed directly using the average oil saturation and the historical water cut data.
9. The coupled CRM model is fast and only requires minimum information. Even though the algorithm and computation are more complicated than the current CRM model, the computation time doesn't increase significantly. For synthetic reservoirs, we found the computation time is almost the same as the current CRM model.
10. The internal and external validation procedures we proposed are effective to verify the coupled CRM model. The validation procedures provide confidence to further use the model parameters. Therefore, they are recommended as a standard practice in the coupled CRM model.
11. The coupled CRM model can be used to improve oil recovery. An improved accurate oil rate prediction enables us to further optimize the injection rate using the coupled

CRM. In the case study we performed, the optimized injection scheme is able to give 8% additional oil production in a synthetic mature water flood and 12% additional oil production in an immature water flood.

6.3 FUTURE WORK

1. Chapter 3 mentioned that laboratory scale relative permeability models are used in the coupled CRM model, which is a large scale model. As discussed, it is not a problem unique to the coupled CRM model; other models such as the traditional reservoir simulations also have similar scale issues by using the laboratory scale relative permeability. Nevertheless, upscaling relative permeability to the CRM scale using the production and injection data should be explored.
2. This dissertation developed the coupled CRM model for a producer-based drainage volume. It will be desirable to develop the coupled CRM model based on a smaller drainage volume between a particular producer-injector pair. In this way, we might gain more information since it is a more detailed version of the coupled CRM model.
3. In the prediction capability, we used the explicit algorithm. It also worth trying the implicit prediction approach, which may achieve a higher accuracy in the quality of oil rate prediction.
4. We have applied the coupled CRM model to many synthetic reservoirs. It is highly recommended to further test the model on field cases. Since the field data are often noisy, we must improve the coupled CRM model's capability to handle these actual production and injection data. Moreover, the application to the field cases provides ultimate validation of the coupled CRM, which is helpful to improve the model.

5. The coupled CRM model gives the average oil saturation within each producer's drainage volume. Therefore, it might provide insights to identify areas with bypass oil since these areas are often associated with a large remaining oil saturation.
6. The coupled CRM model has provided information such as connectivity, time constant and saturation. It is desirable if we could use this information to assist other reservoir evaluation/prediction methods. For example, if we can use the connectivity obtained to better understand the reservoir geology, it will be helpful to construct the geology model in reservoir simulation and reduce the geological uncertainty. Also, down-scaling the information from the CRM model and using it in the reservoir simulation are also interesting research directions.
7. It is recommended to explore different injection strategies. In this dissertation, we adopt the one to maximize the field total oil production while retaining constant injection rates in each injector. However, it is worth trying other injection schemes using different objective functions and constraints in the optimization problem.
8. We should develop better visualization tools for the coupled CRM model. Since the coupled CRM model can describe the average oil saturation, it will be helpful to visualize the oil saturation distribution in the field. Figure 6.1 illustrates such an oil saturation bubble map. This map shows the drainage volume of each producer and the average oil saturation within it.

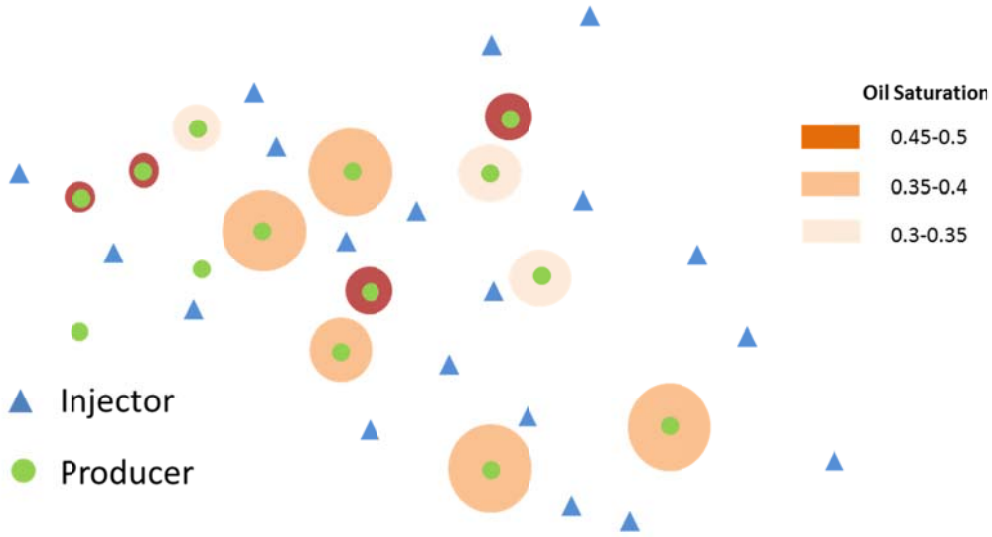

Figure 6.1 Schematic of oil saturation distribution visualization

9. A quick fix to the current CRM model regarding the poor oil prediction quality could be implementing the Koval approach at the early stage of water flood. In the mature water flood region, one needs to switch back to use the Gentil's fractional flow model.
10. Since the CRM model is similar to streamline models. Streamline models produce results such as well allocation factor and time of flight, which are similar to the connectivity and time constants in the CRM model. We recommend comparing the CRM results to the streamline model. A comprehensive comparison can lead to better understanding of both models.

APPENDICES

APPENDIX A: DERIVATION OF KOVAL EQUATION SOLUTIONS

The Koval fractional flow expression is the same as the Buckley-Leverett water fractional flow expression in a water flood when oil and water phases have straight-line relative permeabilities. In such a case, we write the fractional flow of water in the following form:

$$f_w = \frac{1}{1+\frac{(1-S)}{K_{val}(S)}} \tag{A.1}$$

where K_{val} is the Koval factor, and S is the reduced water saturation defined as:

$$S = \frac{S_w - S_{wr}}{1 - S_{wr} - S_{or}} \tag{A.2}$$

We take the derivative of water cut with respect to saturation in Eq. A.1 to give:

$$f_w' = \frac{1}{K_{val}\left[S + \frac{1}{K_{val}}(1-S)\right]^2} \tag{A.3}$$

According to Buckley and Leverette (1942), the specific velocity of a constant saturation is equal to the derivative of the fractional flow curve at that saturation. Therefore, we can arrive at the following expression:

$$f_w' = v_s = \frac{x_D}{t_D} \tag{A.4}$$

where v_s is the velocity of the displacement wave, x_D and t_D are the dimensionless distance and time, respectively.

We will have a spreading wave if:

$$f_w'|_{s=0} > f_w'|_{s=1} \tag{A.5}$$

Using Eq. A.3, Eq. A.5 becomes:

$$K_{val} > \frac{1}{K_{val}} \tag{A.6}$$

Eq. A.6 implies that the Koval factor should be greater than 1 in case of a spreading wave.

To solve for the saturation profile, using Eqs. A.3-A.4 leads to:

$$\frac{1}{K_{val}\left[S+\frac{1}{K_{val}}(1-S)\right]^2}=\frac{x_D}{t_D} \tag{A.7}$$

Rearranging Eq. A.7, we have:

$$\frac{x_D}{t_D}\left(K_{val}-1\right)^2 S^2+\frac{2x_D}{t_D}\left(K_{val}-1\right)S+\frac{x_D}{t_D}-K_{val}=0 \tag{A.8}$$

Solving the equation above, we can obtain:

$$S=\frac{\left(K_{val}\frac{x_D}{t_D}\right)^{1/2}-1}{K_{val}-1} \tag{A.9}$$

Because $0 \le S \le 1$, we rewrite Eq. A.9 in the following form:

$$S=\begin{cases} 0 & t_D \le \dfrac{1}{K_{val}} \\ \dfrac{\left(K_{val}x_D/t_D\right)^{1/2}-1}{K_{val}-1} & \dfrac{1}{K_{val}} < t_D < K_{val} \\ 1 & t_D \ge K_{val} \end{cases} \tag{A.10}$$

Substituting Eq. A.10 into Eq. A.1, we obtain another expression in terms of water cut as follows:

$$f_w\big|_{x_D=1}=\begin{cases} 0 & t_D < \dfrac{1}{K_{val}} \\ \dfrac{K_{val}-\sqrt{\dfrac{K_{val}}{t_D}}}{K_{val}-1} & \dfrac{1}{K_{val}} < t_D < K_{val} \\ 1 & t_D > K_{val} \end{cases} \tag{A.11}$$

APPENDIX B: APPLICATION OF THE CRM MODEL IN A HIGHLY HETEROGENEOUS CO_2 FLOODED FIELD WITH UNALLOCATED WELL TEST DATA

The Cranfield field, which is part of the Mississippi salt basin, is located approximately 20 km east of city of Natchez in Adams and Franklin Counties, southwest Mississippi, USA (Figure B.1). The reservoir is located at 10,000 ft (3,000 m) depth and is a near circular anticline about 4 miles in diameter. A gas cap, an oil ring and a downdip water leg existed before development (Weaver and Anderson, 1966). A fault that is sealing, except in the north part of the field, divides the productive formation into two reservoirs (Figure B.2).

The field was discovered in 1943 and produced oil and gas condensate until 1965 (Weaver and Anderson, 1966). It was pressure depleted and wells plugged and abandoned in 1965. The reservoir has been under CO_2-flooding for EOR since 2008 (Lu et al. 2013).

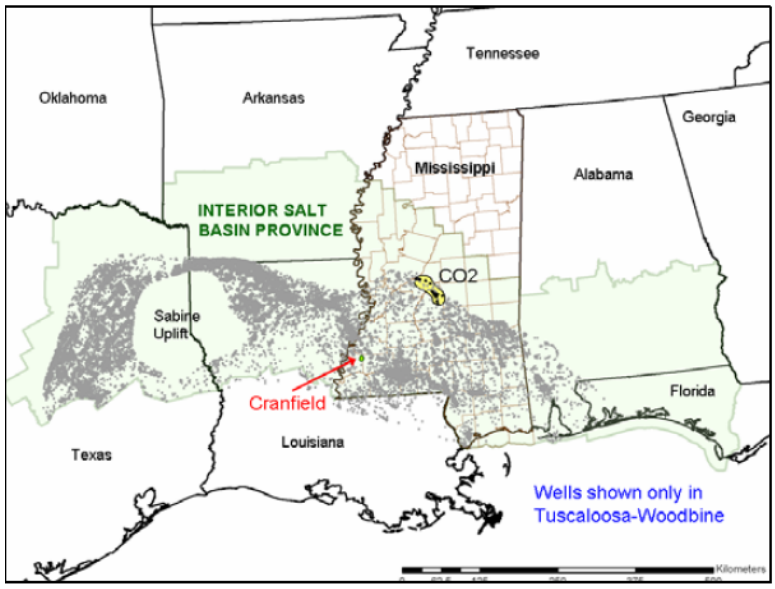

Figure B.1 Location of Cranfield field site in southwest Mississippi (Meckel and Hovorka, 2009).

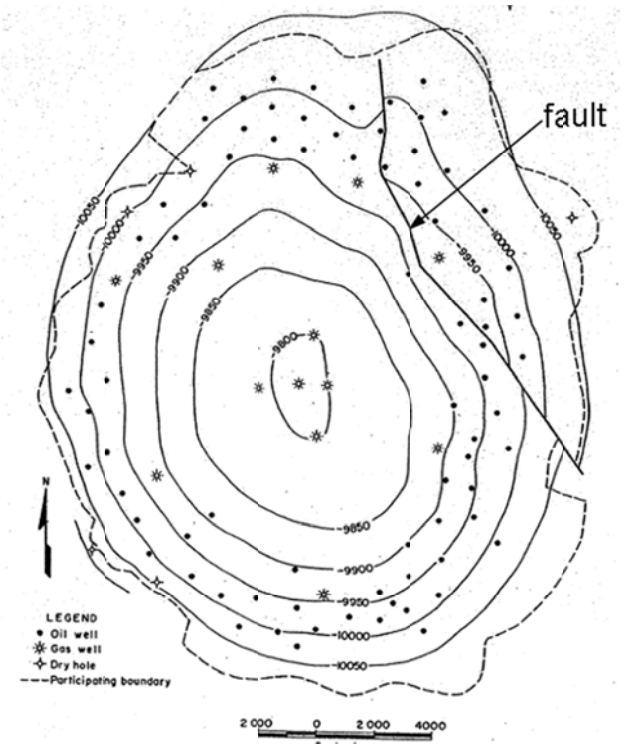

Figure B.2 Cranfield reservoir geology (Weaver and Anderson, 1966).

B.1 The CRM Model for Well Test Data

Unlike most field cases, which provide monthly allocated production rate data, this field only provides randomly and sparsely distributed well test production data, which can lead to difficulties in the application of the current CRM model. Therefore, we modify the objective function and constraints in the current CRM model accordingly to tackle this problem.

Figure B.3 illustrates part of a well test data set. The well test rates are often discontinuous and randomly taken for individual producers. However, the field total production rates are available at each time.

Day	Prod 1 (bbl/day)	Prod 2 (bbl/day)	Prod 3 (bbl/day)	Prod 4 (bbl/day)	Total production (bbl/day)
1	56	89		100	589
2			56		738
3				108	637
4	35		90		499
5		45			552
6	70			89	690

Figure B.3 Portion of a well test data set.

Considering the well test data characteristics, we propose the objective function to be modified in the following way:

$$\min z = \sum_{k=welltest} \sum_{j=1}^{n_p} (q_{tj}^{k\_obs} - q_{tj}^{k\_cal})^2 \qquad \text{B.1}$$

Eq. B.1 is similar to the objective function in the current CRM model except that the summation of the squared difference in rates of each producer is only made over the time steps when a well test rate is available. This objective function is constrained by Eqs. 3.14-3.15. Additionally, the following equation is also applied as a constraint:

$$\sum_j q_{tj}^{k\_cal} = q_t^{k\_obs} \qquad \text{B.2}$$

where $q_t^{k\_obs}$ is the observed field total production rate at time step *k*.

Eq. B.2 corresponds to the measured total production rate. It implies that the summation of the calculated production rate over all producers should be equal to the field total production rate observed at each time step. One can relax this equality constraint by imposing upper and lower bounds to allow Eq. B.2 to be approximately satisfied as the following

$$Lower\_bound \times q_t^{k\_obs} \le \sum_j q_{tj}^{k\_cal} \le q_t^{k\_obs} \times upper\_bound \qquad \text{B.3}$$

With a new objective function and additional constraints, we are able to use well test data directly in the CRM model to perform history match and estimate inter-well connectivities.

B.2 The CRM Model Application

The studied area of Cranfield is focused mainly on the north part of the field with injectors and producers in an irregular five-spot pattern. There are a total of 23 CO_2 injectors and 20 producers. CO_2 is in supercritical state under the reservoir conditions. Daily CO_2 injection rates in each injector are provided. The periodic unallocated well test data (oil/gas/water rates) are available in individual producers. Meanwhile the field total production of oil, gas and water are available on a daily basis.

Through history match, the inter-well connectivity obtained is in Figure B.4. In this field, we explored different distance limits for application. The connections are different when distance limits change. Nevertheless, all results show active connections between wells across the fault in the north part of the field. Connectivities are parallel to the fault in the south part, which correspond reasonably with the knowledge of the field geology. We should work with the Cranfield reservoir engineers who are familiar with the field condition to decide which distance limit to use. Figure B.5 shows the total production history match results in some producers, which gives decent fitting quality.

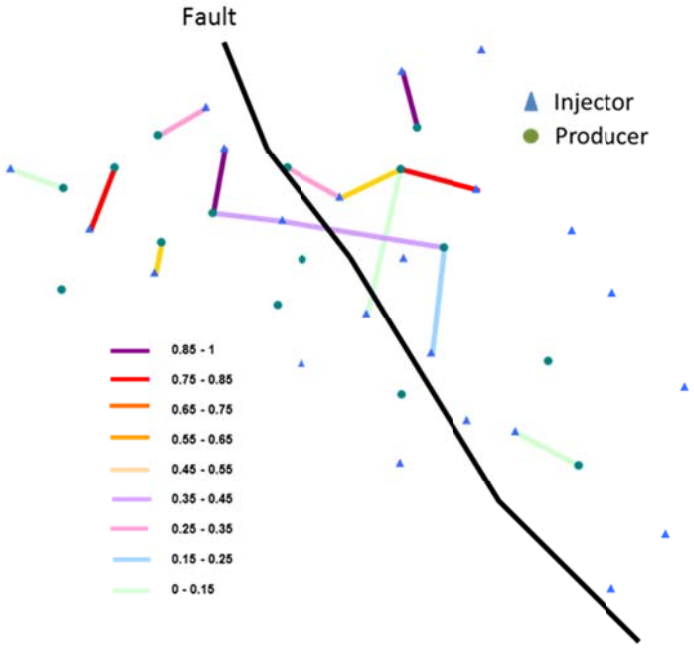

a). Distance limit of 2000 ft.

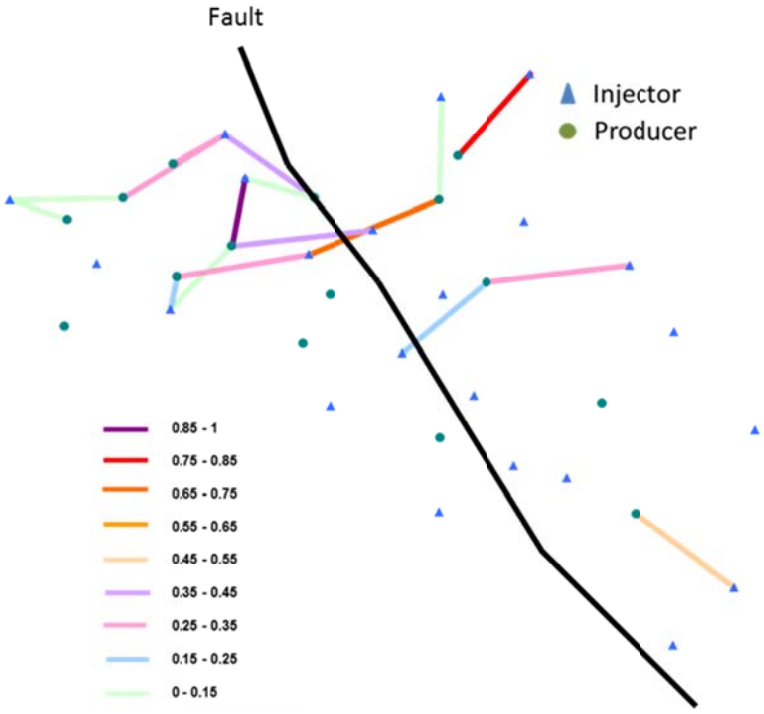

b). Distance limit of 3000 ft

Figure B.4 Cranfield field connectivity maps (Continued on next page).

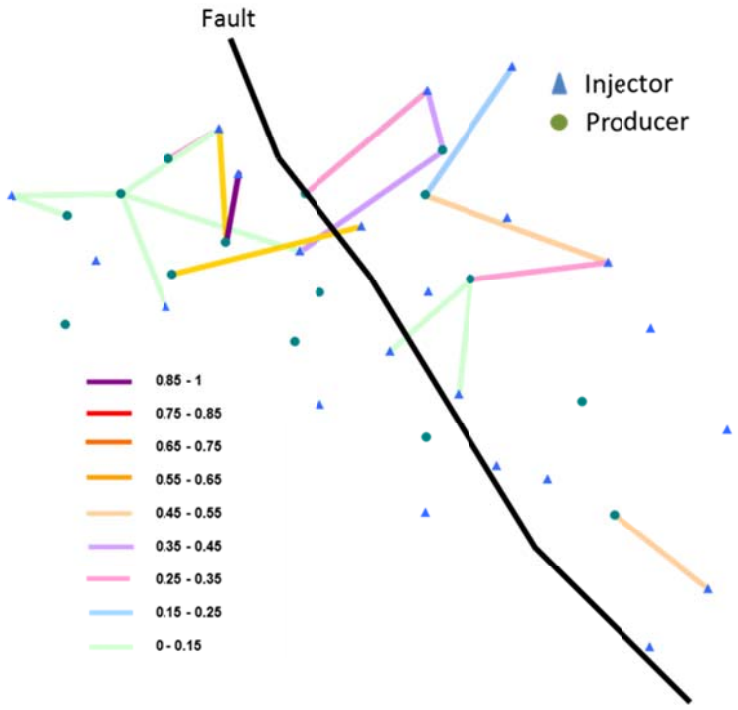

c). Distance limit of 4000 ft

Figure B.4 Cranfield field connectivity maps.

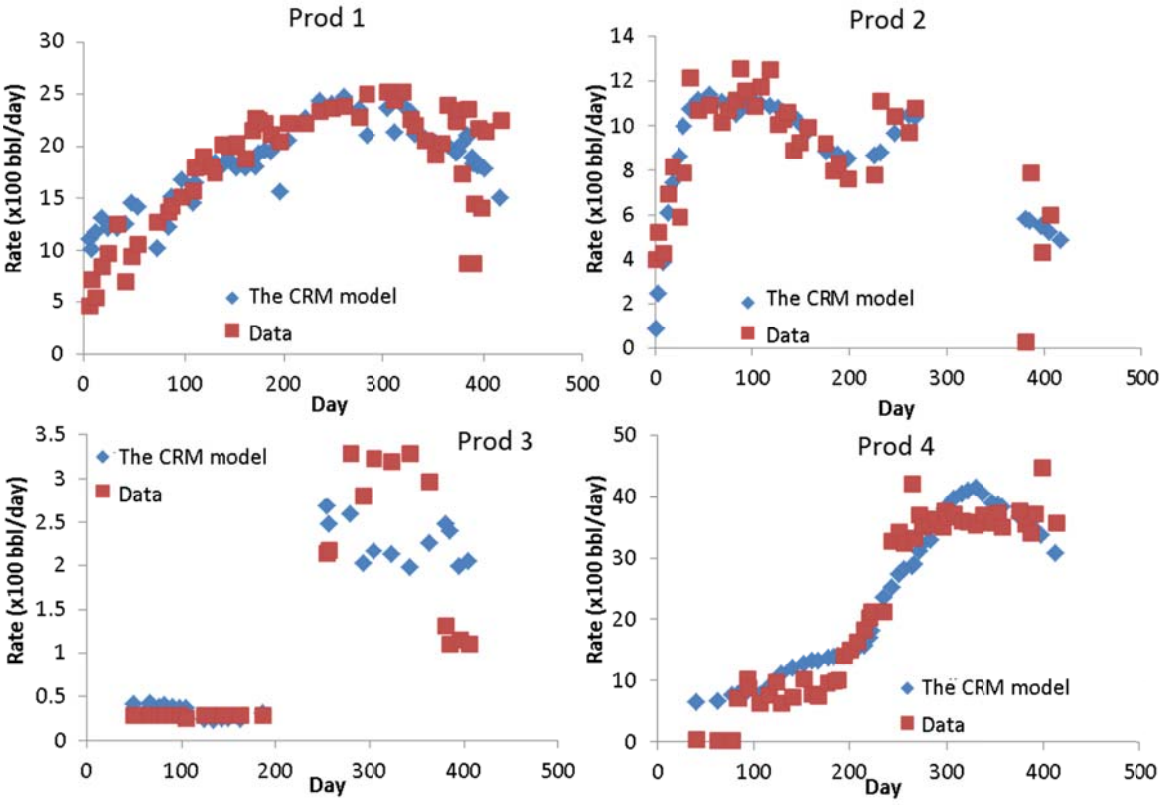

Figure B.5 Total production history match in selected producers.

APPENDIX C: DERIVATION OF THE PRESSURE EQUATION FOR THE COUPLED CRM MODEL

The pressure equation for a producer-based drainage volume has the form:

$$V_p c_t \frac{d}{dt}\left(\frac{q_t(t)}{J_t(t)} + P_{wf}\right) = i(t) - q_t(t) \qquad \text{C.1}$$

We assume the bottom-hole pressure is constant, and rearrange the equation:

$$\frac{dq_t(t)}{dt} + \frac{1}{\tau(t)} q_t(t) = \frac{i(t)}{\tau(t)} \qquad \text{C.2}$$

As the time constant changes with time, the above equation is a first order non-linear ordinary differential equation. The general solution to this ODE is:

$$q_t(t) = C_1\left(e^{-\int \frac{1}{\tau(t)}dt}\right) + e^{-\int \frac{1}{\tau(t)}dt} \int \frac{1}{e^{-\int \frac{1}{\tau(t)}dt}} \frac{i(t)}{\tau(t)} dt \qquad \text{C.3}$$

where C_1 is the integration constant.

We denote:

$$F(t) = \int \frac{1}{\tau(t)} dt \qquad \text{C.4}$$

And rewrite the solution to Eq. C.3 as:

$$q_t(t) = C_1\left(e^{-F(t)}\right) + e^{-F(t)} \int_{t_o}^{t} \frac{1}{e^{-F(t)}} \frac{i(t)}{\tau(t)} dt \qquad \text{C.5}$$

At the initial time when $t=t_0$, Eq. C.5 becomes:

$$q_t(t_0) = C_1\left(e^{-F(t_0)}\right) \qquad \text{C.6}$$

We then solve for the integration constant C_1 as:

$$C_1 = q_t(t_0) e^{F(t_0)} \qquad \text{C.7}$$

Substituting Eq. C.7 into Eq. C.5 gives:

$$q_t(t) = q_t(t_0) e^{F(t_0)-F(t)} + e^{-F(t)} \int_{t_o}^{t} \frac{1}{e^{-F(t)}} \frac{i(t)}{\tau(t)} dt \qquad \text{C.8}$$

Note that:

$$
\begin{aligned}
de^{F(t)} &= e^{F(t)} dF(t) \\
&= \frac{1}{e^{-F(t)}} \frac{1}{\tau(t)} dt
\end{aligned}
\tag{C.9}
$$

Thus, the last term in the solution Eq. C.8 becomes:

$$
\int_{t_o}^{t} \frac{1}{e^{-F(t)}} \frac{i(t)}{\tau(t)} dt = \int_{t_o}^{t} i(t)\, de^{F(t)} \tag{C.10}
$$

We integrate Eq. C.10 by parts to give:

$$
\begin{aligned}
\int_{t_o}^{t} i(t)\, de^{F(t)} &= i(t) e^{F(t)} \Big|_{t_0}^{t} - \int_{t_o}^{t} e^{F(t)} di(t) \\
&= i(t) e^{F(t)} \Big|_{t_0}^{t} - \int_{t_o}^{t} e^{F(t)} \frac{di(t)}{dt} dt
\end{aligned}
\tag{C.11}
$$

Substituting Eq. C.11 into solution Eq. C.8 leads to:

$$
q_t(t) = q_t(t_0) e^{F(t_0)-F(t)} + e^{-F(t)} \left[i(t) e^{F(t)} \Big|_{t_0}^{t} - \int_{t_o}^{t} e^{F(t)} \frac{di(t)}{dt} dt \right] \tag{C.12}
$$

Similarly, if we apply this to the previous time step t-1, we can obtain an expression as the following:

$$
q_t(t) = q_t(t-1) e^{F(t-1)-F(t)} + e^{-F(t)} \left[i(t) e^{F(t)} \Big|_{t-1}^{t} - \int_{t-1}^{t} e^{F(t)} \frac{di(t)}{dt} dt \right] \tag{C.13}
$$

It is reasonable to assume that J_t is a constant from time t-1 to t if the time step is small (usually monthly). This is because the average saturation within the producer's drainage volume usually changes slowly. Consequently, J_t changes slowly with time. Therefore, we can perform discretization in time, assuming that the injection rate and the time constant are constant over each time step. Then, we can reach a semi-analytical solution as:

$$
q_t(t) = q_t(t-1) e^{F(t-1)-F(t)} + i(t) \left[1 - e^{F(t-1)-F(t)} \right] \tag{C.14}
$$

According to Eq. C.4, we have:

$$F(t)-F(t-1)=\int_{t-1}^{t}\frac{1}{\tau(t)}dt \qquad \text{C.15}$$

Substituting Eq. C.15 into Eq. C.13 gives:

$$q_t(t)=q_t(t-1)e^{-\int_{t-1}^{t}\frac{1}{\tau(t)}dt}+i(t)\left[1-e^{-\int_{t-1}^{t}\frac{1}{\tau(t)}dt}\right] \qquad \text{C.16}$$

Since we have assumed constant τ for each time step k, we can obtain the solution as:

$$q_t^k=q_t^{k-1}e^{\frac{-\Delta t}{\tau^k}}+\left(1-e^{\frac{-\Delta t}{\tau^k}}\right)i^k \qquad \text{C.17}$$

Adding the connectivity to account for the injection loss, we arrive at the final pressure equation solution for a producer j at time step k as:

$$q_{tj}^k=q_{tj}^{k-1}e^{\frac{-\Delta t}{\tau_j^k}}+\left(1-e^{\frac{-\Delta t}{\tau_j^k}}\right)\left(\sum_i f_{ij}i_i^k\right) \qquad \text{C.18}$$

APPENDIX D: INPUT PARAMETERS OF THE COUPLED CRM MODEL IN SYNTHETIC STUDY CASE 4

Input		Value
Reservoir/fluid properties	μ_w(cp)	0.72
	μ_o(cp)	1.63
	k_{rw}	$k_{rw}^o\left(\frac{S_w - S_{wr}}{1 - S_{wr} - S_{or}}\right)^2$
	k_{ro}	$k_{ro}^o\left(\frac{1 - S_w - S_{or}}{1 - S_{wr} - S_{or}}\right)^2$
	S_{wr}	0.3
	S_{or}	0.4
	k_{rw}^o	0.3
	k_{ro}^o	1

Table D.1 Input parameters of the coupled CRM model in synthetic study case 4.

NOMENCLATURE

A	Drainage area (ft^2)
c_f	Pore compressibility (psi^{-1})
c_o	Oil compressibility (psi^{-1})
c_w	Water compressibility (psi^{-1})
c_t	Total compressibility (psi^{-1})
C_A	Shape factor
E	Effective viscosity ratio for Koval method
F_s	Solvent fractional flow
f_o	Oil fractional flow
f_w	Water fractional flow
f_{ij}	The connectivity between injector *i* and producer *j*
g	Gravity ($ft \cdot day^{-2}$)
H_K	A measurement of heterogeneity for Koval method
h	Thickness of the drainage volume
i	Injection rate ($bbl \cdot day^{-1}$)
I	Injection rate ($bbl \cdot day^{-1}$)
J_t	Total productivity index ($bbl \cdot day^{-1} \cdot psi^{-1}$)
k	Absolute permeability (darcy)
k_{ro}	Oil relative permeability
k_{rw}^0	Endpoint water relative permeability
k_{ro}^0	Endpoint oil relative permeability
k_{rw}	Water relative permeability
K_{val}	Koval factor

M_t	Total mobility ratio (cp^{-1})
M_t^0	Endpoint total mobility ratio (cp^{-1})
n_i	Total injector number
n_1	Exponent of water relative permeability
n_2	Exponent of oil relative permeability
P	Pressure (psi)
$\overline{P}$	Average pressure in a drainage pore volume (psi)
P_{cow}	Oil-water capillary pressure (psi)
P_{wf}	Well bottom hole pressure (psi)
q_o	Oil production rate ($bbl \cdot day^{-1}$)
q_w	Water production rate ($bbl \cdot day^{-1}$)
q_t	Total production rate ($bbl \cdot day^{-1}$)
r_w	Well radius (ft)
S_o	Oil saturation
S_w	Water saturation
S_{or}	Residual oil saturation
S_{wr}	Irreducible water saturation
S_s	Solvent saturation
$\overline{S}_o$	Average oil saturation in a drainage pore volume
$\overline{S}_w$	Average water saturation in a drainage pore volume
S_{o2}	Oil saturation at the outlet of a producer
t	Time (day)
V_P	Drainage volume (ft^3)
V_b	Bulk control volume of a producer (ft^3)
v_s	Velocity of the displacement wave ($ft \cdot day^{-1}$)

z	Objective function

Greek Symbols

μ_w	Water viscosity (cp)
μ_o	Oil viscosity (cp)
γ	Euler constant
τ	Time constant (day)
ϕ	Porosity

Superscripts

k	Time step index
obs	Observed value
cal	Calculated value

Subscripts

i	Injector index
j	Producer index
o	Oil
w	Water
s	Solvent
t	Total

REFERENCES

Albertoni, A., and Lake, L. W. 2003. Inferring Connectivity Only From Well-Rate Fluctuations in Waterfloods. *SPEREE* **6**(1):6-16.

Albertoni, A. 2002. *Inferring Interwell Connectivity Only From Well-Rate Fluctuations in Waterfloods*. M.S. Thesis, The University of Texas at Austin, Austin, Texas

Arps, J.J. 1945. Analysis of Decline Curves. *Trans. AIME* **160**:228-247.

Baker, R. 2001. Streamline Technology: Reservoir History Matching and Forecasting : Its Success Limitations and Future. *JCPT* **40**(04):23-28.

Brooks, R.H., and Corey A.T. 1964. *Hydraulic Properties of Porous Media*. Hydrological Papers, Colorado State University, Fort Collins.

Bruce, W. A. 1943. An Electrical Device for Analyzing Oil-Reservoir Behavior. *Trans. AIME* **151**(01):112-124.

Buckley S. E., and Leverett M. C. 1942. Mechanism of Fluid Displacement in Sands. *Trans. AIME* **146**:107-116.

Cao, F., Luo, H., and Lake, L. W. 2014. Development of a Fully Coupled Two-phase Flow Based Capacitance Resistance Model (CRM). Paper SPE 169486, presented at the SPE Improved Oil Recovery Symposium, Tulsa, OK, Apr., 12-16.

Can, B., and Kabir, C. S. 2012. Simple Tools for Forecasting Waterflood Performance. Paper SPE 156956, presented at the SPE Annual Technical Conference and Exhibition, San Antonio, TX, Oct., 8-10.

Corey, A.T. 1954. The Interrelation Between Gas and Oil Relative Permeabilities. *Producer Monthly* **19**(11):38-41.

Craft, B. C., Hawkins, M. F., and Terry, R. E. 1959. *Applied Petroleum Reservoir Engineering (Vol. 9)*. Englewood Cliffs, NJ: Prentice-Hall.

Craig, F .F. 1993. *The Reservoir Engineering Aspects of Waterflooding*. SPE, Richardson, Texas.

Datta-Gupta, A., and King, M. J. 2007. *Streamline simulation: theory and practice.* SPE, Richardson, TX.

Dykstra, H., and Parsons, R. L. 1950. The Prediction of Oil Recovery by Waterflood. *Secondary Recovery of Oil in the United States* **2**:160-174.

Ershaghi, I., and Omorigie, O. 1978. A Method for Extrapolation of Cut vs Recovery Curves. *JPT* **30**(02):203-204.

Fetkovich, M.J. 1980. Decline Curve Analysis Using Type Curves. *JPT* **32**(6): 1065-1077.

Gentil, P. H. 2005. *The Use of Multilinear Regression Models in Patterned Waterfloods: Physical Meaning of the Regression Coefficients*. M.S. Thesis, The University of Texas at Austin, Austin, Texas.

Honarpour, M., Koederitz, L. F., and Harvey, A. H. 1982. Empirical Equations For Estimating Two-Phase Relative Permeability in Consolidated Rock. *JPT* **34**(12):2905-2908.

Izgec, O., and Kabir, C. S. 2009. Establishing Injector/Producer Connectivity Before Breakthrough During Fluid Injection. Paper SPE 121203, presented at the SPE Western Regional Meeting, San Jose, CA, Mar., 24-26.

Izgec, O., and Kabir, C. S. 2010. Quantifying Nonuniform Aquifer Strength at Individual Wells. *SPEREE* **13**(02):296-305.

Kaviani, D., and Jensen, J. L. 2010. Reliable Connectivity Evaluation in Conventional and Heavy Oil Reservoirs: A Case Study From Senlac Heavy Oil Pool Western Saskatchewan. Paper SPE 137504, presented at the Canadian Unconventional Resources and International Petroleum Conference, Calgary, Alberta, Canada, Oct., 19-21.

Kaviani, D., Jensen, J. L., and Lake, L. W. 2012. Estimation of Interwell Connectivity in the Case of Unmeasured Fluctuating Bottomhole Pressures. *JPSE* **90**:79-95.

Kbiob, D. G. 1951. A Statistical Approach to Some Basic Mine Valuation Problems on the Witwatersrand. *Journal of Chemical, Metallurgical, and Mining Society of South Africa*.

Koval, E. J. 1963. A Method for Predicting the Performance of Unstable Miscible Displacement in Heterogeneous Media. *SPEJ* **3**(2): 145-154.

Lake, L. W. 2006. *Petroleum Engineering Handbook*. SPE, Richardson, Texas.

Lake, L.W. 1989. *Enhanced Oil Recovery*. Prentice Hall, Englewood Cliffs, New Jersey.

Laochamroonvorap, R. 2013. *Advances in The Development and Application of A Capacitance-Resistance Model*. M.S. Thesis, The University of Texas at Austin, Austin, Texas.

Lee, K. H., Ortega, A., Ghareloo, A., and Ershaghi, I. 2011. An Active Method for Characterization of Flow Units Between Injection/Production Wells by Injection-Rate Design. *SPEREE* **14**(4):433-445.

Leverett, M., and Lewis, W. B. 1941. Steady Fow of Gas-Oil-Water Mixtures Through Unconsolidated Sands. *Trans. AIME* **142**(01):107-116.

Liang, X., Weber, D.B., Edgar, T.F., Lake, L.W., Sayarpour, M., and Yousef, A.A. 2007. Optimization of Oil Production Based on a Capacitance Model of Production and Injection Rates. Paper SPE 107713, presented at the SPE Hydrocarbon Economics and Evaluation Symposium, Dallas, TX, Apr., 1-3.

Lipták, B. G. (Ed.). 2005. *Instrument Engineers' Handbook, Volume Two: Process Control and Optimization*. CRC press.

Lo, K. K., Warner Jr, H. R., and Johnson, J. B. 1990. A Study of the Post-Breakthrough Characteristics of Waterflood. Paper SPE 20064, presented at the SPE California Regional Meeting, Ventura, CA, Apr., 4-6.

Lu, J., Kordi, M., Hovorka, S. D., Meckel, T. A., and Christopher, C. A. 2013. Reservoir characterization and complications for trapping mechanisms at Cranfield CO_2 injection site. I*nternational Journal of Greenhouse Gas Control* **18**:361-374.

Mahdavi, Z., and Khademi, M. 2012. Prediction of Oil Production with Data Mining, Neuro-Fuzzy and Linear Regression. *International Journal of Computer Theory and Engineering* **4**(3):446-447.

Mao, S., and Journel, A. G. 1999. *Generation of a Reference Petrophysical/Seismic Data Set.* The Stanford V Report, Stanford, California.

Meckel, T., and Hovorka, S. 2009, January. Results From Continuous Downhole Monitoring (PDG) at a Field-Scale CO_2 Sequestration Demonstration Project Cranfield MS. SPE paper 127087, presented at the SPE International Conference on CO2 Capture Storage and Utilization, San Diego, CA, Nov., 2-4.

Nguyen A. P. 2012. *Capacitance Resistance Modeling for Primary Recovery, Waterflood and Water-CO_2 Flood*. Ph.D. Dissertation. The University of Texas at Austin, Austin, Texas.

Nowak, M., and Verly, G. 2005. The Practice of Sequential Gaussian Simulation, in *Geostatistics Banff 2004* **14**:387-398. Springer, Netherlands.

Parekh, B., and Kabir, C. S. 2011. Improved Understanding of Reservoir Connectivity in an Evolving Waterflood with Surveillance Data. Paper SPE 146637, presented at the SPE Annual Technical Conference and Exhibition, Denver, CO, Oct, 30-Nov., 2.

Peaceman, D. W. 1983. Interpretation of Well-Block Pressures in Numerical Reservoir Simulation with Nonsquare Grid Blocks and Anisotropic Permeability. *SPEJ* **23**(03):531-543.

Pope, G. A. 1980. The Application of Fractional Flow Theory to Enhanced Oil Recovery. *SPEJ* **20**(03):191-205.

Purvis, R. A. 1985. Analysis of Production-Performance Graphs. *JCPT* **24**(04).

Salazar-Bustamante, M., Gonzalez-Gomez, H., Matringe, S., and Castineira, D. 2012. Combining Decline-Curve Analysis and Capacitance/Resistance Models To Understand and Predict the Behavior of a Mature Naturally Fractured Carbonate Reservoir Under Gas Injection. Paper SPE 153252, presented at the SPE Latin America and Caribbean Petroleum Engineering Conference, Mexico City, Mexico, Apr., 16-18.

Saltelli, A., Ratto, M., Andres, T., Campolongo, F., Cariboni, J., Gatelli, D., Saisana, M., and Tarantola, S. 2008. *Global Sensitivity Analysis: The Primer*. John Wiley & Sons, England.

Samizo, N. 1983. *Numerical Simulation of Two Phase Compressible Flow by the Moving Point Method*. M.S. Thesis, The University of Texas at Austin, Austin, Texas.

Sayarpour, M., Zuluaga, E., Kabir, C.S. and Lake, L.W. 2007. The Use of Capacitance-Resistive Models for Rapid Estimation of Waterflood Performance and Optimization. Paper SPE 110081, presented at the SPE Annual Technical Conference and Exhibition, Anaheim, CA, Nov., 11-14.

Sayarpour, M. 2008. *Development and Application of Capacitance-Resistive Models to Water/CO_2 Floods*. Ph.D. Dissertation, The University of Texas at Austin, Austin, Texas.

Sayarpour, M., Kabir, C. S., and Lake, L. W. 2009. Field Applications of Capacitance-Resistance Models in Waterfloods. *SPEREE* **12**(06):853-864.

Sitorus, J. H., Sofyan, A., and Abdulfatah, M. Y. 2006. Developing A Fractional Flow Curve from Historic Production to Predict Performance of New Horizontal Wells Bekasap Field Indonesia. Paper SPE 101144, presented at the SPE Asia Pacific Oil & Gas Conference and Exhibition, Adelaide, Australia, Sep., 11-13.

Solomatine, D., See, L. M., and Abrahart, R. J. 2008. Data-Driven Modelling: Concepts, Approaches and Experiences, in *Practical Hydroinformatics* **68**:17-30. Springer, Berlin Heidelberg.

Soroush, M., Jensen, J., and Kaviani, D. 2013. Interwell Connectivity Evaluation in Cases of Frequent Production Interruptions. Paper SPE 165567, presented at the 2013 SPE Heavy Oil Conference, Calgary, Alberta, Canada, Jun., 11-13.

Stiles, W.E. 1949. Use of Permeability Distribution in Water Flood Calculations. *Trans*. *AIME* **186**:9-13.

Tafti, A., Ershaghi, T., Rezapour, I., and Ortega, A. 2013. Injection Scheduling Design for Reduced Order Waterflood Modeling. Paper SPE 165355, presented at the SPE Western Regional & AAPG Pacific Section Meeting, 2013 Joint Technical Conference, Monterey, CA, Apr., 19-25.

Thiele, M. R., Batycky, R. P., and Fenwick, D. H. 2010. Streamline Simulation For Modern Reservoir-Engineering Workflows. *JPT* **62**(01):64-70.

Timmerman, E. H. 1971. Predict Performance of Water Floods Graphically. *Petroleum Engineering (United States)* **43**(12):77-80.

Wahl, W. L., Mullins, L. D., Barham, R. H., and Bartlett, W. R. 1962. Matching the Performance of Saudi Arabian Oil Fields With an Electrical Model. *JPT* **14**(11):1275-1282.

Walsh, M. P., and Lake, L. W. 2003. *A Generalized Approach to Primary Hydrocarbon Recovery*. Elsevier Science, Netherlands.

Wang, W. 2011. *Reservoir Characterization Using a Capacitance Resistance Model in Conjunction with Geomechanical Surface Subsidence Models*. M.S. Thesis, The University of Texas at Austin, Austin, Texas.

Weaver, L. K., and Anderson, K. F. 1966. *Cranfield Field, Cranfield Unit, Basal Tuscaloosa reservoir, Adams and Franklin Counties, Mississippi*. Mississippi Oil and Gas Board, Mississippi.

Weber, D.B., Edgar, T.F., Lake, L.W., Lasdon, L.S., Kawas, S., and Sayarpour, M. 2009. Improvements in Capacitance-Resistive Modeling and Optimization of Large Scale Reservoirs. Paper SPE 121299, presented at the SPE Western Regional Meeting, San Jose, CA, Mar., 24-26.

Weber, D.B. 2009. *The Use of Capacitance-Resistance Models to Optimize Injection Allocation and Well Location in Water Floods,* Ph.D. Dissertation, University of Texas at Austin, Austin, Texas.

Welge H. J. 1952. A Simplified Method for Computing Oil Recovery by Gas or Water Drive. *Trans. AIME* **195**:99-108.

Wiess, B., Patterson, O. L., and Montague, K. E. 1951. High-speed Electronic Reservoir Analyzer. presented at Drilling and Production Practice, New York, NY, Jan. 1.

Wie, B. 1998. *Space Vehicle Dynamics and Control*. American Institute of Aeronautics and Astronautics, Virginia, USA.

Willhite, G. P. 1986. *Waterflooding.* SPE, Richardson, Texas.

Yousef, A. A., Gentil, P.H., Jensen, J. L., and Lake, L. W. 2006. A Capacitance Model to Infer Interwell Connectivity from Production and Injection Rate Fluctuations. *SPEREE* **9**(5):630-646.

Yousef, A. A. 2005. *Investigating Statistical Techniques to Infer Interwell Connectivity from Production and Injection Rate Fluctuations.* Ph.D. Dissertation, The University of Texas at Austin, Austin, Texas.